TAILORING PROSTATE CANCER SURGERY

RADIO- AND FLUORESCENCE GUIDANCE TO IMPROVE SURGICAL ACCURACY

Anne Claire Berrens

Tailoring Prostate Cancer Surgery

Radio- and Fluorescence Guidance to Improve Surgical Accuracy

Anne Claire Berrens

The work described in this thesis was performed at the Netherlands Cancer Institute – Antoni van Leeuwenhoek, Amsterdam, the Netherlands

Cover and design: Anne Claire Berrens
Layout: Henry Smaal, persoonlijkproefschrift.nl
Printing: Ridderprint, ridderprint.nl
ISBN: 978-94-6537-110-8

Printing and distribution was kindly supported by the Netherlands Cancer Institute – Oncology Graduate School (OOA), Curium Pharma, Bayer, Mayumana Healthcare, Wellspect, MedicoCare, Science Plus Group, Chipsoft, ABN Amro

VRIJE UNIVERSITEIT

Tailoring Prostate Cancer Surgery

radio- and fluorescence guidance to improve surgical accuracy

ACADEMISCH PROEFSCHRIFT

ter verkrijging van de graad Doctor aan
de Vrije Universiteit Amsterdam,
op gezag van de rector magnificus
prof.dr. J.J.G. Geurts,
volgens besluit van de decaan
van de Faculteit der Geneeskunde
in het openbaar te verdedigen
op maandag 23 februari 2026 om 11.45 uur
in de universiteit

door

Anne Claire Berrens

geboren te Leiden

promotoren:	prof.dr. H.G. van der Poel prof.dr. F.W.B. van Leeuwen
copromotoren:	dr. P.J. van Leeuwen prof.dr. R.J.A. van Moorselaar
promotiecommissie:	prof.dr. A.N. Vis prof.dr. H.P. Beerlage prof.dr. J.P.M. Sedelaar dr. D.D.D. Rietbergen dr. R.C.N. van den Bergh

Paranimfen

Jetske LB Gunster
Lotte M de Roode

Si piensas que la aventura es peligrosa, prueba la rutina.
Es mortal.

Paulo Coelho

Contents

Appendices

Based on:

- Implementation of Radioguided Surgery in Prostate Cancer. Berrens AC, van Leeuwen PJ, Maurer T, Hadaschik BA, Krafft U. *Q J Nucl Med Mol Imaging. 2021 Sep;65(3):202-214*
- Robot-assisted Radical Prostatectomy: Advanced Surgical Techniques - Bookchapter on Fluorescence Guided Node Dissection. Berrens AC, Özman O, Maurer T, van Leeuwen FWB, van der Poel HG. *Published by Springer 2022*

Chapter 1

General Introduction

The prostate

The prostate is a gland, located caudal to the bladder and is present only in men. It is about the size of a walnut and surrounds the urethra through which urine and ejaculate passes from the bladder to the exterior of the body (Figure 1A). The prostate and seminal vesicles, located dorsally at the base of the prostate, play an important role in male fertility. Sperm produced in the testes travels through the vas deferens, passing the prostate where supportive components are added during ejaculation and enters the prostatic urethra through the ejaculatory ducts (Figure 1B) [1].

Prostate Cancer

Prostate cancer is the second most commonly diagnosed malignancy in males worldwide, following closely behind lung cancer [2]. In 2023, 14.560 men were diagnosed with prostate cancer in the Netherlands, 36% of whom were age 75 or older [3]. Prostate cancer is asymptomatic in the majority of early cases. In later stages, and only when located in the peripheral zone or transitional zone (Figure 1B) one can imagine the urethra is affected, causing symptoms that are also linked to benign prostatic hyperplasia including urinary difficulties such as nocturia and increased frequency. Metastases to the bone may eventually lead to skeletal pain [4], signifying that in case of symptoms the cancer has already spread. Although the overall mortality of prostate cancer has decreased considerably in the Netherlands in the past 20 years (corrected for age distribution: 63.5/100.000 yearly deaths in 2000 vs 41/100.000) the difference in survival is still very depended of the stage it was diagnosed. The relative 10-year survival for patients with cancer located only in the prostate is >95%. In patients with advanced disease (tumor growing outside the prostate or with lymph-/ distant metastases), the 10-year survival rate drops to ~30% [3]. This emphasizes the importance of early detection.

Initial staging

Because prostate cancer is usually asymptomatic, patients suspected for prostate cancer usually present themselves with an elevated serum concentration of prostate-specific antigen (PSA) and/or an abnormal digital rectal examination at the general practitioner and referred to a urologist [5]. A large randomized trial showed that screening for PSA led to 50 % reduction of metastatic disease and 20 % reduction of prostate cancer specific death in men between 55-74 years old [6]. However, PSA-based screening also induced overdiagnosis. According to current European Association of Urology (EAU)-Guidelines a magnetic resonance imaging (MRI) is advised in all patients referred to a urologist [7]. On the MRI, the presence, localization and size of the suspected lesion(s), as well as the local radiological tumor (T)-stage, are determined. When a suspected lesion is visualized on MRI, targeted (and/or systematic) prostate biopsies are performed for histopathological diagnosis. Prostate carcinoma is histopathologically classified into different grades expressed as the Gleason score, based on the growth

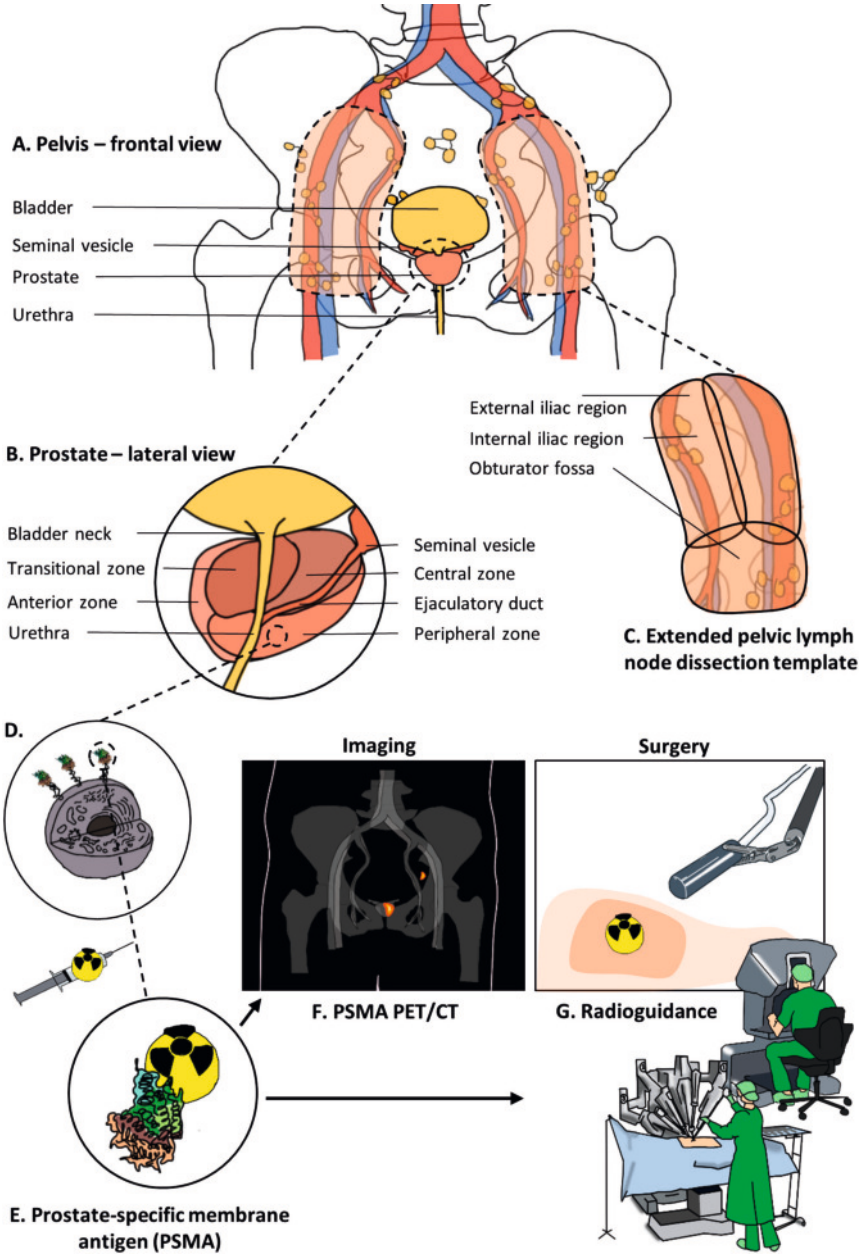

Figure 1. Overview of anatomical structures and terminology mentioned in this thesis in relation to eachother. A) Frontal view of the pelvis and the localization of the prostate in relation to the bladder and the pelvic lymph nodes. B) Lateral view of the prostate and the different zones. C) Extended pelvic lymph node dissection template with the three different regions used for localization. D) Prostate cancer cell with prostate-specific membrane antigen (PSMA). E) PSMA labeled with a radioisotope. F) PSMA PET/CT, the imaging modality where PSMA labeled with radioisotopes is used to localise the prostate cancer. G) PSMA labeled with radioisotopes used for intraoperative identification of prostate cancer.

pattern of the tumor. The Gleason score can in turn be categorized into grade groups (group 1-5), according to international society of urological pathologists (ISUP) standards [8]. Combining all these clinical findings, patients are categorized in one of three risk categories (low/intermediate/high). In case of intermediate or high-risk additional imaging can be performed. Conventional imaging such as bone scintigraphy and CT-scan, or increasingly common in Western Europe: prostate-specific membrane antigen (PSMA) positron emission tomography (PET)/CT.

PSMA PET/CT

PSMA is a transmembrane glycoprotein present in normal prostate cells and overexpressed in prostate cancer cells (Figure 1D) [9]. PET is a nuclear medicine imaging technique, which uses positron emitting isotopes, such as ^{18}Fluoride and ^{68}Gallium, to visualize the distribution of radioactive tracers that bind to PSMA (Figure 1E). Together with the CT that is made for anatomical reference, these images combined give 3D insight to the location of the primary tumor and possible lymph or bone metastases (Figure 1F). For lymph node metastases, a moderate sensitivity (41-42%, 95% CI 19-67%) and high specificity (91-94%, 95% CI 79-98%) is found [10 11]. In other words, the absence of uptake on PSMA PET scan does not guarantee the absence of metastases, but a positive scan is highly predictive of finding tumor-positive lymph nodes. Especially lymph nodes <2mm are still sometimes missed [10]. However, the 5-mm spatial resolution of PET is still an improvement compared with the detection limits of CT and MRI (i.e. > 10 mm) which may explain why PSMA PET was 27% more accurate than conventional imaging (92% vs 65%) [12].

Primary treatment

Patients with low-risk prostate cancer are eligible for active surveillance. This means that PSA levels are regularly checked, and tumor growth is monitored using MRI. Patients who have intermediate- to high-risk prostate cancer without distant metastases (M0) are eligible for treatment with curative intent. Three main treatment types can be distinguished with similar oncological outcomes: brachytherapy, external beam radiotherapy and radical prostatectomy [13]. When deciding on the treatment several factors such as medical history, age, comorbidities and the location and extent of the tumor play an important role.

Prostatectomy

In case of surgical treatment, a radical prostatectomy is performed, meaning the entire prostate gland, seminal vesicles and the fat surrounding the prostate are removed. Neurovascular bundles playing a crucial role in erectile function and urinary continence encircle the prostate [14]. As a result, urinary incontinence and erectile dysfunction are the most common complications. It is a delicate balance between ensuring a wide

margin for oncological safety and minimizing the margin for optimal functional outcomes. Prostatectomy can be conducted as an open, laparoscopic or robot-assisted procedure. The latter being most commonly practiced in the Netherlands nowadays since the introduction of the da Vinci Robot (Intuitive Inc) in 2000.

Extended pelvic lymph node dissection

In addition to the prostatectomy, a bilateral extended pelvic lymphode dissection (ePLND) can be performed (Figure 1C). An ePLND is done only for staging and is not considered a therapeutic procedure as it has not been proven to improve oncological outcomes [15]. Furthermore, surgical disruption of the lymphatic flow, crucial for tissue-fluid balance, eliminating waste and immunity [16 17], can lead to complications [18 19]. Lymphoceles (up to 15%) and lymphedema (up to 14%) being reported the most often [20 21]. Although, possibly underrated as lymphedema is one of the least studied complications of cancer treatment despite its considerable impact on health-related quality of life [22 23]. In spite of the high risk of comorbidities, ePLND is still considered the gold standard to determine nodal involvement [24]. Promising alternatives include the aforementioned PSMA PET/CT and prospective studies are on the way to research its place in the diagnostic work-up. For now, there are two ways to minimize unnecessary removal of lymph nodes. One is to make the dissection template more specific, for which more insight is needed into the drainage patterns from different organs within the pelvis. Second, careful selection of patients who will benefit from an ePLND is crucial. To assist in this decision-making process, several nomograms have been developed [25 26]. In this thesis, the Briganti 2012 nomogram is used [27].

Recurrent disease

Post-surgery PSA levels should be undetectable within approximately six weeks. However, although treated with curative intent, in 20-40% biochemical recurrence (BCR) may occur. BCR is defined as two consecutive PSA measurements of ≥ 0.2ng/ml. In case of BCR, in most countries, the standard treatment is to give radiotherapy on the prostatic fossa. In the Netherlands, the preferred approach is to perform imaging (staging) before starting treatment.

Staging

The next step after finding an increase in PSA levels is to determine where the recurrence is located. Before PSMA PET/CT this was also done by conventional imaging (CT or bone scintigraphy) or PET CT that was not specific for prostate cancer (^{18}F-Choline PET/CT). Since recent literature compared ^{18}F-Choline PET/CT) heads on with ^{68}Gallium-PSMA PET/CT and found a superior detection rate for the latter (especially in PSA <0.5ng/ml; 50% vs 12.5%) current EAU-guidelines recommend performing a PSMA PET/CT in patients with recurrent disease [28].

Salvage treatment

In case evidence of metastatic disease is found on imaging, either (delayed) systemic therapy may be proposed or metastases directed therapies. This is usually referred to as "salvage" treatment, with the underlying meaning that it is no longer intended to be curative but to delay the disease. However, some studies show that in example salvage radiation therapy of the prostatic fossa after local recurrence results in disease-free survival for a long period of time in about 50% [13]. Which patients will be within that 50% that benefits can be calculated using a novel nomogram [29]. Besides radiotherapy on the prostatic fossa, the pelvis can be included in the radiation field when nodal recurrence is suspected. For oligometastatic disease, metastasis-directed stereotactic radiotherapy can be considered. The preferred method for the best oncological outcomes is still unknown but a large, randomized study has been completed and first data did show no difference in toxicity comparing metastases directed therapy and elective nodal pelvic radiotherapy [30].

PSMA-targeted surgery

Surgical options for nodal recurrence include (bilateral) salvage lymph node dissection or PSMA-targeted lymph node dissection. Similar to PSMA PET imaging, a tracer that targets PSMA on the tumorous tissue is labeled with a radioisotope (mostly Technetium; ^{99m}Tc) which can then be identified during surgery with a gamma probe (Figure 1G). This technique has been developing since 2015 and has proven feasible in open as well as robot-assisted surgery [31 32]. Retrospective analysis of over 500 patients has shown that a biochemical response of <0.1 ng/ml was predictive of a longer therapy-free survival [33]. A randomized study is currently running to research the oncological benefit of the addition of PSMA-targeted salvage lymph node dissection to androgen deprivation therapy (ADT) compared to ADT only [34]. PSMA-targeted can be achieved using the two main image-guided surgery approaches: fluorescence or radioguidance, as described in detail below.

Image-guided surgery

Image-guided surgery can be defined as any surgical procedure where preoperative or intraoperative images are used in order to directly or indirectly guide the procedure. Because of its ability to visually discriminate targeted tissue from surrounding tissue the demand for new image-guided surgery has increased and new ways to provide real-time guidance have developed rapidly.

Radioguided surgery

Radioguided surgery involves the use of radioactive substances, called radiotracers, which are injected into the patient before surgery. These radiotracers accumulate in the target tissue, making it detectable by specific detectors. By rotating detectors around the patient, a single photon emission computed tomography (SPECT)/CT can be made.

This produces a 3D-image of the location of the radiotracer in regard of the anatomical structures similar to PET/CT. The SPECT/CT gives the surgeon the roadmap for the location. During surgery radiotracers can be detected by e.g. gamma probes for isotopes like ^{99m}Tc or beta-probes for ^{68}Gallium, guiding the surgeon to the exact location of the tissue that needs to be removed.

In prostate cancer, sentinel node procedure is the most common type of radioguided surgery. ^{99m}Tc- labeled colloids are used that become trapped in the first lymph nodes it encounters from the injection site (in this case the prostate). Nowadays, the hybrid tracer ^{99m}Tc- indocyanine green (ICG)-nanoscan has become standard of care that accommodates both radioguidance and fluorescence guidance. Radioguidance can also be used for removing lymph nodes during salvage surgery. Intraoperative detection of small (oligometastatic) prostate cancer lesions within the pelvis could be facilitated by the aforementioned radioactive labeled PSMA tracers. In brief, patients receive an intravenous injection of ^{99m}Tc-PSMA-I&S or ^{111}In-PSMA-I&T roughly 16-24 hours prior to salvage surgery. Again, SPECT/CT imaging is performed to cross-validate findings of preoperative PSMA PET/CT and to serve as quality control for tracer injection and distribution.

Fluorescence guided surgery

Fluorescence is the spontaneous emission of light radiation from a substance that is electronically excited by a light source. Meaning that light needs to go in first (excitation) and a light-sensitive camera is required to detect the emitted light (emission). The excitation and emission aspects of a specific dye are dictated by the size and shape of conjugated system in their molecular structure, meaning each specific molecule has a unique excitation maximum (λex max). When a fluorescent dye is excited in its particular absorption spectrum, the molecule can convert to an unstable excited energy state. The energy that is lost by the decay back to the stable state, converts it into light of a longer wavelength that provides the emitted fluorescent light. The strength (also called brightness) of a fluorescence emission is a combination of a couple of factors including concentration of the dye, intensity of the excitation light source, efficiency by which the excitation light is absorbed by the molecule (called extinction coefficient) and the conversion of the absorbed energy into a fluorescent emission (called quantum yield) [35].

The emission spectrum of tracers intended for medical use encompasses UV-light (400 nm), visible light (400–650 nm), far-red light (650–780 nm), and near-infrared range of 780–2000 nm [36]. A frequently used (non-conjugated) dye in surgery is fluorescein (λex 480nm, λem 520nm). When administered intravenously, it can be used for e.g. angiography [37]. In the far-red and near-infrared range, cyanine dyes with similar structures are common. E.g. Cy5 (λem 651 nm) and ICG (λem 820 nm) [38-40]. ICG, although not having a specific moiety for chemical conjugation, has the tendency to

bind to proteins such as human serum albumin when injected intravenously [41]. As a result, ICG does not extravasate and remains intravascular for up to 20–30 min, after which it is hepatically cleared via bile [42 43]. Following local injections, ICG, bound to serum proteins, provides an effective lymphangiographic agent [44].

As stated before, in prostate cancer surgery, ICG bound to nanoparticles like nanocolloid/ nanoscan- labeled with the radioisotope ^{99m}Tc is used for sentinel node procedures. Fluorescence guided surgery has also been developing rapidly towards a tumor-targeted approach. Multiple PSMA-targeted fluorescent tracers have been studied in recent first-in-human trials (OTL78, IS-002, IR800-IAB2M) [45-47]. These studies focus mainly on margin assessment of the primary tumor instead of nodal removal.

Aim and outline of the thesis

This thesis focuses on gaining more insights in anatomical structures and surgical accuracy in primary and nodal surgery. **Part I** addresses several aspects of PSMA-targeted surgery. In **Chapter 2**, we delve deeper into the known tracers and applications of PSMA-targeted surgery. **Chapter 3** evaluates the current vision of an international panel of experts on PSMA-targeted surgery by means of a Delphi consensus. In **Chapter 4**, the correlation between preoperative intraoperative values of PSMA targeting is researched. **Chapter 5** explores the fluorescent behavior of a novel hybrid PSMA-targeted tracer when *ex vivo* applied to fresh prostatic tissue.

Part II discusses different approaches and challenges of image-guided surgery. **Chapter 6** and **7** prospectively examine the lymphatic drainage patterns within the ePLND template to identify an approach with fewer lymphatic-related complications. **Chapter 8** explores the impact of renally cleared tracers on the surgical field and potential implications for surgical accuracy. **Chapter 9 and 10** examine an alternative approach to target visualization in radioguided surgery by acquiring an intraoperative SPECT and overlaying this with the anatomical image as seen by the operating surgeon.

Chapter 11 discusses the key findings and future perspectives.

References

1. Drake RL, Vogl W, Mitchell AWM, Gray H. Gray's Anatomy for students. 3rd ed: Churchill Livingstone/Elsevier, Philadelphia, PA, 2015, 2015.
2. Cancer International Agency for Cancer Research. Cancer today. 2022. ttps://gco.iarc.fr/today/en/dataviz
3. IKNL. Prostaatkanker. Last updated: 2-4-2024. https://iknl.nl/kankersoorten/prostaatkanker/reg istratie.
4. Barsouk A, Padala SA, Vakiti A, et al. Epidemiology, Staging and Management of Prostate Cancer. Med Sci (Basel) 2020;8(3).
5. Thompson IM, Pauler DK, Goodman PJ, et al. Prevalence of prostate cancer among men with a prostate-specific antigen level < or =4.0 ng per milliliter. N Engl J Med 2004;350(22):2239-46.
6. Hugosson J, Roobol MJ, Mansson M, et al. A 16-yr Follow-up of the European Randomized study of Screening for Prostate Cancer. Eur Urol 2019;76(1):43-51.
7. Mottet N, van den Bergh RCN, Briers E, et al. EAU- EANM-ESTRO-ESUR-SIOG Guidelines on Prostate Cancer-2020 Update. Part 1: Screening, Diagnosis, and Local Treatment with Curative Intent. Eur Urol 2021;79(2):243-62.
8. van Leenders G, van der Kwast TH, Grignon DJ, et al. The 2019 International Society of Urological Pathology (ISUP) Consensus Conference on Grading of Prostatic Carcinoma. Am J Surg Pathol 2020;44(8):e87-e99.
9. O'Keefe DS, Bacich DJ, Huang SS, Heston WDW. A Perspective on the Evolving Story of PSMA Biology, PSMA-Based Imaging, and Endoradiotherapeutic Strategies. J Nucl Med 2018;59(7):1007-13.
10. Jansen BHE, Bodar YJL, Zwezerijnen GJC, et al. Pelvic lymph-node staging with (18) F-DCFPyL PET/CT prior to extended pelvic lymph-node dissection in primary prostate cancer - the SALT trial. Eur J Nucl Med Mol Imaging 2021;48(2):509- 20.
11. van Kalmthout LWM, van Melick HHE, Lavalaye J, et al. Prospective Validation of Gallium-68 Prostate Specific Membrane Antigen-Positron Emission Tomography/Computerized Tomography for Primary Staging of Prostate Cancer. J Urol 2020;203(3):537-45.
12. Hofman MS, Lawrentschuk N, Francis RJ, et al. Prostate-specific membrane antigen PET-CT in patients with high-risk prostate cancer before curative-intent surgery or radiotherapy (proPSMA): abprospective, randomised, multicentre study. Lancet 2020;395(10231):1208- 16.
13. Hamdy FC, Donovan JL, Lane JA, et al. Active monitoring, radical prostatectomy and radical radiotherapy in PSA-detected clinically localised prostate cancer: the ProtecT three-arm RCT. Health Technol Assess 2020;24(37):1-176.
14. Maruo M, Goto Y, Miyazaki K, et al. Novel nerve- sparing robot-assisted radical prostatectomy with endopelvic fascia preservation and long-term outcomes for a single surgeon. Sci Rep 2024;14(1):926.
15. Fossati N, Willemse PM, Van den Broeck T, et al. The Benefits and Harms of Different Extents of Lymph Node Dissection During Radical Prostatectomy for Prostate Cancer: A Systematic Review. Eur Urol 2017;72(1):84-109.
16. Padera TP, Meijer EF, Munn LL. The Lymphatic System in Disease Processes and Cancer Progression. Annu Rev Biomed Eng 2016;18:125- 58.
17. Randolph GJ, Ivanov S, Zinselmeyer BH, Scallan JP. The Lymphatic System: Integral Roles in Immunity. Annu Rev Immunol 2017;35:31-52.
18. Briganti A, Chun FK, Salonia A, et al. Complications and other surgical outcomes associated with extended pelvic lymphadenectomy in men with localized prostate cancer. Eur Urol 2006;50(5):1006-13.
19. Keegan KA, Cookson MS. Complications of pelvic lymph node dissection

for prostate cancer. Curr Urol Rep 2011;12(3):203-8.

20. Orvieto MA, Coelho RF, Chauhan S, Palmer KJ, Rocco B, Patel VR. Incidence of lymphoceles after robot-assisted pelvic lymph node dissection. BJU Int 2011;108(7):1185-90.
21. Clinckaert A, Callens K, Cooreman A, et al. The Prevalence of Lower Limb and Genital Lymphedema after Prostate Cancer Treatment: A Systematic Review. Cancers (Basel) 2022;14(22).
22. Thorsteinsdottir T, Stranne J, Carlsson S, et al. LAPPRO: a prospective multicentre comparative study of robot-assisted laparoscopic and retropubic radical prostatectomy for prostate cancer. Scand J Urol Nephrol 2011;45(2):102-12.
23. Bianchi LMG, Irmici G, Ce M, et al. Diagnosis and Treatment of Post-Prostatectomy Lymphedema: What's New? Curr Oncol 2023;30(5):4512-26.
24. Dong B, Zhan H, Luan T, Wang J. The role and controversy of pelvic lymph node dissection in prostate cancer treatment: a focused review. World J Surg Oncol 2024;22(1):68.
25. Di Pierro GB, Salciccia S, Frisenda M, et al. Comparison of Four Validated Nomograms (Memorial Sloan Kettering Cancer Center, Briganti 2012, 2017, and 2019) Predicting Lymph Node Invasion in Patients with High-Risk Prostate Cancer Candidates for Radical Prostatectomy and Extended Pelvic Lymph Node Dissection: Clinical Experience and Review of the Literature. Cancers (Basel) 2023;15(6).
26. Vis AN, Meijer D, Roberts MJ, et al. Development and External Validation of a Novel Nomogram to Predict the Probability of Pelvic Lymph-node Metastases in Prostate Cancer Patients Using Magnetic Resonance Imaging and Molecular Imaging with Prostate-specific Membrane Antigen Positron Emission Tomography. Eur Urol Oncol 2023;6(6):553-63.
27. Briganti A, Larcher A, Abdollah F, et al. Updated nomogram predicting lymph node invasion in patients with prostate cancer undergoing extended pelvic lymph node dissection: the essential importance of percentage of positive cores. Eur Urol 2012;61(3):480-7.
28. Morigi JJ, Stricker PD, van Leeuwen PJ, et al. Prospective Comparison of 18F-Fluoromethylcholine Versus 68Ga-PSMA PET/CT in Prostate Cancer Patients Who Have Rising PSA After Curative Treatment and Are Being Considered for Targeted Therapy. J Nucl Med 2015;56(8):1185-90.
29. Meijer D, van Leeuwen PJ, Eppinga WSC, et al. Development and Internal Validation of a Novel Nomogram Predicting the Outcome of Salvage Radiation Therapy for Biochemical Recurrence after Radical Prostatectomy in Patients without Metastases on Restaging Prostate-specific Membrane Antigen Positron Emission Tomography/Computed Tomography. Eur Urol Open Sci 2024;61:37-43.
30. Ost P, Siva S, Brabrand S, et al. PEACE V-Salvage Treatment of OligoRecurrent nodal prostate cancer Metastases (STORM): Acute Toxicity of a Randomized Phase 2 Trial. Eur Urol Oncol 2024;7(3):462-68.
31. de Barros HA, van Oosterom MN, Donswijk ML, et al. Robot-assisted Prostate-specific Membrane Antigen-radioguided Salvage Surgery in Recurrent Prostate Cancer Using a DROP-IN Gamma Probe: The First Prospective Feasibility Study. Eur Urol 2022;82(1):97-105.
32. Maurer T, Weirich G, Schottelius M, et al. Prostate- specific membrane antigen-radioguided surgery for metastatic lymph nodes in prostate cancer. Eur Urol 2015;68(3):530-4.
33. Knipper S, Lischewski F, Koehler D, et al. Biochemical Response of <0.1 ng/ml Predicts Therapy-free Survival of Prostate Cancer Patients following Prostate-specific Membrane Antigen- targeted Salvage Surgery. Eur Urol Oncol 2024.
34. Zuur LG, De Barros HA, Van Oosterom MN, et al. 99mTcPSMA-radioguided surgery in oligorecurrent prostate cancer:

the randomised TRACE-II trial. BJU International 2024.

35. Tian Y, Halle J, Wojdyr M, Sahoo D, Scheblykin IG. Quantitative measurement of fluorescence brightness of single molecules. Methods Appl Fluoresc 2014;2(3):035003.
36. Sheppard N, Willis HA, Rigg JC. Names, symbols, definitions and units of quantities in optical spectroscopy (Recommendations 1984). Pure and Applied Chemistry 1985;57(1):105-20.
37. Baddam DO, Ragi SD, Tsang SH, Ngo WK. Ophthalmic Fluorescein Angiography. Methods Mol Biol 2023;2560:153-60.
38. Dell'Oglio P, de Vries HM, Mazzone E, et al. Hybrid Indocyanine Green-(99m)Tc-nanocolloid for Single-photon Emission Computed Tomography and Combined Radio- and Fluorescence-guided Sentinel Node Biopsy in Penile Cancer: Results of 740 Inguinal Basins Assessed at a Single Institution. Eur Urol 2020;78(6):865-72.
39. Vries HM, Bekers E, van Oosterom MN, et al. c- MET Receptor-Targeted Fluorescence on the Road to Image-Guided Surgery in Penile Squamous Cell Carcinoma Patients. J Nucl Med 2022;63(1):51-56.
40. Leung K. IRDye 800CW-Human serum albumin. Secondary IRDye 800CW-Human serum albumin. 17-5-2012 2007. https://www.ncbi.nlm.nih.gov/books/NBK23077/ table/HSA800.T.nc_chemical_nameirdye_800cwh uma/.
41. Bunschoten A, Buckle T, Kuil J, et al. Targeted non- covalent self-assembled nanoparticles based on human serum albumin. Biomaterials 2012;33(3):867-75.
42. Cacciamani GE, Shakir A, Tafuri A, et al. Best practices in near-infrared fluorescence imaging with indocyanine green (NIRF/ICG)-guided robotic urologic surgery: a systematic review-based expert consensus. World J Urol 2020;38(4):883-96.
43. Dip F, LoMenzo E, Sarotto L, et al. Randomized Trial of Near-infrared Incisionless Fluorescent Cholangiography. Ann Surg 2019;270(6):992-99.
44. Manny TB, Patel M, Hemal AK. Fluorescence- enhanced robotic radical prostatectomy using real-time lymphangiography and tissue marking with percutaneous injection of unconjugated indocyanine green: the initial clinical experience in 50 patients. Eur Urol 2014;65(6):1162-8.
45. Stibbe JA, de Barros HA, Linders DGJ, et al. First-in- patient study of OTL78 for intraoperative fluorescence imaging of prostate-specific membrane antigen-positive prostate cancer: a single-arm, phase 2a, feasibility trial. Lancet Oncol 2023;24(5):457-67.
46. Nguyen HG, van den Berg NS, Antaris AL, et al. First-in-human Evaluation of a Prostate-specific Membrane Antigen-targeted Near-infrared Fluorescent Small Molecule for Fluorescence-based Identification of Prostate Cancer in Patients with High-risk Prostate Cancer Undergoing Robotic-assisted Prostatectomy. Eur Urol Oncol 2024;7(1):63-72.
47. Hamdy FC, Lamb AD, Tullis IDC, et al. First-in-man study of the PSMA Minibody IR800-IAB2M for molecularly targeted intraoperative fluorescence guidance during radical prostatectomy. Eur J Nucl Med Mol Imaging 2024.

Part I

PSMA-Targeted Image-Guided Surgery

Berrens AC, Knipper S, Marra G, van Leeuwen PJ, van der Mierden S, Donswijk ML, Maurer T, van Leeuwen FWB, van der Poel HG

Eur Urol Open Sci. 2023 Jun 16;54:43-55

Chapter 2

State of the Art in Prostate-specific Membrane Antigen-targeted Surgery — A Systematic Review

Abstract

Context. Identifying malignant tissue and leaving adjacent structures undisturbed is an ongoing challenge in prostate cancer (PCa) surgery. Image and radio-guided surgical technologies targeting the prostate-specific membrane antigen (PSMA) receptor may facilitate identification and removal of diseased tissue.

Objective. A systematic review of the clinical studies on PSMA-targeted surgery.

Evidence acquisition. MEDLINE (OvidSP), Embase.com and Cochrane Library databases were searched. Identified reports were critically appraised according to the Idea, Development, Exploration, Assessment, Long-term framework criteria. Risk of bias (RoB) was assessed as per the Risk Of Bias In Non-randomized Studies – of Interventions tool. Strengths and limitations of techniques and corresponding oncological outcomes were extracted as areas of interest. Data was reported according to the Preferred Reporting Items for Systematic Reviews and Meta-Analyses guidelines.

Evidence synthesis. 29 reports were selected, including eight prospective studies, 12 retrospective analyses, and nine case reports. All with high or unclear RoB. In 72.4% of studies PSMA targeting was achieved via radioguided surgery (RGS), predominantly using ^{99m}Tc-PSMA-I&S (66.7%). Hybrid approaches that complement RGS with optical guidance are emerging. The majority of studies retrieved were pilot studies with short follow-up. In 13 reports salvage lymph node surgery was discussed (44.8%). In 12 more recent reports (41.4%), PSMA targeting was studied in primary PCa surgery (50.0% lymph nodes, 50.0% surgical margins) and four studied both primary and salvage surgery (13.8%). Overall, specificity was higher than sensitivity (median 98.9% and 84.8%, respectively). Oncological outcomes were only discussed in reports on the use of ^{99m}Tc-PSMA-I&S in salvage surgery (median follow-up of 17.2 month). PSA decline of >90% ranged from 22.0 to 100.0% and biochemical recurrence from 50.0 to 61.8% of patients.

Conclusions. In PSMA-targeted surgery most studies address salvage PSMA-RGS using ^{99m}Tc-PSMA I&S. Available evidence suggests that the specificity of intraoperative PSMA targeting is higher than the sensitivity. The studies that included follow-up did not yet objectify a clear oncological benefit. Lacking solid outcome data, PSMA-targeted surgery remains investigational.

Introduction

During both primary and salvage prostate cancer (PCa) surgery, identifying the target PCa tissue amongst the surrounding healthy tissue provides a key challenge [1]. Patients are significantly more likely to have biochemical recurrence (BCR) and undergo adjuvant or early salvage cancer treatment when tumor-containing tissue remains in situ following PCa surgery. In general, surgeons rely on experience, anatomical knowledge, and the ability to correctly interpret preoperative imaging to resect PCa tissue [2]. The use of intraoperative imaging and radioguidance helps to better distinguish between cancerous and healthy tissue during surgery [3 4].

The prostate-specific membrane antigen (PSMA) is a transmembrane glycoprotein that is highly overexpressed in prostate cancer cells and is used as the target for PET imaging [5]. Due to its high specificity it is more accurate for nodal staging than MRI, abdominal contrast-enhanced CT, or choline PET/CT. Making its use increasingly common in staging of primary and recurrent PCa [5 6]. However, the technique is less reliable for identifying small lymph node metastases (micro metastases <3mm) and the PSMA-PET tracers are typically excreted by the kidneys, making it difficult to locate the primary cancer site [5 7].

PSMA targeting has been proposed to extend beyond cancer diagnosis and into surgical guidance [7]. Multiple groups have explored a variety of tracer designs to realize this application, leading to the development of e.g. ^{99m}Tc-PSMA-targeted radiotracers [8 9]. Tracers that support non- invasive Single Photon Emission Computed Tomography (SPECT)/CT, providing a surgical roadmap, as well as allow for intraoperative image guidance (Figure 1) [5].

As of today, different PSMA-targeting surgical approaches have been used in PCa patients. In order to provide a comprehensive overview of techniques and initial outcome data, a systematic review of the available clinical literature was conducted.

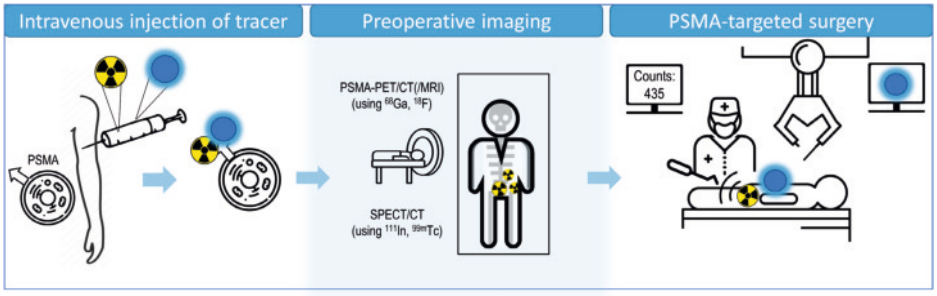

Figure 1. Schematic overview of clinical implementation of prostate specific membrane antigen (PSMA)-guided surgery. Preoperative imaging can be either a PSMA-Positron Emission Tomography (PET)/CT or Single Photon Emission Computed Tomography (SPECT)/CT.

Evidence acquisition

Protocol registration and search strategy

The protocol was registered on PROSPERO (CRD42022304195) in January 2022. A systematic web search was conducted using MEDLINE (OvidSP), Embase.com and Cochrane Library (Figure 2).

The search was last updated in August 2022. The search was executed with the help of an expert information specialist (S.vdM.) and checked by a second information specialist. Search terms can be found in the supplementary data (1). Conference abstracts from Embase.com were removed based on their indexed publication type. Citation chasing was done by one person. No other methods to acquire additional reports and no other limits were used. The results were deduplicated in EndNote 20 using Bramer's method [10]. After removal of duplicates, two authors (A.C.B and A.S.K.) screened all abstracts and reviewed the full-text reports for eligibility using Rayyan software [11]. Discrepancies were resolved through consensus or by consultation of a third author (G.M.). Data collection focused on demographics, surgical and oncological outcomes and was collected by two authors in a pre- specified form in Excel. The review was reported according to the Preferred Reporting Items for Systematic Reviews and Meta-analyses (PRISMA) guidelines [12].

Inclusion and exclusion criteria

As the first reports on the subject of PSMA targeting in surgery became available in 2015, the included studies in this review date from 2015-2022. Our review incorporated research that assessed the effectiveness of intraoperative PSMA-targeted surgical guidance in directing the surgeon towards the targeted tissue *in vivo* or that could confirm the target through *ex vivo* analysis at the back table. Surgical procedures only assisted by a preoperative PSMA PET for decision making without intraoperative or back table guidance where excluded. Only studies that were registered with a study protocol were considered prospective. Given the dynamic growth of PSMA-targeted surgery activities, case reports were included as well. Only original English-language literature full text reports were considered. Pure preclinical work was excluded.

Assessment of risk of bias

The studies were defined according to the IDEAL (Idea, Development, Exploration, Assessment, Long- term) framework (Table 1) [13]. Risk of bias was assessed through the risk of bias of tool for non- randomized studies of interventions (ROBINS-I) (Figure 3) [14]. Because the bias of case reports is not contributory, they were excluded from the assessment of risk of bias.

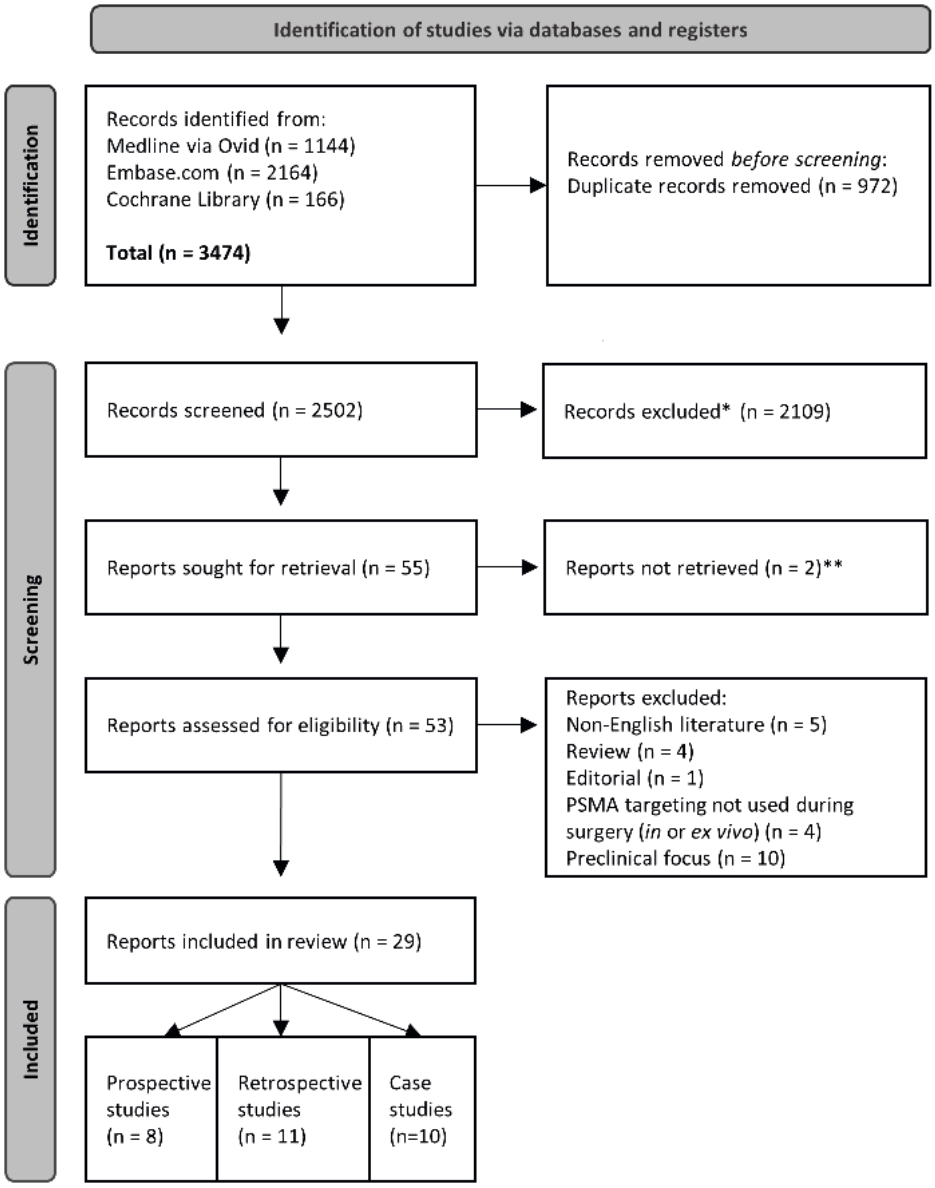

Figure 2. PRISMA flowchart for literature search and selection. *non-automated. Records excluded by the author using Rayyan. ** only abstract available.

Table 1. IDEAL Framework and surgical outcomes

Author, year	IDEAL Framework stage	Number of patients	PSMA agent, administration, type of guidance	Type of surgery	Modality used	*In* or *ex vivo*	Total targets identified				Sensitivity of surgical intervention	Specificity of surgical intervention	Metastases size in mm at histopathology
Focus on lymph nodes							PSMA PET/CT (/MRI)	SPECT/CT	Intra operatively/ ex vivo	Tumor + at histopathology/ total removed	% (95% CI)	% (95% CI)	Median (IQR)
Maurer, 2015	1	5	111In-PSMA-I&T, IV, R	Open RP + ePLND sLND	γ-probe declipse SPECT	*In* and *ex vivo*	13	-	15	15/NR	NR	NR	2.0-12.0^^
Rauscher, 2017	2a	31	111In-PSMA-I&T, IV, R	Open sLND	γ-probe	*In* and *ex vivo*	NR	-	54 FP = 6 FN = 4	52/145	92.3 (83.2–96.7)	93.5 (81.7–97.9)	NR
Knipper, 2018	2a	42 (13)	99mTc-PSMA-I&S, IV, R	Open sLND	γ-probe	*In* and *ex vivo*	2.31' [1–6]^^	NR	NR	5' (1–15)^^/ range 2-53	NR	NR	NR
Maurer, 2018	2a	31	99mTc-PSMA-I&S, IV, R	Open sLND	γ-probe	*In* and *ex vivo*	44	25	46 FP = 0 FN = 12	58/ 132	83.6 (70.9–91.5)	100 (-)	12.0 (3.0-25.0)^^
Mix, 2018	2a	6	111In-PSMA-617, IV, R	Open RP + ePLND sLND	γ-probe HGD	*In* and *ex vivo*	NR	NR	35 FP = 2 FN = 3	38/ 318 single samples	92.1 (-)	98.8 (-)	NR
Horn, 2019	2b	121	111In-PSMA-I&T 99mTc-PSMA-I&S, IV, R	Open sLND	γ-probe	*In* and *ex vivo*	175	NR	180	214/ median 11	NR	NR	3.0 (of regions)
Collamati, 2020	1	7	68Ga-PSMA-11, IV, R	RA RP + ePLND	β-probe	*Ex vivo*	LNs: 4	-	LNs: 4 FP = 1	LNs: 3 / NR	NR	NR	smallest identified node 7mm
Jilg, 2020	2	23 (21)	111In-PSMA-617 IV, R	Open RP + ePLND sLND	γ-probe HGD	*In* and *ex vivo*	87	NR	γ-probe: 72 HGD: 79	104 /864	γ-probe: 62.1 (-) HGD: 71.2 (-)	γ-probe: 96.3 (-) HGD: 96.9 (-)	NR
Mix, 2021	1	6	99mTc-PSMA-I&S, IV, R	Open RP sLND	γ-probe	*In* and *ex vivo*	NR	NR	118	154/ 516	76.6 (0.69-0.83)	94.0 (0.91-0.97)	NR
de Barros, 2022	2a	20	99mTc-PSMA-I&S, IV, R	RA sLND	γ-probe	*In* and *ex vivo*	21	13	19 FN=3	21/21	86.0 (-)	100 (-)	8.4 (3.9–15.0)
Gondoputro, 2022	2a	12	99mTc-PSMA-I&S, IV, R	RA RP + ePLND	γ-probe CT-guided hookwire	*In* and *ex vivo*	11	4	18 FP=2 FN=5	22/74	*in vivo* 76.0 (53.0-92.0) *ex vivo* 76.0 (53.0-92.0)	*in vivo* 69.0 (55.0-81.0) *ex vivo* 96.0 (87.0-99.0)	9.0 (6.3-11.2) smallest <1mm

Focus on lymph nodes							**PSMA PET/CT (/MRI)**	**SPECT/ CT**	**Intra operatively/ ex vivo**	**Tumor + at histo-pathology/ total removed**	**% (95% CI)**	**% (95% CI)**	**Median (IQR)**
Knipper, 2022	2b	364	111In-PSMA-I&T 99mTc-PSMA-I&S, IV, R	Open sLND	γ-probe	*In* and *ex vivo*	364	NR	364 FP = 21	343/NR	NR	NR	NR
Yilmaz, 2022	1	15	99mTc-PSMA-I&S, IV, R	RA RP + ePLND	γ-probe	*In* and *ex vivo*	NR	NR	18	18/297	100 (-)	100 (-)	NR
Gandaglia, 2022	1	12	99mTc-PSMA-I&S, IV, R	RA RP + ePLND	γ-probe	*In* and *ex vivo*	2	2	5 FP=1 FN =4	4/96 specimens	50.0	99.0	NR
Koehler, 2022	1	9	99mTc-MIP-1404, IV, R	Open sLND	γ-probe	*In* and *ex vivo*	19	12	21	24/154	87.5	100.0	6 (2-4.5)
Case reports													
Schottelius, 2015	1	1	111In-PSMA-I&T, IV, R	Open sLND	γ-probe	*In* and *ex vivo*	NR	NR	NR	NR/NR	NR	NR	NR
Maurer, 2016	1	1	111In-PSMA-I&T, IV, R	Open sLND	γ-probe	*In* and *ex vivo*	1	-	1	1/NR	NR	NR	NR
Robu, 2017	1	2 (1)	99mTc-PSMA-I&S, IV, R	Open RP + ePLND	γ-probe	*In* and *ex vivo*	1	-	1	1/NR	NR	NR	NR
Kratzik, 2018	1	1	99mTc-PSMA-I&S, IV, R	Open sLND left-sided	γ-probe	*In* and *ex vivo*	1	1	1	1/NR	NR	NR	NR
Darr, 2020	1	1	68Ga-PSMA-11, IV, O	Open sLND	CLI	*Ex vivo*	1	-	1	2/17	NR	NR	-
van Leeuwen, 2020	1	1	99mTc-PSMA-I&S, IV, R	RA sLND	γ-probe	*In* and *ex vivo*	1	1	1	1/NR	NR	NR	NR
Aras, 2021	1	10 (2)	18F-BF3-Cy3-ACUPA IV, O	Open RP + ePLND	Solis 525C LED illuminator with CMOS camera	*Ex vivo*	NR	NR	4	2/NR	NR	NR	NR
Erfani, 2022	1	1	99mTc-PSMA IV, R	Open sLND	γ-probe	*In* and *ex vivo*	2	2	2	2/8	NR	NR	NR

							PSM intraoperatively/ ex vivo		PSM at histopathology		% (95% CI)	% (95% CI)	
Focus on prostate/local recurrence													
Knipper, 2020	2b	40	111In-PSMA-I&T 99mTc-PSMA-I&S, IV, R	Open sLND	γ-probe	*In* and *ex vivo*	NR	NR	NR	NR	NR	NR	NR
Darr, 2020	1	10	68Ga-PSMA-11, IV, O	Open RP	CLI	*Ex vivo*	2		3		NR	NR	NA
olde Heuvel, 2020	1	5	68Ga-PSMA-11, IV, O	RA RP	CLI	*Ex vivo*	5 FP = 2 FN = 0		3		NR	NR	NA
olde Heuvel, 2022	1	15	68Ga-PSMA-11, IV, O	RA RP	CLI	*Ex vivo*	6 hotspots FP = NR FN = 4 hotspots		10 hotspots		NR	NR	NA
Darr, 2021	1	7	68Ga-PSMA-11, IV, O	Open RP	CLI + 550nm-OF	*Ex vivo*	3		3		NR	NR	NA
Case reports													
Eder, 2021	1	1	68Ga-PSMA-914, IV, O	RA RP	NR	*In* and *ex vivo*	1	-	1	NR	NR	NR	NA

‘ = Mean (± SD), ~=maximum, ^^ =Range, CLI=Cerenkov Luminescence Imaging, CMOS= Complementary Metal Oxide Semiconductor, ePLND=extended pelvic lymph node dissection, Ga=Gallium, HGD= Highpurity Germanium Detector, IDEAL=Idea, Development, Exploration, Assessment, Long-term I&S=Imaging and surgery, I&T=Imaging and therapy, In=Indium, IQR=Interquartile Range, IV=Intravenous, NA = Not applicable, NR= Not reported, O= Optical guidance, OF= optical short-pass filter, R= Radioguidance, RA = Robot Assisted, RP= Radical Prostatectomy, sLND =salvage lymph node dissection

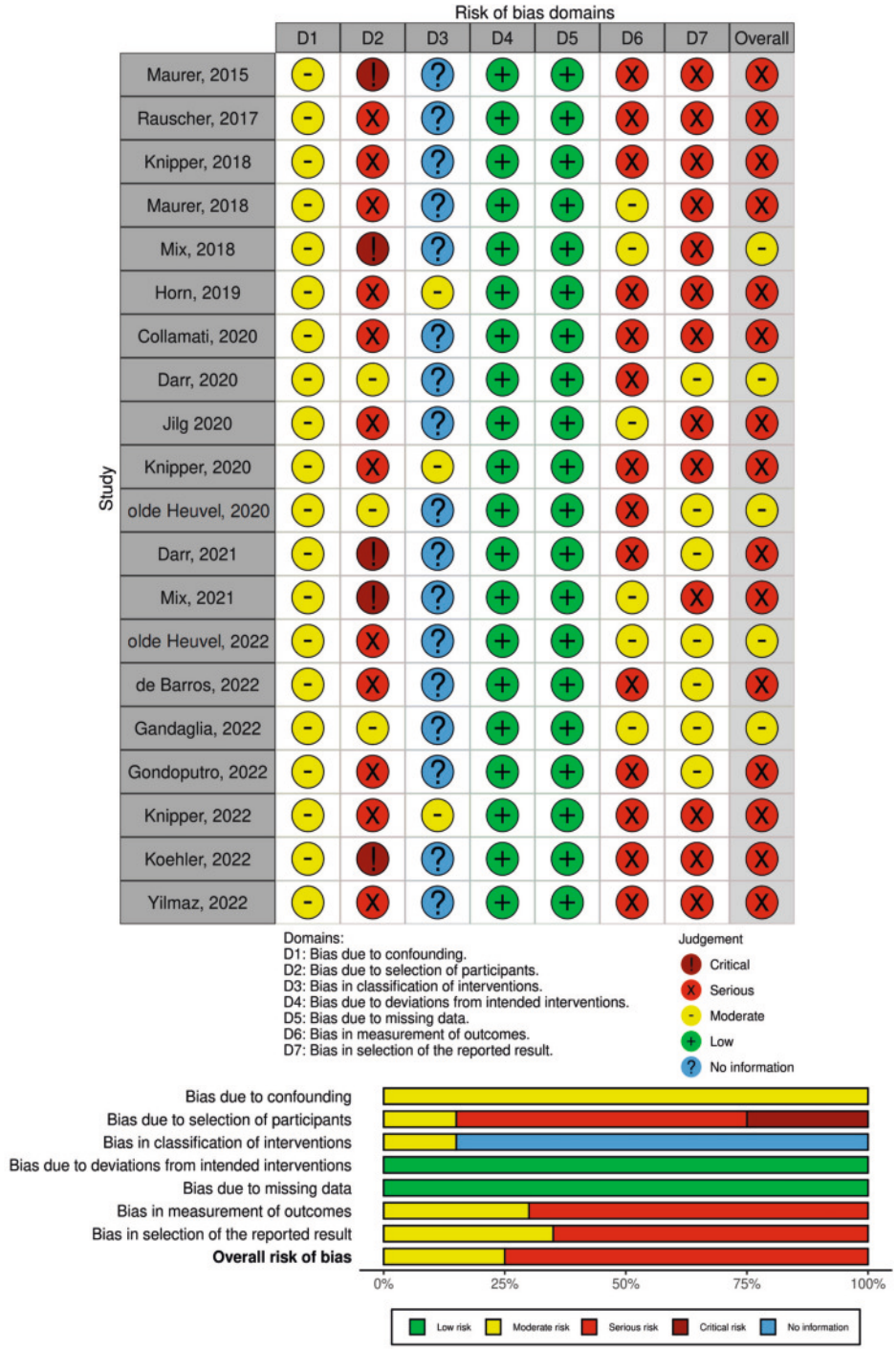

Figure 3. Bias table according to Risk Of Bias In Non-randomized Studies - of Interventions (ROBINS-I). Case reports were excluded from this bias analysis

Data analysis and objectives

Due to the high heterogeneity found among the included studies in terms of different procedures, different reporting and different definition of outcomes a meta-analysis was not possible. A comprehensive narrative synthesis of included studies was performed. Descriptive statistics were used to summarize baseline characteristics data.

Evidence synthesis

Study quality and baseline features

We included 29 reports on PSMA-targeted surgery of which eight prospective studies [15-22] 12 retrospective analyses [4 23-33] and nine case reports [34-42] (Figure 2). Generally, a small number of patients were included: in 8/29 (28%) of reports ≥ 20 patients were included of which two (retrospective) studies included > 100 patients (7%). The remaining 72% of studies can be considered small-scale pilots or first-in-man reports (Figure 4). In the primary setting (~41% of reports), patients included were intermediate or high-risk with or without nodal involvement. In the salvage setting (~45% of reports), patients included had recurrent disease on PSMA PET/CT (in local recurrence a maximum of one lesion, in nodal recurrence a maximum of five) and were eligible for surgery. Standard Uptake Values (SUV)-max of the PSMA PET/CT scans were not taken into account. A detailed description of patients' demographics can be found in supplementary data 2.

Seventeen studies (59%; including ten case reports) were considered stage 1 according to the IDEAL framework: proof of concept or first-in-man. These studies describe clinical use of novel tracers or an adapted version of a previously studied tracer. Nine were considered exploring stage (stage 2a; 31%) and three in developmental stage (stage 2b; 10%). None of the studies could be considered stage 3 or higher (assessment and long-term) (Table 1) [13].

Preoperative features

Surgical resections were always guided by preoperative imaging roadmaps acquired more than 24 hours prior to surgery (PSMA PET/CT (97%), and (additional) PET/MRI (7%) [28 40]). In general the guidance provided by the PSMA PET/CT was considered leading even in cases were a SPECT/CT was done (see below). Fifteen (52%) of the studies reported on the outcomes of the PSMA PET/CT on lesion level. Out of 473 tumor positive lesions at histopathology, PSMA PET/CT identified 382 (81%). The smallest lesion identified on PSMA PET was 3 mm [4].

For the most commonly used tracers (^{99m}Tc-PSMA-I&S and ^{111}In-PSMA-I&T), the mean injection time to surgery was around 24 hours (range 16-28 hours), with a median injected activity varying between 541-638 MBq and 140-150 MBq, respectively. Studies

using ^{68}Ga-PSMA-11 injected between 76 and 127 MBq [16 21]. A detailed description of timing and injected activity of all tracers can be found in the supplementary data (3).

When ^{111}In- or ^{99m}Tc-labeled PSMA tracers were used, an additional preoperative SPECT/CT was performed within 24 hours before surgery (in 43% of the procedures with ^{111}In, in 93% of ^{99m}Tc). Of the studies that included a SPECT/CT only seven reported their findings. Indicating 60 out of 133 histopathological confirmed tumor positive lesions (45%) could be identified by SPECT/CT. The only studies that described all lesions being identified on SPECT/CT were case reports with a maximum of two lesions on the PSMA PET/CT [37 38 42].

Radioguidance

Clinically, PSMA guidance is employed in two main approaches: radio- and optical-guidance. The former, being the most frequently described (22/29 reports (76%); (ranging from n=1 to 364 patients) and makes use of gamma/beta-emitting radioisotopes. Clinical use of gamma-emitting radioisotopes started with the use of ^{111}In-PSMA-I&T, followed not shortly by studies using ^{99m}Tc-PSMA-I&S and ^{111}In- PSMA-617 [29 32 41]. In all these reports the guidance was facilitated by real-time tracing using a gamma probe. The design of the gamma probe varied depending on the surgical approach. A hand- held gamma probe for open surgery was used in 17/29 studies (59%; ranging from n= 1 to 364 patients). One study reported the combined use with a probe-based freehandSPECT scan [30]. The development of a drop-in gamma probe design enabled the performance of the first robotic PSMA- targeted surgery a technique that was used in 5/29 studies (17%; ranging from n= 1 to 20 patients). In one study a robotic drop-in beta probe has been employed *ex vivo* to confirm presence of ^{68}Ga-PSMA- 11 in the prostate and nodal tissue [15].

Since 2018 all groups originally reporting use of ^{111}In-PSMA tracers (gamma emissions 171 kilo electron Volt (keV) & 245 keV; t1/2 = 2.8 days) converted to the use of ^{99m}Tc-PSMA-I&S; the 141 keV gamma emission and 6h half-life of ^{99m}Tc is more compatible with the everyday clinical workflow and suffers less from background signals [40] (details on tracer properties can be found in supplementary data 4 and 5). Figure 4 shows that in 2020 ^{111}In-PSMA-617 ceases to be reported on and that new ^{99m}Tc- based tracers like ^{99m}Tc-MIP-1404 are still being introduced.

Optical guidance

A different approach of PSMA guidance relies on converting the beta-emission of tracers such as ^{68}Ga- PSMA-11 into a secondary optical signal (Cerenkov Luminescence; $\lambda_{em\ max}$ <450 nm) that has a very limited degree of tissue penetration (<3mm) but can be recorded in a back-table (*ex vivo*) dark-room environment via highly sensitive optical detectors [43]. A strategy that was used in 5/29 (17%) of the studies reported (n=37 patients).

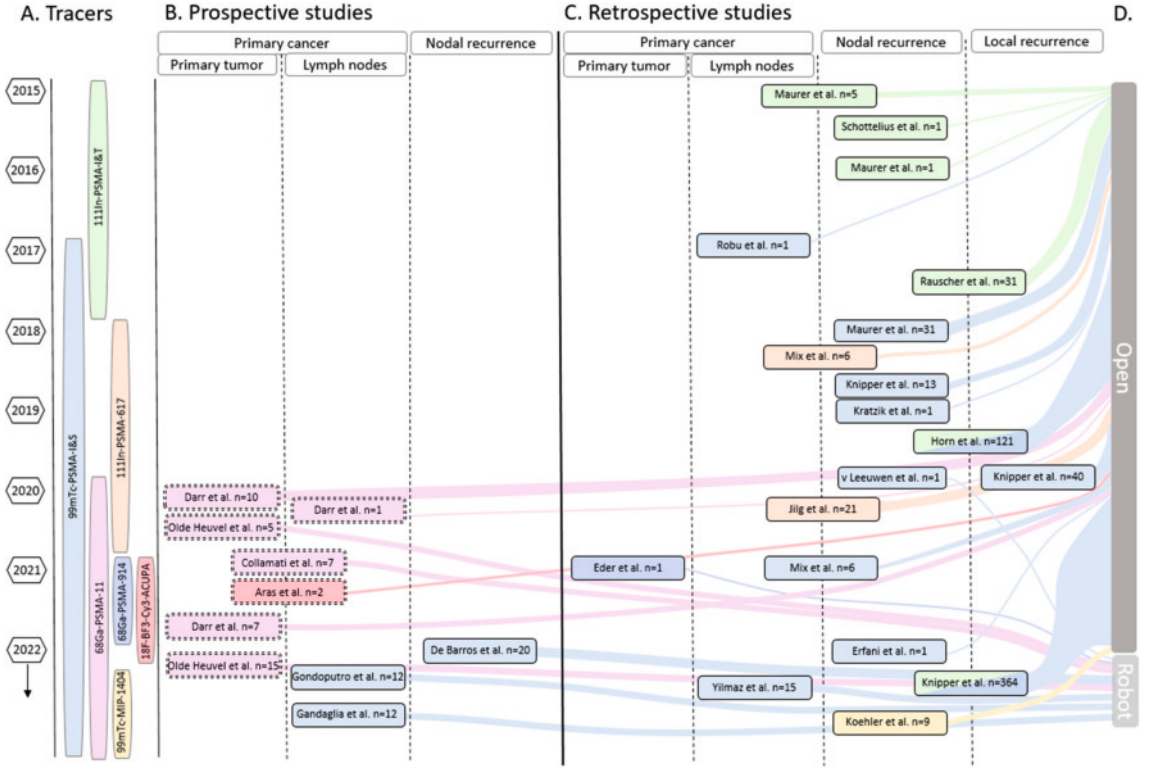

Figure 4. An overview of all reviewed literature. On the y-axis from top to bottom in chronological order the year in which the studies were published. A) All tracers aligned with the years studies were published on the subject. B) Overview of prospective studies. Color matches the tracer that was studied. Position on y-axis indicates year of publication. Position on x-axis indicates type of prostate cancer studied. C) Overview of studies that retrospectively analyzed the data. Color indicates type of tracer studied. Position on y-axis indicates year of publication. Position on x-axis indicates type of prostate cancer studied. D) Sankey diagram entwined in B and C showing the distribution between open and robot-assisted surgical procedures by number of patients. The color matches the tracer that was studied. == Only *ex vivo* measurements were performed. ═ *In* and *ex vivo* measurements were performed.

An alternative approach to combining beta emissions and optical guidance, makes use of so- called hybrid (radioactive- and fluorescently- labeled) PSMA-tracers [34 36]. A strategy that was used in 2/29 (7%) of the studies (n=3 patients). Eder et al. reported the use of a PSMA-11-derived hybrid molecular tracer, PSMA-914 (^{68}Ga-PSMA-914) using fluorescence imaging [36 44]. While Aras et al. used ^{18}F-BF3-Cy3-ACUPA in an *ex vivo* setting [34]. Unfortunately, the dyes 800 CW ($\lambda_{em\ max}$ =789 nm) and Cy3 ($\lambda_{em\ max}$ = 565 nm) are not optimally compatible with the da Vinci Firefly endoscope, which is designed for the detecting indocyanine green (ICG; $\lambda_{em\ max}$ = 820 nm) (Supplementary data 3 and 4). As a result the fluorescence of ^{18}F-BF3-Cy3-ACUPA was only imaged *ex vivo*. For neither compound was investigated if radio-and optical guidance could complement each other.

Tumor-to-background values

Comparison between tracers or modalities was difficult as the in and *ex vivo* reporting of tumor-to- background ratio (TBR) was not consistent and different cutoffs to consider a lesion positive were used [18 28]. Mostly this was defined as at least twice the background, with different definitions of the background (fatty tissue, lymph nodes, psoas muscle). TBR ranged from 2.1 to 8.0 for ^{99m}Tc-PSMA-I&S (*in vivo* analysis (drop-in) gamma probe, background: different types of tissue near the lesion) and from 10.0 to 30.0 for ^{99m}Tc-MIP-1404 (*ex vivo* analysis, hand-held gamma probe, background: fatty tissue) [17 28].

Surgical outcomes

As illustrated in figure 4, 69% of the reports studied open surgical interventions (tracers used *in vivo*: ^{111}In-PSMA-I&T, ^{99m}Tc-PSMA-I&S, ^{99m}Tc-MIP-1404; *ex vivo*: ^{68}Ga-PSMA-11, ^{18}F-BF3-Cy3-ACUPA) and 31% robot-assisted (tracers used *in vivo*: ^{99m}Tc-PSMA-I&S, ^{68}Ga-PSMA-914; *ex vivo*: ^{68}Ga-PSMA-11). Six studies (21%) focused only on the identification of margins in primary cancer (tracers used *in vivo*: ^{68}Ga-PSMA-914, *ex vivo*: ^{68}Ga-PSMA-11) or local recurrence (*in vivo:* ^{99m}Tc-PSMA-I&S), two (7%) on both prostate and lymph nodes (tracers used *ex vivo*: ^{68}Ga-PSMA-11, ^{18}F-BF3-Cy3-ACUPA), and 21 (72%) on identifying tumor positive lymph nodes during primary or salvage lymph node dissection (LND) (tracers used *in vivo*: ^{111}In-PSMA-617, ^{111}In-PSMA-I&T, ^{99m}Tc-PSMA-I&S, ^{99m}Tc-MIP-1404).

In nodal surgery, the accuracy of identifying tumor-containing lymph nodes was reported in 11 studies (38%); 7/11 salvage LND, 4/11 primary LND,) (tracers used *in* and *ex vivo*: ^{111}In-PSMA-617, ^{111}In- PSMA-I&T, ^{99m}Tc-PSMA-I&S, ^{99m}Tc-MIP-1404, tracers used only *ex vivo*: ^{68}Ga-PSMA-11). Generally, specificity (median 96.3 [IQR] 93.8- 99.4) was higher than sensitivity (median 80.1 [IQR] 76-92.1). Gondoputro et al. reported the only discrepancy with an *in vivo* specificity of 69% (sensitivity of 76%; ^{99m}Tc-PSMA-I&S; robotic procedure) [19]. A notable outlier was a sensitivity of 50% reported by Gandaglia et al. in primary LND using ^{99m}Tc-PSMA-I&S [18]. The influence of the tracers and the approach (open/

robotic) on the accuracy could not be assessed given the different preoperative patient characteristics, differences in timing of injection, differences in location of the lesions and differences in reporting.

In vivo identified PCa lesions ranged between <1 mm to 25 mm in size for ^{99m}Tc-PSMA-I&S where the smallest lesion (<1mm) was identified during robot assisted surgery using a drop-in gamma probe [19]. For ^{111}In-PSMA-I&T the range was 2 mm – 12 mm. Four studies (14%) report identifying tumor positive lesions via ^{99m}Tc-PSMA-I&S that did not show on preoperative PET [18 19 29]. False negatives, when reported, where lesions <5 mm [17-19]. An overview of the surgical outcomes can be found in table 1.

In prostate-focused surgery, the accuracy of identifying positive surgical margins *in vivo* by RGS was only described in one patient by Gondoputro et al. They successfully removed residual cancerous tissue but advised caution due to potential urinary contamination [19]. The *ex vivo* evaluation of ^{68}Ga- PSMA-11 with the drop-in beta probe correctly identified positive surgical margins in 40% (n=7 patients) [15]. *Ex vivo* Cerenkov imaging of ^{68}Ga-PSMA-11 yielded 60-83% (n=37 patients) agreement with histopathology [16 20-22]. Eder et al. and Aras et al. describe the visibility of the fluorescent component of the tracer (*in* and *ex vivo*, respectively) but did not quantify their results [34 36].

(Oncological) outcomes

Between the studies the evidence varied as shown in table 1, no study exceeded IDEAL framework stage 2b "development".

Follow-up data after PSMA-targeted salvage surgery was analyzed retrospectively in 10 studies (34%) reporting a median follow-up of 1 to 25.7 months and was only provided for ^{99m}Tc-PSMA I&S and ^{111}In-PSMA-I&T. Nothing has yet been reported on the difference in oncological outcomes between these tracers.

Post-operative PSA decline was reported in six of the 22 reports addressing salvage lymph node surgery [4 23 27 45]. The PSA decline ranged between 67-100% of the patients and a decline of >90% in 22-100% (Table 2), indicating variations in treatment effectiveness. Knipper et al. was the first to look at the difference in PSA decline after conventional salvage LND versus the addition of PSMA- targeted radioguidance (^{99m}Tc-PSMA I&S, n=42 patients) and found a significantly better outcome for the latter. However, long term follow-up data is missing [4].

Table 2. Follow-up

Author, year	Number of patients	PSMA agent, administration, type of guidance	Duration in months	Additional treatment after PSMA GS needed	PSA progression	BCR/BCRFS	Survival	Complications (Clavien-Dindo)			
Focus on lymph nodes			Median (IQR)	in n (%)	PSA at FU: Median (IQR) cBR/decline: n (%)	n (%) BCRFS n in months (95% CI)	n (%)	I/II n (%)	III n (%)	IV n (%)	V n (%)
Maurer, 2015	5	111In-PSMA-I&T, IV, R	NR	NR	NR	NR	NR	NR	NR	NR	NR
Rauscher, 2017	31	111In-PSMA-I&T, IV, R	11.1 (2.7–19.4)^^	10 (33.0) after median of 4.1 mo	cBR: 2 (22.0) with FT 15 (75.0) without FT Decline >50 %: 23 (76.7) Decline >90%: 16 (53.3)	NR	NR	6 (20.0)	4 (13.0)	0 (0.0)	0 (0.0)
Knipper, 2018	42 (13)	99mTc-PSMA-I&S, IV, R	NR	NR	0.069 (<0.01-3,3)^^ ng/mL Decline >50% (92.0) Decline >90% (53.0)	NR	NR	NR	NR	NR	NR
Maurer, 2018	31	99mTc-PSMA-I&S, IV, R	13.8 (-)	11 (35.0) after median of 3.7 mo	Decline >50 %: 24 (80.0) Decline >90%: 17 (57.0)	BCR: 17 (55.0) after median of 1.9 mo	NR	12 (38.7)	1 (3.2)	0 (0.0)	0 (0.0)
Mix, 2018	6	111In-PSMA-617, IV, R	24 (-)	NR	at FU: 0.51 (0.03 -4.85)	NR	NR	NR	NR	NR	NR
Horn, 2019	121	111In-PSMA-I&T 99mTc-PSMA-I&S, IV, R	NR	39 (32.2) after median of 4.6 mo	cBR: 77 (66%) Decline >50% 88 (77.0) Decline >90% 55 (48.0)	41.8% BCRFS of at least 12 mo. No significant difference between tracers	NR	29 (24.0)	11 (9.0)	0 (0.0)	1 (1.0)
Collamati, 2020	7	68Ga-PSMA-11, IV, R	NR	NR	NR	NR	NR	NR	NR	NR	NR
Jilg, 2020	23 (21)	111In-PSMA-617 IV, R	25.7 (-)	10 (43.5)	NR	14/23 clinical progression	NR	NR	NR	NR	NR
Mix, 2021	6	99mTc-PSMA-I&S, IV, R	19.4 (17.0-22.7)	6 (100.0)	at FU: 1.45 (0.15-17.1)	NR	AWD 6 (100.0)	NR	NR	NR	NR
de Barros, 2022	20	99mTc-PSMA-I&S, IV, R	15.0~	NR	Decline >50% (67.0) Decline >90% (22.0)	BCR: 14/18 (88.0)	overall 18/19 (94.7)	5 (26.3)	0 (0.0)	0 (0.0)	1 (5.3)
Gondoputro, 2022	12	99mTc-PSMA-I&S, IV, R	13 (4-22)	6 (50.0)	pPSA 5/12 (42.0)	BCR: 2/12 (16.7)	overall 12/12 (100.0)	1 (8.3)	0 (0.0)	0 (0.0)	0 (0.0)

Focus on lymph nodes			**Median (IQR)**	**in n (%)**	**PSA at FU: Median (IQR)** **cBR/decline: n (%)**	**n (%)** **BCRFS n in months (95% CI)**	**n (%)**	**I/II** **n (%)**	**III** **n (%)**	**IV** **n (%)**	**V** **n (%)**
Knipper, 2022	364	111In-PSMA-I&T 99mTc-PSMA-I&S, IV, R	no BCR 10.8 (1.2-25.1) no treatm 10.3 (2.3-24.0)	121 (33.2)	cBR 165 (45.3)	BCR 225 (61.8) BCRFS 7.8 (5.4-10.5)	NR	94 (25.6)	23 (6.3)	1 (0.28)	0 (0.0)
Yilmaz, 2022	15	99mTc-PSMA-I&S, IV, R	23.5' (14-30)^^	5 (33.3)	Decline >90% (100.0)	at 2.5yrs fu BCRFS rate 86.7%	overall 15/15 (100.0)	NR	0 (0.0)	0 (0.0)	0 (0.0)
Gandaglia, 2022	12	99mTc-PSMA-I&S, IV, R	1	3 (25.0)	pPSA 3/12 (25.0)	NR	overall 12/12 (100.0)	0 (0.0)	3 (25.0)	0 (0.0)	0 (0.0)
Koehler, 2022	9	99mTc-MIP-1404, IV, R	NR	NR	cBR: 5 (56.0)	NR	NR	NR	NR	NR	NR
Case reports											
Schottelius, 2015	1	111In-PSMA-I&T, IV, R	NR	NR	NR	NR	NR	NR	NR	NR	NR
Maurer, 2016	1	111In-PSMA-I&T, IV, R	NR	0 (0.0)	<0.07 1 (100.0)	NR	overall 1 (100.0)	NR	NR	NR	NR
Robu, 2017	2 (1)	99mTc-PSMA-I&S, IV, R	NR	NR	NR	NR	NR	NR	NR	NR	NR
Kratzik, 2018	1	99mTc-PSMA-I&S, IV, R	1	NR	<0.01 1 (100.0)	NR	NR	0 (0.0)	0 (0.0)	0 (0.0)	0 (0.0)
Darr, 2020	1	68Ga-PSMA-11, IV, O	NR	NR	NR	NR	NR	NR	NR	NR	NR
van Leeuwen, 2020	1	99mTc-PSMA-I&S, IV, R	NR	NR	<0.03	NR	NR	NR	NR	NR	NR
Aras, 2021	10 (2)	18F-BF3-Cy3- ACUPA IV, O	NR	NR	NR	NR	NR	0 (0.0)	0 (0.0)	0 (0.0)	0 (0.0)
Erfani, 2022	1	99mTc-PSMA IV, R	NR	NR	NR	NR	NR	NR	NR	NR	NR

Focus on prostate/local recurrence			Median (IQR)		PSA at FU: Median (IQR)			I/II n (%)	III n (%)	IV n (%)	V n (%)
Knipper, 2020	40	111In-PSMA-I&T 99mTc-PSMA-I&S, IV, R	24.4 (11.8-41.9)	12 (30.0)	cBR: 31 (77.5)	BCR: 22 (55.0) 23.7 (9.8- not reached)	NR	4 (10.0)	3 (7.5)	0 (0.0)	0 (0.0)
Darr, 2020	10	68Ga-PSMA-11, IV, O	NR	NR	NR	NR	NR	NR	NR	NR	NR
olde Heuvel, 2020	5	68Ga-PSMA-11, IV, O	NR	NR	NR	NR	NR	NR	NR	NR	NR
olde Heuvel, 2022	15	68Ga-PSMA-11, IV, O	NR	NR	NR	NR	NR	NR	NR	NR	NR
Darr, 2021	7	68Ga-PSMA-11, IV, O	NR	NR	NR	NR	NR	NR	NR	NR	NR
Case reports											
Eder, 2021	1	68Ga-PSMA-914, IV, O	NR	NR	NR	NR	NR	NR	NR	NR	NR

‘ =Mean (± SD), ~=maximum, ^^ =Range, AWD=Alive with disease, BCR=biochemical recurrence, defined as PSA >0.2ng/ml, BCRFS= BCR free survival, cBR =complete biochemical response (PSA<0.2 ng/ml), CI = confidence interval, FT=Further Treatment, Ga=Gallium, I&S=Imaging and surgery, I&T=Imaging and therapy, In=Indium, IQR=Interquartile Range, IV=Intravenous, NA = Not applicable, NR= Not reported, O= Optical guidance, R= Radioguidance

BCR was reported in five of 22 studies regarding salvage surgery, ranging from 50-62% of the patients with a follow-up ranging from 10.3 to 25.7 months. One study looked at BCR in the primary setting and found a BCR of 16.7% within a median of 13 months (IQR 4-22) [19]. Horn et al. concluded from their biochemical recurrence-free survival (BCRFS) data that patients with low preoperative PSA and a single lesion on preoperative PSMA-PET benefitted most of PSMA-targeted surgery [24]. A range of 0 to 100% of the patient populations was in need of additional treatment after PSMA-targeted surgery within a median ranging from 1 to 25.7 months.

Complications were classified according to Clavien-Dindo [46]. Seven from the 10 studies that reported on complications report on patients with a grade I/II complication, with a percentage ranging from 8 to 39%. Five studies observed complications grade 3 (percentage ranging from 3 to 25%) and only three patients from the total population of all studies experienced a complication ≥ grade IV [17 24 27]. None of the complications were ascribed to the tracer or image guidance procedure. The overall survival was again mentioned only in studies using ^{99m}Tc-PSMA-I&S and ^{111}In-PSMA-I&T and was 95-100% after a median ranging from 1.0 to 23.5 months. Details concerning follow-up and outcomes can be found in table 2.

Discussion

This systematic review summarized the existing literature on PSMA-targeted surgery in PCa patients. PSMA targeting provides a promising strategy to identify prostate cancer both pre- and intra- operatively and it seems we have only just begun to find out what this technique can offer. Currently, the most widely implemented approach is PSMA-RGS using ^{99m}Tc-PSMA I&S (~50% of the studies on this topic and the study with the largest number of patients (n=364)). Studies that used a conventional open surgical approach were the majority (69%) in comparison to robot-assisted surgery (31%).

Most studies present data on the value of PSMA-RGS in men with nodal recurrence (salvage surgery). One study suggested a benefit of PSMA-RGS versus conventional salvage LND [4]. Sensitivity for detecting nodal metastases during salvage surgery was dependent on size and location of the lesion and widely ranged from 50 to 100% (eight trials). One of the most critical factors is selection of patients. Men with a lower preoperative PSA and one lesion on imaging were most likely to benefit from RGS surgery with complete biochemical response rate of 45-66% in the largest series.

PSMA-PET imaging is known to be less dependable in identifying lesions under 3mm [6 7]. This corresponds to our findings for intraoperative detection, where the median size of metastases found in this review ranged from 2 to 9 mm. Smaller nodes (<3 mm) were most frequently missed [17 19]. The level of reporting of correlation between RGS findings and histology in studies varied, with some reporting at the nodal level and others

at the patient level. Moreover, whether *ex vivo* analysis corresponded to intraoperative findings was not reported in all studies. This makes it difficult to compare detection rates among studies.

Tracer choice may also impact on detection accuracy. A choice usually based on pharmacokinetics and pharmacodynamics as well as the sensitivity and specificity of the tracer. The studies with the largest patient groups (ranging from n= 1 to 364) included in these trials received RGS facilitated by ^{99m}Tc-PSMA I&S. The properties of ^{99m}Tc-PSMA I&S are well known but this cannot be said for many of the other tracers and comparative studies are lacking [47]. As ^{99m}Tc-PSMA I&S has been successfully used in both the primary and salvage setting, it is currently the favored tracer.

The oncological benefit of PSMA-targeted surgery was mainly studied using biochemical response as an endpoint. Looking at all the data combined there was a large variation in PSA decline. Knipper et al. showed that adding PSMA guidance to conventional salvage LND improved PSA decline suggesting that PSMA-RGS may improve outcome in men with recurrent nodal disease when compared conventional surgery [26]. Around 50% of salvage RGS patients was BCR-free at a median follow-up of 13.2 months. Hereby a low preoperative PSA and a single lesion on preoperative PSMA PET yielded a better BCRFS after salvage RGS [24].

In six studies PSMA-RGS was used in primary LND. Sensitivity and specificity for detection of nodal metastases was comparable to the salvage setting but considering the short reported follow-up no other oncological outcome data are available. Optical cancer detection by Cerenkov or fluorescence imaging has only been studied in the primary setting. No study has proven the oncological value of PSMA-targeted surgical margin imaging. PSMA tracers that solely rely on fluorescence are in development [48 49]. However, preclinical or first-in-man data may not immediately translate to patient care. In fact, our search worryingly suggests that thus far only two optical (hybrid) tracers mentioned in preclinical reviews (^{68}Ga-PSMA-914 and ^{18}F-BF3-Cy3-ACUPA) were tested clinically in two case series [8 9 50].

This review is limited by the retrospective nature of the majority of the included studies with an unclear overlap in numbers of patients. The included studies had a high or unclear risk of bias, were non-comparative, lacked a standardized way of reporting outcomes, and follow-up was short. Furthermore, the sample sizes were generally small. Direct comparison of studies is also hampered by overlapping patient populations in several studies. Only one prospective first-in-human study that presented proof of concept data contained ≥20 patients so far. Based on results from this review it is essential that further clinical trials are based on standardized methodology and proper study endpoints. Also consensus on what PSMA-targeted surgery should provide for wider clinical implementation is desirable.

Conclusion

Consolidating the existing literature on PSMA-targeted guidance during surgery in PCa indicates the most common technique used is by radioactive gamma-tracing in the open salvage setting. Techniques for use in robotic surgery and the addition of optical detection possibilities are in the pipeline. Intraoperative PSMA targeting has proven to be technically sound, but no clear oncological benefit has yet been objectified. Lacking solid outcome data, currently PSMA-targeted surgical guidance should be considered an experimental treatment. Randomized controlled studies may be considered after consensus on the optimal surgical approaches and most valid clinical endpoints.

References

1. Eastham JA, Scardino PT, Kattan MW. Predicting an optimal outcome after radical prostatectomy: the trifecta nomogram. J Urol 2008;179(6):2207-10; discussion 10-1.
2. Zhang R, Li T, Ye L, Lin L, Wei Y. The Evidence Behind Robot-Assisted Abdominopelvic Surgery. Ann Intern Med 2022;175(3):W22.
3. Dell'Oglio P, Mottrie A, Mazzone E. Robot- assisted radical prostatectomy vs. open radical prostatectomy: latest evidences on perioperative, functional and oncological outcomes. Curr Opin Urol 2020;30(1):73-78.
4. Knipper S, Tilki D, Mansholt J, et al. Metastases- yield and Prostate-specific Antigen Kinetics Following Salvage Lymph Node Dissection for Prostate Cancer: A Comparison Between Conventional Surgical Approach and Prostate- specific Membrane Antigen-radioguided Surgery. Eur Urol Focus 2019;5(1):50-53.
5. Perera M, Papa N, Roberts M, et al. Gallium-68 Prostate-specific Membrane Antigen Positron Emission Tomography in Advanced Prostate Cancer-Updated Diagnostic Utility, Sensitivity, Specificity, and Distribution of Prostate-specific Membrane Antigen-avid Lesions: A Systematic Review and Meta-analysis. Eur Urol 2020;77(4):403-17.
6. Uprimny C, Kroiss AS, Decristoforo C, et al. 68Ga- PSMA-11 PET/CT in primary staging of prostate cancer: PSA and Gleason score predict the intensity of tracer accumulation in the primary tumour. European Journal of Nuclear Medicine and Molecular Imaging 2017;44(6):941-49.
7. Mottet N, van den Bergh RCN, Briers E, et al. EAU- EANM-ESTRO-ESUR-SIOG Guidelines on Prostate Cancer-2020 Update. Part 1: Screening, Diagnosis, and Local Treatment with Curative Intent. Eur Urol 2021;79(2):243-62.
8. Hensbergen AW, van Willigen DM, van Beurden F, et al. Image-Guided Surgery: Are We Getting the Most Out of Small-Molecule Prostate- Specific-Membrane-Antigen-Targeted Tracers? Bioconjug Chem 2020;31(2):375-95.
9. Derks YHW, Lowik D, Sedelaar JPM, et al. PSMA- targeting agents for radio- and fluorescence- guided prostate cancer surgery. Theranostics 2019;9(23):6824-39.
10. Bramer WM, Giustini D, De Jonge GB, Holland L, Bekhuis T. De-duplication of database search results for systematic reviews in EndNote. Journal of the Medical Library Association 2016;104(3).
11. Ouzzani M, Hammady H, Fedorowicz Z, Elmagarmid A. Rayyan-a web and mobile app for systematic reviews. Syst Rev 2016;5(1):210.
12. Page MJ, McKenzie JE, Bossuyt PM, et al. The PRISMA 2020 statement: an updated guideline for reporting systematic reviews. Rev Esp Cardiol (Engl Ed) 2021;74(9):790-99.
13. Ergina PL, Barkun JS, McCulloch P, Cook JA, Altman DG. IDEAL framework for surgical innovation 2: observational studies in the exploration and assessment stages. BMJ 2013;346(jun18 3):f3011-f11.
14. Sterne JA, Hernan MA, Reeves BC, et al. ROBINS- I: a tool for assessing risk of bias in non- randomised studies of interventions. BMJ 2016;355:i4919.
15. Collamati F, van Oosterom MN, De Simoni M, et al. A DROP-IN beta probe for robot-assisted (68)Ga-PSMA radioguided surgery: first *ex vivo* technology evaluation using prostate cancer specimens. EJNMMI Res 2020;10(1):92.
16. Darr C, Fragoso Costa P, Kesch C, et al. Prostate specific membrane antigen-radio guided surgery using Cerenkov luminescence imaging- utilization of a short-pass filter to reduce technical pitfalls. Transl Androl Urol 2021;10(10):3972-85.
17. de Barros HA, van Oosterom MN, Donswijk ML, et al. Robot-assisted Prostate-specific Membrane Antigen-

radioguided Salvage Surgery in Recurrent Prostate Cancer Using a DROP-IN Gamma Probe: The First Prospective Feasibility Study. Eur Urol 2022;82(1):97-105.

18. Gandaglia G, Mazzone E, Stabile A, et al. Prostate-specific membrane antigen Radioguided Surgery to Detect Nodal Metastases in Primary Prostate Cancer Patients Undergoing Robot-assisted Radical Prostatectomy and Extended Pelvic Lymph Node Dissection: Results of a Planned Interim Analysis of a Prospective Phase 2 Study. Eur Urol 2022;82(4):411-18.
19. Gondoputro W, Scheltema MJ, Blazevski A, et al. Robot-Assisted Prostate-Specific Membrane Antigen-Radioguided Surgery in Primary Diagnosed Prostate Cancer. J Nucl Med 2022;63(11):1659-64.
20. olde Heuvel J, de Wit-van der Veen BJ, van der Poel HG, et al. Cerenkov Luminescence Imaging in Prostate Cancer: Not the Only Light That Shines. J Nucl Med 2022;63(1):29-35.
21. olde Heuvel J, de Wit-van der Veen BJ, van der Poel HG, et al. (68)Ga-PSMA Cerenkov luminescence imaging in primary prostate cancer: first-in-man series. Eur J Nucl Med Mol Imaging 2020;47(11):2624-32.
22. Darr C, Harke NN, Radtke JP, et al. Intraoperative (68)Ga-PSMA Cerenkov Luminescence Imaging for Surgical Margins in Radical Prostatectomy: A Feasibility Study. J Nucl Med 2020;61(10):1500- 06.
23. Yilmaz B, Sahin S, Ergul N, et al. (99m) Tc-PSMA targeted robot-assisted radioguided surgery during radical prostatectomy and extended lymph node dissection of prostate cancer patients. Ann Nucl Med 2022;36(7):597-609.
24. Horn T, Kronke M, Rauscher I, et al. Single Lesion on Prostate-specific Membrane Antigen-ligand Positron Emission Tomography and Low Prostate-specific Antigen Are Prognostic Factors for a Favorable Biochemical Response to Prostate-specific Membrane Antigen-targeted Radioguided Surgery in Recurrent Prostate Cancer. Eur Urol 2019;76(4):517-23.
25. Jilg CA, Reichel K, Stoykow C, et al. Results from extended lymphadenectomies with [(111)In]PSMA-617 for intraoperative detection of PSMA-PET/CT-positive nodal metastatic prostate cancer. EJNMMI Res 2020;10(1):17.
26. Knipper S, Ascalone L, Ziegler B, et al. Salvage Surgery in Patients with Local Recurrence After Radical Prostatectomy. Eur Urol 2021;79(4):537- 44.
27. Knipper S, Mehdi Irai M, Simon R, et al. Cohort Study of Oligorecurrent Prostate Cancer Patients: Oncological Outcomes of Patients Treated with Salvage Lymph Node Dissection via Prostate-specific Membrane Antigen- radioguided Surgery. Eur Urol 2023;83(1):62-69.
28. Koehler D, Sauer M, Klutmann S, et al. Feasibility of (99m)Tc-MIP-1404 for SPECT/CT Imaging and Subsequent PSMA-Radioguided Surgery in Early Biochemically Recurrent Prostate Cancer: A Case Series of 9 Patients. J Nucl Med 2023;64(1):59- 62.
29. Maurer T, Weirich G, Schottelius M, et al. Prostate-specific membrane antigen-radioguided surgery for metastatic lymph nodes in prostate cancer. Eur Urol 2015;68(3):530-4.
30. Maurer T, Robu S, Schottelius M, et al. (99m)Technetium-based Prostate-specific Membrane Antigen-radioguided Surgery in Recurrent Prostate Cancer. Eur Urol 2019;75(4):659-66.
31. Mix M, Reichel K, Stoykow C, et al. Performance of (111)In-labelled PSMA ligand in patients with nodal metastatic prostate cancer: correlation between tracer uptake and histopathology from lymphadenectomy. Eur J Nucl Med Mol Imaging 2018;45(12):2062-70.
32. Mix M, Schultze-Seemann W, von Buren M, et al. (99m)Tc-labelled PSMA ligand for radio- guided surgery in nodal metastatic prostate cancer: proof of principle. EJNMMI Res 2021;11(1):22.
33. Rauscher I, Duwel C, Wirtz M, et al. Value of (111) In-prostate-specific membrane

antigen (PSMA)-radioguided surgery for salvage lymphadenectomy in recurrent prostate cancer: correlation with histopathology and clinical follow-up. BJU Int 2017;120(1):40-47.

34. Aras O, Demirdag C, Kommidi H, et al. Small Molecule, Multimodal, [(18) F]-PET and Fluorescence Imaging Agent Targeting Prostate- Specific Membrane Antigen: First-in-Human Study. Clin Genitourin Cancer 2021;19(5):405- 16.
35. Darr C, Krafft U, Fendler WP, et al. First-in-man intraoperative Cerenkov luminescence imaging for oligometastatic prostate cancer using (68)Ga-PSMA-11. Eur J Nucl Med Mol Imaging 2020;47(13):3194-95.
36. Eder AC, Omrane MA, Stadlbauer S, et al. The PSMA-11-derived hybrid molecule PSMA-914 specifically identifies prostate cancer by preoperative PET/CT and intraoperative fluorescence imaging. Eur J Nucl Med Mol Imaging 2021;48(6):2057-58.
37. Erfani S, Sadeghi R, Aghaee A, Ghorbani H, Roshanravan V. Prostate-Specific Membrane Antigen Radioguided Surgery for Salvage Pelvic Lymph Node Dissection in a Man With Prostate Cancer. Clin Nucl Med 2022;47(2):e174-e76.
38. Kratzik C, Dorudi S, Schatzl M, Sinzinger H. Tc- 99m-PSMA imaging allows successful radioguided surgery in recurrent prostate cancer. Hell J Nucl Med 2018;21(3):202-04.
39. Maurer T, Schwamborn K, Schottelius M, et al. PSMA Theranostics Using PET and Subsequent Radioguided Surgery in Recurrent Prostate Cancer. Clin Genitourin Cancer 2016;14(5):e549- e52.
40. Robu S, Schottelius M, Eiber M, et al. Preclinical Evaluation and First Patient Application of 99mTc-PSMA-I&S for SPECT Imaging and Radioguided Surgery in Prostate Cancer. J Nucl Med 2017;58(2):235-42.
41. Schottelius M, Wirtz M, Eiber M, Maurer T, Wester HJ. [(111)In]PSMA-I&T: expanding the spectrum of PSMA-I&T applications towards SPECT and radioguided surgery. EJNMMI Res 2015;5(1):68.
42. van Leeuwen FWB, van Oosterom MN, Meershoek P, et al. Minimal-Invasive Robot- Assisted Image-Guided Resection of Prostate- Specific Membrane Antigen-Positive Lymph Nodes in Recurrent Prostate Cancer. Clin Nucl Med 2019;44(7):580-81.
43. Chin PT, Welling MM, Meskers SC, Valdes Olmos RA, Tanke H, van Leeuwen FW. Optical imaging as an expansion of nuclear medicine: Cerenkov- based luminescence vs fluorescence-based luminescence. Eur J Nucl Med Mol Imaging 2013;40(8):1283-91.
44. Meershoek P, KleinJan GH, van Willigen DM, et al. Multi-wavelength fluorescence imaging with a da Vinci Firefly-a technical look behind the scenes. J Robot Surg 2021;15(5):751-60.
45. Meershoek P, van Oosterom MN, Simon H, et al. Robot-assisted laparoscopic surgery using DROP-IN radioguidance: first-in-human translation. Eur J Nucl Med Mol Imaging 2019;46(1):49-53.
46. Clavien PA, Barkun J, de Oliveira ML, et al. The Clavien-Dindo classification of surgical complications: five-year experience. Ann Surg 2009;250(2):187-96.
47. Aalbersberg EA, van Andel L, Geluk-Jonker MM, Beijnen JH, Stokkel MPM, Hendrikx J. Automated synthesis and quality control of [(99m)Tc]Tc-PSMA for radioguided surgery (in a [(68)Ga]Ga-PSMA workflow). EJNMMI Radiopharm Chem 2020;5(1):10.
48. Kularatne SA, Thomas M, Myers CH, et al. Evaluation of Novel Prostate-Specific Membrane Antigen-Targeted Near-Infrared Imaging Agent for Fluorescence-Guided Surgery of Prostate Cancer. Clin Cancer Res 2019;25(1):177-87.
49. Nguyen A, Antaris AL, van den Berg N, Xue L, Greenberg S, Carroll P. Abstract Results of the Phase 1 Safety and Efficacy Prostate Specific Membrane Antigen (Psma) Targeting Fluorophore for Image Guided Surgery in Patients Undergoing

Robotic Prostatectomy. Journal of Urology 2022(207):(Supplement 5).

50. Derks YHW, van Lith SAM, Amatdjais-Groenen HIV, et al. Theranostic PSMA ligands with optimized backbones for intraoperative multimodal imaging and photodynamic therapy of prostate cancer. Eur J Nucl Med Mol Imaging 2022;49(7):2425-35.

Supplementary 1. Full search on Medline, Embase.com and Cochrane library

Medline (OvidSP):
((exp "prostatic neoplasms"/) OR ((prostat*) ADJ3 (cancer* OR neoplas* OR carcinom* OR adenocarcinoma* OR malignan* OR tumor* OR tumour* OR sarcoma* OR lymphom* OR oncolog* OR metastas*) OR PCa).ti,ab,kf.) AND (("gallium 68 PSMA-11" OR "177Lu-EB-PSMA-617" OR "(18)F-PSMA- 11" OR "PSMA-617" OR "18F-JK-PSMA-7" OR "89Zr-Df-IAB2M" OR "68Ga-DKFZ-PSMA-11" OR "177Lu- PSMA-617" OR "PSMA-1007" OR "PSMA-BCH").nm. OR (PSMA OR "prostate specific membrane antigen*" OR "PSM antigen*" OR "gallium gozetotide GA-68" OR "89Zr-Df-IAB2M" OR "vipivotide tetraxetan").ti,ab,kf.) AND (exp "Surgical Procedures, Operative"/ OR exp "Prostatic Neoplasms"/su OR (surger* OR surgical* OR prostatectom* OR salvage OR ("lymph node*" ADJ3 (dissection* OR biops* OR excision*)) OR LND OR PLND OR ePLND OR sLND).ti,ab,kf.)

Embase.com:
(('prostate tumor'/exp) OR (((prostat*) NEAR/3 (cancer* OR neoplas* OR carcinom* OR adenocarcinoma* OR malignan* OR tumor* OR tumour* OR sarcoma* OR lymphom* OR oncolog* OR metastas*)) OR PCa):ti,ab,kw) AND (('prostate specific membrane antigen'/exp OR 'gallium gozetotide ga 68'/de OR 'vipivotide tetraxetan lutetium lu 177'/de OR 'vipivotide tetraxetan'/de) OR (PSMA OR "prostate specific membrane antigen*" OR "PSM antigen*" OR "gallium gozetotide GA-68" OR "89Zr- Df-IAB2M" OR "vipivotide tetraxetan"):ti,ab,kw) AND (surgery/exp OR (surger* OR surgical* OR prostatectom* OR salvage OR (("lymph node*" NEAR/3 (dissection* OR biops* OR excision*)) OR LND OR PLND OR ePLND OR sLND)):ti,ab,kw)

Cochrane library:
#1 MeSH descriptor: [Prostatic Neoplasms] explode all trees
#2 ((prostat*) NEAR/3 (cancer* OR neoplas* OR carcinom* OR adenocarcinoma* OR malignan* OR tumor* OR tumour* OR sarcoma* OR lymphom* OR oncolog* OR metastas*)):ti,ab,kw OR (PCa):ti,ab,kw
#3 #1 OR #2
#4 (PSMA OR "prostate specific membrane antigen*" OR "PSM antigen*" OR "gallium gozetotide GA-68" OR "89Zr-Df-IAB2M" OR "vipivotide tetraxetan"):ti,ab,kw
#5 MeSH descriptor: [Surgical Procedures, Operative] explode all trees
#6 MeSH descriptor: [Prostatic Neoplasms] explode all trees and with qualifier(s): [surgery - SU]
#7 (surger* OR surgical* OR prostatectom* OR salvage):ti,ab,kw OR ("lymph node*" NEAR/3 (dissection* OR biops* OR excision*)):ti,ab,kw OR (LND OR PLND OR ePLND OR sLND):ti,ab,kw
#8 #5 OR #6 OR #7
#9 #3 AND #4 AND #8

Supplementary 2. Table on study features and baseline patient characteristics

Author, year	Number of patients	Age	Type PCa	Preoperative PSA*	ISUP					Pathological T-stage			
	n (n PSMA guidance)	Years Median (IQR)		ng/m Median (IQR)	1 n (%)	2 n (%)	3 n (%)	4 n (%)	5 n (%)	2 n (%)	3a n (%)	3b n (%)	4 n (%)
Maurer, 2015	5	75 (64-75)^^	Recurrent Disease or primary N+	2.45 (0.42-244)^^	1 (20.0)	1 (20.0)	1 (20.0)	1(20.0)	1 (20.0)	2 (40.0)	1(20.0)	1(20.0)	1(20.0)
Rauscher, 2017	31	68.2 (60.5-73.5)^^	Recurrent disease	1.3 (0.57-2.53)	5 (16.1)	15 (48.5)		10 (32.3)		12 (38.7)	16 (51.6)		1 (3.2)
Knipper, 2018	42 (13)	61.8' (52–76)^^	Recurrent disease	3.5' (0.15-16.3)^^	0 (0.0)	11 (84.6		2 (15.4)		8 (61.5)	5 (38.5)		
Maurer, 2018	31	66.7 (60.5-73.5)	Recurrent disease	1.13 (0.71-2.35)	4 (12.9)	8 (25.8)	7 (22.6)	5 (16.1)	7 (22.6)	14 (45.2)	16 (51.6)		
Mix, 2018	6	71 (65-77)	Recurrent disease or primary N+	7.03 (0.93 -12.16)	0 (0.0)	0 (0.0)	3 (50.0)	2 (33.3)	1 (16.7)	NR	NR	NR	NR
Horn, 2019	121	70 (63-74)	Recurrent disease	1.13 (0.53-2.16)	13 (11.0)	48 (48.0)		44 (36.0)		12 (38.7)	16 (51.6)		1 (3.2)
Collamati, 2020	7	63 (55-71)	Primary high-risk	5.3 (4.4-8.3)	0 (0.0)	0 (0.0)	0 (0.0)	4 (0.57)	3(0.43)	NR	NR	NR	NR
Darr, 2020	10	72 (63-81)^^	Primary high-risk	9.04 (3.3-77.7)^^	0 (0.0)	2 (20.0)	3 (30.0)	1 (10.0)	4(40.0)	2 (20.0)	5 (50.0)	3 (30.0)	0 (0.0)
Jilg, 2020	23 (21)	67(52–78)^^	Recurrent disease or primary N+	1.8 (0.03–56.2)^^	0 (0.0)	0 (0.0)	4 (17.0)	7 (31.0)	12 (52.0)	NR	NR	NR	NR
Knipper, 2020	40	67 (63-67)	Recurrent disease or Primary cN+	0.9 (0.5-1.7)	7 (17.5)	12 (30.0)	6 (15.0)	7 (17.5)	7 (17.5)	18 (45.0)	15 (37.5)	7 (17.5)	0 (0.0)
olde Heuvel, 2020	5	67 (60.5-72)	Primary high-risk	6.4 (4.85-19.1)	0 (0.0)	0 (0.0)	0 (0.0)	3 (60.0)	2 (40.0)	2 (40.0)	2 (40.0)	1 (20.0)	0 (0.0)
Mix, 2021	6	64 (54.8-67.3)	Recurrent Disease or primary cN+	33.3 (4.6-64.4)	0 (0.0)	0 (0.0)	2 (33.3)	3 (50.0)	1 (16.7)	NR	NR	NR	NR
olde Heuvel, 2022	15	67 (64-72.5)	Primary high-risk	7.9 (5.2-9.25)	0 (0.0)	1 (6.7)	2 (13.3)	7 (46.7)	5(33.3)	4 (26.7)	6 (40.0)	5 (33.4)	0 (0.0)
Darr, 2021	7	66 (59- 69)	Primary high-risk	12.0 (5.6-16.0)	0 (0.0)	1 (14.3)	2 (28.6)	2 (28.6)	2 (28.6)	5 (71.0)	2 (29.0)	0 (0.0)	0 (0.0)
de Barros, 2022	20	68 (66-72)	Recurrent disease	1.02 (0.46-2.43)	NR	NR	NR	NR	NR	NR	NR	NR	NR
Gondoputro, 2022	12	68 (57-69)	Primary high-risk	9.15 (6.0-21.2)	0 (0.0)	0 (0.0)	0 (0.0)	3 (25.0)	9 (75.0)	6 (50.0)	1 (8.3)	3 (25.0)	0
Knipper, 2022	364	67 (62-71)	Recurrent disease	1.0 (0.5-1.9)	27 (7.2)	96 (26.0)	127 (35.0)	40 (11.0)	60 (16.0)	145 (40.0)	105 (29.0)	107 (29.0)	0 (0.0)
Yilmaz, 2022	15	63.3' (56-74)^^	Intermediate -/ high-risk	40.9' (4-309)^^	0 (0.0)	3 (20.0)	4 (26.7)	1 (26.7)	7 (46.7)	NR	NR	NR	NR
Gandaglia, 2022	12	70 (66-71)	Intermediate-/ high-risk	8.7 (4.8-15.5)	0 (0.0)	1 (8.3)	5 (42.0)	4 (33.0)	2 (17.0)	0 (0.0)	8 (66.7)	4 (33.3)	0 (0.0)
Koehler, 2022	9	62 (61 – 67)	Recurrent disease	0.74 (0.41 – 1.54)	0 (0.0)	1 (11.1)	5 (55.5)	2 (22.2)	0 (0.0)	2 (22.2)	3 (33.3)	4 (44.4)	0 (0.0)

	n (n PSMA guidance)	Years Median (IQR)		ng/ml Median(IQR)	1 n (%)	2 n (%)	3 n (%)	4 n (%)	5 n (%)	2 n (%)	3a n (%)	3b n (%)	4 n (%)
Case reports													
Schottelius, 2015	1	51	Recurrent disease	63	0 (0.0)	0 (0.0)	0 (0.0)	0 (0.0)	1 (100.0)	NR	NR	NR	NR
Maurer, 2016	1	63	Recurrent disease	0.23	0 (0.0)	0 (0.0)	0 (0.0)	0 (0.0)	1 (100.0)	0 (0.0)	1 (100.0)	0 (0.0)	0 (0.0)
Robu, 2017	2 (1)	72	Intermediate risk	13	0 (0.0)	0 (0.0)	1 (100.0)	0 (0.0)	0 (0.0)	1 (100.0)	0 (0.0)	0 (0.0)	0 (0.0)
Kratzik, 2018	1	78	Recurrent disease	13.1	0 (0.0)	0 (0.0)	0 (0.0)	0 (0.0)	1 (100.0)	1 (100.0)	0 (0.0)	0 (0.0)	0 (0.0)
Darr, 2020	1	68	Primary cN+	NR	0 (0.0)	0 (0.0)	1 (100.0)	0 (0.0)	0 (0.0)	1 (100.0)	0 (0.0)	0 (0.0)	0 (0.0)
Van Leeuwen, 2020	1	NR	Recurrent disease	0.58	NR	NR	NR	NR	NR	NR	NR	NR	NR
Aras, 2021	10 (2)	66' (57-74)^^	Intermediate -/ high-risk	31' (0.25-199)^^	0 (0.0)	1 (10.0)	4 (40.0)	3 (30.0)	0 (0.0)	3 (30.0)	6(60.0)		0 (0.0)
Eder, 2021	1	71	Primary high-risk	7	0 (0.0)	0 (0.0)	0 (0.0)	0 (0.0)	1 (100.0)	NR	NR	NR	NR
Erfani, 2022	1	75	Recurrent disease	0.3	NR	NR	NR	NR	NR	NR	NR	NR	NR

*Preoperative PSA is the value before Prostate Specific Membrane Antigen(PSMA)-targeted surgery, not primary surgery. '=Mean (± SD), ^^ =Range, ISUP= International Society of Urological Pathology, IQR=Interquartile Range, NR = not reported, PCa=Prostate cancer, PSA=Prostate specific antigen

Supplementary 3. Table on preoperative imaging features

Author, year	Number of patients	PSMA agent, administration, type of guidance	Injection time to surgery	Injected activity MBq	Preoperative imaging
Focus on lymph nodes			Median (IQR)	Median (IQR)	
Maurer, 2015	5	111In-PSMA-I&T, IV, R	24h	146' (110-169)^^	68Ga-PSMA-PET/CT
Rauscher, 2017	31	111In-PSMA-I&T, IV, R	22.9' ± 3 h (16.7–28.0)^^	150' (86-298)^^	68Ga-PSMA-PET/CT
Knipper, 2018	42 (13)	99mTc-PSMA-I&S, IV, R	NR	NR	68Ga-PSMA-PET/CT + SPECT/CT
Maurer, 2018	31	99mTc-PSMA-I&S, IV, R	19.7h' (15.8-24.9)^^	571' (221-857)^^	68Ga-PSMA-PET/CT SPECT/CT
Mix, 2018	6	111In-PSMA-617, IV, R	48h	108.5 (104-113)	68Ga-PSMA-PET/CT SPECT/CT
Horn, 2019	121	111In-PSMA-I&T 99mTc-PSMA-I&S, IV, R	24h	NR	68Ga-PSMA-PET/CT SPECT/CT
Collamati, 2020	7	68Ga-PSMA-11, IV, R	150 (120-172.5)	68 (63.5–82)	18F-DCFPyl-PSMA-PET/CT
Jilg, 2020	23 (21)	111In-PSMA-617 IV, R	44' ± 10h	110' ± 14	68Ga-PSMA-PET/CT SPECT/CT
Mix, 2021	6	99mTc-PSMA-I&S, IV, R	24h	638' (537-692)^^	68Ga-PSMA-PET/CT 18F-PSMA-PET/CT SPECT/CT
de Barros, 2022	20	99mTc-PSMA-I&S, IV, R	19-23h^^	541 (526–578)	68Ga-PSMA-PET/CT 18F-PSMA-PET/CT SPECT/CT
Gondoputro, 2022	12	99mTc-PSMA-I&S, IV, R	18h	500	68Ga-PSMA-PET/CT SPECT/CT
Knipper, 2022	364	111In-PSMA-I&T 99mTc-PSMA-I&S, IV, R	NR	NR	68Ga-PSMA-PET/CT SPECT/CT
Yilmaz, 2022	15	99mTc-PSMA-I&S, IV, R	17' ± 2h	630' (555-770)^^	68Ga-PSMA-PET/CT SPECT/CT
Gandaglia, 2022	12	99mTc-PSMA-I&S, IV, R	NR	735 (731-738)	68Ga-PSMA-11 PET/CT SPECT/CT
Koehler, 2022	9	99mTc-MIP-1404, IV, R	20.8h 30 – 24.0	747 (710 – 764)	68Ga-PSMA I&T PET/MRI SPECT/CT
Case reports					
Schottelius, 2015	1	111In-PSMA-I&T, IV, R	24h	155	68Ga-PSMA-PET/CT SPECT/CT

Focus on lymph nodes			**Median (IQR)**	**Median (IQR)**	
Maurer, 2016	1	111In-PSMA-I&T, IV, R	24h	NR	68Ga-PSMA-PET/CT
Robu, 2017	2 (1)	99mTc-PSMA-I&S, IV, R	16h	497 (-)	68Ga-PSMA-PET/MRI SPECT/CT
Kratzik, 2018	1	99mTc-PSMA-I&S, IV, R	18h	800 (-)	68Ga-PSMA-PET/CT SPECT/CT
Darr, 2020	1	68Ga-PSMA-11, IV, O	234min	116 (-)	68Ga-PSMA-11 PET/CT
van Leeuwen, 2020	1	99mTc-PSMA-I&S, IV, R	24h	NR	68Ga-PSMA-11 PET/CT SPECT/CT
Aras, 2021	10 (2)	18F-BF3-Cy3-ACUPA IV, O	24h	6.5 '(± 3.2 mCi)	[18F]-BF3-Cy3-ACUPA PET/CT + PET/MRI
Erfani, 2022	1	99mTc-PSMA IV, R	NR	20 mCi	68Ga-PSMA-PET/CT SPECT/CT
Focus on prostate/local recurrence			**Median (IQR)**	**Median (IQR)**	
Knipper, 2020	40	111In-PSMA-I&T 99mTc-PSMA-I&S, IV, R	24h	NR	68Ga-PSMA-PET/CT 18F-PSMA PET/CT
Darr, 2020	10	68Ga-PSMA-11, IV, O	223min(153-328)^^	119' (95-202^^)	68Ga-PSMA-PET/CT
Olde Heuvel, 2020	5	68Ga-PSMA-11, IV, O	73' ± 14 min	76 (66.5-103)	68Ga-PSMA-PET/CT
Olde Heuvel, 2022	15	68Ga-PSMA-11, IV, O	70'min (44-105)^^	69' (23-121)^^	68Ga-PSMA-PET/CT
Darr, 2021	7	68Ga-PSMA-11, IV, O	316min (283-331)	127 (116-179)	68Ga-PSMA-PET/CT
Case reports					
Eder, 2021	1	68Ga-PSMA-914, IV, O	1h	NR	68Ga-PSMA-914-PET/CT

' =Mean (± SD), ~=maximum, ^^ =Range, Ga=Gallium, I&S=Imaging and surgery, I&T=Imaging and therapy, In=Indium, IQR=Interquartile Range, IV=Intravenous, MBq= Megabecquerel, mCi=milliCurie, NR= Not reported, O= Optical guidance, R = Radioguidance, Tc= Technetium

Supplementary 4. Figure on chemical structures of PSMA-tracers for PSMA-targeted surgery

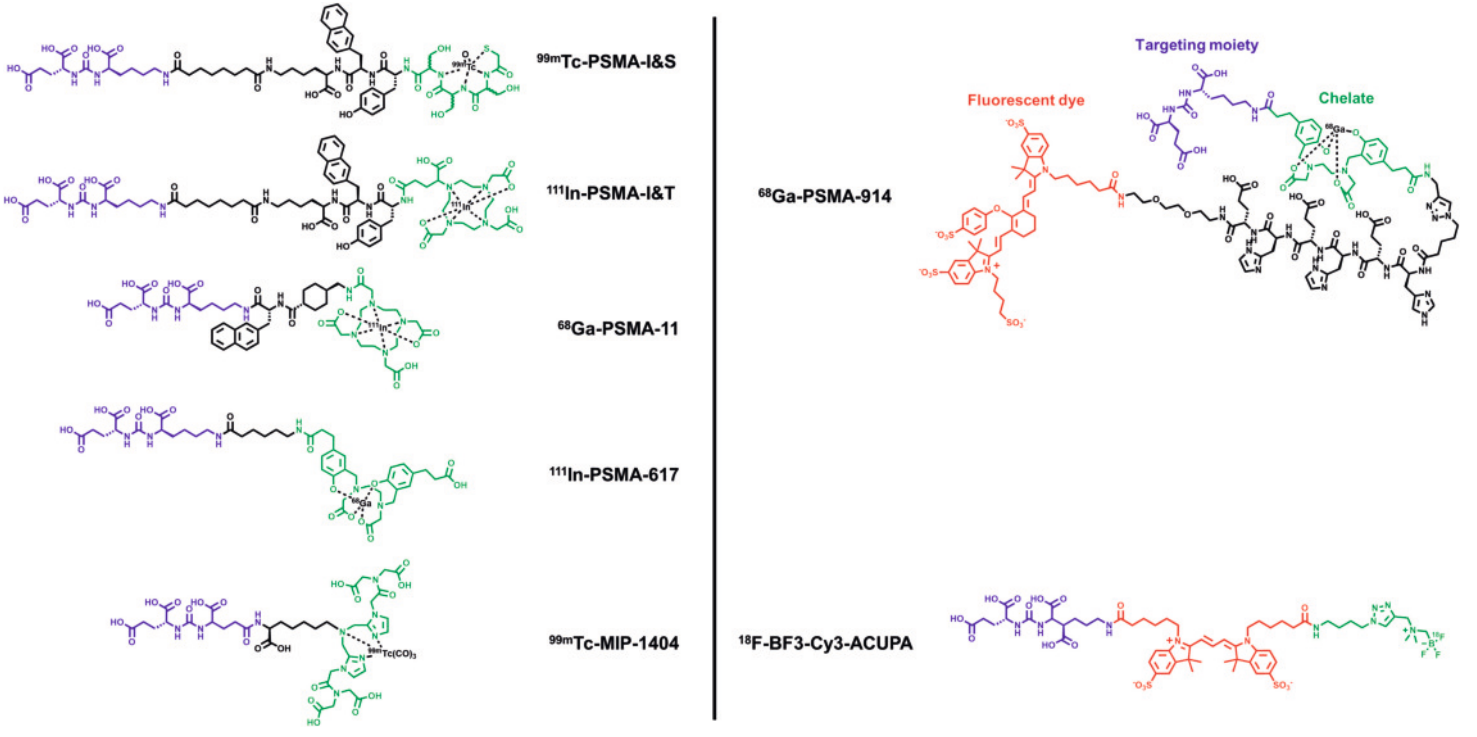

Supplementary 5. Table on chemical properties of Prostate Specific Membrane Antigen (PSMA)-tracers for PSMA-targeted surgery

	Injection	Preparation Time	Half-life	Radiochemical purity	IC50 [nM]	Fraction of protein-bound tracer (human plasma)	Stability	Clearance pathway	$\lambda_{em\ max}$ (nm)
^{111}In-PSMA-I&T	IV	10 min (labeling)	2.8 d		7.5 ± 1.5	83%	5-7 days	Renal	NA
^{111}In-PSMA-617	IV	30 min (synthesis)	2.81 d (^{111}In)	100.0±0.0%	Kd=5.4±0.8 nM	NR	NR	Renal	NA
^{99m}Tc-PSMA-I&S	IV	90 min	27h	98%	39.7 ± 1.2	94%	for up to 6h	Renal and hepatobilliary	NA
^{68}Ga-PSMA-11	IV	15 min (synthesis)	68 min	>99%	7.5 ± 2.2	NR	NR	Renal, minimal lung and spleen	450 for Cerenkov
^{18}F-BF3-Cy3- ACUPA	IV	25 min (labeling)	18 min	31-14% decay uncorrected	NR	NR	NR	Renal, minimal hepatic accumulation	565
^{68}Ga-PSMA-914	IV	10 min (labeling)	68 min	>99%	35.54±2.94	NR	NR	Renal, minimal splenic clearance	789
^{99m}Tc-MIP-1404	IV	NR	13.2	95%	Kd = 0.75 ± 0.32 nM	NR	NR	Renal and minimal hepatobilliary	NA

Ga=Gallium, IC50 = Half maximal inhibitory concentration, I&S=Imaging and surgery, I&T=Imaging and therapy, In=Indium, IV=Intravenous, Kd= Equilibrium dissociation constant, $\lambda_{em\ max}$ = maximum emission wavelength, mCi=milliCurie, nm = nanometer, [nM] = nano molar concentration, NR= Not reported, Tc= Technetium

Berrens AC, Scheltema M, Maurer T, Hermann K, Hamdy FC, Knipper S, Dell'Oglio P, Mazzone E, de Barros HA, Sorger JM, van Oosterom MN, Stricker PD, van Leeuwen PJ, Rietbergen DDD, Valdes Olmos RA, Vidal-Sicart S, Carroll PR, Buckle T, van der Poel HG, van Leeuwen FWB

Eur J Nucl Med Mol Imaging. 2024 Aug;51(10):2893-2902

Chapter 3

Delphi Consensus Project on Prostate-specific Membrane Antigen (PSMA)-targeted Surgery — Outcomes from an International Multidisciplinary Panel

Abstract

Purpose. Prostate-specific membrane antigen (PSMA) is increasingly considered as a molecular target to achieve precision surgery for prostate cancer. A Delphi consensus was conducted to explore expert views in this emerging field, and to identify knowledge and evidence gaps as well as unmet research needs that may help change practice and improve oncological outcomes for patients.

Methods. One hundred and five statements (scored by a 9-point Likert scale) were distributed through SurveyMonkey®. Following evaluation, a consecutive second round was performed to evaluate consensus (16 statements; 89% response rate). Consensus was defined using the disagreement index, assessed by the research and development project/University of California, Los Angeles appropriateness method.

Results. Eighty-six panel participants (72.1% clinician; 8.1% industry; 15.1% scientists and 4.7% other) participated, most with a urological background (57.0%), followed by nuclear medicine (22.1%). Consensus was obtained on: 1) The diagnostic PSMA-ligand PET/CT should ideally be taken <1 month before surgery, 1-3 months is acceptable, 2) a 16-20 hours interval between injection of the tracer and surgery seems to be preferred, 3) PSMA targeting is most valuable for identification of nodal metastases, 4) gamma-, fluorescence- and hybrid-imaging are the preferred guidance technologies, and 5) randomized controlled clinical trials are required to define oncological value. Regarding surgical margin assessment, the view on the value of PSMA-targeted surgery was neutral or inconclusive. A high rate of “cannot answer” responses indicate further study is necessary to address knowledge gaps (e.g. Cerenkov or beta-emissions).

Conclusions. This Delphi consensus provides guidance for clinicians and researchers that implement or develop PSMA-targeted surgery technologies. Ultimately, however, the consensus should be backed by randomized clinical trial data before it may be implemented within the guidelines.

Introduction

The emergence of prostate-specific membrane antigen (PSMA), a transmembrane glycoprotein that is highly overexpressed in prostate cancer (PCa) cells (Figure 1a), has greatly changed the identification of PCa on imaging. With the incorporation of PSMA-ligand positron emission tomography (PET)/computed tomography (CT) in international guidelines [1], this biomarker has proven its clinical value [2 3]. Exploitation of imaging biomarkers for surgical guidance is also becoming increasingly popular (Figure 1b/c), where distinguishing benign tissue from malignant tissue constitutes a challenge. More accurate intraoperative tumour delineation is expected to help advance surgical precision. A recent systematic review on the first efforts in the area of PSMA-targeted surgery, summarized the results on intraoperative technologies for detecting PSMA expressing PCa cells, both *in* and *ex vivo* (total approximately n=793 patients) [4]. This overview of the literature revealed that many of these pioneering studies deviate in (technical) set-up and data analysis. Reports using radioguidance facilitated by the tracer [^{99m}Tc]Tc-PSMA-I&S (for imaging and surgery) currently dominate the field [5].

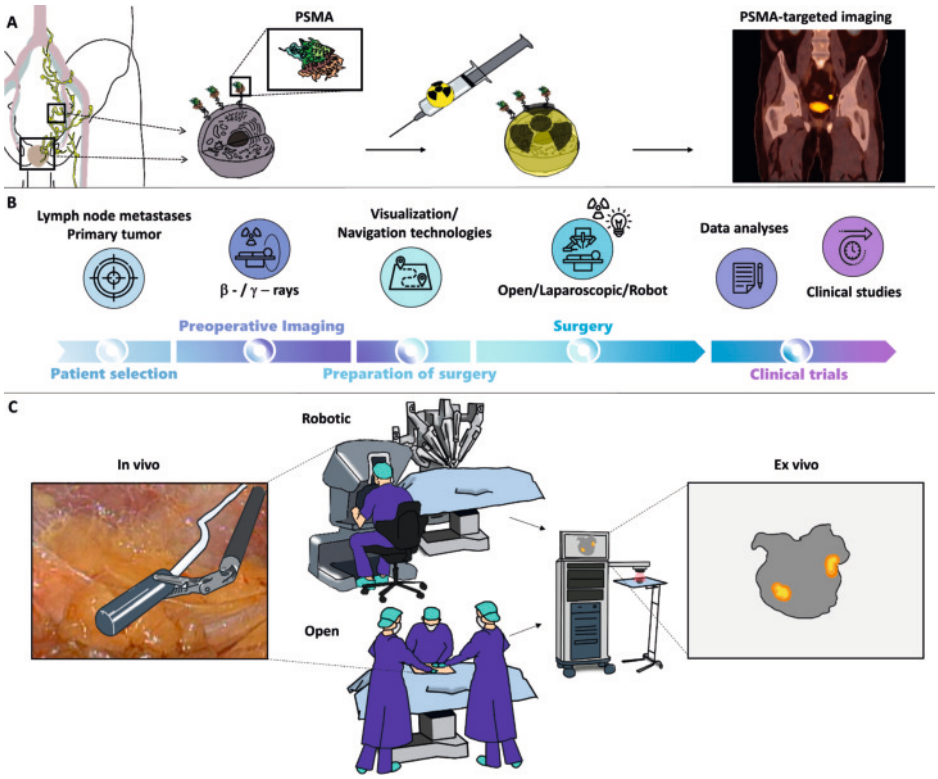

Figure 1. A) Prostate Specific Membrane Antigen (PSMA) targeting B) Clinical workflow PSMA-targeted surgery C) Surgical settings: Illustration of open and minimally invasive robotic surgery with examples of *in vivo* drop-in probe and *ex vivo* specimen imaging (e.g. Cerenkov or fluorescence imaging).

With the exception of two studies (121 and 364 patients) [6 7], most literature on PSMA-targeted surgery represent smaller, often retrospective, series (range 1-40 patients). This may be related to the novelty of the subject and current reimbursement. Studies describe different types of tracers and detection modalities, each having their own strengths and limitations [4]. Literature on PSMA-targeted surgery also suffers from considerable heterogeneity of definitions, and inconsistencies in the reporting of approaches and outcomes such as the cut-off metrics used for a positive signal (signal-to-background ratios (SBR) ranging from 1.5 to 17) [8-10]. Although there appears to be a growing demand for technologies that support PSMA-targeted PCa surgery, criteria for evaluating the outcomes and the optimal approach for future studies are unknown. Furthermore, evidence is lacking to demonstrate the benefits of the technology in improving outcomes for men with PCa such as disease-specific mortality and quality of life. This raises questions about how the technology might affect clinical practice.

In recognition of the importance of consensus on requirements, indications and assessment criteria, a Delphi consensus was initiated. A widely accepted strategy in the surgical field to establish guidelines based on clinical evidence and increasingly used for relatively new technologies that have not yet been implemented at a large scale e.g. for strategies in image-guided surgery [11-13]. By conducting a Delphi consensus project at this early stage of PSMA-targeted surgery development it becomes possible to identify and address knowledge/evidence gaps and unmet needs. The pursuit of consensus among the stake holders in multiple disciplines helps standardize approaches and establish best practices in order to speed up the further maturation of the field. A forward-thinking strategy that helps reduce the chance that patients are subject to sub-optimal treatment paradigms. The objective of this study was to advance insight into the current and future applications of PSMA-targeted surgery early on, and with that help set the stage for future research and clinical implementation.

Methods

Delphi consensus project

The consensus project was conducted in six phases. In the first phase, a steering committee was established comprising 12 experts from across the globe purposively selected to represent urologic end-users (46%), enabling nuclear medicine physicians (31%) and researchers (23%) in the field of image-guided surgery. In an iterative process the steering committee decided on the topics and wording of the initial 105 statements. To accommodate for difference in backgrounds, statements were included with different levels of complexity and could be answered with “cannot answer”. The second phase involved distributing the statements through SurveyMonkey® (Momentive Inc. San Mateo, California, USA). In the third phase, the answers were analysed. In the fourth phase, the steering committee met to discuss the need for clarifying certain statements

and drafting new ones. The fifth phase consisted of a second round of 16 statements that were distributed to the panel participants, again followed by anonymous answering (89% response rate). The sixth and final phase included the analysis of the answers and drafting of the manuscript. The steering committee guided the project and jointly drafted and authored the manuscript.

Participants and recruitment

Participants were identified through their authorship of studies on PSMA-targeted surgery or other individual relevant experience in this field, independent of the hospital, affiliation or geographical origin. Industrial participants were invited because their company provided key enabling technologies for PSMA-targeted surgery studies. To avoid bias, two participants per company were invited. Eligible panel participants were invited directly by the steering committee to participate, explaining the projects aim and methodology and requesting their agreement to participate. Final selection was influenced by the need to achieve an acceptable representation of key stakeholder groups. In total 86 panel participants answered the statements (62 (72.1%) clinician; 7 (8.1%) industry; 13 (15.1%) scientists and 4 (4.7%) other), most with a urological background (57.0%), followed by nuclear medicine (22.1%). Further details on participants are available in supplementary 1.

Definition of consensus

The initial statements could be divided into two main categories: clinical and technological. Statements could be scored using a 9-point Likert scale ranging from disagree (1) to agree (9), or "cannot answer" [14]. A median score of 1–3 represented disagreement with the statement, a score between 4-6 neutrality on the statement and a score of 7–9 reflected agreement. Consensus was defined using the disagreement index (DI). DI was assessed using the research and development project (RAND)/University of California, Los Angeles (UCLA) appropriateness method, using the formula: DI = interpercentile range (IPR) / interpercentile range adjusted for symmetry (IPRAS) [14]. IPR was defined as the difference between the 30th and 70th percentiles. The IPRAS was derived using the formula IPRAS = 2.35 + (asymmetry index [AI] x 1.5), where AI was the absolute difference between five and the central point of the IPR. A DI >1.0 indicated a large dispersion of scores and therefore no consensus. The smaller the DI, the less dispersion, meaning a stronger consensus. The level of dispersion was illustrated by boxplots. The colour of the boxplots refers to the median score (1-3 red; 4-6 orange; 7-9 green). Grey reflects 'no consensus'.

Results/Discussion

Molecular targeting methods for PCa surgery

The panel participants concurred that PSMA is, to date, the best available molecular target (median 9.0) (Figure 1a) but other targets should continue to be explored (median 8.0).

For a surgical roadmap, the panel participants agreed on the use of PSMA-ligand PET scans, ideally undertaken less than 1 month prior to PSMA-targeted surgery (Figure 2a/b). It was agreed that both ^{18}F- and ^{68}Ga-PSMA-ligand PET tracers can be used interchangeably (median 7.5), thereby addressing the plurality of available PSMA-ligand PET tracers [15]. PSMA-ligand PET could be used to indicate the target location prior to surgery and provide a roadmap to support surgical navigation. While PET was the leading modality in PSMA-targeted surgery, an additional PSMA-ligand SPECT was also considered of value (median 7.0) (Figure 2a). A secondary roadmap (either PET or SPECT), acquired the day before surgery or on the day of surgery, was scored to be of neutral additional value (median 6.0). Overall, the lesions identified at preoperative imaging were considered leading for PSMA-targeted surgery. The intraoperative identification of additional lesions was considered a bonus as it may support the identification of lesions <3mm since these are easy to miss on preoperative imaging [16].

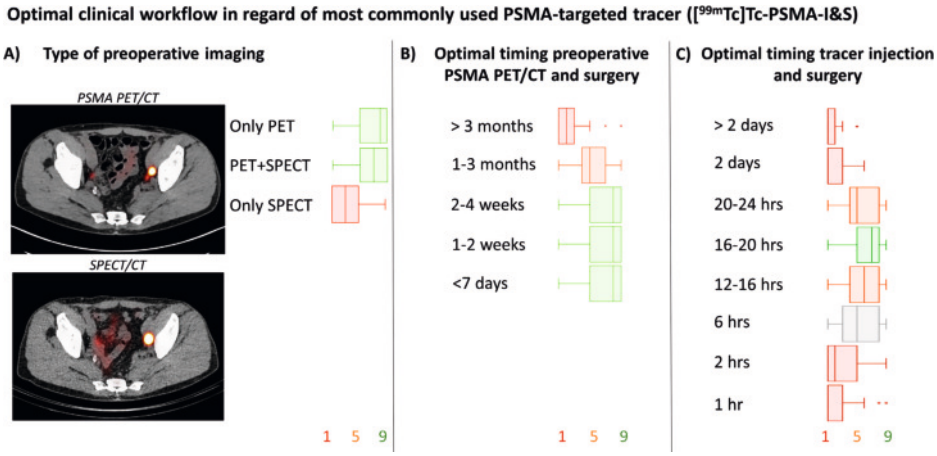

Figure 1. Optimal clinical workflow in regard of most commonly used PSMA-targeted tracer ([^{99m}Tc]Tc-PSMA-I&S) A) Left, top image: PSMA PET/CT, bottom image: SPECT/CT. Right: level of consensus of only SPECT/CT, both PET and SPECT or only SPECT as preferred type of preoperative imaging. B) Level of consensus on optimal timing between preoperative PSMA PET/CT and surgery. C) Level of consensus on optimal timing between tracer injection and surgery. Scale: 9-point Likert scale. Legend: red = disagree (median 1-3), orange = neutral (median 4-6) green = agree (median 7-9), grey = no consensus.

Based on the available data from [^{99m}Tc]Tc-PSMA-I&S, a time range of 16-20h between injection and surgery was regarded as optimal for the clinical workflow (Figure 2c). However, as tracers may differ in imaging signature and pharmacokinetic properties, the timing between injection of the tracer and surgery may differ accordingly and it was agreed that this should be determined for each tracer separately. The panel participants concurred that next to the pharmacokinetics the quantity of PSMA-tracer injected has influence on lesion staining, timing of administration and background signal (median 8.0). A recent study using the fluorescent PSMA analogues OTL78, which used a therapeutic dosing range, indicate that the sensitivity and specificity of staining are highly dependent on the quantity of tracer administered [17].

Indications for PSMA-targeted surgery

Despite the limited evidence provided thus far [4] the panel participants were neutral on the statement that PSMA targeted surgery has already proven its value in routine patient care. Hereby taking into consideration that routine care is depended on the geographical origin of the panel participants.

Use of PSMA targeting strategies differ in clinical requirements and evidence for primary and salvage surgery [4]. Where indicated, the statements therefore addressed primary cancer surgery separately from salvage surgery (Figure 3a). There was consensus on the value of PSMA targeting during nodal identification in both primary and salvage surgery, especially outside the standard surgical template, with the strongest consensus for nodes surrounding the rectum, the bladder and the aortic bifurcation. Despite literature describing use of PSMA targeting for margin detection during primary prostatectomy [8 10 18-20], no consensus was reached on its value (median 6.0, DI=1.01). The view on the value of PSMA-targeting technologies for the assessment of resection margins during salvage prostatectomy was neutral (Figure 3a). Local recurrence, however, was seen as an indication that could benefit from a PSMA-targeted approach. This statement is supported by the recent report of Knipper et al [21].

In general, it was considered valuable to identify lesions that lay deeper below the tissue surface, in addition to the identification of superficial lesions. This is in line with the reliance on PSMA- ligand PET as a surgical roadmap (see clinical workflow, Figure 1b). While there was consensus that PSMA targeting strategies should facilitate open, laparoscopic, and robotic surgery, the consensus on its value in the latter setting was the most evident (median 9.0 with a DI=0.0). This is contrary to the current predominant literature of PSMA-targeted approaches in open surgery [4] (Figure 4a). In particular, (real-time) *in vivo* guidance technologies were considered useful (median 7.0). Complementary value was seen in *ex vivo* specimen analysis (median 8.0). In line with the outcomes reported in a general Delphi consensus on image-guided surgery [13]. In this back-table set-up, the (margins of) excised tumour specimens are analysed for PSMA expressing tissue.

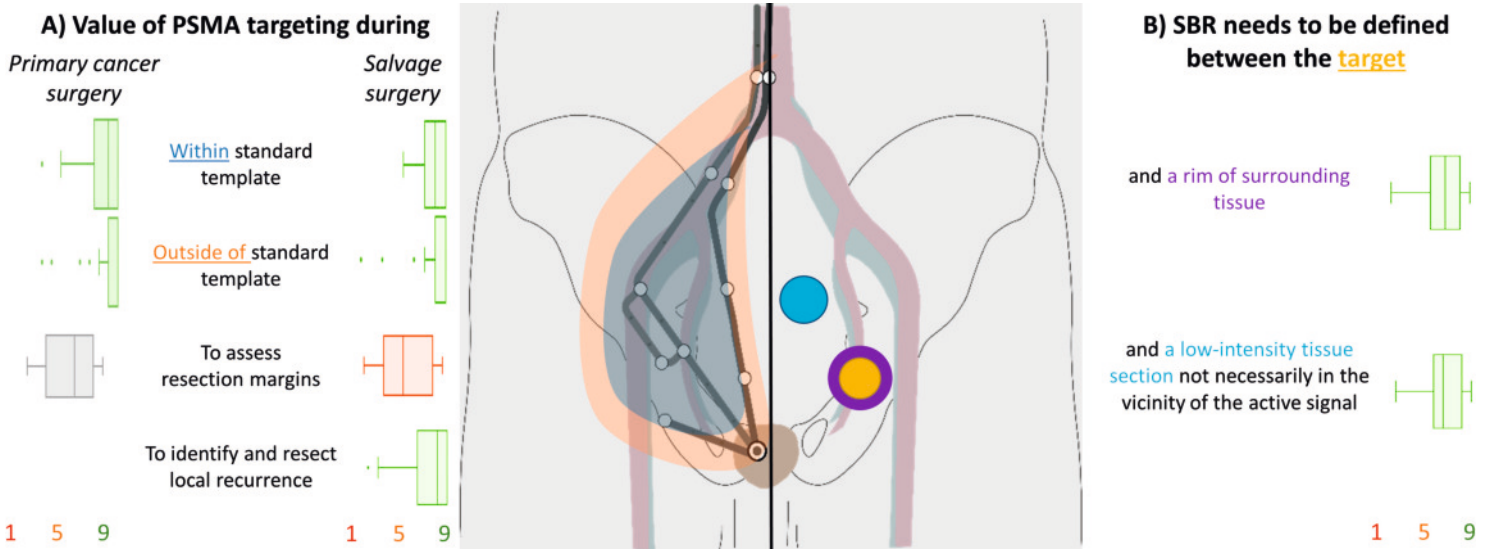

Figure 3. A) Level of consensus on the value of PSMA targeting during primary or salvage surgery in different settings. B) Level of consensus on how to define the Signal-to-background Ratio (SBR). Scale: 9-point Likert scale. Legend: red = disagree (median 1-3), orange = neutral (median 4-6), green = agree (median 7-9), grey = no consensus.

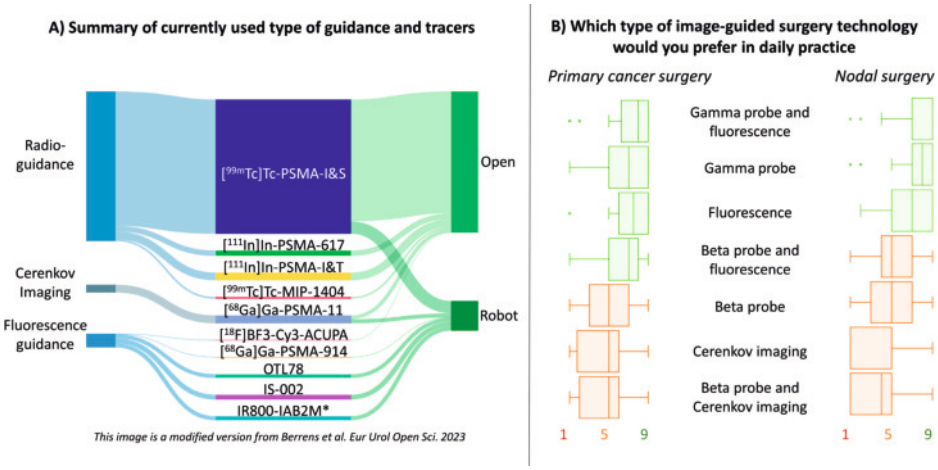

Figure 4. A) Summary of currently used types of PSMA-ligand guidance and their distribution over open and robotic surgery [4]. B) Level of consensus on which type of guidance would be preferred in daily practice (ranked based on declining consensus of nodal surgery) on a 9-point Likert scale. Legend: red = disagree (median 1-3), orange = neutral (median 4-6, green = agree (median 7-9), grey = no consensus. *not yet published.

Guidance modalities

There are a variety of technologies that can be used to help realize PSMA-targeted surgical guidance, ranging from radioactive to optical approaches [9 10 18 22]. While it is often argued that non-ionizing methods are preferred, the panel participants remained neutral when asked whether non-radioactive guidance approaches are preferred over radioactive approaches (median 6.0). Combined with the strong consensus that radioactive PSMA-ligands provide a valid method for PSMA-targeted surgery (median 8.0), this indicates that the exposure to ionizing radiation during guided surgery is not considered to be an issue. It should be noted that this view could be region specific, but radiation burden on patient and personnel for ^{99m}Tc-based technologies is minimal [23 24].

Gamma-emission provides in-depth guidance (>10cm), while fluorescence, Cerenkov, and beta-emission provide superficial guidance (<1 cm) [18 25]. The depth at which a signal can be detected constitutes a fundamental feature for the impact that a technology can offer during either nodal resections (in-depth signal detection most desirable) and primary tumour margin detection (superficial signal detection desirable). When asked which guidance technology was preferred for radical prostatectomy, the panel participants most strongly agreed on the use of a hybrid combination of gamma- and fluorescence-guidance, or fluorescence-guidance only (Figure 4b). Interestingly, panel participants did not reach consensus on whether the in-depth nature of gamma-guidance supported resection margin evaluation. In addition, in primary tumour margin evaluation a hybrid combination of beta- and fluorescence-guidance was valued, while use of a

beta-probe only resulted in a neutral response. Use of Cerenkov also yielded a neutral response, hereby it is worth mentioning that Cerenkov imaging is only employed *ex vivo*. The statements regarding the use of Cerenkov or beta- probes generated exceptionally high cannot answer rates (27-47%). This indicates more education is needed regarding the use of these technologies for PSMA-targeted surgery applications, something recently attempted by Costa et al [26]. The panel participants answered neutral on whether the location of the tumour lesion affects the choice of imaging modality (median 6.0).

When asked which guidance technology was preferred for lymph node dissection, the response changed slightly (Figure 4b). For this indication, there was consensus on the use of gamma- and/or fluorescence-guidance. While lesion location on preoperative imaging was considered essential for the selection of the best imaging modality, there was no consensus on whether the superficial nature of fluorescence imaging allows accurate identification of nodal metastases (median 5.0, DI=1.15). There was a strong consensus to use radio-gamma and hybrid-gamma supporting approaches (median 8.0 and 9.0, respectively) and a neutral view on the use of the hybrid combination of beta- and fluorescence-guidance (median 5.0) or beta probe combined with Cerenkov imaging (median 4.0). Again, only Cerenkov and only beta-emissions scored neutral including a high percentage of "cannot answer" (29-43%).

When asked about what type of readout was preferred (quantitative or qualitative and visual or acoustic) the strongest consensus was on a quantitative and visual image-based readout (median 8.0 and 7.0, respectively). As a quantitative read-out is affiliated with radioguidance (gamma and beta), while an image-based readout is affiliated with optical technologies (fluorescence and Cerenkov), only hybrid approaches appear to tick both boxes.

Besides the choice of a modality, the surgeon's ability to use image-guided technology during surgery also is critical. For example, the integration of the Firefly fluorescence camera in the da Vinci surgical system (Intuitive Surgical, Inc., Sunnyvale, CA, USA) has paved the way for the pursuit of robotic fluorescence-guidance applications [27]. In extension to this, the operating surgeon should be able to autonomously select and control the modalities needed to implement PSMA-targeted surgery instead of e.g. the bedside assistant (median 8.0). There was consensus that guidance modalities are preferably integrated in existing surgical instruments, but it appears that more research is needed on this topic. This need for integration aligns with technical concepts such as intelligent robotics that are currently under investigation [28 29].

Performance assessment

In the gathering of evidence for PSMA-targeted approaches it was agreed that is important to assess the impact on the success of the surgical procedure. Oncological

outcomes (e.g. surgical margins, biochemical recurrence, disease free survival) were defined as the most valuable endpoint (median 9.0), followed by improvement in dexterity and decision-making (median 8.0) and complications (median 7.0). There was a neutral view on the role of length of surgery or blood loss as endpoints (median 5.0). On top of this, the panel participants agreed on the need for technologies that support scoring of proficiency in the use of PSMA-technologies. A trend that is in line with the use of proficiency scoring in urological training programs and the relation between outcomes and surgical quality [30 31].

When asked whether specificity should be central even when sensitivity is reduced, the opinion was neutral (median 6.0) and the answers were scattered (DI=0.97). There was consensus that sensitivity is preferred, even when this reduces specificity (median 7.0). It is worth noting that the widely employed method of ^{99m}Tc-PSMA radioguidance exhibits greater specificity than sensitivity [9 32 33]. Recent studies describe fluorescent PSMA-ligands to exhibit the same, although this was highly dose-dependent [17 34]. Further enquiries revealed that there was a strong consensus that during primary tumour resection false-positive signal needs to be avoided (median 8.0). During lymph node dissection, false positivity was voted on to be less of an issue (median 7.0).

There was consensus on the need to define SBR values during surgery and that these values are critical for decision-making, a finding that is supported by earlier literature [35]. In line with the variations of SBR assessments reported in literature [8 9], there was no consensus on the best way to perform SBR measurements; variations considered were the individual target versus the direct surrounding rim of tissue, or all the targets versus a distant low-intensity tissue (Figure 3b). As SBRs are the driving factor for a surgeon's ability to isolate a target from its background environment, one can question the value of measures that rely on SBRs based on distant low-intensity tissue. Although in current clinical practice the *ex vivo* SBR is often taken into account [32 36], it was agreed that the SBR should be measured *in vivo* (median 8.0). There was a preference for SBR> 2 as cut-off for detection and it was mutually understood there is a need to standardize the way SBRs are measured and reported. Hence it seems more studies are required that address the role of SBR values during PSMA-targeted surgery. During primary tumour resection, background signal coming from the intestines was considered acceptable (median 7.0). On background signal coming from urine, however, no consensus was reached (median 4.0, DI=1.36). Here one should realize that urine can contaminate the operating field during prostatectomy [37]. It should be noted that literature on PSMA-targeted surgery rarely describes the idea, development, exploration, assessment and long-term study (IDEAL) framework criteria [4 38]. Logically adopting the IDEAL criteria would improve standardization.

Before the individual PSMA-targeted surgery strategies put forward in feasibility studies can be accepted as valid treatment option, individual tracers and modalities

need to be independently analysed, preferably in prospective randomized controlled trials (RCTs). Multicentre RCTs with identical procedures (median 9.0), or with the same procedure but different tracers (median 8.0) and different modalities (median 7.0) were considered valuable. There was strong consensus that clinical data acquisition needs to be standardized (median 8.0). The panel participants remained inconclusive, however, on whether the data that is gathered on one specific PSMA-targeting tracer provides sufficient evidence to support the use of alternative PSMA-targeting tracers for the same indication (median 5.0, DI=0.97). Further studies are thus required to define how e.g. higher dose fluorescence approaches [17] relate to micro-dosing based radioguided approaches [7 21 39].

One performance aspect that was considered too early to investigate is the learning curve. This because only a very limited selection of the participants had enough clinical experience to define which metrics define procedural proficiency. In line with the consensus on the value of dexterity and decision-making analysis, studies are now emerging on technologies that can objectively assess these features during PSMA-targeted surgery [40]. Following further growth of performance assessment technologies, the impact of learning curves on PSMA-targeted surgery could be addressed in future consensus activities.

Conclusions

While conducted at an early phase in clinical implementation, the present Delphi consensus project provides guidance for clinicians and researchers that have an interest in pursuing PSMA as a surgical biomarker in PCa. Key stakeholders from urology, nuclear medicine, research, and industry, with experience in PSMA-targeted surgery were involved. As the different participants often applied the technology in a different setting (e.g. primary vs salvage surgery) or using different technologies (e.g. radio-or fluorescence-guided surgery), a balanced view of the field could be provided. This project demonstrated areas of consensus, identified disagreements, highlighted ongoing knowledge gaps, and revealed unanswered clinical needs. Consensus indicated that PSMA-ligand PET/CT is ideally undertaken within one month before surgery. The preferred time between injection of tracer and surgery seems to be 16-20 hours. The timing should, however, be determined per tracer, imaging signature, and in relation to the pharmacokinetics and dosing. *In vivo* guidance and SBR measurements are preferred, with an additional value of *ex vivo* confirmation. Looking at indication, the strongest consensus was found for the use of PSMA-targeted guidance in nodal surgery outside of the template, independent of primary or salvage setting. As imaging modality, a hypothetical hybrid combination of gamma- and fluorescence guidance yielded the strongest consensus. The answers also clearly indicated knowledge gaps in areas such as Cerenkov, the use of beta-emission or their combination (high percentages of “cannot answer”), suggesting more education and research is needed to assess the

value of these unconventional approaches. Regarding the value of PSMA as biomarker in surgical margin assessment, the view was neutral or inconclusive. Again, indicating more evidence is needed before widespread clinical implementation is pursued. For gathering evidence, the field should move beyond feasibility and future emphasis should be on well-designed RCTs with the same procedures using standardized values, and relevant endpoints to improve outcomes in patients receiving surgical treatment for their PCa. This Delphi consensus project provides a valuable reference by addressing clinical needs and recommendations for research and clinical trials.

References

1. Fendler WP, Eiber M, Beheshti M, et al. PSMA PET/CT: joint EANM procedure guideline/SNMMI procedure standard for prostate cancer imaging 2.0. Eur J Nucl Med Mol Imaging 2023;50(5):1466-86.
2. Perera M, Papa N, Roberts M, et al. Gallium-68 Prostate-specific Membrane Antigen Positron Emission Tomography in Advanced Prostate Cancer-Updated Diagnostic Utility, Sensitivity, Specificity, and Distribution of Prostate-specific Membrane Antigen-avid Lesions: A Systematic Review and Meta-analysis. Eur Urol 2020;77(4):403-17.
3. Mottet N, van den Bergh RCN, Briers E, et al. EAU- EANM-ESTRO-ESUR-SIOG Guidelines on Prostate Cancer-2020 Update. Part 1: Screening, Diagnosis, and Local Treatment with Curative Intent. Eur Urol 2021;79(2):243-62.
4. Berrens AC, Knipper S, Marra G, et al. State-of- the-art in Prostate Specific Membrane Antigen (PSMA)-targeted surgery– a systematic review Eur urol Open Science 2023;54:43-55.
5. Robu S, Schottelius M, Eiber M, et al. Preclinical Evaluation and First Patient Application of 99mTc-PSMA-I&S for SPECT Imaging and Radioguided Surgery in Prostate Cancer. J Nucl Med 2017;58(2):235-42.
6. Horn T, Kronke M, Rauscher I, et al. Single Lesion on Prostate-specific Membrane Antigen-ligand Positron Emission Tomography and Low Prostate-specific Antigen Are Prognostic Factors for a Favorable Biochemical Response to Prostate-specific Membrane Antigen-targeted Radioguided Surgery in Recurrent Prostate Cancer. Eur Urol 2019;76(4):517-23.
7. Knipper S, Mehdi Irai M, Simon R, et al. Cohort Study of Oligorecurrent Prostate Cancer Patients: Oncological Outcomes of Patients Treated with Salvage Lymph Node Dissection via Prostate-specific Membrane Antigen- radioguided Surgery. Eur Urol 2023;83(1):62-69.
8. Gondoputro W, Scheltema MJ, Blazevski A, et al. Robot-Assisted Prostate-Specific Membrane Antigen-Radioguided Surgery in Primary Diagnosed Prostate Cancer. J Nucl Med 2022;63(11):1659-64.
9. Maurer T, Weirich G, Schottelius M, et al. Prostate-specific membrane antigen-radioguided surgery for metastatic lymph nodes in prostate cancer. Eur Urol 2015;68(3):530-4.
10. Darr C, Harke NN, Radtke JP, et al. Intraoperative (68)Ga-PSMA Cerenkov Luminescence Imaging for Surgical Margins in Radical Prostatectomy: A Feasibility Study. J Nucl Med 2020;61(10):1500- 06.
11. van der Poel HG, Wit EM, Acar C, et al. Sentinel node biopsy for prostate cancer: report from a consensus panel meeting. BJU Int 2017;120(2):204-11.
12. Fanti S, Goffin K, Hadaschik BA, et al. Consensus statements on PSMA PET/CT response assessment criteria in prostate cancer. Eur J Nucl Med Mol Imaging 2021;48(2):469-76.
13. Dell'Oglio P, Mazzone E, Buckle T, et al. Precision surgery: the role of intra-operative real-time image guidance - outcomes from a multidisciplinary European consensus conference. Am J Nucl Med Mol Imaging 2022;12(2):74-80.
14. Fitch K, Bernstein SJ, Aguilar MD, et al. The RAND/UCLA Appropriateness Method User's Manual. In: Corporation R, ed. Santa Monica, CA, 2001.
15. Niaz MJ, Sun M, Skafida M, et al. Review of commonly used prostate specific PET tracers used in prostate cancer imaging in current clinical practice. Clin Imaging 2021;79:278-88.
16. Maurer T, Gschwend JE, Rauscher I, et al. Diagnostic Efficacy of (68)Gallium-PSMA Positron Emission Tomography Compared to Conventional Imaging for Lymph Node Staging of 130 Consecutive Patients with Intermediate to High Risk Prostate Cancer. J Urol 2016;195(5):1436-43.

17. Stibbe JA, de Barros HA, Linders DGJ, et al. First- in-patient study of OTL78 for intraoperative fluorescence imaging of prostate-specific membrane antigen-positive prostate cancer: a single-arm, phase 2a, feasibility trial. Lancet Oncol 2023;24(5):457-67.
18. Collamati F, van Oosterom MN, De Simoni M, et al. A DROP-IN beta probe for robot-assisted (68)Ga-PSMA radioguided surgery: first *ex vivo* technology evaluation using prostate cancer specimens. EJNMMI Res 2020;10(1):92.
19. olde Heuvel J, de Wit-van der Veen BJ, van der Poel HG, et al. (68)Ga-PSMA Cerenkov luminescence imaging in primary prostate cancer: first-in-man series. Eur J Nucl Med Mol Imaging 2020;47(11):2624-32.
20. Eder AC, Omrane MA, Stadlbauer S, et al. The PSMA-11-derived hybrid molecule PSMA-914 specifically identifies prostate cancer by preoperative PET/CT and intraoperative fluorescence imaging. Eur J Nucl Med Mol Imaging 2021;48(6):2057-58.
21. Knipper S, Ascalone L, Ziegler B, et al. Salvage Surgery in Patients with Local Recurrence After Radical Prostatectomy. Eur Urol 2021;79(4):537- 44.
22. Aras O, Demirdag C, Kommidi H, et al. Small Molecule, Multimodal, [(18) F]-PET and Fluorescence Imaging Agent Targeting Prostate- Specific Membrane Antigen: First-in-Human Study. Clin Genitourin Cancer 2021;19(5):405- 16.
23. Bunschoten. Tracers applied in radioguided surgery. In: Herrmann K, Nieweg O, Povoski S, eds. Radioguided surgery: current applications and innovative directions in clinical practice. , 2016.
24. Aalbersberg EA, Verwoerd D, Mylvaganan- Young C, et al. Occupational Radiation Exposure of Radiopharmacy, Nuclear Medicine, and Surgical Personnel During Use of [(99m)Tc]Tc- PSMA-I&S for Prostate Cancer Surgery. J Nucl Med Technol 2021;49(4):334-38.
25. Ciarrocchi E, Belcari N. Cerenkov luminescence imaging: physics principles and potential applications in biomedical sciences. EJNMMI Phys 2017;4(1):14.
26. Costa PF, Shi K, Holm S, et al. Surgical radioguidance with beta-emitting radionuclides; challenges and possibilities: A position paper by the EANM. Submitted 2023.
27. Meershoek P, KleinJan GH, van Willigen DM, et al. Multi-wavelength fluorescence imaging with a da Vinci Firefly-a technical look behind the scenes. J Robot Surg 2021;15(5):751-60.
28. Zhu J, Lyu L, Xu Y, et al. Intelligent Soft Surgical Robots for Next-Generation Minimally Invasive Surgery. Advanced Intelligent Systems 2021;3(5):2100011.
29. Wendler T, van Leeuwen FWB, Navab N, van Oosterom MN. How molecular imaging will enable robotic precision surgery. Eur J Nucl Med Mol Imaging 2021;48:4201-24.
30. Vanlander AE, Mazzone E, Collins JW, et al. Orsi Consensus Meeting on European Robotic Training (OCERT): Results from the First Multispecialty Consensus Meeting on Training in Robot-assisted Surgery. Eur Urol 2020;78(5):713-16.
31. Hung AJ, Chen J, Jarc A, Hatcher D, Djaladat H, Gill IS. Development and Validation of Objective Performance Metrics for Robot-Assisted Radical Prostatectomy: A Pilot Study. J Urol 2018;199(1):296-304.
32. Maurer T, Robu S, Schottelius M, et al. (99m)Technetium-based Prostate-specific Membrane Antigen-radioguided Surgery in Recurrent Prostate Cancer. Eur Urol 2019;75(4):659-66.
33. de Barros HA, van Oosterom MN, Donswijk ML, et al. Robot-assisted Prostate-specific Membrane Antigen-radioguided Salvage Surgery in Recurrent Prostate Cancer Using a DROP-IN Gamma Probe: The First Prospective

Feasibility Study. Eur Urol 2022;82(1):97-105.

34. Nguyen H, Alexander A, van den Berg N, et al. Preliminary phase 1 safety and efficacy results of a prostate specific membrane antigen (psma) targeting fluorophore in patients undergoing robotic prostatectomy. Journal of Urology 2021;206:e1067.
35. Azargoshasb S, Boekestijn I, Roestenberg M, et al. Quantifying the Impact of Signal-to- background Ratios on Surgical Discrimination of Fluorescent Lesions. Mol Imaging Biol 2023;25(1):180-89.
36. Rauscher I, Duwel C, Wirtz M, et al. Value of (111) In-prostate-specific membrane antigen (PSMA)-radioguided surgery for salvage lymphadenectomy in recurrent prostate cancer: correlation with histopathology and clinical follow-up. BJU Int 2017;120(1):40-47.
37. van Leeuwen FW, van der Poel HG. Surgical Guidance in Prostate Cancer: "From Molecule to Man" Translations. Clin Cancer Res 2016;22(6):1304-6.
38. Ergina PL, Barkun JS, McCulloch P, Cook JA, Altman DG. IDEAL framework for surgical innovation 2: observational studies in the exploration and assessment stages. BMJ 2013;346(jun18 3):f3011-f11.
39. Gandaglia G, Mazzone E, Stabile A, et al. Prostate-specific membrane antigen Radioguided Surgery to Detect Nodal Metastases in Primary Prostate Cancer Patients Undergoing Robot-assisted Radical Prostatectomy and Extended Pelvic Lymph Node Dissection: Results of a Planned Interim Analysis of a Prospective Phase 2 Study. Eur Urol 2022;82(4):411-18.
40. Azargoshasb S, de Barros HA, Rietbergen DDD, et al. Artificial Intelligence-Supported Video Analysis as a Means to Assess the Impact of DROP-IN Image Guidance on Robotic Surgeons: Radioguided Sentinel Lymph Node versus PSMA- Targeted Prostate Cancer Surgery. Advanced Intelligent Systems 2023;5(10):2300192.

Supplementary 1. Panel participants' characteristics

Working as, n (%)	
Clinician	63 (73.3)
Industry	7 (8.1)
Scientist	14 (16.3)
Other (please specify) [a]	2 (2.3)
Background, n (%)	
Nuclear Medicine	19 (22.1)
Pathology	1 (1.2)
Radiology	2 (2.3)
Urology	49 (57.0)
Other (please specify) [b]	15 (17.4)
Gender, n (%)	
Male	67 (77.9)
Female	19 (22.1)
Origin, n (%)	
Europe	71 (82.6)
the Middle East	4 (4.7)
North America	5 (5.8)
Oceania	4 (4.7)
South America	2 (2.3)
Years of experience (IQR)	
In own field	15 (9-20)
With PSMA	3.25 (1-5)

[a] Radiopharmacist/clinical scientist and trial investigator
[b] Chemistry/Technical Medicine/Physics/Molecular Imaging/Pharmacy
IQR = Interquartile Range, PSMA = Prostate-specific membrane antigen

Supplementary 2. Statements round 1

Nr	Statement
1	PSMA is, so far, the best available molecular target for identifying prostate cancer
2	In pursuit of precision prostate cancer identification, we should continue to explore imaging targets alternative to PSMA, e.g. Bombesin
3	Preoperative imaging e.g. PSMA-PET provides a surgical roadmap and as such opens the way for so-called surgical navigation (e.g. image-guided surgery)
4	When PSMA targeted surgery is considered, preoperative imaging roadmaps should be used to highlight the target location
	Preoperative identification of PSMA-positive lesions can be based on:
5	only PET (PET/CT, PET/MRI etc)
6	only SPECT
7	the combination of PET and SPECT
8	either one
9	other
10	A secondary preoperative image (PET or SPECT), taken the day before surgery or at the day of surgery, adds value to the diagnostic PET (or SPECT) image (often taken weeks prior to surgery)
	The timing between the diagnostic evaluation with PSMA -PET and PSMA-targeted surgery can be:
11	≥3 months
12	1-3 months
13	2-4 weeks
14	1-2 weeks
15	≤7 days
	PSMA-targeted strategies should facilitate:
16	open surgery
17	laparoscopic surgery
18	robot-assisted surgery
	PSMA targeting has potential to provide value:
19	during primary radical prostatectomy: to assess resection margins
20	during primary lymph node dissection: metastases directed surgery of lymph nodes within standard ePLND template
21	during primary lymph node dissection: metastases directed surgery of lymph nodes outside of standard ePLND template
22	during salvage prostatectomy: to assess resection margins
23	during salvage lymph node dissection: metastases directed surgery of lymph nodes within standard template
24	during salvage lymph node dissection: metastases directed surgery of lymph nodes outside of standard template
25	during salvage surgery: To identify/resect a local prostate cancer recurrence
	Which kind of image-guided surgery technology would you prefer to use in daily clinical practice? For radical prostatectomy:
26	gamma probe (possibly with navigation)
27	beta probe (possibly with navigation)
28	fluorescence imaging
29	Cerenkov imaging (possibly with navigation)
30	combination of gamma probe and fluorescence (possibly with navigation)
31	combination of beta probe and fluorescence (possibly with navigation)
32	combination of beta probe and Cerenkov (possibly with navigation)
33	depends on the location of the lesion as defined on preoperative imaging
34	none of the above
	Which kind of image-guided surgery technology would you prefer to use in daily clinical practice? For lymph node dissection:
35	gamma probe (possibly with navigation)
36	beta probe (possibly with navigation)

Nr	Statement
37	fluorescence imaging
38	Cerenkov imaging (possibly with navigation)
39	combination of gamma probe and fluorescence (possibly with navigation)
40	combination of beta probe and fluorescence (possibly with navigation)
41	combination of beta probe and Cerenkov (possibly with navigation)
42	depends on the location of the lesion as defined on preoperative imaging
43	none of the above
44	There is a difference in the preferred image-guided surgery technology in primary or salvage lymph node dissection.
	PSMA-targeted lymph node dissection would be valuable in lymph nodes located
45	within the dissection template (e.g. internal and external iliac + obturator)
46	presacral
47	pararectal
48	paravesical
49	at aortic bifurcation and common iliac vessels
50	above aortic bifurcation
51	The timing between injection of the tracer used for surgical guidance and actual surgical procedure depends on the tracer
	Most commonly used in PSMA-targeted surgery is [99mTc]Tc-PSMA-I&S what would be the most optimal timeframe between injection and surgery in regard of clinical workflow?:
52	>2 days
53	2 days
54	24 hours
55	12 hours
56	6 hours
57	2 hours
58	1 hour
59	More evidence is needed to support recommendations on timing
	When implemented in routine surgical procedure. Image-guided surgery modalities are preferably:
60	separate tools additional to the standard robotic tools (e.g. dedicated optical camera or (gamma/beta) probe
61	integrated in existing surgical tools (e.g. camera of the robot, standard robotic tools such as grasper, forceps, scissors)
62	Radioactive PSMA-agents provide a valid image-guided surgical technique despite the potential difficulties in getting such tracers into the OR, e.g. due to the radiation exposure
63	Due to the lack of radiation exposure, non-radioactive image guidance approaches are preferred over radioactive approaches
	Intraoperative identification of additional PSMA positive lesions, that were not defined at diagnostic or preoperative imaging (PSMA-PET/PSMA-SPECT), is considered to be:
64	A bonus as the primary aim of PSMA-targeted surgery is to remove preoperatively defined PSMA avid lesions
65	Desirable as preoperative imaging is unable to accurately diagnose lesions < 3mm
66	Required to demonstrate value for PSMA-targeted surgery
	Intraoperatively there is:
67	a demand for technologies that help identify superficially located lesions (<1 cm beneath the surface)
68	a demand for technologies that help identify also deeper lying lesions
69	a demand for technologies that are able to do both: help identify superficially and deeper lying lesions
	In PSMA-targeted surgery:
70	*in vivo* directional guidance is more desirable than obtaining *ex vivo* confirmation
71	*ex vivo* confirmation is more valuable than obtaining real-time *in vivo* directional guidance
72	both *in vivo* guidance and *ex vivo* confirmation are required
73	During surgery, qualitative readout of the accumulated signal intensity is sufficient
74	During surgery, a quantitative readout of the accumulated signal intensity is desirable
75	An image- based readout of the tracer accumulation in the lesion is required

Nr	Statement
76	Visual (image-based) feedback is preferred over sensory acoustic/numerical feedback
77	During surgery it is required to accurately define signal to background ratios.
	Signal to background values:
78	are critical for surgical decision making
79	need to be defined between the target and a rim of surrounding tissue, as the reference will vary for each PSMA-positive target
80	need to be defined between the target and a low-intensity tissue section not necessarily in the vicinity of the active signal, giving a single reference for al PSMA-positive targets
81	Ideally a quantitative cut-off such as signal to background ratio or minimum signal intensity (e.g. counts) is used to determine whether tissue should be resected or not
	The minimal cutoff for the signal to background ratio during PSMA targeted surgery is a
82	signal to background ratio > 1.5
83	signal to background ratio >2.0
84	signal to background ratio = >3.0
85	The operating surgeon should have autonomy in selecting the modalities needed to implement image guided surgery
86	The operating surgeon should be the one to control the image guiding modality (instead of e.g. the bedside assistant)
87	PSMA targeted surgery has already proven its value in routine patient care and can be implemented in routine care
88	It would be of value to know if and how PSMA-targeted surgery impacts the surgeon's ability to accurately resect tissue (intraoperative performance; dexterity and decision making).
89	Technologies are needed to score the proficiency in use of PSMA-guidance technologies. e.g. automated video-analysis
	The value of PSMA-targeted surgery should be based on the endpoint(s):
90	OR time and blood loss
91	improved surgical dexterity and decision making
92	complications
93	oncological outcomes
94	The evidence gathered for PSMA-targeted surgery is independent of the modality used (radioactive SPECT vs radioactive PET vs fluorescence). Meaning: extensive studies using one specific PSMA-targeted-tracer provide sufficient evidence to support use of alternative PSMA-targeted- tracers
95	Clinical data acquisition needs to be standardized for all PSMA-targeting approaches
	Innovations in PSMA targeted surgery should focus on:
96	realizing a high specificity, even when this reduces the sensitivity
97	realizing a high sensitivity, even when this reduces the specificity
98	PSMA targeted surgery efforts should focus on gathering evidence needed to get the procedure into urological guidelines.
	Acceptance of PSMA targeted surgery as a valid clinical treatment option requires:
99	retrospective single centre cohort studies
100	prospective single centre cohort studies
101	prospective single centre studies using identical clinical procedures
102	prospective multicentre studies using different clinical procedures and a different PSMA-tracer
103	randomized controlled multicentre studies using identical clinical procedures
104	randomized controlled multicentre studies using different clinical procedures but the same PSMA-tracer
105	randomized controlled multicentre studies using different clinical procedures and a different PSMA-tracer

e.g.= example given, ePLND = extended pelvic lymphnode dissection, I&S = imaging and surgery, OR = Operating Room, PET = Positron emission topography, PSMA= Prostate Specific Membrane Antigen, SPECT = Single-photon emission computed tomography, Tc = Technetium

Supplementary 3. Statements round 2

Nr	Statement
1	18F- and 68Ga- tracers for PSMA-PET (such as [18F]DCFPyl, [18F]JK-PSMA-7, [18F]PSMA-1007, [68Ga]Ga-PSMA-11 etc.) can be used interchangeably for preparation of PSMA-targeted surgery
	Acceptance of PSMA-targeted surgery as valid treatment option requires:
2	multicentre randomized controlled trials using the same procedure but different modalities
3	multicentre randomized controlled trials using different procedures and different modalities
4	The superficial nature/low tissue penetration of fluorescence imaging allows accurate PSMA-based nodal metastases identification. (Note: the signal intensity will be much lower than with sentinel node procedures)
5	The in-depth nature/high tissue penetration of gamma imaging allows accurate PSMA-based identification of resection margins? (Note: in depth detection also means the gamma technology is more sensitive to background signals)
6	Optimal timing between tracer administration and surgery should be determined for each tracer separately
7	The quantity of PSMA-agent injected is of influence on the surgical findings, timing of administration and background signal. (note: PSMA-PET tracers are used in a <100microgram/patient dose and some fluorescent agents are used in a > 5mg/patient dose)
	The optimal timing between tracer administration and surgery for clinical implementation is:
8	12-16 hours
9	16-20 hours
10	20-24 hours
11	During primary tumour resection, false-positive signal needs to be avoided to ensure optimal tissue preservation such as nerves
12	During lymph node dissection, false-positive signal is less of a concern as removal of additional nodal tissue is not likely to generate additional complications
13	There is a need to standardize the way signal-to-background values are measured and reported (thus allowing comparison between studies)
14	Signal-to-background values need to be determined *in vivo*
15	Background signal coming from the intestines is acceptable during primary tumour resection
16	Background signal coming from urine is acceptable during primary tumour resection

PET = Positron emission topography, PSMA = Prostate Specific Membrane Antigen

Berrens AC*, Sorbi MA*, Donswijk ML, De Barros HA, Azargoshasb S, van Oosterom MN, Rietbergen DDD, Bekers EM, van der Poel HG, van Leeuwen FWB, van Leeuwen PJ
J Nucl Med. 2024 Apr 1;65(4):548-554
*These authors contributed equally
A translation of this article was published in Tijdschrift voor Urologie
Tijdschr Urol 14, 182–190 (2024)

Chapter 4

Strong Correlation SUV_{max} on PSMA PET/CT and Numerical Drop-In Gamma Probe Signal for Intraoperative Identification of Prostate Cancer Lesions

Abstract

Introduction. Prostate Specific Membrane Antigen (PSMA) Positron Emission Tomography (PET) is used to select recurrent prostate cancer patients for metastasis-directed therapy. A surgical approach can be achieved through radio-guided surgery (RGS), using a drop-in gamma probe that traces lesions that accumulate the radioactive signal. With the aim to guide patient selection for salvage surgery, we studied the correlation between the standardized uptake value (SUV_{max}) of lesions on the preoperative PSMA PET/CT and their intraoperative counts/second measured using the drop-in gamma probe.

Methods. A secondary analysis based on the prospective, single-arm and single-center feasibility study was conducted (NCT03857113). Patients (*n*= 29) with a biochemical recurrence after previous curative- intent therapy and a maximum of three suspicious lesions within the pelvis on preoperative PSMA PET/CT were included. Patients treated with androgen deprivation therapy within 6 months prior to surgery were excluded. All patients received an intravenous injection of ^{99m}Technetium-PSMA-I&S one day before surgery. Radioguidance was achieved using a drop-in gamma probe (Eurorad S.A., Eckbolsheim, France). Correlation was determined using Spearman's correlation coefficient (ρs). Subgroup analysis was based on the median SUV_{max}.

Results. In total, 33 lesions were visible on the PSMA PET/CT with a median overall SUV_{max} of 6.2 (interquartile range [IQR] 4.2-9.7). RGS facilitated removal of 31 lesions. The median drop-in counts/second were 134 (IQR 81-219) *in vivo* and 109 (IQR 72-218) *ex vivo*. Hereby the intensity of the values correlated with the SUV_{max} values (ρs 0.728 and 0.763; p<0.001, respectively). Subgroup analysis based on the median SUV_{max} showed in the SUV_{max} <6 group no statistically significant correlation with the numerical signal *in vivo* (ρs 0.382; p=0.221), or the signal-to-background-ratio (ρs 0.245; p=0.442), whilst the SUV_{max} ≥6 group showed respective statistically significant positive correlations of ρs 0.774 (p<0.001) and ρs 0.647 (p=0.007).

Conclusions. Our findings indicate that there is a direct relation between the SUV_{max} values on PSMA PET/CT and the readout recorded by the surgical drop-in probe. Thereby indicating SUV_{max} values can be used to select patients for PSMA-RGS. For more definitive subgroup definitions for treatment recommendations further studies are necessary to validate present findings.

Introduction

Despite curative intent treatment in primary prostate cancer, recurrences occur in 20-40% [1 2]. Targeting the prostate-specific membrane antigen (PSMA), a protein that is highly overexpressed on the surface of most prostate cancer cells, supports positron emission tomography (PET) imaging. A technology that has substantially enhanced the diagnosis of prostate cancer metastases in intermediate and high-risk primary patients [3]. PSMA PET/CT can detect metastatic lesions in patients with biochemical recurrence at PSA values <0.5 ng/ml [4 5]. Thereby enabling curative metastases directed treatment options like salvage radiotherapy, salvage lymph node dissection and metastasis-directed therapy.

To accommodate PSMA-targeted surgery, gamma-emitting PSMA-ligands have been developed that facilitate image-guided surgery [6 7]. In a PSMA-guided workflow, PSMA PET/CT provides the surgical roadmap and a secondary PSMA-ligand is used to provide intraoperative guidance. Signal intensities of primary tumor on PSMA PET/CT (the maximum standardized uptake value [SUV_{max}]) have been reported to vary substantially [8].

For guidance during surgery the gamma-emitting ^{99m}Technetium (^{99m}Tc)-based tracer, [^{99m}Tc]Tc-PSMA-I&S has been most frequently used[9]. This agent not only facilitates PSMA-ligand single-photon emission computed tomography (SPECT)/CT, albeit with an inferior performance compared to PSMA PET/CT [10 11], but also facilitates intraoperative lesion localization via gamma tracing (counts/second) [12], so-called radioguided surgery (RGS) (Figure 1). Expanding from traditional gamma probes in open surgery [12-15], the introduction of the miniaturized drop-in gamma probe facilitated dissemination of these procedures to robotic surgery [16-19]. Limited research has been conducted on the SUV_{max} in relation to intraoperative numerical signal. While the intraoperative counts/second vary substantially [18 19], there are indications that these values relate to the SUV_{max} values [20].

The aim of this study is to further corroborate the relation between the SUV_{max} at PSMA PET/CT and surgical signal detected using [^{99m}Tc]Tc-PSMA-I&S. Ultimately, the goal is to identify cut-off values that can be used to refine selection criteria for PSMA-targeted RGS.

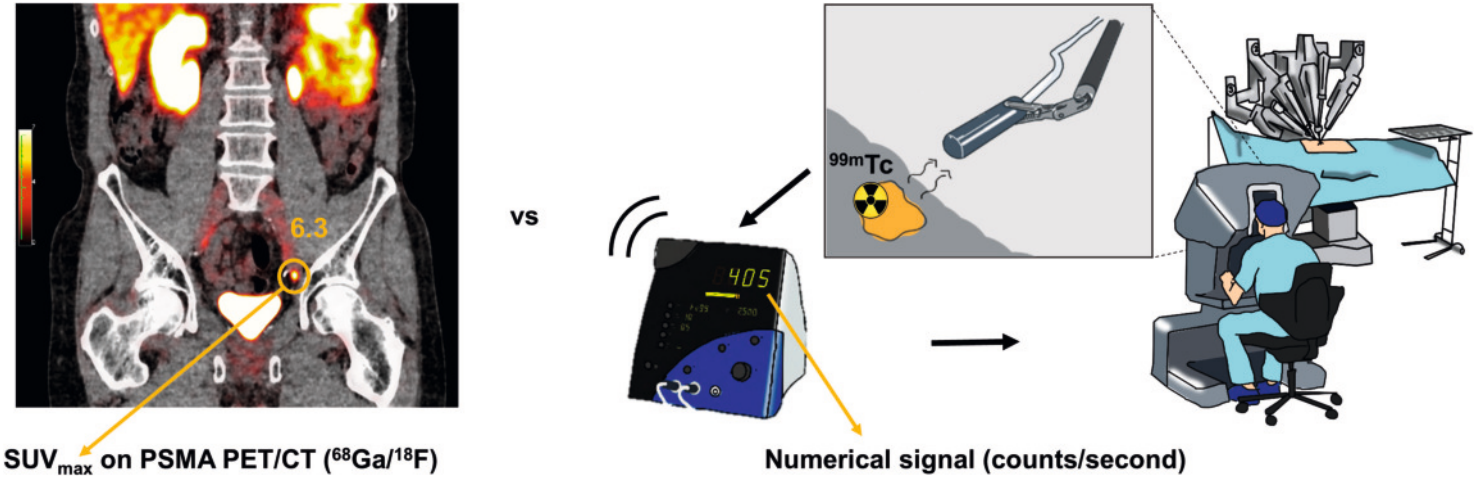

Figure 1. Illustration of PSMA PET/CT versus the numerical signal (counts/second) as seen by the operating surgeon during robot assisted surgery.

Methods

Study design and patient population

A secondary analysis was performed on data of a prospective, single-center, feasibility study that was approved by the local ethics committee at the Netherlands Cancer Institute, Amsterdam, the Netherlands (ClinicalTrials.gov: NCT03857113). All subjects signed a written informed consent. The institutional review board approved this retrospective study (IRBdm21-106). Patients were included in case of biochemical recurrence (PSA between 0.2 and 4 ng/ml at two consecutive measurements) after previous curative intent treatment and a maximum of three soft-tissue lesions (local or nodal recurrences) on PSMA PET/CT. Patients were excluded in case of ongoing androgen deprivation therapy or within 6 months prior to surgery. Patients were treated with robot-assisted ^{99m}Tc-PSMA- targeted salvage RGS between June 2020 and November 2022 [19].

Preoperative imaging and analysis

All patients underwent a PSMA PET/CT scan within Prostate Cancer Network the Netherlands ('Prostaatkankernetwerk Nederland'). Patients were scanned using the ^{68}Ga-bound tracer [^{68}Ga]Ga- PSMA-11 or one of the ^{18}F-labelled tracers [^{18}F]DCFPyl and [^{18}F]JK-PSMA-7 within 125 days before RGS, according to local protocols. Two experienced nuclear medicine physicians (M.L.D, D.D.D.R) reevaluated the first part of preoperative imaging of included patients using Osirix MD (Pixmeo SARL, Switzerland). After comparison and no difference was seen one reevaluated the remaining. On preoperative PSMA PET/CT the SUV_{max} of lesions noted in the clinical report was determined by drawing a volume-of-interest over the lesions. The short-axis diameter of the morphological substrate, if visible on concurrent CT, was measured.

One day before surgery, a single dose of [^{99m}Tc]Tc-PSMA-I&S (Median 541; interquartile range [IQR] 482-559) was injected intravenously and assessed by performing SPECT/CT after a median of 17 h (IQR 17.3-17.8), at the morning of surgery. The preoperative scintigraphy was reevaluated after blinding from clinical or study related data including the preoperative PSMA PET/CT and intraoperative findings. The number and location of suspicious lesions was noted.

Intraoperative measurements

Within a median of 21 h after injection RGS was performed. All surgical procedures were done using a da Vinci Xi robot (Intuitive Surgical, Sunnyvale, CA, USA). Radioguidance was achieved using a DROP- IN gamma probe (Eurorad S.A., Eckbolsheim, France) translating the radiosignal to the numerical signal. First, radioactivity measurements of anatomical landmarks near target prostate cancer lesions (i.e., iliac artery, iliac vein, psoas muscle) were performed to determine the background signal. Second, the location of the suspected prostate cancer lesions were scanned *in vivo* with the drop-in probe to

assess the signal-to-background-ratio (SBR). To confirm successful removal of radioactive tissue *ex vivo* validations were performed using the drop-in probe. A detailed description of the surgical procedures can be found in de Barros et al. 2022 [19].

Histopathological evaluation and Immunohistochemistry

All dissected specimens were sent for histopathological examination with hematoxylin and eosin staining and, if needed, immunohistochemical pancytokeratin AE13 (CK AE1/3) staining. On prostate cancer positive tissues additional immunohistochemical PSMA staining was performed (Clone 3E6; Dako, Carpinteria, CA, USA) to assess the PSMA intensity. The total immunostaining score (TIS) was calculated using:

TIS = the proportion score (PS) x corresponding intensity scores (IS)

The PS represented the percentage of cells that stained positive with a particular intensity and could range between 0 and 100%. The IS represented the intensity of the stained cells and could range between 0 and 3 (0 = no staining; 1 = weak; 2 = moderate; 3 = strong). One pathologist (E.M.B) analyzed all intraoperative obtained tissues. The size of the node was measured in the long axis. The TIS of each tumor-positive region was correlated with the SUV_{max} and the numerical signal of the *in* and *ex vivo* measurements.

Statistical analysis

Data were summarized by frequency and percentage for categorical variables and mean and median with ranges for continuous variables. The numerical signal was normalized to account for differences in injected activity of ^{99m}Tc, using the average injected dose as the standard (550 MBq). For continuous variables normality of distribution was verified with Kolmogorov-Smirnov test. The primary outcome of interest was the correlation of the SUV_{max} of the prostate cancer lesions at pre-operative PSMA PET/CT and the *in vivo* numerical signal recorded with the drop-in probe of the PSMA-positive prostate cancer lesions. Secondary the *ex vivo* signal and the PSMA intensity on histopathology's correlation with the SUV_{max}. All were analyzed using Spearman's rank correlation coefficient (ρs) to determine the correlation. To evaluate the visual perception of a potential correlation, a scatterplot was produced. The different PSMA PET-tracers were compared using a Kruskal-Wallis statistical test and the SPECT/CT subgroups were compared using a Mann-Whitney-U statistical test. To identify meaningful subgroups for clinical applicability median regression with concave fusion penalizations was used [21]. $P < 0.05$ was considered statistically significant. Statistical analysis was carried out with IBM SPSS Statistics V29.0 (SPSS INC., Chicago, Ill).

Results

Patient characteristics

Following staging on PSMA PET/CT, 29 patients who had suspicion of nodal disease (n=25) or locally recurrent prostate cancer (n=4) were included (Figure 2). As primary treatment, 21 patients (72%) underwent radical prostatectomy and eight (28%) radiotherapy. Subsequently, 13 patients (45%) underwent salvage therapy before ^{99m}Tc-PSMA RGS (Table 1).

Table 1. Patient characteristics

Parameter	Result
Median age at ^{99m}Tc-PSMA-RGS (IQR), years	68 (66-72)
Previous primary treatment, n (%)	
RALP	4 (14)
RALP + ePLND	17 (59)
EBRT	2 (7)
EBRT + HT	5 (17)
Brachytherapy	1 (3)
Previous salvage treatment, n (%)	
Radiotherapy fossa	5 (17)
Radiotherapy prostate + pelvis	3 (10)
Salvage prostatectomy + LND	1 (3)
Radiotherapy pelvis	1 (3)
Radiotherapy fossa + SLND	1 (3)
Radiotherapy fossa + lutetium PSMA	1 (3)
Radiotherapy prostate + pelvis + previous SLND	1 (3)
No previous salvage treatment	16 (55)
Type of recurrence, n (%)	
Nodal	25 (86)
Local	4 (14)
PSA before ^{99m}Tc-PSMA-RGS, median (IQR)	0.91 (0.5-2.4)
Number of positive lesions on PSMA PET/CT, n (%)	
1 lesion	25 (86)
2 lesions	4 (14)

PSMA = prostate-specific membrane antigen; RGS = radio guided surgery; IQR = interquartile range; RALP = robot-assisted laparoscopic prostatectomy; ePLND = extended pelvic lymph node dissection; EBRT = external beam radiation therapy; HT = hormone therapy; (S)LND = (salvage) lymph node dissection.

Preoperative imaging and analysis

A total of 33 PSMA avid lesions were identified in the pre-operative PSMA PET/CT. The overall median SUV_{max} on preoperative PSMA PET/CT was 6.2 (IQR 4.2-9.7) and did not differ between the different tracers (p=0.559) (detailed description in table 2). 97% of the PSMA PET/CT scans were conducted on a European Association of Nuclear Medicine Research Ltd (EARL) accredited system [22 23]. Twenty- seven of the 33 (82%) identified lesions were <1cm, with a median size of 4 mm (IQR 3.8-6). The size of the PSMA PET/CT avid lesion was significantly correlated to the SUV_{max} (ρs 0.728; p <0.001). The PSA

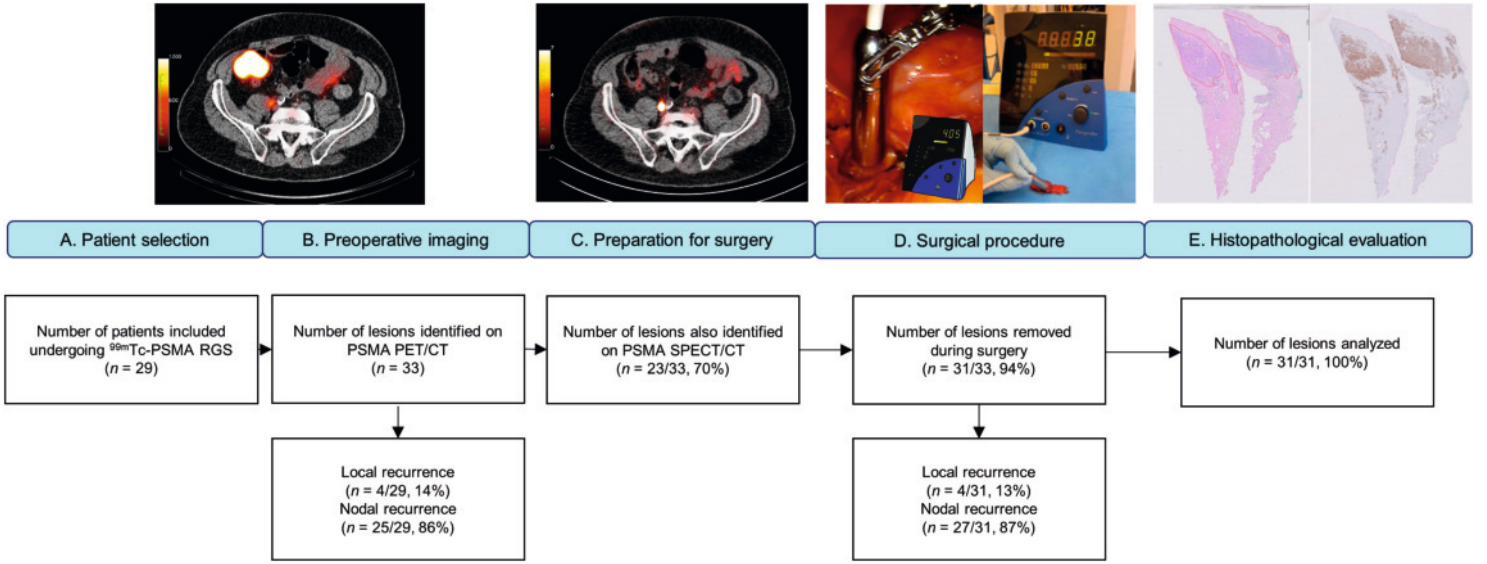

Figure 2. Workflow and inclusions. A) Patient selection for salvage ^{99m}Tc-PSMA-radioguided surgery B) Preoperative PSMA PET/CT and C) [^{99m}Tc]Tc-PSMA-I&S imaging demonstrate a para-iliac lesion in a patient with biochemical recurrence. D) Intraoperative radioactivity measurements with the drop-in probe. E) Immunohistochemistry (PSMA staining) at histopathological examination.

before RGS showed a weak, non-significant correlation with the SUV_{max} (ρs 0.2041; p=0.289), as did the PSA density (defined as PSA before surgery multiplied by the size of the lesion(s) on PSMA PET/CT) (ρs 0.390; p=0.073).

Out of the 33 lesions found on PSMA PET/CT, 23 lesions (70%) were observed on PSMA-I&S SPECT/CT and 10 (30%) were not. Within the group of lesions that were not visible on SPECT/CT, the median SUV_{max} value was 4.9 (IQR 3.3-6.4), while the group of lesions visible on SPECT/CT had a median SUV_{max} value of 7.4 (IQR 5.3-14.3) (p=0.028). The visibility on SPECT/CT was not associated with a higher numerical signal *in vivo* (p=0.237) or a higher SBR (p=0.453).

Table 2. Characteristics of diagnostic preoperative imaging and preparation for surgery

Parameter	Result
Diagnostic preoperative Imaging	
Type PSMA PET/CT, n (%)	
[^{68}Ga]Ga-PSMA	6 (21)
[^{18}F]DCFPyL	13 (45)
[^{18}F]JK-PSMA-7	10 (34)
Median incubation time (IQR), minutes	58 (50-61)
[^{68}Ga]Ga-PSMA	49 (44-52)
[^{18}F]DCFPyL	58 (56-61)
[^{18}F]JK-PSMA-7	61 (58-74)
Median dose of PSMA PET/CT tracer (IQR), MBq	197 (161-201)
[^{68}Ga]Ga-PSMA	146 (134-159)
[^{18}F]DCFPyL	180 (164-203)
[^{18}F]JK-PSMA-7	201 (200-202)
Median SUV_{max} of suspect lesion on PSMA PET/CT overall, (IQR)	6.2 (4.2-9.8)
[^{68}Ga]Ga-PSMA	7.7 (3.0-11.6)
[^{18}F]DCFPyL	5.5 (4.2-9.1)
[^{18}F]JK-PSMA-7	6.4 (4.8-16.2)
Median time from PSMA PET/CT to OR (IQR), days	33 (15-50)
Median size suspect lesion on PSMA PET/CT (IQR), mm	4 (3.8-6.0)
Size suspect lesion on PSMA PET/CT, n (%)	
<1cm	27 (81)
≥1cm	4 (12)
Not measurable	2 (6)
EARL accreditation for PSMA PET/CT, n (%)	
Yes	28 (97)
No	1 (3)
Preparation for surgery	
Median dose of ^{99m}Tc-tracer (IQR), MBq	541 (482-559)
Median time from injection ^{99m}Tc-tracer to SPECT/CT (IQR), hours	17.25 (17.25-17.75)
Lesion visible on PSMA PET/CT also visible on SPECT/CT, n (%)	
Yes	23 (70)
No	10 (30)

PSMA PET/CT = prostate-specific membrane antigen positron emission tomography/computed tomography; IQR = interquartile range; OR = operation; SUV = standardized uptake value; Tc = technetium; SPECT/CT = single photon emission computed tomography/computed tomography

Intraoperative

In total 31/33 (94%) lesions were successfully removed during robot-assisted RGS. One suspicious LN could not be localized due to extensive intestinal adhesions (3mm on PSMA PET/CT SUV_{max} 5.3, and one LN (3 mm on PSMA PET/CT, SUV_{max} 1.8) located in the pararectal fat could not be detected due to high background signal in the rectum as a result of hepatobiliary tracer clearance. The numerical signal of the lesion was recorded both in and *ex vivo* (median 134 counts/second (IQR 81-220) and 109 counts/second (IQR 72-219), respectively). The median SBR *in vivo* was 2.3 (IQR 1.7-3.9). No correlation was seen between the duration of the surgery (median 136 minutes; IQR 101-155) and the SUV_{max} (ρs -1.44; p=0.457) or the counts *in vivo* (ρs -1.38; p=0.492).

Correlation SUV_{max} and intraoperative numerical signal

A significant and strong positive correlation was found between the overall SUV_{max} values and the intraoperative measures (Spearman's rank correlation coefficient (ρs) 0.728 and 0.763; p<0.001, for *in vivo* and *ex vivo* respectively) (Figure 3). Median regression analysis identified two subgroups in SUV_{max} values, SUV_{max} <6 and SUV_{max} ≥6. The SUV_{max} <6 group showed no statistically significant correlation (ρs 0.382; p=0.221), whilst the SUV_{max} ≥6 group had a strong statistically significant correlation (ρs 0.774; p<0.001) with the numerical signal *in vivo*. *Ex vivo* showed similar results (SUV_{max} <6 group ρs 0.308; p=0.284 , SUV_{max} ≥6 group ρs 0.752; p<0.001). A very moderate, non-significant, correlation was observed between the size of the lesion on pre-operative PSMA PET/CT and numerical signal *in vivo* (ρs 0.421; p=0.057) and *ex vivo* (ρs 0.492; p=0.015).

Overall, a moderate correlation was found for the SUV_{max} of the prostate cancer lesions at preoperative PSMA PET/CT and the SBR *in vivo* (ρs 0.524; p = 0.004). Subgroup analysis showed no correlation in the group with SUV_{max} <6 (ρs 0.245; p=0.442) and the SBR, whilst a strong correlation was observed for lesions with a SUV_{max} ≥6 (ρs 0.647; p=0.007).

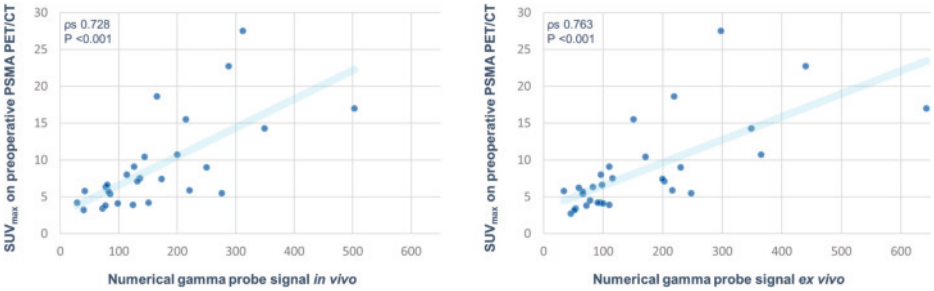

Figure 3. Scatterplot illustrating the correlation between the SUV_{max} on preoperative PSMA PET/CT and in and *ex vivo* numerical signal of the drop-in gamma probe.

Correlation SUV_{max} and PSMA intensity staining

Among the removed lesions, the median TIS was 2.75 (IQR 2.06-3.00) (Table 3). The distribution of PSMA intensity was homogenous in 46% and heterogeneous in 54% of the lesions. The type of distribution had no significant impact on the SUV_{max} (p=0.602). No positive correlation was found between the SUV_{max} and the TIS (ρs -0.433; p=0.015). Multiplying the TIS with the size of the lesion at pathology did not show a correlation with SUV_{max} on preoperative PSMA PET/CT (ρs 0.190; p=0.353).

Table 3. Intraoperative and histopathological outcomes

Parameter	Result
Intraoperative outcomes	
Median time from injection ^{99m}Tc-tracer to OR (IQR), hours	21 (19.75-21.1)
Number of lesions removed during OR, n (%)	31 (94)
Median counts/second drop-in probe *in vivo* (IQR)	134 (81-220)
Median counts/second drop-in probe *ex vivo* (IQR)	109 (72-219)
Median counts/second in suspected lesion to activity in PAV ratio, (IQR)	2.3 (1.7-3.9)
Histopathological outcomes	
Median TIS, (IQR)	2.3 (2.0-3.0)

PSMA = prostate-specific membrane antigen; IQR = interquartile range; OR = operation; PAV = psoas, artery, and vein; TIS = Total Immunostaining Score

Discussion

By directly comparing pre- and intra-operative PSMA-targeting strategies a significant, positive correlation could be established between the SUV_{max} and the drop-in gamma probe measurements. This indicates that there is a greater distinction between the tumor and surrounding structures *in vivo* the higher the SUV_{max} is, suggesting a more reliable roadmap. Lesion identification may seem less straightforward with a lower SUV_{max}, but not impossible since nearly all lesions in the present study were identified and removed. Results are in line with the findings of Gondoputro et al. who performed successful RGS on lesions with median SUV_{max} 4.4) [18]. The SUV_{max} should therefore be considered among various parameters in the case assessment. Not all removed lesions were seen on the preoperative SPECT/CT, which may be due to timing and background interference [11]. Although one might assume that the greater the distinction the shorter the duration of the surgery, current results are inconclusive. This might be explained by other influential factors on the duration such as adhesions, the location of the lesion in regard to its surroundings and the learning curve of the operating surgeon. Two subgroups in SUV_{max} were defined based on median regression that showed clear differences in sensitivity and specificity for SUV_{max} values <6 and ≥6. However, external validation of these findings is needed in larger series since subgroups were not defined a priori. Nevertheless, with an increasing population subjected to oligometastatic treatment by PSMA-RGS [9], definitions of optimal subgroups for RGS are desired.

For clinical applicability it would be less time consuming to base the preoperative assessment on the size of the lesion. This study showed, however, that lesion size was not a significant predictor for the number of intraoperative numerical signal, whilst SUV_{max} appeared to be a strong and significant predictor and should therefore be preferred when selecting patients.

No positive correlation was observed between the SUV_{max} and the PSMA intensity staining defined as the TIS. This could be explained by the fact that the SUV_{max} values varied widely and the TIS mostly ranged from moderate to strong. Another influential factor could be the reporting of lymph node size solely as diameter, and the TIS being evaluated per slide, which omits the consideration of its 3D dimensions. Little is known regarding TIS and SUV_{max} of prostate cancer positive lymph nodes. Looking at radical prostatectomy specimens Rüschoff et al. also described no significant correlation between SUV_{max} on PSMA PET and immunohistochemical PSMA intensity expression [24], whereas Jiao and Vetrone et al. do describe a correlation [25 26], possibly explained by different tumor characteristics and/or growth patterns [8].

Limitations include the high variability in a relatively small number of included patients and the retrospective nature of the secondary analysis. For the scope of this article only PSMA PET/CT positive nodes were included. The inclusion criteria of the prospective study introduce a possible selection bias [19]. The nature of surrounding tissue is always a consideration when measuring radioactivity *in vivo*. To minimize the effect of background signal, in the prospective study the values were documented real-time after careful positioning of the drop-in gamma probe. A limitation remains however, that the surrounding tissue type was not taken into account in this secondary analysis. In addition, the applicability in open surgery was not studied.

Subgroup analysis was performed although subgroups were not specified *a priori*, so inferential issues might emerge. Subgroups based on the median are depended of the cohort and may alter slightly after validation in larger cohorts. Furthermore, although an accurate representation of daily clinical practice, different PSMA PET/CT tracers and systems have been used with different median SUV_{max} values. Although the groups were much smaller, the differences were similar to de Bie et al, where a non-significant higher SUV_{max} of recurrent prostate cancer was seen in the [^{68}Ga]Ga- PSMA-11 group [27]. In addition, all surgical procedures were performed in one tertiary center experienced in the use of ^{99m}Tc-tracers and the drop-in gamma probe.

With the growing implementation of PSMA-RGS and minimally invasive robotic surgery, it is expected that PSMA PET/CT will assume a fundamental role in the selection of patients. Thereby helping to optimize the treatment of patients with oligometastatic prostate cancer recurrence, and perhaps also during primary treatment.

Conclusion

This study shows a positive significant correlation between the SUV_{max} on preoperative PSMA PET/CT and the intraoperative numerical signal measured by the drop-in gamma probe. Thereby indicating SUV_{max} values can be considered as a parameter to select patients for PSMA-RGS. For more definitive subgroup definitions for treatment recommendations further studies are necessary to validate present findings.

References

1. Boorjian SA, Houston Thompson R, Tollefson MK, Rangel LJ, Bergstralh EJ, Blute ML. Long-term risk of clinical progression after biochemical recurrence following radical prostatectomy: the impact of time from surgery to recurrence. European Urology 2011;June(59(6)):893-9.
2. Suardi N, Porter CR, Reuther AM, et al. A nomogram predicting long-term biochemical recurrence after radical prostatectomy. Cancer 2008;112(6):1254-63.
3. Hofman MS, Lawrentschuk N, Francis RJ, et al. Prostate-specific membrane antigen PET-CT in patients with high-risk prostate cancer before curative-intent surgery or radiotherapy (proPSMA): a prospective, randomised, multicentre study. Lancet 2020;395(10231):1208-16.
4. Morigi JJ, Stricker PD, van Leeuwen PJ, et al. Prospective Comparison of 18F-Fluoromethylcholine Versus 68Ga-PSMA PET/CT in Prostate Cancer Patients Who Have Rising PSA After Curative Treatment and Are Being Considered for Targeted Therapy. J Nucl Med 2015;56(8):1185-90.
5. Perera M, Papa N, Roberts M, et al. Gallium-68 Prostate-specific Membrane Antigen Positron Emission Tomography in Advanced Prostate Cancer-Updated Diagnostic Utility, Sensitivity, Specificity, and Distribution of Prostate-specific Membrane Antigen-avid Lesions: A Systematic Review and Meta-analysis. Eur Urol 2020;77(4):403-17.
6. Hensbergen AW, van Willigen DM, van Beurden F, et al. Image-Guided Surgery: Are We Getting the Most Out of Small-Molecule Prostate- Specific-Membrane-Antigen-Targeted Tracers? Bioconjug Chem 2020;31(2):375-95.
7. Derks YHW, van Lith SAM, Amatdjais-Groenen HIV, et al. Theranostic PSMA ligands with optimized backbones for intraoperative multimodal imaging and photodynamic therapy of prostate cancer. Eur J Nucl Med Mol Imaging 2022;49(7):2425-35.
8. Demirci E, Kabasakal L, Sahin OE, et al. Can SUV_{max} values of Ga-68-PSMA PET/CT scan predict the clinically significant prostate cancer? Nucl Med Commun 2019;40(1):86-91.
9. Berrens AC, Knipper S, Marra G, et al. State-of- the-art in Prostate Specific Membrane Antigen (PSMA)-targeted surgery– a systematic review Eur urol Open Science 2023;54:43-55.
10. Koehler D, Sauer M, Klutmann S, et al. Feasibility of (99m)Tc-MIP-1404 for SPECT/CT Imaging and Subsequent PSMA-Radioguided Surgery in Early Biochemically Recurrent Prostate Cancer: A Case Series of 9 Patients. J Nucl Med 2023;64(1):59- 62.
11. Berliner C, Steinhelfer L, Chantadisai M, et al. Delayed Imaging Improves Lesion Detectability in [(99m)Tc]Tc-PSMA-I&S SPECT/CT in Recurrent Prostate Cancer. J Nucl Med 2023;64(7):1036- 42.
12. Maurer T, Weirich G, Schottelius M, et al. Prostate-specific membrane antigen-radioguided surgery for metastatic lymph nodes in prostate cancer. Eur Urol 2015;68(3):530-4.
13. Robu S, Schottelius M, Eiber M, et al. Preclinical Evaluation and First Patient Application of 99mTc-PSMA-I&S for SPECT Imaging and Radioguided Surgery in Prostate Cancer. J Nucl Med 2017;58(2):235-42.
14. Rauscher I, Duwel C, Wirtz M, et al. Value of

(111) In-prostate-specific membrane antigen (PSMA)-radioguided surgery for salvage lymphadenectomy in recurrent prostate cancer: correlation with histopathology and clinical follow-up. BJU Int 2017;120(1):40-47.

15. Kratzik C, Dorudi S, Schatzl M, Sinzinger H. Tc- 99m-PSMA imaging allows successful radioguided surgery in recurrent prostate cancer. Hell J Nucl Med 2018;21(3):202-04.
16. van Leeuwen FWB, van Oosterom MN, Meershoek P, et al. Minimal-Invasive

Robot- Assisted Image-Guided Resection of Prostate- Specific Membrane Antigen-Positive Lymph Nodes in Recurrent Prostate Cancer. Clin Nucl Med 2019;44(7):580-81.

17. Erfani S, Sadeghi R, Aghaee A, Ghorbani H, Roshanravan V. Prostate-Specific Membrane Antigen Radioguided Surgery for Salvage Pelvic Lymph Node Dissection in a Man With Prostate Cancer. Clin Nucl Med 2022;47(2):e174-e76.
18. Gondoputro W, Scheltema MJ, Blazevski A, et al. Robot-Assisted Prostate-Specific Membrane Antigen-Radioguided Surgery in Primary Diagnosed Prostate Cancer. J Nucl Med 2022;63(11):1659-64.
19. de Barros HA, van Oosterom MN, Donswijk ML, et al. Robot-assisted Prostate-specific Membrane Antigen-radioguided Salvage Surgery in Recurrent Prostate Cancer Using a DROP-IN Gamma Probe: The First Prospective Feasibility Study. Eur Urol 2022;82(1):97-105.
20. Azargoshasb S, de Barros HA, Rietbergen DDD, et al. Artificial Intelligence-Supported Video Analysis as a Means to Assess the Impact of DROP-IN Image Guidance on Robotic Surgeons: Radioguided Sentinel Lymph Node versus PSMA- Targeted Prostate Cancer Surgery. Advanced Intelligent Systems 2023;5(10):2300192.
21. Zhang Y, Wang HJ, Zh Z. Robust Subgroup Identification. Statistica Sinica 2019;29:1873-89.
22. Werner RA, Hartrampf PE, Fendler WP, et al. Prostate-specific Membrane Antigen Reporting and Data System Version 2.0. Eur Urol 2023.
23. Aide N, Lasnon C, Veit-Haibach P, Sera T, Sattler B, Boellaard R. EANM/EARL harmonization strategies in PET quantification: from daily practice to multicentre oncological studies. Eur J Nucl Med Mol Imaging 2017;44(Suppl 1):17-31.
24. Ruschoff JH, Ferraro DA, Muehlematter UJ, et al. What's behind (68)Ga-PSMA-11 uptake in primary prostate cancer PET? Investigation of histopathological parameters and immunohistochemical PSMA expression patterns. Eur J Nucl Med Mol Imaging 2021;48(12):4042-53.
25. Jiao J, Kang F, Zhang J, et al. Establishment and prospective validation of an SUV(max) cutoff value to discriminate clinically significant prostate cancer from benign prostate diseases in patients with suspected prostate cancer by (68) Ga-PSMA PET/CT: a real-world study. Theranostics 2021;11(17):8396-411.
26. Vetrone L, Mei R, Bianchi L, et al. Histology and PSMA Expression on Immunohistochemistry in High-Risk Prostate Cancer Patients: Comparison with (68)Ga-PSMA PET/CT Features in Primary Staging. Cancers (Basel) 2023;15(6).
27. de Bie KCC, Veerman H, Bodar YJL, et al. Higher Preoperative Maximum Standardised Uptake Values (SUV(max)) Are Associated with Higher Biochemical Recurrence Rates after Robot- Assisted Radical Prostatectomy for [(68)Ga]Ga-PSMA-11 and [(18)F]DCFPyL Positron Emission Tomography/Computed Tomography. Diagnostics (Basel) 2023;13(14).

Berrens AC, Contieri R, Buckle T, Ottens VA, van Willigen DM, Donswijk ML, Da Silva Guimaraes M, van der Poel HG, van Leeuwen FWB

Submitted 2025

Chapter 5

Molecular Imaging of Primary Prostate Cancer Specimens Using a Novel Hybrid PSMA Tracer

Abstract

Introduction. Prostate-specific membrane antigen (PSMA) is an imaging target for prostate cancer and is used to guide precision surgery. Such guidance is generally pursued using either radio- or fluorescence guidance. Combining best of both worlds, this study assessed the tumor-identification accuracy of our recently developed hybrid PSMA-tracer (*h*PSMA).

Methods. Patients (n=15) with preoperative PSMA PET/CT avid prostate tumors were included. Following prostatectomy, the freshly excised prostate was sliced at tumor level and incubated in 500 nM *h*PSMA (fluorescent component cyanine 5 (Cy5)). After incubation (30 min) the tissue was imaged macroscopically using a fluorescence laparoscope. Specimens were formalin fixed (48 h), sectioned and imaged again. In-house developed imaging software was used to process the images. After paraffin-embedding, sections were microscopically and (immuno)histopathologically analyzed.

Results. The location of Cy5 signal corresponded with PSMA PET/CT in fresh tissue in 74% (95% CI 63.4- 84.5) and in formalin-fixed slices in 71% (95% CI 56.9-84.3). Cy5 signal and PSMA PET/CT corresponded with tumor location on HE in 70% (95% CI 52.5-87.5) and HE 71(95% CI 56.1-87.2), respectively. Lesions missed by PSMA PET/CT and fluorescence imaging were median size 3.7 mm (IQR 2.3-7.1) and predominantly (86%) Gleason grade 3. The main limitations were related to the *ex vivo* set-up.

Conclusion. *Ex vivo* use of the *h*PSMA tracer showed a high accuracy for identifying PSMA-PET/CT avid lesions and tumor lesions stained with HE. Gleason grade and lesion size were predictive of identifying lesions seen on HE. *Ex vivo* limitations are expected to be overcome at first-in-human (intravenous) application.

Introduction

Prostate cancer ranks as the second most prevalent cancer and the fifth leading cause of cancer-related mortality in men. One of the primary interventions for prostate cancer is radical prostatectomy, a procedure that revolves around achieving an equilibrium between complete resection of the primary tumor and preservation of critical functional structures. While staging and diagnostic accuracy of preoperative imaging have significantly improved, the surgery itself still exhibits a non-negligible 6-50% rate of positive surgical margins, depending on e.g. tumor stage [1-3]. Positive margins that express themselves as biochemical persistence or recurrence create a need for additional treatment. To overcome this challenge, techniques are needed that help visualize tumor tissue that is not visible by eye or under white light endoscopy [4].

In prostate cancer, the most widely used means of intraoperative margin assessment is neuroSAFE [5]. The surgeon harvests tissue so that a pathologist at a different location in the hospital can perform frozen section analysis [5]. This technique has been shown to allow for 20-30% more nerve-sparing without an increase in positive surgical margin rates [6]. It is, however, a time-consuming and logistically challenging procedure. Preferably margin assessments are performed in the operating room itself, ideally using *in-situ* tumor visualization [7]. In prostate cancer, the transmembrane protein prostate-specific membrane antigen (PSMA) has firmly been established as a molecular target [8]. Intraoperative molecular imaging solutions for PSMA make use of radiopharmaceuticals (gamma- and beta-rays), fluorescent agents, or the convergence of both in hybrid agents (fluorescence/gamma-rays, fluorescence/beta-rays, or beta-rays with induced Cerenkov) [9-12]. The hybrid approaches help overcome the limitations associated with the individual modalities' signatures, essentially providing a best-of-both-worlds scenario.

Our chemical and preclinical efforts have indicated that a hybrid analogue of the commonly used [^{99m}Tc]Tc-PSMA I&S, namely ^{99m}Tc-EuK-(SO3)Cy5-mas3 (in short ^{99m}Tc-*h*PSMA) holds potential for intraoperative PSMA imaging [13 14]. An exploratory micro-dosing study in a porcine model (intravenous injection) further substantiated this assumption [15]. While venous application underlies the foreseen clinical targeting route for PSMA, there are several studies that indicate that findings at back-table (*ex vivo*) imaging can be a surrogate for *in vivo* use [16-19], and feasibility for *h*PSMA to stain PSMA has also been shown [15].

This study explored the correlation between fluorescent PSMA-staining achieved after *ex vivo* tissue incubation and preoperative imaging as a means to further bridge between preclinical research and in-patient tracer application. This was done by assessing the potential of *h*PSMA to illuminate PSMA- expressing tissues in freshly excised human prostate specimens in relation to preoperative MRI and PSMA- PET imaging and histopathology.

Methods

Human prostates were obtained from patients undergoing robot assisted radical prostatectomy (RARP) at a tertiary cancer center. Patients were included if they had 1) biopsy proven prostate cancer, 2) a tumor larger than 5 mm on MRI, 3) a tumor located more than 1 cm from the apex, and 4) a preoperative PSMA PET/CT demonstrating increased intraprostatic tracer accumulation (Figure 1). A prostate that was not incubated with tracer was included as reference for native background fluorescence. Patient consent for *ex vivo* use of tissue specimens was acquired upon general hospital registration. This study was approved by the local Institutional Review Board (IRBm19-273). All samples and corresponding data were handled and stored anonymized and handled and stored in accordance with the ethical standards of the local ethics committee of The Netherlands Cancer Institute - Antoni van Leeuwenhoek Hospital and with the 1964 Helsinki declaration and its later amendments or comparable ethical standards.

Preoperative imaging

Prebiopsy MRI was used in all men guiding targeted biopsies. After prostate cancer diagnosis patients were scanned using different PSMA PET-tracers ([^{18}F]PSMA-JK-7, [^{68}Ga]Ga-PSMA-11, [^{18}F]DCFPyL, [^{18}F]PSMA-1007) within 125 days before surgery, according to local protocols. One nuclear medicine physician (MLD) reevaluated the PET imaging by drawing a volume of interest (VOI) and calculating the SUV_{max} using Osirix MD (Pixmeo SARL) software and classified the lesions according to the PRIMARY score [20].

Hybrid tracer synthesis

The Cy5 fluorescent hybrid tracer *h*PSMA (MW = 1411.6 g/mol; KD = 19.2 ± 5.8 nM) for fluorescent imaging was synthesized according to previously described methods [13]. For this experiment, radiolabeling with ^{99m}Tc was omitted.

Ex vivo *tissue incubation*

Ex vivo imaging was performed based on previously described methods [18 21] that were slightly adapted to accommodate incubation of the larger samples of the prostate. Directly after surgery the freshly excised prostate was inked, measured and cut in two in the transverse plane at the level of the tumor. With the dissection plane facing up, the prostatic tissue was placed in a custom 3D-printed ring and incubated in a 5 ml solution of *h*PSMA (500 nM; λex max =650 nm, λem max=670 nm) on the surface. After incubation for the duration of 30 minutes in a dark environment, the fresh tissue was rinsed thrice with Dulbecco's Phosphate-Buffered Saline (DPBS; ±100 ml; Gibco^{tm}, Thermo Fisher Scientific, Waltham, MA, USA) to remove unbound tracer and patted dry.

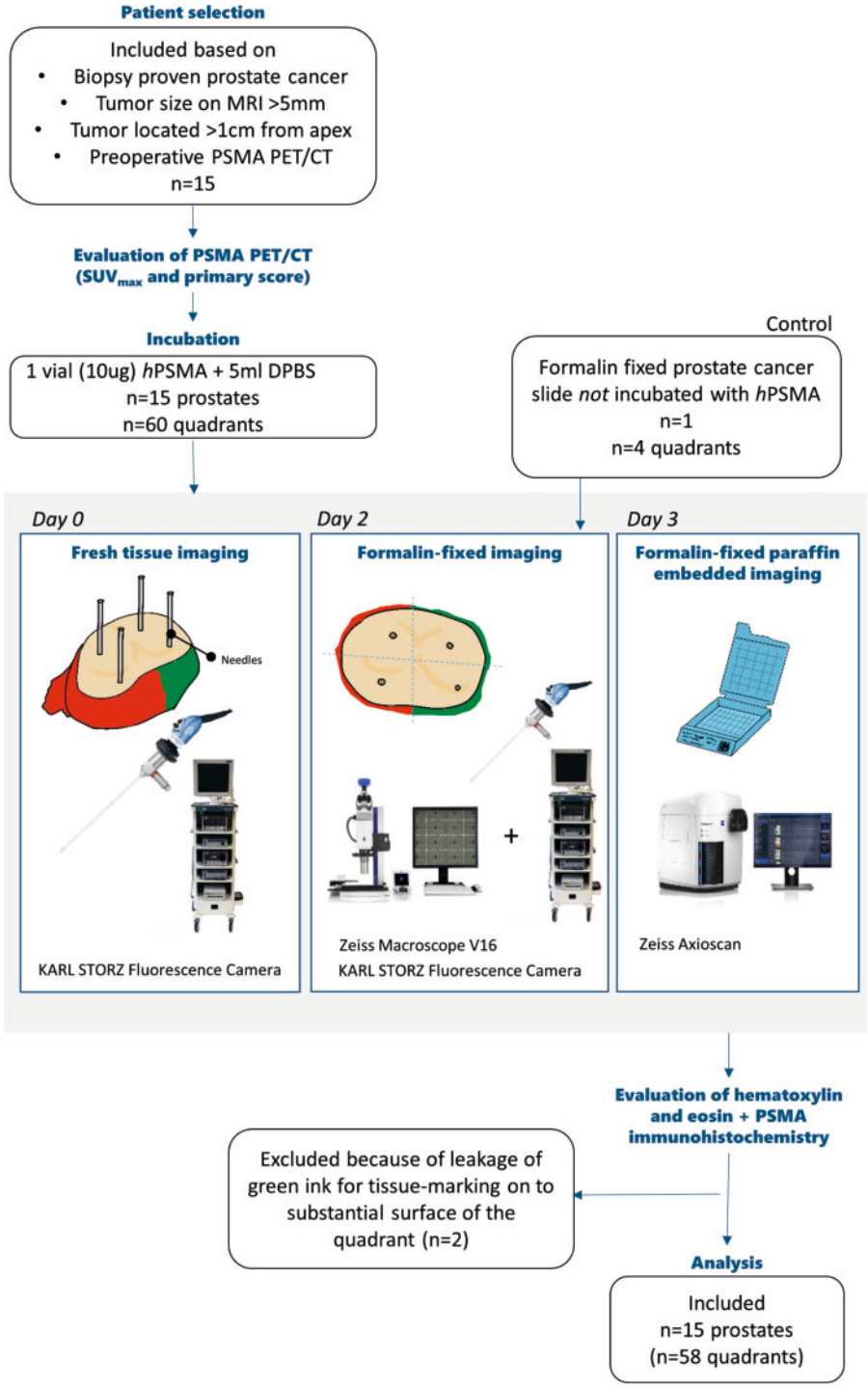

Figure 1. Flowchart inclusions and imaging methods of prostate cancer tissue quadrants.

Imaging

At day 0 the dissection plane was imaged macroscopically using a clinical grade Cy5-enabled IMAGE 1 S camera system equipped with a 30° laparoscope (Karl Storz Endoscopie Nederland B.V., Amersfoort, the Netherlands [18 22]. The imaging conducted by the fluorescence camera was complemented with in- house–developed image-processing software that allowed color-coding of the fluorescence signal for improved visualization and distinction of Cy5 intensity differences. Following imaging, four needles were placed in the fresh tissue to facilitate alignment between imaging and (immuno) histopathology (Figure 1).

The specimens were subsequently formalin fixed for two days and sectioned according to standard protocol. The sectioned slice of interest, meaning the same fresh slice that was incubated an imaged as fresh tissue, was again macroscopically imaged using the camera system and laparoscope (Karl Storz; see above). A Cy5 source (1mM Cy5) was used to analyze autoscaling. Additional images were collected using a Zeiss AxioZoom Macroscope V16 with a Axiocam 512m camera using 1x 0.25 NA objective set to 12.4 magnification, Zeiss 50HE filterset for CY5 staining and GFP 38HE filterset for autofluorescence, and transmitted light. The Zeiss macroscope does not use autoscaling. It collects many smaller tiles of the image. These tiles were corrected for shading and stitched to make one complete image using ZEN v3.4.

Histopathological evaluation

Histopathological evaluation of the prostate specimens was performed as per standard of care according to International Society of Urological Pathology (ISUP) protocols by an experienced uropathologist on formalin-fixed, paraffin-embedded slides after haematoxylin and eosin (HE) staining [23]. Additional to standard protocol, the same uropathologist delineated and graded tumor-positive regions on the sequential microscopic HE slides and scored tumor density (no tumor/intermediate/dense). Fluorescence microscopy was done on the first blanco slide (3 µm) using a Zeiss Axioscan Z1 with an Orca FLASH 4.0 V3 camera using a 0.8 NA objective and the same filter set as described above. The imaged slides were used for PSMA immunohistochemistry (IHC), performed on a BenchMark Ultra autostainer (Ventana Medical Systems, Tucson, Arizona, USA) (Clone EPR6253; Abcam, Cambridge, UK) (detailed description in supplementary 1). The uropathologist microscopically evaluated all slides while remaining blinded to the results of preoperative imaging and perioperative fluorescence imaging. A four-point immunoreactive score (IRS) classification was used considering the grade of membranous staining intensity (0: no color reaction; 1: mild; 2: moderate; 3: intense reaction) and percentage of positive cells [24 25]. To quantify intra-patient heterogeneity the Shannon–Diversity Index was calculated per lesion for IHC outcomes by weighing positive areas and intensity [26]. The minimal Shannon–Diversity Index is 0, which represents homogeneity.

Image analysis

All images of the fresh and formalin-fixed tissue were split in four quadrants in line with the transversal plane of the prostate (anterior-posterior/left-right) (Figure 1). Needle positions provided reference for the relative position of the different images generated. All imaging approaches were compared to each other to score if the areas considered 'positive' overlaid. Hereby no attempts were made to use 'warping' to compensate for tissue deformations, but rather the analyses were done per quadrant. Cy5 intensity was scored and areas with a score of >4 were considered 'positive'. PSMA intensity score on IHC of >2 was considered 'positive'. Additional to analysis of the quadrants, analysis was also done in more detail on tumor lesion level based on HE. In case of more than one lesion of the prostate on PSMA PET and MRI, the lesion in the corresponding anatomical location as the imaged formalin-fixed slice was used for analysis. A lesion was considered 'positive' when it was described as such by the nuclear medicine physician and radiologist. The lesion(s) annotated by the pathologist on HE was considered tumor 'positive'.

Statistical Analysis

Fifteen patients were included based on the sensitivity of PSMA PET (~90%) and the known presence of tumor in our population with a marginal error of 15% and α= 0.05 [27]. For continuous variables, the median and interquartile range (IQR) is reported. Accuracy is reported using the mean and 95% confidence intervals (CI). A p-value of less than 0.05 was considered significant. Spearman's correlation coefficient was used to identify correlation between not-normally distributed data.

Results

Patient characteristics

Prostatic tissue from 15 prostate cancer patients was incubated. In two patients, one of the quadrants contained green tissue-marking ink which made interpretation of fluorescence unreliable. Therefore 58/60 quadrants were included for analysis (Figure 1). Patients were nearly equally divided between intermediate (53%) and high risk (47%) with a median initial PSA of 8.1 ng/ml (IQR 6.8, 17.3). Primary tumor lesions on PSMA PET/CT had a median SUV_{max} of 15.4 (IQR 8.1-19.3) and predominantly classified as PRIMARY score 5 (67%). Detailed patient demographics are provided in table 1.

Table 1. Patient demographics

Parameter	Overall (n=15)
Median age at surgery, yr (IQR)	74 (65.0 - 74.0)
Median initial prostate-specific antigen, ng/ml (IQR)	8.1 (6.8 - 17.3)
Clinical T stage	
T1c, n (%)	9 (60.0)
T2, n (%)	6 (40.0)
>T2b, n (%)	0 (0.0)
T3a, n (%)	0 (0.0)
Radiological (m)T stage, n (%)	
T2, n (%)	4 (26.7)
T2a, n (%)	2 (13.3)
T2b, n (%)	1 (6.7)
T2c, n (%)	5 (33.3)
T3a, n (%)	2 (13.3)
T3b, n (%)	1 (6.7)
Radiological (mi)N-stage	
N0, n (%)	11 (73.3)
N1, n (%)	1 (6.7)
Median risk of LNI according to Briganti 2012, % (IQR)	13 (9.0-22.0)
Median prostate volume (cc)	39 (33.0 - 66.0)
PSMA PET/CT tracer	
[^{18}F]PSMA-JK-7	7 (46.6)
[^{68}Ga]Ga-PSMA-11	6 (40.0)
[^{18}F]DCFPyL	1 (6.7)
[^{18}F]PSMA-1007	1 (6.7)
Median SUV_{max} (IQR)	15.4 (8.1-19.3)
Primary score, n (%)	
1-3	0 (0.0)
4	4 (26.7)
5	10 (66.7)
Pathological ISUP grade group, n (%)	
2	2 (13.3)
3	7 (46.7)
4	2 (13.3)
5	4 (26.7)
Surgical margins, n (%)	
R0	13 (86.7)
R1	2 (13.3)

Accuracy of fluorescence staining by hPSMA in identifying positive lesions

Cy5 staining was visible in specimens of all 15 patients The overall accuracy of PSMA-related staining to identify the same lesions as on PSMA PET/CT was high for the fresh tissue (74%; 95% CI 63.4-84.5) as well as the formalin-fixed slices (71%; 95% CI 56.9-84.3) (Figure 2 and 3A-E). False positive staining reduced specificity to 59%, whereas sensitivity was 100% on the quadrant level. While false positive staining poses an inherent challenge when tissues are being incubated with markers [28]. In this case,

autoscaling of the Storz fluorescence camera (Supplementary 3A-B) and bulging of the prostate after cutting the fresh tissue (Supplementary 3C-F) challenged matters further. While autoscaling helps detect low intensity signals it also means that a reference for 'true' PSMA-specific fluorescence may be replaced by background staining. The imaging from the Zeiss macroscope (Figure 3E) showed the results without autoscaling. The formalin-fixed reference slice (also imaged with the Zeiss macroscope) showed very little Cy5 signal (Supplementary 3G-I). Bulging on the other side, may have caused deformations of several millimeters, limiting the correlation with histopathological references.

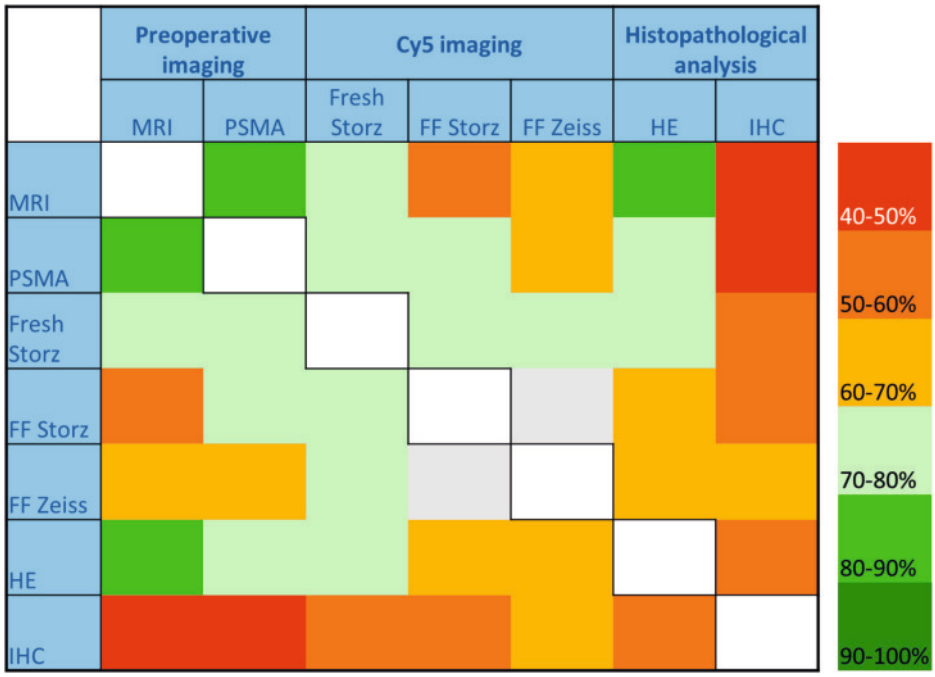

Figure 2. Heatmap of correlation between all imaging modalities. The color indicates the percentage of accurate overlay as depicted on the left. Cy5 = Cyanine 5, FF = Formalin-fixed tissue (Storz = fluorescence laparoscope; Zeiss = Zeiss macroscope), HE = hematoxylin and eosin, IHC = immunohistochemistry

As HE was considered the gold standard for the uropathologist, we studied the presence of PSMA-related Cy5 signal in the fresh tissue specimens. Cy5 corresponded with HE in 70% of cases (95% CI 52.5-87.5) (Figure 2 and 3C and G). The correspondence decreased to 65% for formalin-fixed slices (95% CI 52.5-82.9) (Figure 2 and 3D, E, and G). Indicating the fixation process has a negative influence on the fluorescence detection. Nevertheless, the correspondence was alike the relation between PSMA PET/CT and HE (71%; 95% CI 56.1-87.2) (Figure 2 and 3B and G).

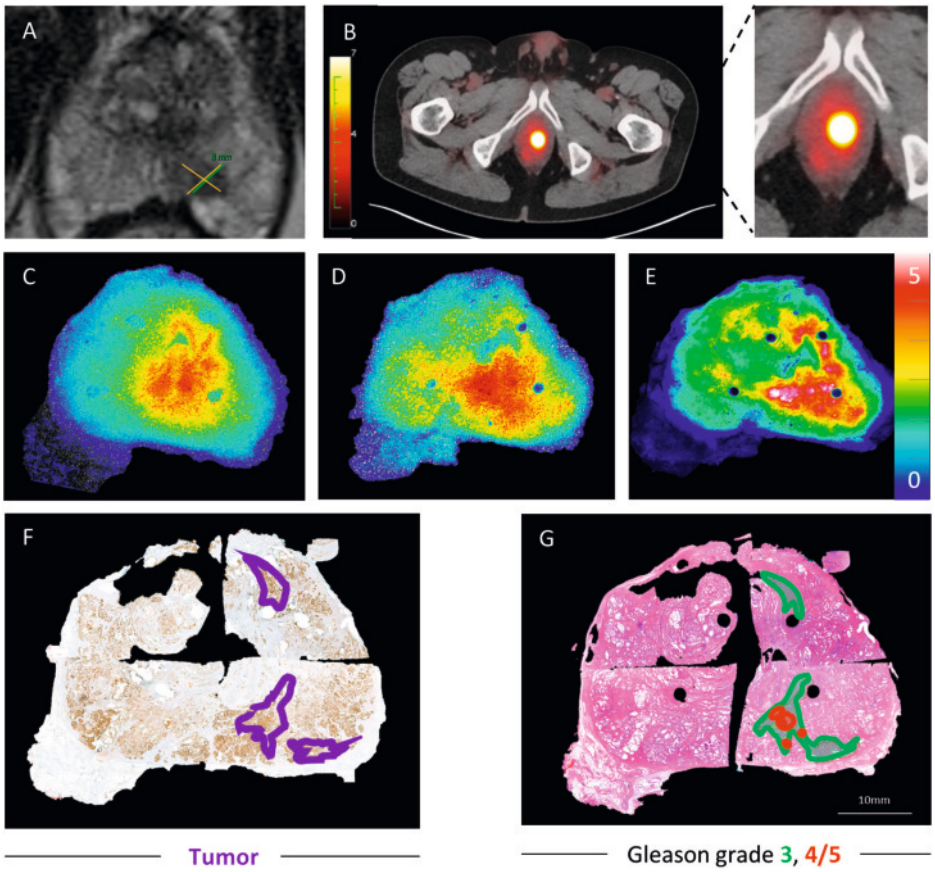

Figure 3. Patient example of A) MRI imaging (tumor marked by the orange cross). B) PSMA PET/CT imaging (tumor visible as white-yellow spot). Cy5 intensity after incubation of C) fresh prostatic tissue (fluorescence endoscope). D) formalin-fixed (+48 h) slice (fluorescence endoscope), and E) the same formalin-fixed (+48 h) slice imaged by Zeiss macroscope. Heatmaps display the signal intensities relative to the minimal signal observed. F) PSMA immunohistochemistry staining with delineated tumor areas (in purple). G) Hematoxylin and eosin staining with tumor areas delineated according to the Gleason grade (3 in green, 4/5 in red) by the uropathologist.

Analysis per tumor positive lesion according to HE

When looking at the lesions instead of per quadrant there were a total of 33 tumor positive lesions (in 15 patients) seen on HE. These were used as reference standard for this per lesion analysis. Sixteen of these were identified by fluorescence imaging (median size of 17.5 mm (IQR 10.6-19.8); 19% Gleason grade 3) (Figure 4). Of the 17 tumor foci that were identified on HE but were missed by fluorescence imaging (as well as by PSMA PET/CT) >75% were Gleason grade 3 with a median size of 5.5 mm (IQR 2.8-7.9). The median IRS was 6 (IQR 4–9). Clear intra-patient and interpatient heterogeneity as calculated by the Shannon-diversity index was observed with values ranging from 0.325–1.366 (Figure 4). Demonstrating the differences in PSMA intensity within lesions

PSMA PET/CT			Cy5 imaging			HE analysis		PSMA IHC analysis					
Primary score	SUVmax	Identified	Fresh tissue	FF storz	FF zeiss	Size in mm	Gleason score	%cells intensity 0+	%cells intensity 1+	%cells intensity 2+	%cells intensity 3+	Shannon index	IRS
						1,2	4/5	30	10	10	50	1,168	6
						1,8	3	50	20	20	10	1,221	
						2,4	3	No tumour identified on IHC					
						2,7	3	10	20	30	40	1,280	6
						2,9	3	IHC missing part of tissue so NR					
						3,3	3	50	20	20	10	1,221	
						3,7	4/5	0	0	80	20	0,500	8
						4,8	3	No tumour identified on IHC					
						5,5	3	10	40	30	20	1,280	2
						6,6	3	20	10	70	0	0,802	4
						6,6	3	0	20	50	30	1,030	6
						7,5	3 en 4/5	0	10	85	5	0,518	8
						7,6	4/5	0	0	80	20	0,500	8
						8,2	3	0	0	90	10	0,325	8
						8,6	3	30	20	40	10	1,280	4
						10,4	3	20	60	20	0	0,950	2
						16,8	3	10	30	40	20	1,280	4
4	3,7					18,0	3 en 4/5	5	5	75	15	0,799	6
4	5,7					19,6	4/5	5	0	90	5	0,394	8
4	6,8					11,8	4/5	20	60	0	20	0,950	3
5	8,2					6,7	3	0	30	60	10	0,898	6
4	8,2					19,5	3	40	20	10	30	1,280	0
4	8,2					23,7	3 en 4/5	30	20	30	20	1,366	4
5	8,6					8,0	3 en 4/5	0	35	25	40	1,080	8
4	10,4					19,8	3 en 4/5	10	20	50	20	1,221	4
5	12,9					8,5	3	0	5	95	0	0,199	8
5	15,4					15,6	4/5	10	0	40	50	0,943	6
5	16,9					10,2	3 en 4/5	0	5	5	90	0,246	12
5	18,5					12,3	3 en 4/5	0	0	80	20	0,500	8
5	19,3					19,2	3 en 4/5	0	20	30	50	1,030	9
5	21,2					24,4	3 en 4/5	0	20	10	70	0,802	9
5	34,0					17,0	4/5	0	0	5	95	0,199	12
5	50,9					44,7	4/5	0	0	20	80	0,500	9

Figure 4. Overview of per lesion analysis as identified on hematoxylin and eosin staining. All lesions were ordered ascending, first according to and second by size. From left to right: Primary score depicted in shades of grey (dark grey depicting the highest number). SUV_{max} values (heatmap: light orange = low SUV_{max}, dark orange = high SUV_{max}). Dark green depicts if the lesion was identified by the imaging type. Dark red if it was not identified (Storz = fluorescence laparoscope; Zeiss = Zeiss macroscope). Size (heatmap: light yellow = small, dark yellow = large). Gleason score depicted in shades of grey (dark grey depicting the highest number). Percentage of cells with intensity 0-3 depicted in shades of light green. Degrees of heterogeneity in PSMA protein expression and PSMA-ligand uptake were measured by Shannon–Diversity Index and depicted as heat map ranging from low heterogeneity (light blue) to high heterogeneity (dark blue). Intensity of PSMA membranous expression quantified by IRS are depicted in shades of grey (dark grey depicting the highest number). IHC = immunohistochemistry, IRS = immunoreactive score, PSMA = prostate-specific membrane antigen.

even within the same patient. A strong, significant positive correlation was observed between the IRS and SUV_{max} (ρ=0.729, p=0.001) indicating the more cells within the tumor with high PSMA intensity, the higher the SUV_{max}.

Microscopic evaluation

At microscopic evaluation the signal accumulated in PSMA-positive cells according to the outcomes of IHC. For example, in glandular tissue (Figure 5). The intensity of Cy5 signal was highest on PSMA-positive tissue borders, but failed to illuminate denser, more solid tumor tissue (Figure 5B and C). In fact, several denser tumor lesions showed no Cy5 signal where it would have been expected based on the IHC. This suggests that the lack of tracer diffusion through denser tissues could in some cases compromise accessibility of PSMA-positive tissues.

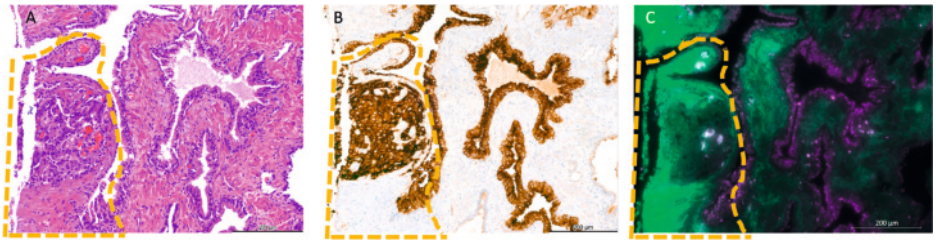

Figure 5. Example of microscopic evaluation ofPSMA-related Cy5 signal presence in prostatic tissue where both tumor (dotted line) and healthy tissue are represented. A) Hematoxylin and eosin staining. B) PSMA immunohistochemistry. C) Cy5 imaging using the Zeiss axioscan: pink representing Cy5, green representing background staining.

Discussion

In this fluorescence imaging study, we evaluated the potential of *h*PSMA *ex vivo* on human prostate specimens to reliably detect intraprostatic cancer lesions. Following extensive evaluation, we found that fluorescence imaging of *h*PSMA yielded a comparable accuracy in identifying cancerous lesions as PSMA PET/CT.

Both the false positive and false negative fluorescent staining seem to be intrinsic to the back-table 'tissue incubating' set up, including the demonstrated factors like tissue bulging and autoscaling. Additionally, fluorescence cameras are more prone to detect signal in tissues that are positioned close to the camera and were approached from different angles (preoperative scans vs sliced tissue, 30° endoscope vs 0° macroscope and microscope), which may cause false positives. Within 30 minutes the results from the microscopic evaluation showed that the penetration of hPSMA into the tissue specimen is limited and more restricted for solid tumor tissue. It is unknown how far the hPSMA can get into the tissue during fresh tissue incubation, but it has been suggested in literature that the denser the tumor tissue, the less a tracer penetrates when incubated [29]. This means that *ex vivo* findings fail to reliably represent the (pharmaco)physiological

tracer input that occurs following intravenous tracer administration. Based on preclinical data [13 15], it is expected that intravenous *h*PSMA administration in humans will suffer less from background signals and will yield adequate intraprostatic PSMA-straining. Although the needle holes could be used for a more accurate overlay, discrepancies between macroscopic and microscopic imaging remained. This could be attributed to the steps taken before paraffin embedding (including washing with 70% and 100% alcohol plus isopropanol) and the delay of at least 72 h after incubation.

With regard to histopathology, the discrepancy between HE and PSMA-IHC in the identification of cancerous tissue causes a major challenge. PSMA-targeted agents, like *h*PSMA, are designed to target PSMA and will do so independent on the type of tissue that expresses the receptor. Meaning that in case of a PSMA-negative lesions the accumulation of *h*PSMA does not have to be related to the tumor location. There was a number of lesions (nearly 50%) when analyzing the correlation on a lesion level, that was identified on HE but was not identified by PSMA PET/CT and/or fluorescence imaging. As the majority (76%) of these lesions was Gleason grade 3 and relatively small (median 5.5 mm; Figure 4) it should be taken into account that this method of *ex vivo* staining may be more successful in higher Gleason grades and larger lesions.

In line with our findings, other studies have demonstrated significant heterogeneity within prostate cancer lesions [25 30 31]. This variability affects both the SUV_{max} and the Gleason grade, as is proven by the strong correlation between IRS and SUV_{max} (and shown in Figure 4). Consequently, this heterogeneity can lead to variations in imaging results. This was recently confirmed by Waibel et al., who showed differences in PSMA expression within a tumor can lead to variations in PET imaging results [32]. Their study found a strong correlation between the intensity of PSMA staining (using an IRS-equivalent score) and SUV_{max} values on PSMA PET. This indicates that areas with higher or lower PSMA expression within the same lesion may be visible as corresponding differences in SUV_{max}. The heterogeneity of PSMA expression influences not only PET imaging but also intraoperative imaging, considering prior work confirmed a positive correlation between SUV_{max} of PSMA PET lesions and the intraoperative signal of similar PSMA-targeted (radio)tracers [33 34].

Ex vivo incubation has given us valuable insight into the workings of the *h*PSMA tracer when applied to human prostatic tissue. However, it cannot predict the exact performance when administered intravenously. A first-in-human clinical study is currently being instigated.

Conclusion

Despite the challenges accompanying the *ex vivo* incubation approach, the majority of prostate cancer lesions (~70%) could be identified using the hybrid PSMA (*h*PSMA; Cy5) tracer. On fresh prostate cancer tissue as well as on formalin-fixed tissue, it was found in the same regions as lesions on PSMA PET/CT and histopathology. The main limitations were related to the *ex vivo* set-up and are expected to be overcome in the first-in-human (intravenous) application.

References

1. Martini A, Gandaglia G, Fossati N, et al. Defining Clinically Meaningful Positive Surgical Margins in Patients Undergoing Radical Prostatectomy for Localised Prostate Cancer. Eur Urol Oncol 2021;4(1):42-48
2. Moris L, Gandaglia G, Vilaseca A, et al. Evaluation of Oncological Outcomes and Data Quality in Studies Assessing Nerve-sparing Versus Non-Nerve-sparing Radical Prostatectomy in Nonmetastatic Prostate Cancer: A Systematic Review. Eur Urol Focus 2022;8(3):690-700
3. Pellegrino F, Falagario UG, Knipper S, et al. Assessing the Impact of Positive Surgical Margins on Mortality in Patients Who Underwent Robotic Radical Prostatectomy: 20 Years' Report from the EAU Robotic Urology Section Scientific Working Group. Eur Urol Oncol 2024;7(4):888-96
4. van Leeuwen FWB, Buckle T, van Oosterom MN, Rietbergen DDD. The Rise of Molecular Image- Guided Robotic Surgery. J Nucl Med 2024;65(10):1505-11
5. van der Slot MA, den Bakker MA, Tan TSC, et al. NeuroSAFE in radical prostatectomy increases the rate of nerve-sparing surgery without affecting oncological outcome. BJU Int 2022;130(5):628-36
6. Kroon LJ, van der Slot MA, van den Bergh RCN, Roobol MJ, van Leenders G. Neurovascular Structure-adjacent Frozen-section Examination (NeuroSAFE) During Radical Prostatectomy: A Systematic Review and Meta-analysis. Eur Urol Oncol 2024
7. Berrens AC, Scheltema M, Maurer T, et al. Delphi consensus project on prostate-specific membrane antigen (PSMA)-targeted surgery-outcomes from an international multidisciplinary panel. Eur J Nucl Med Mol Imaging 2023
8. Hofman MS, Lawrentschuk N, Francis RJ, et al. Prostate-specific membrane antigen PET-CT in patients with high-risk prostate cancer before curative-intent surgery or radiotherapy (proPSMA): a prospective, randomised, multicentre study. Lancet 2020;395(10231):1208-16
9. Berrens AC, Knipper S, Marra G, et al. State-of-the- art in Prostate Specific Membrane Antigen (PSMA)- targeted surgery– a systematic review Eur urol Open Science 2023;54:43-55.
10. Stibbe JA, de Barros HA, Linders DGJ, et al. First- in-patient study of OTL78 for intraoperative fluorescence imaging of prostate-specific membrane antigen-positive prostate cancer: a single-arm, phase 2a, feasibility trial. Lancet Oncol 2023;24(5):457-67
11. Nguyen HG, van den Berg NS, Antaris AL, et al. First-in-human Evaluation of a Prostate-specific Membrane Antigen-targeted Near-infrared Fluorescent Small Molecule for Fluorescence-based Identification of Prostate Cancer in Patients with High-risk Prostate Cancer Undergoing Robotic- assisted Prostatectomy. Eur Urol Oncol 2024;7(1):63-72
12. Hamdy FC, Lamb AD, Tullis IDC, et al. First-in-man study of the PSMA Minibody IR800-IAB2M for molecularly targeted intraoperative fluorescence guidance during radical prostatectomy. Eur J Nucl Med Mol Imaging 2024
13. Hensbergen AW, Buckle T, van Willigen DM, et al. Hybrid Tracers Based on Cyanine Backbones Targeting Prostate-Specific Membrane Antigen: Tuning Pharmacokinetic Properties and Exploring Dye-Protein Interaction. J Nucl Med 2020;61(2):234-41
14. Hensbergen AW, van Willigen DM, van Beurden F, et al. Image-Guided Surgery: Are We Getting the Most Out of Small-Molecule Prostate-Specific- Membrane-Antigen-Targeted Tracers? Bioconjug Chem 2020;31(2):375-95
15. Dell'Oglio P, van Willigen DM, van Oosterom MN, et al. Feasibility of fluorescence imaging at microdosing using a hybrid PSMA tracer during robot-

assisted radical prostatectomy in a large animal model. EJNMMI Res 2022;12(1):14

16. Jager NA, Westra J, van Dam GM, et al. Targeted folate receptor beta fluorescence imaging as a measure of inflammation to estimate vulnerability within human atherosclerotic carotid plaque. J Nucl Med2012;53(8):1222-9
17. Elekonawo FMK, de Gooyer JM, Bos DL, et al. Ex Vivo Assessment of Tumor-Targeting Fluorescent Tracers for Image-Guided Surgery. Cancers (Basel) 2020;12(4)
18. Vries HM, Bekers E, van Oosterom MN, et al. c- MET Receptor-Targeted Fluorescence on the Road to Image-Guided Surgery in Penile Squamous Cell Carcinoma Patients. J Nucl Med 2022;63(1):51-56
19. Hao H, Wang X, Qin Y, et al. *Ex vivo* near-infrared targeted imaging of human bladder carcinoma by ICG-anti-CD47. Front Oncol 2023;13:1083553
20. Emmett L, Papa N, Buteau J, et al. The PRIMARY Score: Using Intraprostatic (68) Ga-PSMA PET/CT Patterns to Optimize Prostate Cancer Diagnosis. J Nucl Med 2022;63(11):1644-50
21. Buckle T, van Alphen M, van Oosterom MN, et al. Translation of c-Met Targeted Image-Guided Surgery Solutions in Oral Cavity Cancer-Initial Proof of Concept Data. Cancers (Basel) 2021;13(11)
22. van Willigen DM, van den Berg NS, Buckle T, et al. Multispectral fluorescence guided surgery; a feasibility study in a phantom using a clinical-grade laparoscopic camera system. Am J Nucl Med Mol Imaging 2017;7(3):138-47
23. van Leenders G, van der Kwast TH, Grignon DJ, et al. The 2019 International Society of Urological Pathology (ISUP) Consensus Conference on Grading of Prostatic Carcinoma. Am J Surg Pathol 2020;44(8):e87-e99
24. Heetman JG, Hermsen R, Exterkate L, et al. Immunohistochemical and histopathological validation of (18) F-PSMA-1007 PET/CT for intraprostatic cancerous lesions. Prostate 2023;83(14):1332-41
25. Wang H, Remke M, Horn T, et al. Heterogeneity of prostate-specific membrane antigen (PSMA) and PSMA-ligand uptake detection combining autoradiography and postoperative pathology in primary prostate cancer. EJNMMI Res 2023;13(1):99
26. Maley CC, Aktipis A, Graham TA, et al. Classifying the evolutionary and ecological features of neoplasms. Nat Rev Cancer 2017;17(10):605-19
27. Jansen BHE, Bodar YJL, Zwezerijnen GJC, et al. Pelvic lymph-node staging with (18) F-DCFPyL PET/CT prior to extended pelvic lymph-node dissection in primary prostate cancer - the SALT trial. Eur J Nucl Med Mol Imaging 2021;48(2):509-20
28. Buchwalow I, Samoilova V, Boecker W, Tiemann M. Non-specific binding of antibodies in immunohistochemistry: fallacies and facts. Sci Rep 2011;1:28
29. Netti PA, Baxter LT, Boucher Y, Skalak R, Jain RK. Time-dependent behavior of interstitial fluid pressure in solid tumors: implications for drug delivery. Cancer Res 1995;55(22):5451-8.
30. Ruschoff JH, Ferraro DA, Muehlematter UJ, et al. What's behind (68)Ga-PSMA-11 uptake in primary prostate cancer PET? Investigation of histopathological parameters and immunohistochemical PSMA expression patterns. Eur J Nucl Med Mol Imaging 2021;48(12):4042-53
31. Vetrone L, Mei R, Bianchi L, et al. Histology and PSMA Expression on Immunohistochemistry in High-Risk Prostate Cancer Patients: Comparison with (68)Ga-PSMA PET/CT Features in Primary Staging. Cancers (Basel) 2023;15(6)
32. Waibel PMA, Glavynskyi I, Fechter T, et al. Can PSMA PET detect intratumour heterogeneity in histological PSMA expression of primary prostate cancer? Analysis of [(68)Ga]Ga-PSMA-11 and [(18)F]PSMA-1007. Eur J Nucl Med Mol Imaging 2025;52(6):2023-33

33. Berrens AC, Sorbi MA, Donswijk ML, et al. Strong Correlation Between SUV(max) on PSMA PET/CT and Numeric Drop-In gamma-Probe Signal for Intraoperative Identification of Prostate Cancer Lesions. J Nucl Med 2024;65(4):548-54
34. Azargoshasb S, Boekestijn I, Roestenberg M, et al. Quantifying the Impact of Signal-to-background Ratios on Surgical Discrimination of Fluorescent Lesions. Mol Imaging Biol2023;25(1):180-89

Supplementary 1. PSMA immunohistochemistry

Paraffin sections were cut at 3 µm, heated at 75 °C for 28 min and deparaffinized at 72°C in the instrument with EZ prep solution (Ventana Medical Systems). Heat-induced antigen retrieval was carried out using Cell Conditioning 1 (CC1, Ventana Medical Systems) for 32 min at 95 °C. Prostate-specific membrane antigen was detected using clone EPR 26253 (Abcam) (1/40 dilution, 32 min 37 °C). Bound antibody was visualized using the OptiView DAB Detection Kit (Ventana Medical Systems). Slices were counterstained with hematoxylin and bluing reagent (Ventana Medical Systems).

Supplementary 2. Examples of complicating factors on *ex vivo* fluorescence imaging

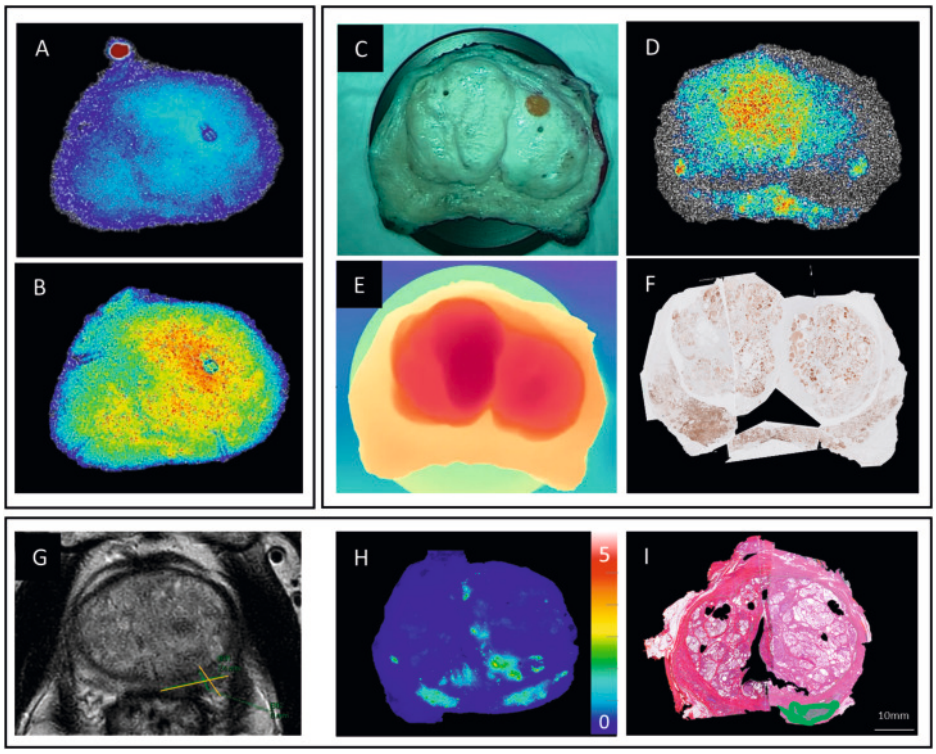

Examples of complicating factors (A-F) and reference slice for presence of Cy5 fluorescence (G-I). Starting with complicating factors: A) Example of fresh prostatic tissue with a Cy5 source (1 mM Cy5) next to it that indicates how autoscaling of the camera system can influence imaging findings in comparison to B) where the source is removed. C) Example of tissue bulging of prostatic tissue formalin-fixed slice. D) Example of heightened signal at the location of bulging tissue. E) Example of depth where dark red is closest to the imaging system and blue is furthest away. F) Corresponding immunohistochemistry. An example of a reference slice of prostatic tissue where tracer incubation was omitted, but the specimens were subjected to the same imaging sequence: G) MRI image with the tumor marked by the orange cross. H) Cy5 signal intensity of the formalin-fixed (+48 h) slice imaged by Zeiss macroscope. I) Hematoxylin and eosin staining with delineated tumor areas Gleason grade 3 (no 4/5 present).


Part II

Applications and Challenges in Image-guided Surgery

Berrens AC, van Oosterom MN, Slof LJ, van Leeuwen FWB, van der Poel HG, Buckle T
Eur J Nucl Med Mol Imaging 50, 1262–1263 (2023)

Chapter 6a

Three-way Multiplexing in Prostate Cancer Patients — Combining a Bimodal Sentinel Node Tracer with Multicolor Fluorescence Imaging. Image of the Month

We present images from a 71-year-old prostate cancer patient who underwent a robot-assisted radical prostatectomy and extended pelvic lymph node dissection (ePLND) complemented with experimental sentinel node (SN) resection [1]. Additional intraoperative lymphangiography was performed to highlight lymphatic structures that should ideally be spared. This concept is part of a prospective trial wherein we aim to use the presented approach to reduce the 20% complication rate associated with ePLND procedures [2]. For SN identification, the bimodal/hybrid tracer ICG-^{99m}Tc-nanoscan (218 MBq in 2 ml) was used, which has replaced the well-known ICG-^{99m}Tc-nanocolloid [3]. Preoperative (lymphoscintigraphy and SPECT/CT) and intraoperative SN imaging (gamma and fluorescence imaging) were performed after intraprostatic tracer injection. Previous work indicates that the hybrid tracer and the visible-dye fluorescein both stain lymphatic structures, but with different kinetics [4]. It is also known that multi-color fluorescence imaging can be used to differentiate between lymphatics of different organs [5 6]. With this first-in-human implementation (see Scheme), we underscore that lymphatic ducts draining the left upper leg can be made visible using fluorescein (80 mg in 4 ml; yellow, dotted triangle) and that this drainage can be distinguished from the SNs visualized with ICG-^{99m}Tc-nanoscan (blue, dotted circle). With that, the former can act as “red-flag” to highlight tissues that should be spared, while the latter provides a “green-flag” for tissues that should be resected. As such, the presented three-way multiplexing approach may help preserve the oncological benefit of ePLND + SN [3], while providing a handle to reduce complication rates.

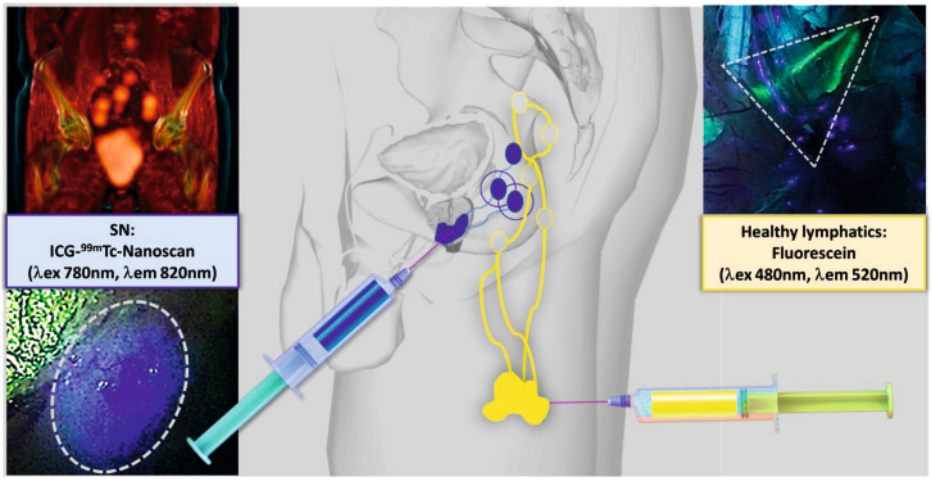

References

1. Wit EMK, Acar C, Grivas N, Yuan C, Horenblas S, Liedberg F, et al. Sentinel node procedure in prostate cancer: a systematic review to assess diagnostic accuracy. Eur Urol. 2017;71:596–605
2. Briganti A, Chun FK, Salonia A, Suardi N, Gallina A, Da Pozzo LF, et al. Complications and other surgical outcomes associated with extended pelvic lymphadenectomy in men with localized prostate cancer. Eur Urol. 2006;50:1006–13.
3. Mazzone E, Dell'Oglio P, Grivas N, Wit E, Donswijk M, Briganti A, et al. Diagnostic value, oncologic outcomes, and safety profile of image-guided surgery technologies during robot-assisted lymph node dissection with sentinel node biopsy for prostate cancer. J Nucl Med. 2021;62:1363–71.
4. van den Berg NS, Buckle T, KleinJan GH, van der Poel HG, van Leeuwen FW. Multispectral fluorescence imaging during robotassisted laparoscopic sentinel node biopsy: a first step towards a fluorescence- based anatomic roadmap. Eur Urol. 2016
5. Kobayashi H, Longmire MR, Ogawa M, Choyke PL, Kawamoto S. Multiplexed imaging in cancer diagnosis: applications and future advances. Lancet Oncol. 2010;11:589–95.
6. Meershoek P, KleinJan GH, van Willigen DM, Bauwens KP, Spa SJ, van Beurden F, et al. Multi- wavelength fluorescence imaging with a da Vinci Firefly—a technical look behind the scenes. J Robot Surg. 2021;15:751–60.

Berrens AC, Buckle T, van Oosterom MN, Slof LJ, van Leeuwen PJ, Wit EMK, Bekers EM, Donswijk ML, van Leeuwen FWB, van der Poel HG.
Ann Surg Oncol 32, 1372–1381 (2025)

Chapter 6b

Multispectral Fluorescence Imaging as a Tool to Distinguish Pelvic Lymphatic Drainage Patterns During Lymph Node Dissection in Prostate Cancer

Abstract

Background. The invasive nature of extended pelvic lymph node dissection (ePLND) prompts the need for alternative lymphatic mapping technologies. To change the focus to "sparing nodes that are not involved" the first step is to research the feasibility of intraoperatively distinguishing the lymph drainage patterns of the prostate from healthy organs.

Methods. We performed a prospective study (NCT05120973) including sixteen patients that underwent a robot-assisted radical prostatectomy + ePLND + sentinel node (SN) (using Indocyanine green (ICG)-^{99m}Tc- nanocolloid). After general anesthesia, a second fluorescent dye (fluorescein) was injected unilaterally in two deposits into the intradermis of the upper leg (n=8) or abdominal wall (n=8) as these are the most common locations of lymphedema in prostate cancer surgery. To distinguish between the drainage patterns, *in* and *ex vivo* multispectral fluorescence imaging was performed using a fluorescence Endoscope.

Results. ICG and fluorescein were visible in the same regions within the ePLND-template and co- accumulated in lymph vessels *in vivo*. At histopathology, fluorescein was seen in only 10/370 LNs (possibly due to tracer properties), none of which overlapped with ICG, and none were tumor positive. Administration of fluorescein did not result in discomfort or abnormal postoperative recovery.

Conclusion. Multispectral imaging can be used to distinguish lymphatic drainage patterns. Our *in vivo* findings indicate that within the ePLND-template lymphatic drainage patterns of the prostate at least partly overlap with those of upper leg and abdominal wall. The properties of fluorescein render it unsuitable for confirmation of fluorescence at histopathology.

Introduction

European Association of Urology guidelines suggest consulting prostate cancer (PCa) patients on advantages and disadvantages of extended pelvic lymph node dissection (ePLND) when nomogram- or classification-assessed risk of nodal involvement (LNI) exceeds 7% [1-3]. Surgical disruption of lymphatic flow, crucial for tissue-fluid balance [4], can lead to complications [5 6]. Studies have indicated that the risk of complications increases with the number of lymph nodes (LNs) dissected [5 7]. Lymphoceles (up to 15%) and lymphedema (up to 14%) being reported most frequently [8 9]. The invasive nature of ePLND prompts the need for alternative lymphatic mapping to prevent dissection of lymphatic anatomies unrelated to the prostate.

To facilitate a less invasive node dissection template, the distinction of drainage patterns from the prostate and healthy organs is necessary during surgery. Lymphangiographic or sentinel node (SN) targeting techniques are of value [10 11]. For lymphangiography, relatively small (<10nm) organic dyes that flow freely through the lymphatics are used (e.g. blue dye, fluorescein or indocyanine green (ICG)) [12 13]. These lymphatic tracers can be detected in white-light or through fluorescence imaging. SN procedures rely on the use of larger (>20 nm) colloidal particles taken up by macrophages residing in LNs (e.g. nanocolloid) [14 15]. In prostate cancer, on the morning of SN surgery a hybrid tracer combining ICG and Technetium (^{99m}Tc) is administered, followed by static planar lymphoscintigraphy and single photon emission computed tomography (SPECT)/CT to guide intraoperative identification [15 16].

Preclinical studies have indicated that multispectral fluorescence imaging was feasible to differentiate between lymphatic drainage patterns of different anatomies [17]. Insights that recently resulted in multispectral fluorescence studies in porcine models, where the lymphatic drainage of the prostate (ICG- Nanocolloid; λem max = 820 nm) could be separated from that of the lower limbs (fluorescein; λem max = 515 nm) during robot-assisted surgery [18]. In humans, this has not yet been confirmed but shows promise as multicolor/multispectral (fluorescence) imaging was proven effective to study the lymphatic drainage of only one organ e.g prostate or endometrium [19 20].

The aim of this translational trial was to objectify the technical feasibility of multispectral intraoperative fluorescence imaging to separate lymphatic drainage patterns of prostate (ICG-technetium(^{99m}Tc)- nanocolloid;) vs. the upper leg or abdominal wall (fluorescein) within the ePLND-template in humans during robot-assisted surgery.

Methods

Study design and patient population

This single-arm, single-center, prospective, feasibility study was approved by the local ethics committee at the Netherlands Cancer Institute-Antoni van Leeuwenhoek Hospital (NCI-AVL), Amsterdam, The Netherlands (NCT05120973). All patients provided written informed consent.

Sixteen male patients aged 18 years or older, with histopathologically confirmed PCa and a calculated risk of LNI >5% according to Briganti 2012 who were scheduled to undergo robot-assisted radical prostatectomy with ePLND were included between March 2022 and August 2023 [2]. Based on the EAU guidelines, patients routinely underwent PSMA PET/CT [1].

SN identification

ICG-^{99m}Tc-nanocolloid (Nanocoll®/Nanoscan®; GE Healthcare BV, Leiderdorp, the Netherlands) was administered 5 h prior to surgery in four deposits of 0.5 ml into the prostate [16]. At 15 min and 2 h post tracer injection, lymphatic mapping was performed using static planar lymphoscintigraphy and SPECT/CT (Figure 1, Supplementary 1).

Lymphangiography upper leg or abdominal wall

After administering general anesthesia, fluorescein (80mg, $T^{1/2}$ 24 min) was injected unilaterally into the dermis in two deposits of 2 ml each, either at the medial and lateral side of the upper leg (n=8) or at the left or right lower quadrant of the abdominal wall (n=8) (Figure 1, Supplementary 1). The side of injection was chosen based on the side showing the most SNs on SPECT/CT to optimally investigate possible converging drainage patterns. The surgery was performed by four robotic surgeons from the prostate cancer network Netherlands, specialized in prostatectomies and SN procedures. On both sides SN and ePLND was performed. The included lymph nodes in the ePLND-template were removed as obturator combined with internal iliac nodes and external iliac nodes. Malignant looking non-SNs outside the template (Cloquet's node/common iliac/presacral/etc) and SNs from all regions were sent to pathology separately.

In vivo *fluorescence imaging*

After docking the robot (da Vinci Xi Surgical System, Intuitive surgical, Inc, Sunnyvale, CA, USA) the surgeon commenced with SN and ePLND on the side of the fluorescein injection. The integrated Firefly fluorescence camera of the robot was used for initial assessment. It is essential to recognize that Firefly is not able to differentiate between fluorescein or ICG [21]. Based on vd Berg et al. [19], at standardized moments during the procedure, secondary fluorescence imaging was performed using an endoscope combined with the Image 1 HUB HD + D-light P (ICG; λex max =800 nm, λem max = 820 nm) and D-light C (fluorescein; λex max =488 nm, λem max = 515 nm) light

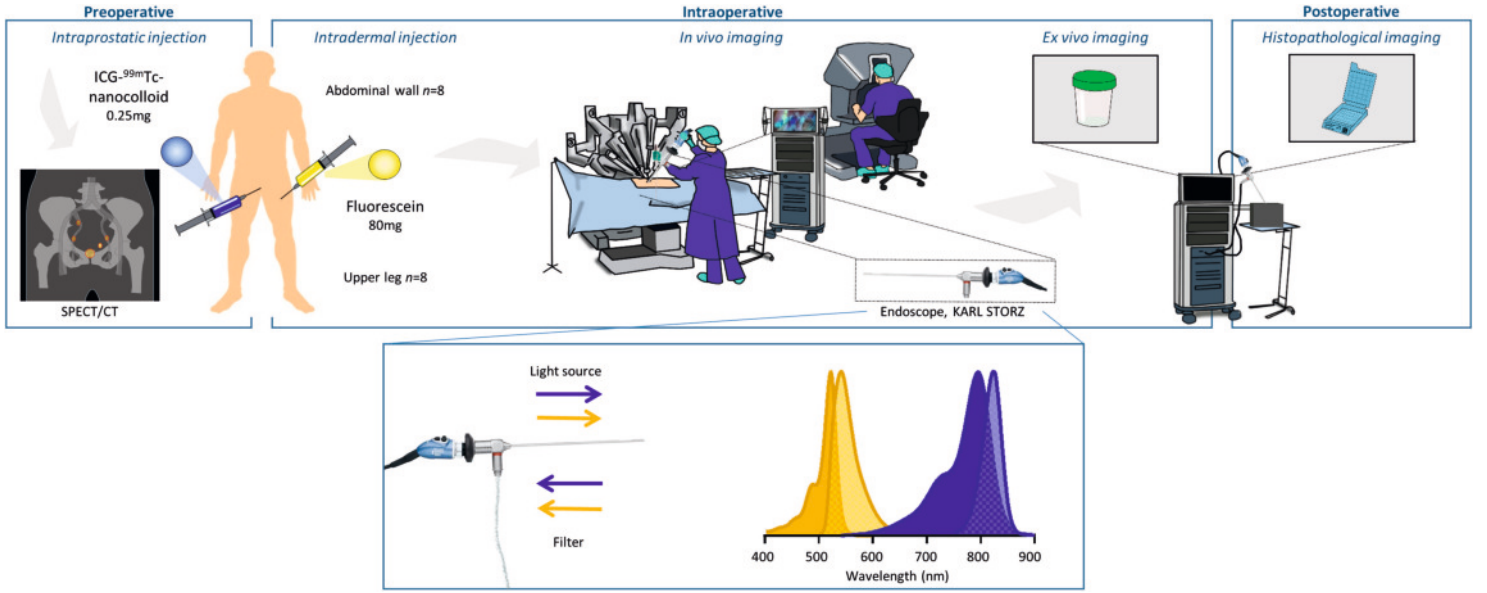

Figure 1. Illustration of perioperative study workflow. According to sentinel node procedure, ICG-^{99m}Tc-nanocolloid was injected into the prostate approximately 5 h preoperatively. Fluorescein was injected intradermally after general anesthesia into the upper leg or abdominal wall, followed by *in* and *ex vivo* imaging directly after removal of tissue in the operating room. After 48 h histopathological imaging was performed on formalin-fixed tissue.

sources (Karl Storz Endoscopie Nederland B.V., Amersfoort, the Netherlands) that allowed visualization of both ICG and fluorescein. The endoscope was maneuvered by the bedside assistant. The view of the endoscope could be seen by could be observed by the operating surgeon by integrating the images using the Tile Pro input. Additional multispectral fluorescence imaging was employed in regions where Firefly indicated a fluorescent signal to distinguish ICG from fluorescein.

Ex vivo *(back table) evaluation*

Ex vivo imaging was performed to validate *in vivo* findings immediately after removal. All excised tissue specimens were examined for the presence of ICG, fluorescein, a combination of both, or absence of staining, using the Karl Storz endoscope (Figure 1). Tissue samples were collected in separate containers or in large tissue samples, areas of interest were marked with sutures. *Ex vivo* evaluated samples of four patients who had not received fluorescein served as negative control.

Histopathological evaluation

After *ex vivo* imaging, tissue samples were put in formalin according to clinical protocol. At least 48h later the samples were examined again for the presence of ICG or fluorescein using the same endoscope and sent for histopathological examination with hematoxylin and eosin staining. From one patient and one control, formalin-fixed paraffin-embedded tissue samples were analyzed for the presence of ICG and fluorescein to determine tracer signal after paraffin-embedding. Dedicated uropathologists microscopically evaluated all slides.

Safety and follow-up

Exclusion criteria were prior abdominal or inguinal surgery, a history of severe allergic reaction and known conditions of the kidney or thyroid. Due to the recognized increased risk of anaphylactic reactions to fluorescein, patients taking beta-blockers were excluded from participation [22]. The injection of fluorescein into the skin was an off-label use. Consequently, the injection sites were monitored for redness or swelling at 15 min intervals throughout the procedure. Immediately after surgery and the next morning, the injection sites were assessed for presence of redness, swelling and fluorescence using an ultraviolet (UV) flashlight. The use of ICG-^{99m}Tc-nanocolloid in SN procedures in PCa is routine care at the NCI-AvL. All adverse events and postoperative surgical complications within 90 days were assessed according to the Clavien Dindo classification [23].

Study endpoints

The primary outcome was the technical feasibility of using multispectral fluorescence imaging to distinguish different lymphatic drainage patterns intraoperatively in primary PCa patients. In case of *in vivo* lymph staining in >10 patients the method was considered feasible. Secondary outcomes included the determination whether and where the lymphatic drainage pattern of the upper leg/abdominal wall converges with that of

the prostate and correlation of presence of ICG-^{99m}Tc-nanocolloid and fluorescein in histopathological samples with tumor.

Statistical analysis

The sample size of 16 patients was not based on statistical power considerations due to the exploratory nature of the study but on the basis of practical and clinical considerations. Interim analysis was performed after five patients. Descriptive statistics are presented as frequencies with percentages or medians and interquartile range (IQR). Statistical tests were done using IBM SPSS version 29. A p-value less than 0.05 was considered statistically significant.

Results

Eighteen patients were enrolled of which 16 patients were included; two patients withdrew consent before surgery. One because of medical reasons and one because of an unforeseen planning delay (Figure 2). Median age at surgery was 66.5 years (IQR 61-69), median initial PSA was 15.3 ng/ml (IQR 7.8-21.9) and 8/16 (50%) of patients were overweight (BMI>25.0). All patients were miN0 on preoperative prostate- specific membrane antigen (PSMA) PET/CT with a median nomogram-assessed risk of LNI of 18.9% (IQR 12.5-33.7) (detailed description on patient demographics in supplementary 2; race/ethnicity is not generally reported in patient files and is therefore not included in the table). SPECT/CT revealed a median of three visible SNs (IQR 3-4). Median OR duration was 244 minutes (IQR 222-256.5).

Intraoperative imaging – prostate (ICG) vs abdominal wall or upper leg (fluorescein)

The median interval between injection and surgical imaging was 4.9 h (IQR 4.8-5.1) for ICG-^{99m}Tc- nanocolloid and 16 min (IQR 15.0-21.5) for fluorescein. *In vivo* most of the fluorescein resided in lymph vessels (LV) (~48 LVs vs. 2 LNs), whilst ICG accumulated primarily in LNs (~42 SNs vs ~3 LVs). Fluorescein was not observed at the contralateral side of the injection. Combining all unilateral visualizations, fluorescein was observed both within the ePLND-template (obturator fossa (75% of patients), external iliac (63%), internal iliac (19%)) and outside the template (lateral to external iliac artery 69%, common iliac (6%) and crossing the umbilical ligament (6%)) (Table 1, Figure 3). Fluorescein was located in Cloquet's node in 75%, whilst ICG was not seen at all at this location. ICG, following the SN pathway of the prostate, was also seen within the ePLND-template (obturator fossa (100%), external iliac (63%), internal iliac (13%)). ICG (or SNs) outside the ePLND-template was distributed lateral to external iliac (13%), around common iliac (6%), pararectal/presacral (25%), crossing the umbilical ligament/paravesical (19%) (Table 1, Figure 3). Twice it was observed that fluorescein and ICG overlapped in a lymph vessel, both times in the internal iliac region.

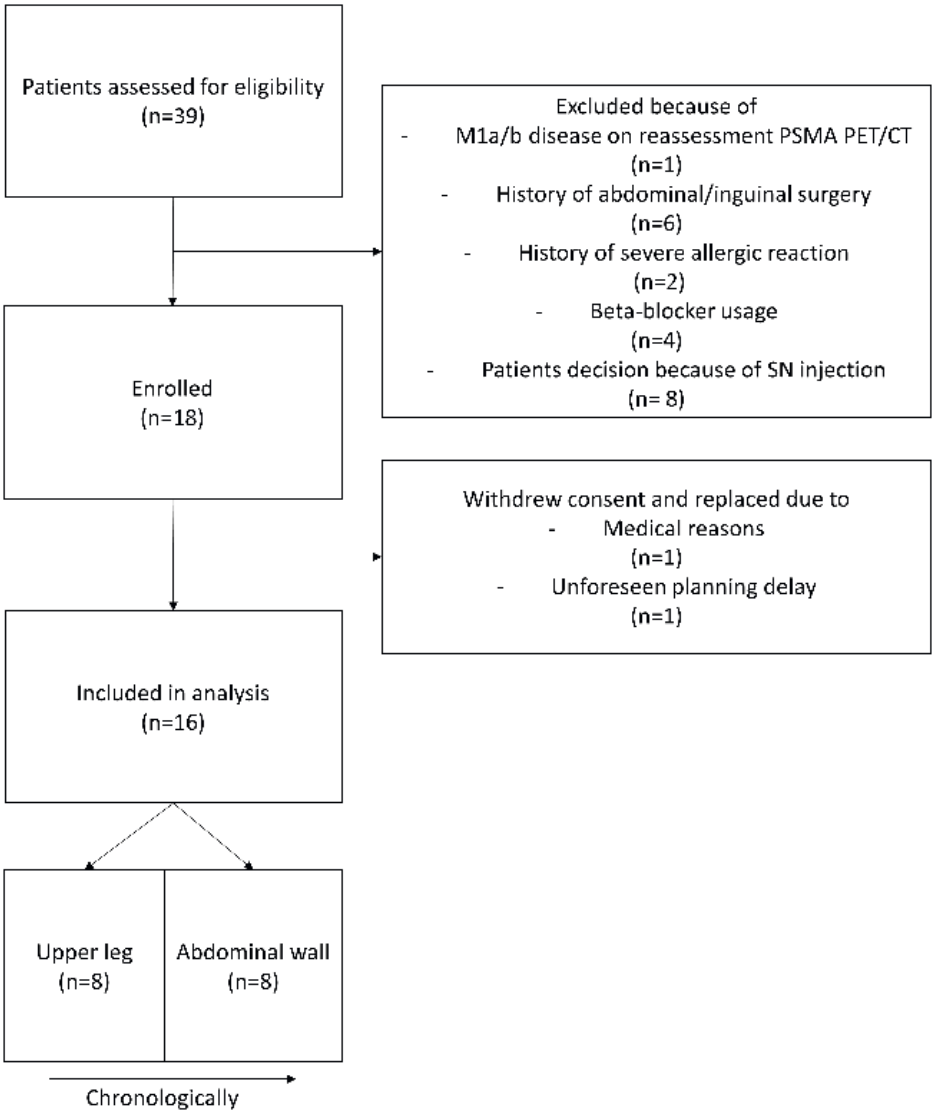

Figure 2. Flowchart of patient assessment and enrollment.

Table 1. Surgical and histopathological outcomes

Parameter	Overall (n=16) (n=8)		Upper leg group (n=8)		Abdominal wall group	
Preoperative						
Median injected dose 99mTc, MBq (IQR)	219.6 (216.3-224.4)		220.1 (213.6-231.9)		219.3 (216.6-220.9)	
Median time injection ICG to first intraoperative imaging, hours (IQR)	4.9 (4.8-5.1)		4.9 (4.8-5.3)		4.9(4.9-5.1)	
Median number of SNs on SPECT/CT, (IQR)	3.0 (3.0-4.0)		3.5 (3.0-4.8)		3.0 (2.3-3.8)	
Intraoperative						
Injection side fluorescein						
Left	7 (43.8)		4 (50.0)		3 (37.5)	
Right	9 (56.3)		4 (50.0)		5 (62.5)	
Median time injection fluorescein to first intraoperative imaging, minutes (IQR)	16 (15.0-21.5)		16.0 (14.5-24.3)		16.0 (16.0-21.5)	
Median OR time, minutes (IQR)	244 (222-256.5)		243 (223-255)		244 (213.3-255.5)	
Distribution of tracers *in vivo*						
Location fluorescein or ICG, n (% of n patients)	*Fluorescein*	*ICG*	*Fluorescein*	*ICG*	*Fluorescein*	*ICG*
Cloquet's	12 (75.0)	0 (0.0)	5 (62.5)	0 (0.0)	7 (87.5)	0 (0.0)
Obturator fossa	12 (75.0)	16 (100.0)	4 (50.0)	8 (100.0)	8 (100.0)	8 (100.0)
External iliac	10 (62.5)	10 (62.5)	4 (50.0)	6 (75.0)	6 (75.0)	4 (50.0)
Lateral to external iliac	11 (68.8)	2 (12.5)	5 (62.5)	2 (25.0)	6 (75.0)	0 (0.0)
Internal iliac	3 (18.8)	2 (12.5)	0 (0.0)	1 (12.5)	3 (37.5)	1 (12.5)
Common Iliac	1 (6.3)	1 (6.3)	0 (0.0)	0 (0.0)	1 (12.5)	1 (12.5)
Medial to umbilical ligament / paravesical	1 (6.3)	4 (25.0)	0 (0.0)	3 (37.5)	1 (12.5)	1 (12.5)
Presacral / pararectal	0 (0.0)	4 (25.0)	0 (0.0)	2 (25.0)	0 (0.0)	2 (25.0)
Histopathological (formalin fixed tissue)						
Location to fluorescein injection side	*Ipsilateral*	*Contra-lateral*	*Total*	*Total*	*Total*	
Total number of LNs (incl SNs) removed, n	202	168	370	181	189	
Total tumor positive LNs, n	9	4	13	10	3	
Total number of LNs containing ICG, n	64	18	98	55	43	
Total number of LNs containing ICG *and* tumor positive, n	9	2	11	9	2	
Total number of LNs containing fluorescein, n	10	0	10	5	5	

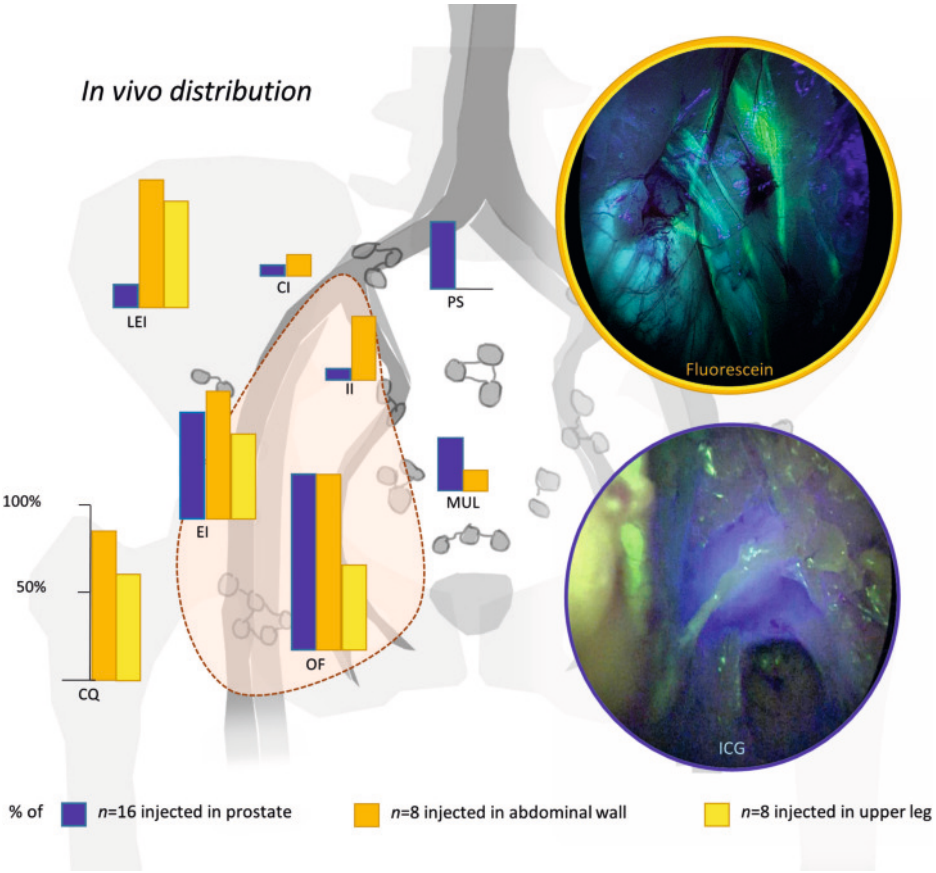

Figure 3. Unilateral representation of distribution of fluorescein (upper leg; yellow, and abdominal wall; orange) and ICG-^{99m}Tc-nanocolloid (prostate; blue) with examples of *in vivo* Karl Storz endoscope imaging filtered for fluorescein (yellow) and ICG (blue). CQ = Cloquet's, OF = Obturator fossa, EI = External Iliac, LEI = Lateral to External Iliac, II = Internal Iliac, CI = Common Iliac, PS = Presacral/pararectal, MUL = Medial to Umbilical Ligament/paravesical.

Intraoperative imaging – upper leg vs abdominal wall (both fluorescein)

Comparing upper leg and abdominal wall, the regions where fluorescein was observed were similar but showed some differences (left and right combined in Table 1, Figure 3). The abdominal wall drainage was seen more frequently and in more regions than the upper leg. Both were seen mainly in Cloquet's node (upper leg 63%, abdominal wall 88%) and lateral to external iliac (upper leg 50%, abdominal wall 75%). Although both visible, the abdominal wall pattern was seen in the obturator fossa in twice as many patients compared to upper leg (100 vs 50%, respectively).

Intraoperative imaging – lymph fluid leakage

In six patients (2/8 upper leg, 4/8 abdominal wall), fluorescein leakage was observed <1cm of the cut lymph vessels. Leakage of lymph fluid >1cm from the cut vessels was only identified when tracer was trapped between layers of fascia (n=2) and after opening the bladder neck (n=16). (Supplementary 3) Leakage of ICG was not observed.

Ex vivo *and histopathological evaluation*

At the back table, in 9/167 (5%) of pathological containers with freshly removed larger tissue samples, fluorescein was seen and in 81/167 (49%) ICG. Two samples contained both fluorescein and ICG.

Approximately 48 h later, formalin-fixed nodal tissue samples were examined before paraffin-embedding for presence of fluorescein and ICG (n=370). In 10/370 (3%) fluorescein was seen (all ipsilateral to injection side; total removed nodes ipsilaterally n=202) (Table 1) and in 98/370 (26%) ICG (of which 64/98 (65%) ipsilateral to fluorescein injection), suggesting a fixation effect on the fluorescence signal. Although at the back table two samples contained both tracers, when examined at nodal level none contained both fluorescein and ICG. Thirteen nodes were tumor positive of which 11 (85%) were ICG stained (SNs) and two (15%) were not (Figure 4). After paraffin-embedding it was possible to identify ICG within LNs but fluorescein staining was not specific (Supplementary 4).

Safety and follow-up

The injection of fluorescein did not trigger any local or systemic reaction. Patients reported no postoperative discomfort or pain at the injection site and no redness or swelling was seen during surgery, directly after surgery or the following day. The presence of yellow skin discoloration lasted up to two days postoperatively (Supplementary 5).

Within 90 days postoperative 12/16 (75%) patients suffered a complication grade Clavien-Dindo I, 5/16 (31%) Clavien-Dindo II, 2/16 (13%) Clavien-Dindo IIIa. Three serious adverse events (re-admission) were observed in one patient (Table 2). All events were considered unrelated to fluorescein or ICG-^{99m}Tc- nanocolloid administration.

One patient reported lymphedema in one leg (6%), seven in one or both legs together with the abdominal wall (44%), and four (25%) reported only lymphedema of the abdominal wall. Five men (35%) complained of a swollen scrotum, all independent of injection site and side. The lymphedema was reported to last between two days and three months. One patient was referred for specialized treatment regarding lymphedema of the abdominal wall. Postoperative PSA was undetectable in 13/16 (81%).

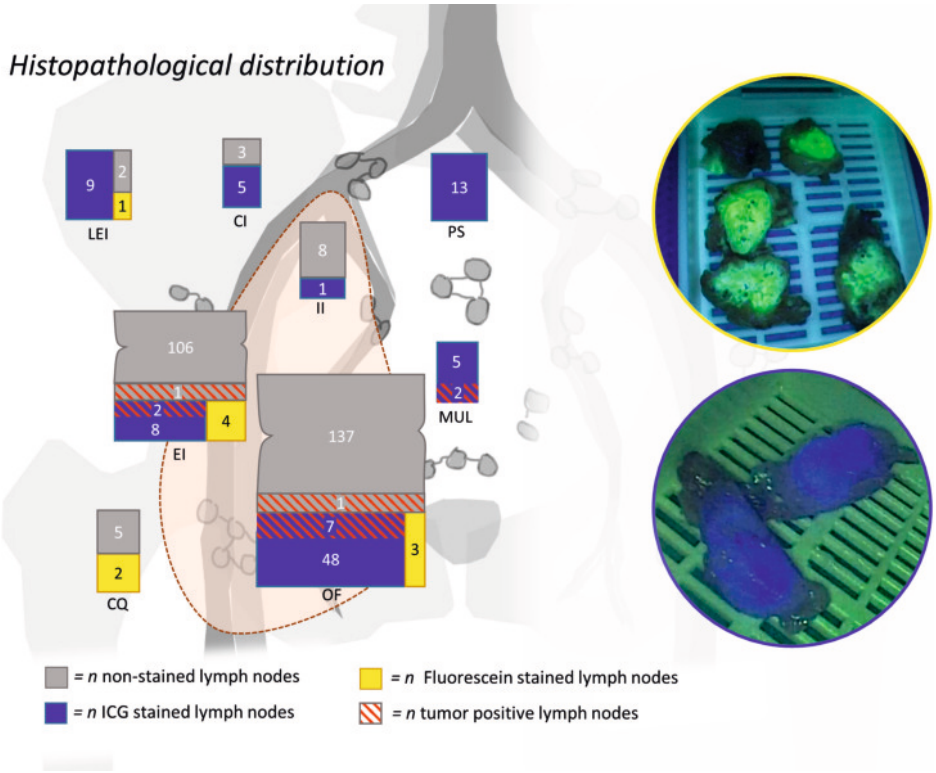

Figure 4. Unilateral representation of the distribution of detected lymph nodes with examples of Karl Storz imaging filtered for ICG and Fluorescein at histopathology. CQ = Cloquet's, OF = Obturator fossa, EI = External Iliac, LEI = Lateral to External Iliac, II = Internal Iliac, CI = Common Iliac, PS = Presacral/pararectal, MUL = Medial to Umbilical Ligament/paravesical.

Table 2. Complications according to Clavien-Dindo <90 days post-surgery

Clavien-Dindo I, n(% of n=16 patients)	
Lymphedema	12 (75%)
Paresthesia	2 (13%)
Mild allergic reaction to ciproxin	1 (6%)
Clavien-Dindo II, n(%)	
Lymphedema >2 months treated with edema therapy	1 (6%)
UTI treated with antibiotics	2 (13%)
TUC replacement	1 (6%)
Prolonged TUC in situ	1 (6%)
Infected urinoma (requiring re-admission)	1 (6%)
Pulmonary embolism	1 (6%)
UTI with signs of bacteremia (requiring re-admission)	1 (6%)
Clavien-Dindo IIIa, n(%)	
Cystoscopy before replacement of TUC	1 (6%)
Urinoma treated with nephrostomy catheter and abdominal drain (requiring re-admission)	1 (6%)

TUC = transurethral catheter, UTI = urinary tract infection

Discussion

This prospective study demonstrated the feasibility of real-time, multispectral fluorescence imaging to visualize lymphatic drainage patterns from different anatomical locations within the ePLND-template. A first step in analyzing future applications where using multispectral imaging of drainage patterns will help distinguish patterns from healthy and diseased organs within the pelvis. Ultimately, the aim would be to spare the lymphatics draining from the healthy organs and reduce morbidity. To translate fundamental multicolor imaging performed in mice [17], via porcine models [18], to humans, the clinically approved dyes ICG and fluorescein were used. Our *in vivo* findings indicate that lymphatic drainage patterns of prostate and other locations are in close relation within the ePLND-template.

When examining the distribution of the prostate in comparison to upper leg or abdominal wall, it became apparent that some features from earlier observations in porcine models were lost [18]. Lowering the fluorescein dose from 500 mg to 80 mg (for safety reasons), may have prevented intraoperative *nodal* visualization but did show fluorescein clearly in lymphatic vessels. Hence, the detection sensitivity for fluorescein was limited and the distinct lymphatic separation observed in porcine models did not translate to the human situation. Still the mapping of the drainage patterns was still possible in regard to ePLND- template regions. That said, the observed patterns of skin or prostate injected tracers were clearly closely related *in vivo*. The main differences being that ICG was not observed around Cloquet's, whereas fluorescein was absent in the presacral/pararectal regions as seen in Figure 3. This correlates with known literature where Cloquet's node is regarded the highest superficial node of the ilioinguinal basin when looking at lower limb drainage and is rarely reported to be a SN of the prostate (<1.1%) [24 25].

The *in vivo* distribution of leg or abdominal wall-injected fluorescein showed only ipsilateral staining, corroborating results in melanoma studies where contralateral nodes are only described in case reports where patients had prior surgery [26-28]. The transient nature of fluorescein and high tissue attenuation of 515 nm fluorescent emissions made fluorescein detectability inferior compared to ICG for LN-imaging at the back table, and after formalin fixation at histopathology. This may explain why only 10/202 of the ipsilateral nodes were clearly fluorescein stained compared to the 64 ipsilateral ICG-stained nodes.

The lymphatic drainage pattern from the abdominal wall was similar to that from the upper leg, although the abdominal drainage pattern was seen more frequently and in more locations within the pelvis. This may be explained by a different drainage velocity or because the patterns slightly differ. The latter may explain why lymphedema of the abdominal wall was more frequently reported (75%) when compared to lymphedema of the upper leg (50%).

In regard of complications, injection of 80 mg fluorescein divided in two deposits in the skin did not result in redness, swelling or other local or systemic events, confirming the results from Chang et al [29]. Notably, our prevalence of lymphedema was higher than reported in existing literature [9]. The numbers may be underrated in current literature [9] as lymphedema is one of the least studied complications of prostate cancer treatment despite its considerable impact on health-related quality of life [10-12]. However, studies on gynecological cancers have reported high prevalence of lymphedema (up to 79%) [30 31]. Prostate cancer related literature generally describes staff-reported lymphedema, which was lower in comparison to patient-reported [32], and data stems from predominantly retrospective studies. In this study, the lymphedema was patient-reported. Consequently, it should also be taken into account that patients' perception of lymphedema was not verified by a physician which may have caused bias. Other factors like body-mass-index may play a role and are reported to have an increased risk of lymphedema in other cancers [33 34]. In prostate cancer the risk of complications in general is reported to be higher in overweight patients but the association with lymphedema remains unknown [35 36].

Limitations of the study include small sample size and the fact it was performed in a single center by different surgeons. In addition, determining whether the drainage patterns overlapped depended on various factors, including choosing the side with the most SNs on SPECT/CT and the location of the SN *in vivo* all contribute to the already high interpatient variability of pelvic lymphatic anatomies [37]. Furthermore, the fluorescence endoscope was maneuvered by the bedside assistant under verbal guidance and *in vivo* fluorescence imaging deep in the pelvis could be challenging using this endoscope. The experimental multispectral imaging set-up described in this manuscript needs further optimization before it can be more widely applied. Hereby logistic refinement can be achieved by using a robot integrated multispectral camera [21]. Overall, precision imaging during surgery tends to cost extra OR time, but may ultimately help reduce costs later on by minimizing the morbidity and reducing the recurrence rates.

Although the multispectral imaging was technically feasible, the *in vivo* closely related lymphatic drainage patterns and the fact fluorescein was relatively inferior indicate that sparing non-disease related (fluorescein containing) lymphatic structures may result in under sampling cancer-containing LNs. As overlapping patterns were not observed at nodal level at histopathology and lymphedema of the abdominal wall was seen more frequently, future studies should focus on possible tumor presence in nodes draining from the abdominal wall.

Conclusions

Multispectral fluorescence imaging of two distinct drainage patterns was technically feasible during robot-assisted PCa surgery. Our initial *in vivo* findings indicate that within the ePLND-template, lymphatic drainage patterns of the prostate overlap with those of upper leg and abdominal wall. The properties of fluorescein render it unsuitable as a tracer for fluorescence histopathological confirmation.

References

1. Mottet N, van den Bergh RCN, Briers E, et al. EAU-EANM-ESTRO-ESUR-SIOG Guidelines on Prostate Cancer-2020 Update. Part 1: Screening, Diagnosis, and Local Treatment with Curative Intent. Eur Urol 2021;**79**(2):243-62.
2. Briganti A, Larcher A, Abdollah F, et al. Updated nomogram predicting lymph node invasion in patients with prostate cancer undergoing extended pelvic lymph node dissection: the essential importance of percentage of positive cores. Eur Urol 2012;**61**(3):480-7.
3. Morizane S, Takenaka H. Current status and therapeutic value of extended pelvic lymph node dissection during radical prostatectomy for prostate cancer Prostate International 2024;**12**(3):117-27.
4. Padera TP, Meijer EF, Munn LL. The Lymphatic System in Disease Processes and Cancer Progression. Annu Rev Biomed Eng 2016;**18**:125-58.
5. Briganti A, Chun FK, Salonia A, et al. Complications and other surgical outcomes associated with extended pelvic lymphadenectomy in men with localized prostate cancer. Eur Urol 2006;**50**(5):1006-13.
6. Touijer KA, Sjoberg DD, Benfante N, et al. Limited versus Extended Pelvic Lymph Node Dissection for Prostate Cancer: A Randomized Clinical Trial. Eur Urol Oncol 2021;**4**(4):532-39.
7. Baas DJH, de Baaij JMS, Sedelaar JPM, et al. Extended pelvic lymph node dissection in robot-assisted radical prostatectomy is an independent risk factor for major complications. J Robot Surg 2024;**18**(1):140.
8. Orvieto MA, Coelho RF, Chauhan S, Palmer KJ, Rocco B, Patel VR. Incidence of lymphoceles after robot-assisted pelvic lymph node dissection. BJU Int 2011;**108**(7):1185-90.
9. Clinckaert A, Callens K, Cooreman A, et al. The Prevalence of Lower Limb and Genital Lymphedema after Prostate Cancer Treatment: A Systematic Review. Cancers (Basel) 2022;**14**(22).
10. Wit EMK, Acar C, Grivas N, et al. Sentinel Node Procedure in Prostate Cancer: A Systematic Review to Assess Diagnostic Accuracy. Eur Urol 2017;**71**(4):596-605.
11. Mazzone E, Dell'Oglio P, Grivas N, et al. Diagnostic Value, Oncologic Outcomes, and Safety Profile of Image-Guided Surgery Technologies During Robot-Assisted Lymph Node Dissection with Sentinel Node Biopsy for Prostate Cancer. J Nucl Med 2021;**62**(10):1363-71.
12. Li C, Xu X, McMahon N, Alhaj Ibrahim O, Sattar HA, Tichauer KM. Paired-Agent Fluorescence Molecular Imaging of Sentinel Lymph Nodes Using Indocyanine Green as a Control Agent for Antibody-Based Targeted Agents. Contrast Media Mol Imaging 2019;**2019**:7561862.
13. Chen QY, Xie JW, Zhong Q, et al. Safety and Efficacy of Indocyanine Green Tracer-Guided Lymph Node Dissection During Laparoscopic Radical Gastrectomy in Patients With Gastric Cancer: A Randomized Clinical Trial. JAMA Surg 2020;**155**(4):300-11.
14. Van Den Berg NS, Buckle T, Kleinjan GI, et al. Hybrid tracers for sentinel node biopsy. Q J Nucl Med Mol Imaging 2014;**58**(2):193-206.
15. Wit EMK, KleinJan GH, Berrens AC, et al. A hybrid radioactive and fluorescence approach is more than the sum of its parts; outcome of a phase II randomized sentinel node trial in prostate cancer patients. Eur J Nucl Med Mol Imaging 2023;**50**(9):2861-71.
16. KleinJan GH, van Werkhoven E, van den Berg NS, et al. The best of both worlds: a hybrid approach for optimal pre- and intraoperative identification of sentinel lymph nodes. Eur J Nucl Med Mol Imaging 2018;**45**(11):1915-25.
17. Kosaka N, Mitsunaga M, Choyke PL, Kobayashi H. In vivo real-time lymphatic draining using quantum-dot optical

imaging in mice. Contrast Media Mol Imaging 2013;**8**(1):96-100.

18. Meershoek P, KleinJan GH, van Oosterom MN, et al. Multispectral-Fluorescence Imaging as a Tool to Separate Healthy from Disease-Related Lymphatic Anatomy During Robot-Assisted Laparoscopy. J Nucl Med 2018;**59**(11):1757-60.
19. van den Berg NS, Buckle T, KleinJan GH, van der Poel HG, van Leeuwen FWB. Multispectral Fluorescence Imaging During Robot-assisted Laparoscopic Sentinel Node Biopsy: A First Step Towards a Fluorescence-based Anatomic Roadmap. Eur Urol 2017;**72**(1):110-17.
20. Zapardiel I, Alvarez J, Barahona M, et al. Utility of Intraoperative Fluorescence Imaging in Gynecologic Surgery: Systematic Review and Consensus Statement. Ann Surg Oncol 2021;**28**(6):3266-78.
21. Meershoek P, KleinJan GH, van Willigen DM, et al. Multi-wavelength fluorescence imaging with a da Vinci Firefly-a technical look behind the scenes. J Robot Surg 2021;**15**(5):751-60.
22. Summary of Product Characteristics - Fluorescite. Brussels: SERB, Last updated 2021.
23. Clavien PA, Barkun J, de Oliveira ML, et al. The Clavien-Dindo classification of surgical complications: five-year experience. Ann Surg 2009;**250**(2):187-96.
24. Joyce KM. Surgical Management of Melanoma. In: Ward WH, Farma JM, eds. Cutaneous Melanoma: Etiology and Therapy. Brisbane (AU), 2017.
25. Plata Bello A, Apatov SE, Benfante NE, et al. Prevalence of High-Risk Prostate Cancer Metastasis to Cloquet's Ilioinguinal Lymph Node. J Urol 2022;**207**(6):1222-26.
26. Hague A, Platford B, Rehman SU, Howes AJ, Brackley P. Multi-nodal basin drainage in lower limb melanoma. JPRAS Open 2024;**39**:71-74.
27. Komenaka IK, Nguyen ET, DeRaffele G, Mitcham J, Hurst-Wicker KS, Kaufman HL. The contralateral sentinel node. Can J Surg 2005;**48**(5):416-7.
28. Zhou C, Louwman M, Wakkee M, et al. Primary Melanoma Characteristics of Metastatic Disease: A Nationwide Cancer Registry Study. Cancers (Basel) 2021;**13**(17).
29. Chang YW, Lee HY, Lee CM, et al. Sentinel lymph node detection using fluorescein and blue light-emitting diodes in patients with breast carcinoma: A single-center prospective study. Asian J Surg 2020;**43**(1):220-26.
30. Kim JH, Choi JH, Ki EY, et al. Incidence and risk factors of lower-extremity lymphedema after radical surgery with or without adjuvant radiotherapy in patients with FIGO stage I to stage IIA cervical cancer. Int J Gynecol Cancer 2012;**22**(4):686-91.
31. Yost KJ, Cheville AL, Al-Hilli MM, et al. Lymphedema after surgery for endometrial cancer: prevalence, risk factors, and quality of life. Obstet Gynecol 2014;**124**(2 Pt 1):307-15.
32. Thorsteinsdottir T, Stranne J, Carlsson S, et al. LAPPRO: a prospective multicentre comparative study of robot-assisted laparoscopic and retropubic radical prostatectomy for prostate cancer. Scand J Urol Nephrol 2011;**45**(2):102-12.
33. Graf N, Rufibach K, Schmidt AM, Fehr M, Fink D, Baege AC. Frequency and risk factors of lower limb lymphedema following lymphadenectomy in patients with gynecological malignancies. Eur J Gynaecol Oncol 2013;**34**(1):23-7.
34. Jammallo LS, Miller CL, Singer M, et al. Impact of body mass index and weight fluctuation on lymphedema risk in patients treated for breast cancer. Breast Cancer Res Treat 2013;**142**(1):59-67.
35. Bianchi LMG, Irmici G, Ce M, et al. Diagnosis and Treatment of Post-Prostatectomy Lymphedema: What's New? Curr Oncol 2023;**30**(5):4512-26.

36. Porcaro AB, Sebben M, Tafuri A, et al. Body mass index is an independent predictor of Clavien-Dindo grade 3 complications in patients undergoing robot assisted radical prostatectomy with extensive pelvic lymph node dissection. J Robot Surg 2019;**13**(1):83-89.
37. Okitsu T, Tsuji T, Fujii T, et al. Natural history of lymph pumping pressure after pelvic lymphadenectomy. Lymphology 2012;**45**(4):165-76.

Supplementary 1. Detailed description of tracer injection

Sentinel node (SN) identification

Indocyanine Green(ICG)-^{99m}Technetium(Tc)-nanocolloid (based on Nanocoll® or Nanoscan®; GE Healthcare BV, Leiderdorp, the Netherlands;) was prepared by mixing 250 ICG in sterile water with 200 MBq ^{99m}Tc-nanocolloid in 2 ml saline. The resulting formulation was administered approximately five hours prior to surgery in four deposits of 0.5 ml into the peripheral zone of the prostate using transrectal ultrasound guidance. At 15 min and two hours post tracer injection, lymphatic mapping was performed using static planar lymphoscintigraphy of the pelvic area, followed by single photon emission computed tomography (SPECT)/CT using a dual head gamma camera (Symbia T, Siemens, Erlangen, Germany). Planar images and SPECT, CT, and fused SPECT/CT including volume-rendering reconstructions were displayed using OsiriX medical imaging software (Pixmeo, Geneva, Switzerland). The images were reviewed by a nuclear medicine physician and the number and location of SNs were reported and communicated with the surgeon.

Lymphangiography upper leg or abdominal wall

In the operating room, after administering general anesthesia, fluorescein (80 mg; 4 ml of 2% fluorescein in saline 0.9%); ½-life 24 min) was injected unilaterally into the dermis in two deposits of 2 ml each, either at the medial and lateral side of the upper leg (n=8) or at the left or right lower quadrant of the abdominal wall (n=8). The injection site was massaged to promote lymphatic flow. The side of injection (left/right) was chosen based on the side showing the most SNs on SPECT/CT to optimally investigate the possibility of imaging converging drainage patterns. On both sides ePLND and SN procedure was performed.

Fluorescent dye	λem max	Extinction coefficient	Fluorescence lifetime t1/2	Quantum yield
ICG	820 nm	1.8 x 105 (HSA)	0.97 (DMSO)	5 (HSA)
Fluorescein	515 nm	0.4 x 105 (HSA)	4 (H2O)	12 (HSA)

*from Meershoek et al. 2020 [20]

Supplementary 2. Patient demographics

	Age, yrs	Clinical TNM stage	MRI T stage	iPSA, ng/mL	Biopsy ISUP grade group	Risk of LNI Briganti 2012	Pathologic al TNM stage	Pathologic al ISUP grade group	Resection margin	PSA at first follow up visit, ng/mL
Patient 1	66	cT2N0M0	T2b	7.8	3	9.8	pT2N0	3	R0	<0.01
Patient 2	68	cT2N0M0	T3a	22.8	3	21.9	pT3aN1	2	R1	1.32
Patient 3	69	cT2bN0M0	T2	13.0	4	17.0	pT2cN1	3	R0	<0.01
Patient 4	71	cT2N0M0	T3a	42.0	3	38.0	pT3aN1	4	R1	0.18
Patient 5	68	cT2N0M0	T3b	16.0	3	32.7	pT3bN0	3	R1	<0.01
Patient 6	75	cT1cN0M0	T2	7.7	3	12.4	pT2N0	3	R0	0.5
Patient 7	57	cT1cN0M0	T2	16.8	5	9.4	pT3aN0	5	R0	0.07
Patient 8	61	cT2N1M0	T3b	14.6	2	12.6	pT3bN1	2	R1	<0.01
Abdominal wall										
Patient 9	60	cT3aN0M0	T3b	24.5	2	50.7	pT3bN0	3	R1	<0.01
Patient 10	64	cT2N0M0	T3a	5.9	3	15.6	pT3aN0	2	R0	<0.05
Patient 11	67	cT2N0M0	T2	14.0	5	19.0	pT2N1	3	0	<0.006
Patient 12	68	cT2N0M0	T3a	5.52	2	7.2	pT3aN0	2	R0	<0.01
Patient 13	62	cT2N0M0	T2	17.5	2	18.8	pT3aN0	3	R0	<0.01
Patient 14	53	cT1cN0M0	T3a	45.6	5	40.3	pT2N0	3	R0	<0.01
Patient 15	65	cT2N0M0	T3a	19.3	3	34.0	pT3bN1	3	R0	<0.01
Patient 16	71	cT2N0M0	T3a	7.9	5	28.5	pT2N0	2	R0	<0.1

iPSA = initial prostate-specific antigen; ISUP = International Society of Urological Pathology; LNI = Lymph node involvement

Supplementary 3. Leakage of lymph fluid when severing lymph vessels

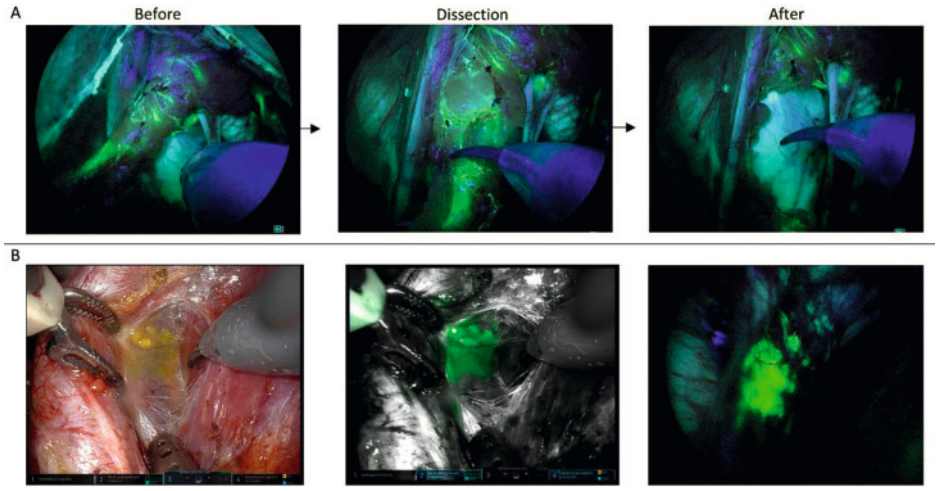

A) Before, during and after fluorescein stained lymph vessels connecting Cloquet's with the obturator fossa are being severed (fluorescein imaging). B) Lymph fluid leakage when trapped between layers of fascia in white light, Firefly integrated camera imaging and fluorescein imaging.

Supplementary 4. Fluorescein in embedded lymph nodes

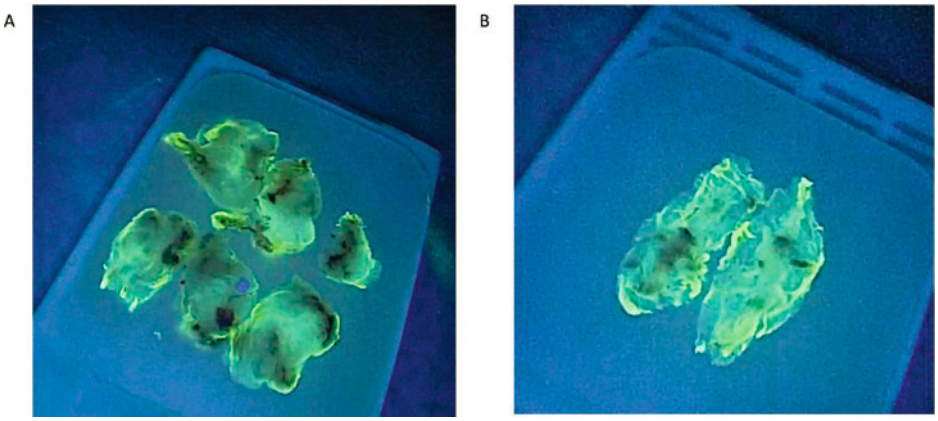

A) Fluorescein imaging after paraffin embedding in a fluorescein stained node at histopathology. B) Fluorescein imaging after paraffin embedding in a control patient.

Supplementary 5. White light and ultraviolet-light imaging the injection site postoperative and 1 day post-surgery

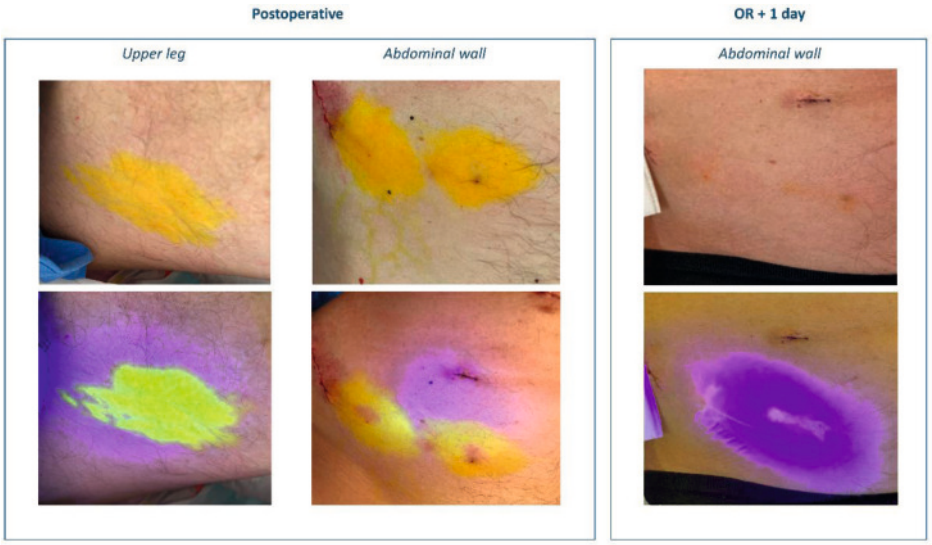

Supplementary 6. The manuscript explained in video available via QR code

Berrens AC, Vis AN, van Leeuwen PJ, Wit EMK, van Leeuwen FWB, van der Poel HG
Lymphat Res Biol. 2025 Nov 20.

Chapter 7

Lymphatic Drainage of the Abdominal Wall Within the Extended Nodal Dissection Template During Prostate Cancer Surgery — Mapping Overlapping Patterns

Abstract

Background. The number of lymph nodes (LN) excised during extended pelvic lymph node dissections (ePLND) in prostate cancer (PCa) are related to complications including lymphoceles (up to 15%) and lymphedema (up to 14%). Approaches that reduce the resection of lymph nodes related to healthy anatomies may help reduce the complication rate. The aim of this study was to unravel the complexity of the pelvic lymphatics by researching to what extent the lymphatics draining the abdominal wall overlap with the ePLND template and the lymphatic metastatic spread of primary PCa lesions.

Methods. This prospective (NCT05120973), single-center study included 10 patients who underwent robot-assisted radical prostatectomy with ePLND. To visualize the lymphatic drainage of the abdominal wall, indocyanine green (ICG) was injected intradermally at four sites distributed over the lower abdomen. *In vivo* fluorescence imaging was performed using the robot integrated fluorescence endoscope. Harvested LNs were assessed for fluorescence and tumor content.

Results. In total, 195 lymph nodes were removed (average 20/patient), 56% of these nodes were fluorescent (average 11.5/patient). Three patients were pN1, yielding 6 positive nodes, of which in two patients the tumor positive nodes were also found to be fluorescent (3 nodes in total (50%)). Indicating overlapping patterns.

Conclusion. Within the ePLND template there is a 56% overlap, on a nodal level, with the lymphatic drainage from the abdominal wall. Three fluorescent LNs also contained metastases, indicating that the lymphatic drainage of healthy tissues directly converges with the drainage of the primary PCa.

Introduction

It is recommended by European Association of Urology guidelines to offer extended pelvic lymph node dissection (ePLND) to prostate cancer (PCa) patients when the nomogram-assessed risk of nodal involvement exceeds 5% [1 2]. Unfortunately, the risk of complications caused by damage to the lymphatic system is related to the number of lymph nodes (LNs) dissected [3-5]. Most common complications being lymphoceles (up to 15%) and lymphedema (up to 14%) [6 7]. Whereby lymphedema is known to have considerable impact on the health-related quality of life [8-11].

The necessity of and ways to reduce invasiveness of lymph node dissection are both highly debated [12- 16] It is important to understand to what extent the ePLND template also provides drainage of healthy anatomies e.g. abdominal wall that can suffer from complications. Insights that may help reduce the extent of ePLND without diminishing oncological outcomes. Melanoma related sentinel node literature indicates that from the abdominal wall superficial lymph vessels below the umbilicus also drain to the inguinal lymph nodes, followed by the external iliac, common iliac and lateral aortic LNs [17 18]. To what extent such drainage overlaps with the drainage of the prostate and primary PCa is unclear. Where studies in porcine models, using multispectral fluorescence imaging, suggested a clear separation between the drainage of the prostate and healthy tissue [19 20], it proved to be impossible to confirm these findings in humans [21]. Meaning a different strategy is required to study this phenomenon in humans.

Using indocyanine green, a lymphangiographic agent commonly used to map the drainage of skin [22] we aimed to assess whether the lymphatic spread of the primary PCa converges with the lymphatic drainage of the abdominal wall. This also allowed us to determine if LNs associated with the healthy abdominal wall could also contain PCa metastases.

Methods

Study design and patient population

The local ethics committee at the Netherlands Cancer Institute-Antoni van Leeuwenhoek Hospital (NCI- AVL), Amsterdam, The Netherlands (NCT05120973) approved this single-arm, single-center, prospective, study. All patients provided written informed consent. Between September 2023 and April 2024, male patients aged 18 years or older, with histopathologically confirmed PCa and an increased risk (>5%) of lymph node involvement (LNI) according to Briganti 2012 nomogram (standard of care) and according to the Amsterdam Brisbane Sydney (ABS) nomogram (taking PSMA PET into account) [2 23], who were scheduled to undergo robot-assisted radical prostatectomy with ePLND were included. Clinical and pathological as well as patients' characteristics were documented.

In vivo *lymphangiography of the abdominal wall*

At the operating room, after administering general anesthesia, ICG-Verdye (Profiplus bvba, Kortessem, Belgium) dissolved in sterile water was injected bilaterally into the abdominal dermis in four deposits of 0.5ml (of 1.25mg ICG) each. This was done at both lower quadrants of the abdominal wall just medial and lateral of the midclavicular line (Figure 1, Supplementary 1). The injection site was massaged to promote lymphatic flow. Using a da Vinci Xi Surgical System (Intuitive surgical, Inc, Sunnyvale, CA, USA) the procedure started with the ePLND followed by prostatectomy and continuous monitoring of ICG lymph drainage with the integrated da Vinci Firefly fluorescence endoscope. During surgery, attempts were made to visualize the dynamics of the fluorescence distribution over time. The fluorescent specimens were collected separate from the non-stained tissue before sending to pathology.

Ex vivo *(back table) evaluation*

For larger tissue specimens or in case of doubt on the presence of fluorescence, further analysis was done *ex vivo* employing a Hamamatsu FIS-00 fluorescence camera (HAMAMATSU PHOTONICS K.K., Tokyo, Japan) designed for open surgery.

Histopathological evaluation

After *ex vivo* imaging, tissue samples were put on formalin according to clinical protocol. The presence of tumor was correlated with the presence of fluorescence on nodal level. The dedicated uropathologist who examined the tissue was not blinded for the presence of fluorescence.

Safety and follow-up

Exclusion criteria included a history of severe allergic reaction and known conditions of the kidney or thyroid and prior inguinal or abdominal surgery [24]. The injection sites were monitored for redness or swelling directly after surgery and the next morning. All adverse events and surgical complications within 90 days postoperatively were scored and reported according to the Clavien-Dindo classification [25].

Statistical analysis

Considering an expected average of 35% risk of LN involvement we aimed to include 10 patients to ensure the probability of >97% of including at least one patient with nodal metastases. Descriptive statistics are presented as medians and interquartile range (IQR) or frequencies with percentages. Statistical tests were done using IBM SPSS version 29. A p-value less than 0.05 was considered statistically significant.

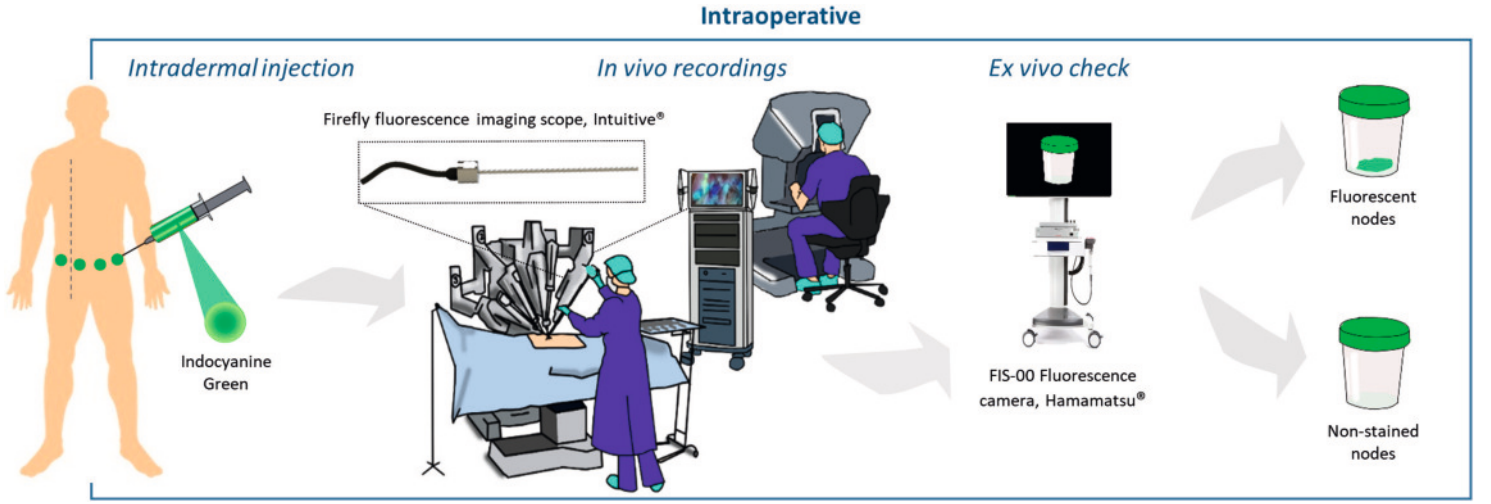

Figure 1. Study workflow. Starting with intradermal injection of ICG after general anesthesia, followed by *in vivo* imaging using the Firefly fluorescence imaging scope. *Ex vivo*, the Hamamatsu Handheld ICG Imaging System (FIS-00) could be used to separate the green (fluorescent) nodes from the non-stained nodes.

Results

Patient characteristics

10 patients were enrolled with a median age at surgery of 72.5 years (IQR 66-75.3) and median initial PSA of 7.9 ng/ml (IQR 6.7-19.7). All patients were miN0 on preoperative prostate-specific membrane antigen (PSMA) PET/CT with a median nomogram-assessed risk of LN involvement of 30.4% (IQR 21.5-40.4) (Table 1).

Table 1. Patient characteristics and surgical outcomes

Parameter	Overall (n=10)
Preoperative	
Median age at surgery, yr (IQR)	72.5 (66.0-75.3)
Median BMI, kg/m2 (IQR)	25.7 (24.7-28.7)
Median initial prostate-specific antigen, ng/ml (IQR)	7.9 (6.7-19.7)
Radiological (m)T stage, n (%)	
T2, n (%)	2 (20)
T2c, n (%)	2 (20)
T3a, n (%)	4 (40)
T3b, n (%)	2(20)
Radiological (mi)N stage	
N0, n (%)	10 (100)
N1, n (%)	0 (0)
Median risk of LN involvement according to Briganti 2012, % (IQR)	30.4 (21.5-40.4)
Median risk of LN involvement according to ABS nomogram, % (IQR)	41.1 (19.6-52.1)
Intraoperative	
Median OR time in min (IQR)	203 (187.5-223.5)
Median time between injection and first ICG visualization in min (IQR)	23.5 (20.0-18.3)
Histopathology	
Pathological T stage	
T2, n (%)	1 (10)
T3a, n (%)	3 (30)
T3b, n (%)	6 (60)
Pathological N stage	
N0, n (%)	7 (70)
N1, n (%)	3 (30)
Pathological ISUP	
2	2 (20)
3	3 (30)
4	1 (10)
5	4 (40)
Surgical margin status	
R0, n (%)	6 (60)
R1, n (%)	4 (40)
Histopathological analysis of FFPE tissue	
Number of non-stained LNs; of which tumor positive (%)	86; 3 (4)
Number of fluorescent LNs; of which tumor positive (%)	109; 3 (3)

ABS= Amsterdam-Brisbane-Sydney BMI = Body Mass Index, FFPE = formalin-fixed paraffin-embedded, ICG = indocyanine green, IQR = interquartile range, ISUP = International Society of Urological Pathology, LN = lymph node involvement, (m) = MRI, (mi) = molecular imaging, OR = operating room, yr = year

Intraoperative findings

In 90% of the patients at first imaging, fluorescent could be observed around the proximal external iliac after a median time of 23.5 min (IQR 20.0-18.3) (Table 1). In the one patient where superficial first imaging did not immediately show fluorescence, the obturator fossa was carefully explored and the first fluorescence was seen at Cloquet's node after 28 min post-injection. At 36 minutes post-injection, the rest of the obturator fossa displayed fluorescence traveling via the proximal external iliac artery towards the common iliac artery and onward. All surgeons started the ePLND on the left side, where fluorescence could be seen at the level of the bifurcation and common iliac at the end of the dissection. This shows that the fluorescence reaches the common iliac between a median of 23.5 and 39 minutes after injection. The lymphatic drainage showed roughly the same pattern in all patients but had some interpatient nuances (Figure 2A).

Overall, the drainage patterns appeared to be symmetric for left and right side (Figure 2A). Because the right sided LND was always performed after completing the left (start right side median of 39 minutes after the first fluorescence was seen on the left), on the right side the common iliac nodes were already stained at the time of resection. This meant that the dynamics around not be reliably monitored on the right. However, it could be deduced that after a median of 39 minutes (range 22-5) the abdominal wall drainage reached the common iliac artery.

All patients showed drainage from Cloquet's node to the obturator fossa where a web of small fluorescent lymph vessels could be appreciated (Figure 3A). In nine patients, fluorescent lymph vessels between the external iliac vein and artery were observed (Figure 3B). Clear and relatively large fluorescent lymph vessels could be seen crossing or encircling the external iliac artery in six patients (Figure 3C; with LNs on both sides (Figure 2D). During the ePLND it became apparent that both small and large lymphatic vessels were severed (Figure 4A). At the end of the procedure (after removal of the prostate) lymph fluid leakage was captured continuously flowing from the location of Cloquet's node on both sides (Figure 4B). Lymph vessels were found to cross over the umbilical ligament into, what appeared to be, the direction from lateral to medial (Figure 2 and figure 3E).

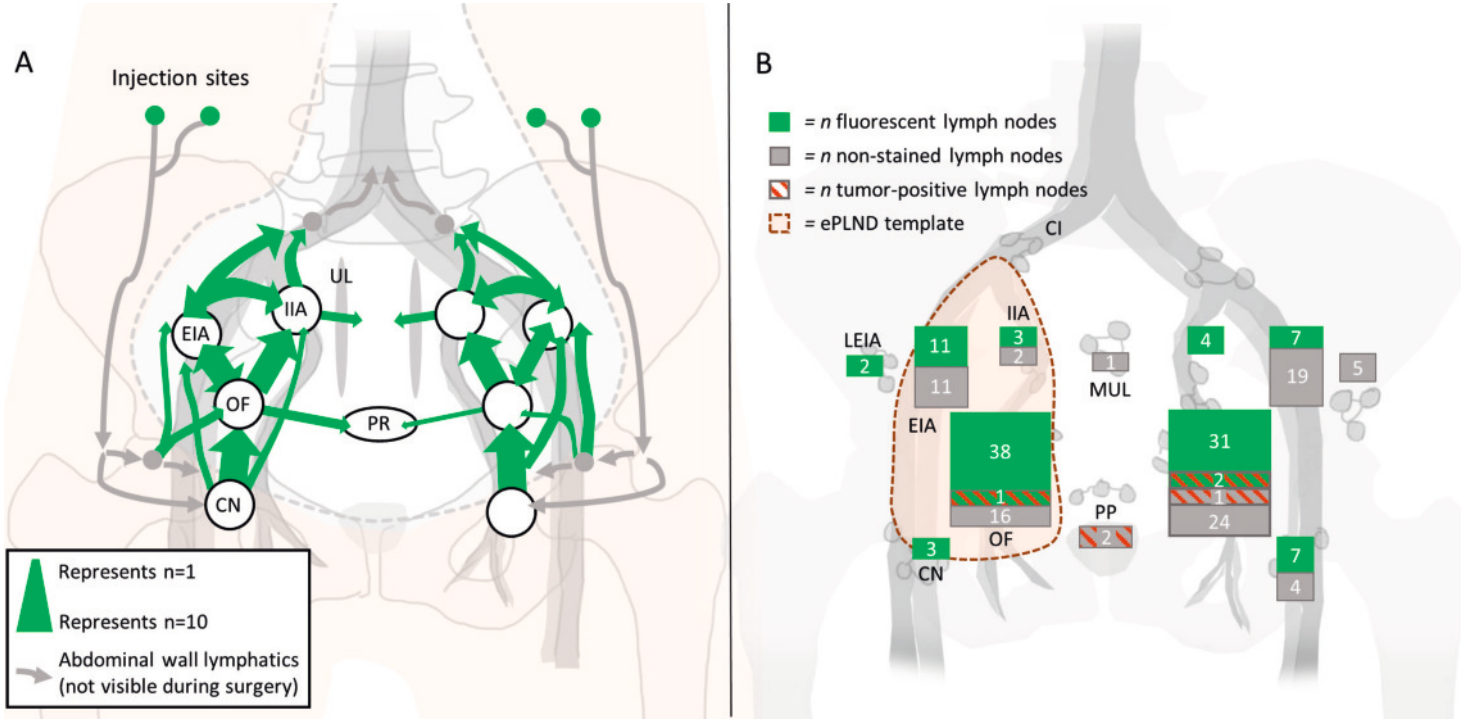

Figure 2. Distribution of *in* and *ex vivo* visualization of fluorescence. A) Presentation of the *in vivo* drainage patterns of the abdominal wall within the pelvic area. The grey arrows represent the drainage patterns as reported by literature but that could not be seen during surgery. The green arrows represent the ICG- stained (fluorescent) flow within the surgical field. In some cases like for internal-external-obturator area, the direction of the flow was unclear and is therefore represented with arrows in both directions. B) Overview of the pelvic area with the amount of lymph nodes visualized per histopathological region. In green the indocyanine green (ICG) stained nodes are depicted and in grey the non-stained nodes. The red-stripes represent the tumor- positive nodes either with a green background corresponding to tumor-positive, fluorescent nodes or with a grey background for tumor-positive, non-stained nodes. Regions: CN= Cloquet's node, EIA = External iliac artery, IIA = Internal iliac artery, LEIA= lateral to external iliac artery MUL = medial to umbilical ligament, OF= obturator fossa, PP= periprostatic, PR= pararectal, UL= umbilical ligament.

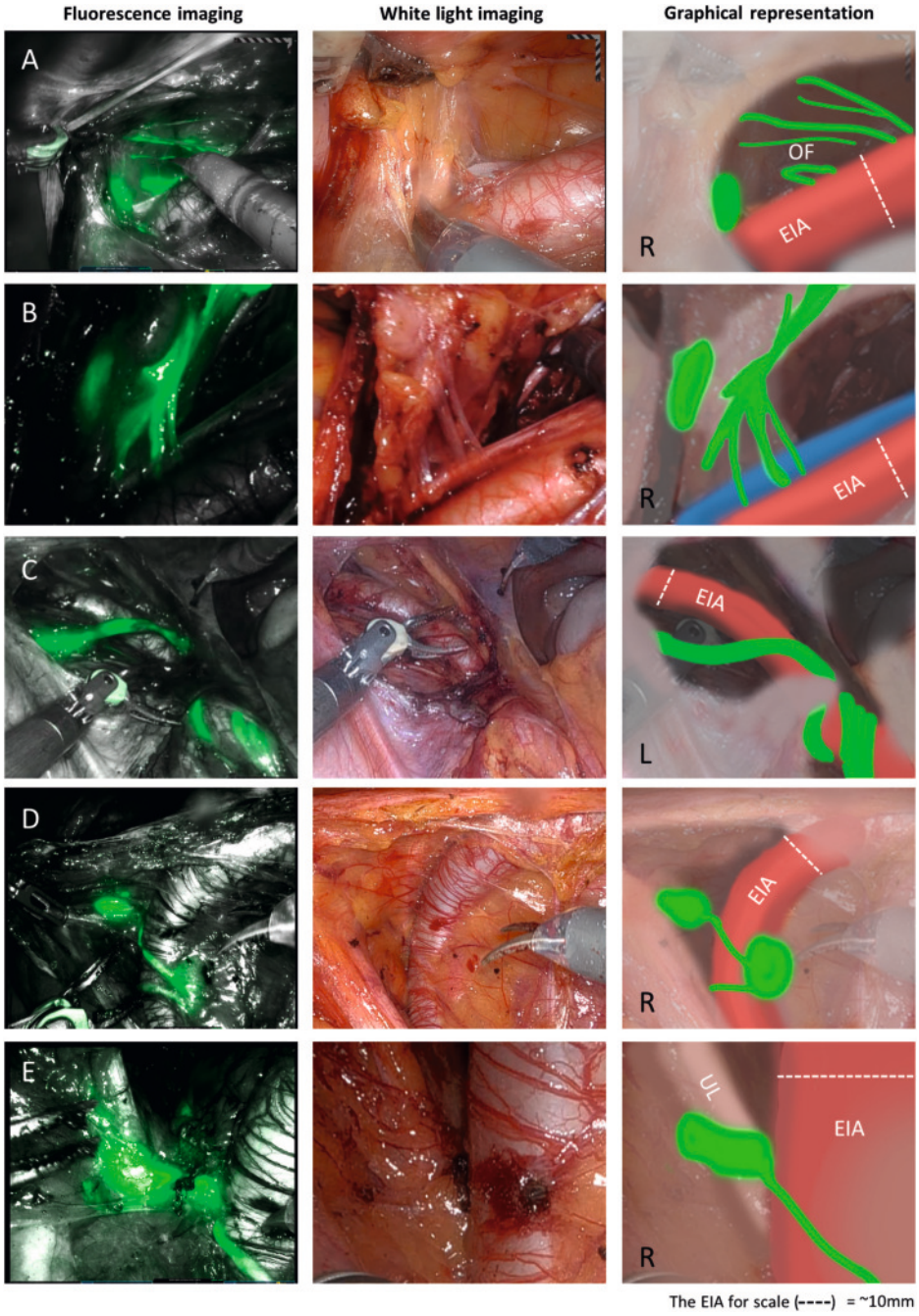

Figure 3. Examples of images as seen during surgery. On the left the image as seen by fluorescence imaging using the Firefly fluorescence imaging scope where the indocyanine green (see in green) represent the lymphatic drainage from the abdominal wall. In the middle the same view but as the surgeons normal (white light) view of the da Vinci robotic surgical system. On the right, the overlay of the surgical view with anatomical landmarks and if the left (L) or right (R)

side is depicted. A) A collection of small lymph vessels in the obturator fossa. B) Lymph vessels passing between the external iliac vein and external iliac artery. C) Lymph vessels encircling the external iliac artery. D) Lymph vessels and two lymph nodes surrounding the external iliac artery. E) Lymph vessel crossing the umbilical ligament and the external iliac artery. EIA = External iliac artery. The EIA is ~10mm in diameter. The dotted line on the EIA represents 10mm for scale. OF= obturator fossa, UL= umbilical ligament.

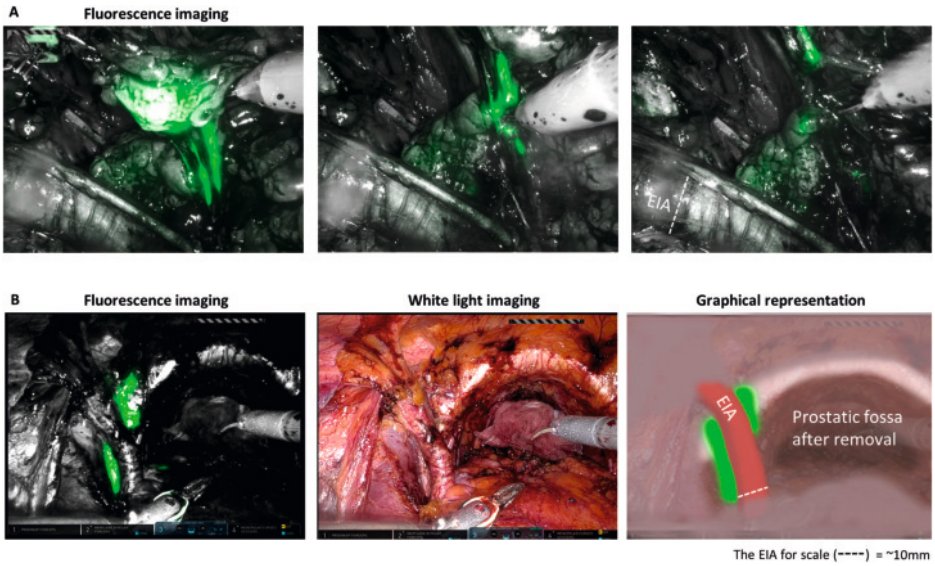

Figure 4. Intraoperative images. A) Transection of lymph vessels of the abdominal wall during ePLND (imaged with Firefly fluorescence camera) B) Leakage of ICG containing lymph fluid coming from the abdominal wall passing behind the EAI (external iliac artery) within the surgical field after removal of the prostate at the end of the prostatectomy. EIA = External iliac artery. The EIA is ~10mm in diameter. The dotted line on the EIA represents 10mm for scale.

Histopathological findings

In all patients, the injection of ICG yielded lymphatic drainage that could be clearly detected during the ePLND. In total, 195 lymph nodes were removed (average 20/patient) of these 56% were fluorescent (11.5/patient). Hereby the only regions that did not show fluorescence where the periprostatic and medial to umbilical ligament/paravesical nodal regions. Of the patients, three proved to be pN1 (30%) yielding a total of six tumor-positive nodes in the obturator fossa and periprostatic region. While none of the periprostatic positive LNs were fluorescent, 75% of the positive LNs in the obturator fossa (distributed over two patients) contained ICG that drained from the abdominal wall. Indicating that prostate and abdominal wall lymphatic drainage converges (Figure 2B).

Safety and follow-up

Patients reported no postoperative discomfort or pain at the injection sites. The presence of green skin discoloration was still clearly visible the morning after surgery in all patients (Supplementary 1). Four patients reported that the ICG injection sites in the skin were visibly green up to 3 weeks postoperatively. No severe adverse events were reported. Seven patients (70%) suffered from postoperative edema located in the abdominal wall, scrotum or upper leg. In our cohort, this was independent of number of LNs removed in total (p=0.337) and of fluorescent nodes removed (p=0.631). Four other complications were registered (1 Clavien-Dindo I and 3 Clavien-Dindo II (Table 2). Postoperative PSA was detectable in one patient (pT3bN0 R1).

Table 2. Complications according to Clavien-Dindo

Clavien-Dindo I, n (% of n=10 patients)	
Lymphedema	7 (70%)
Paresthesia	1 (10%)
Clavien-Dindo II, n (%)	
UTI treated with antibiotics	2 (20%)
TUC replacement	1 (10%)
Long term constipation	1 (10%)

TUC = transurethral catheter, UTI = urinary tract infection

Discussion

This prospective clinical study indicates that a considerable amount (56%) of nodes draining the abdominal wall reside within the ePLND template. As a result, the drainage pathways of the primary PCa and abdominal wall converge and a substantial portion of the tumor containing LNs were directly linked to the fluorescent abdominal wall drainage. Meaning that sparing the LNs that drain the abdominal wall would harm the oncological rigor of the procedure.

In line with literature, we observed that the abdominal lymphatic drainage displayed consistent patterns across the cohort with slight interpatient differences [17]. In all patients Cloquet's node (medial to external iliac artery) was stained as it is regarded the highest superficial node of the ilioinguinal basin and a common route for the superficial lymphatic drainage of the dermis of the lower abdomen [18 21]. Hence, the observed convergence seemed to be originating at Cloquet's node. According to literature, the deeper (below the dermis) lymphatic system of the abdominal wall follows patterns that terminate at the lateral external iliac nodes (e.g. the inferior epigastric pathway: following the inferior epigastric artery to the lateral external iliac nodes or the lumbar/iliac pathway: following the deep circumflex iliac artery) [18]. A mechanism that could indicate that the observed fluorescent pattern that passed to the pelvic area lateral external to the iliac artery before draining towards the obturator fossa or common iliac is related to possibly depositing ICG a little deeper in the skin.

Usually the drainage from the prostate is described to run along the medial side of the umbilical ligament and cross towards the external iliac artery [26]. The current data suggest a bidirectional lymph drainage occurs within the pelvic lymph drainage network (as seen in Figure 4E).

Our analysis was not devoid of limitations. Due to clinical practicality, ICG was administered before the surgical incision. This allowed an interval of ~25 minutes (including skin disinfection, trocar placement and docking of the robotic system) between injection and the start of imaging. This approach limited the ability to capture the initial dynamic phase of lymph flow. Moreover, the precise timing of ICG distribution and uptake was not systematically recorded, as imaging was performed according to the anatomical location rather than at standardized times. Four different surgeons performed the surgical procedures which can cause different interpretations of the patterns intraoperatively and during video analysis.

Conclusion

Our findings indicate that a considerable number of nodes draining the abdominal wall, the most common location for lymphedema after prostate cancer surgery, are situated within the ePLND template. Moreover, 75% of the tumor positive lymph nodes within the obturator fossa converged with the abdominal wall drainage.

References

1. Mottet N, van den Bergh RCN, Briers E, et al. EAU-EANM-ESTRO-ESUR-SIOG Guidelines on Prostate Cancer-2020 Update. Part 1: Screening, Diagnosis, and Local Treatment with Curative Intent. Eur Urol 2021;79(2):243-262,
2. Briganti A, Larcher A, Abdollah F, et al. Updated nomogram predicting lymph node invasion in patients with prostate cancer undergoing extended pelvic lymph node dissection: the essential importance of percentage of positive cores. Eur Urol 2012;61(3):480-7,
3. Briganti A, Chun FK, Salonia A, et al. Complications and other surgical outcomes associated with extended pelvic lymphadenectomy in men with localized prostate cancer. Eur Urol 2006;50(5):1006-13
4. Baas DJH, de Baaij JMS, Sedelaar JPM, et al. Extended pelvic lymph node dissection in robot-assisted radical prostatectomy is an independent risk factor for major complications. J Robot Surg 2024;18(1):140
5. Keegan KA, Cookson MS. Complications of pelvic lymph node dissection for prostate cancer. Curr Urol Rep 2011;12(3):203-8
6. Orvieto MA, Coelho RF, Chauhan S, et al. Incidence of lymphoceles after robot-assisted pelvic lymph node dissection. BJU Int 2011;108(7):1185-90
7. Clinckaert A, Callens K, Cooreman A, et al. The Prevalence of Lower Limb and Genital Lymphedema after Prostate Cancer Treatment: A Systematic Review. Cancers (Basel) 2022;14(22),
8. Rasmusson E, Gunnlaugsson A, Blom R, et al. Low rate of lymphedema after extended pelvic lymphadenectomy followed by pelvic irradiation of node-positive prostate cancer. Radiat Oncol 2013;8(271
9. Finnane A, Hayes SC, Obermair A, Janda M. Quality of life of women with lower-limb lymphedema following gynecological cancer. Expert Rev Pharmacoecon Outcomes Res 2011;11(3):287-97
10. Bianchi LMG, Irmici G, Ce M, et al. Diagnosis and Treatment of Post-Prostatectomy Lymphedema: What's New? Curr Oncol 2023;30(5):4512-4526
11. Thorsteinsdottir T, Stranne J, Carlsson S, et al. LAPPRO: a prospective multicentre comparative study of robot-assisted laparoscopic and retropubic radical prostatectomy for prostate cancer. Scand J Urol Nephrol 2011;45(2):102-12
12. Gandaglia G, Barletta F, Robesti D, et al. Identification of the Optimal Candidates for Nodal Staging with Extended Pelvic Lymph Node Dissection Among Prostate Cancer Patients Who Underwent Preoperative Prostate-specific Membrane Antigen Positron Emission Tomography. External Validation of the Memorial Sloan Kettering Cancer Center and Briganti Nomograms and Development of a Novel Tool. Eur Urol Oncol 2023;6(6):543-552
13. Touijer KA, Vertosick EA, Sjoberg DD, et al. Pelvic Lymph Node Dissection in Prostate Cancer: Update from a Randomized Clinical Trial of Limited Versus Extended Dissection. Eur Urol 2024
14. Chen QY, Xie JW, Zhong Q, et al. Safety and Efficacy of Indocyanine Green Tracer-Guided Lymph Node Dissection During Laparoscopic Radical Gastrectomy in Patients With Gastric Cancer: A Randomized Clinical Trial. JAMA Surg 2020;155(4):300-311
15. Washino S, Kawase M, Shimbo M, et al. Comparison of oncological outcomes between extended and no pelvic lymph node dissection in patients with high- or very high-risk prostate cancer: a multi-institutional study. Prostate International 2024;12(3):160-166
16. Preisser F, van den Bergh RCN, Gandaglia G, et al. Effect of Extended Pelvic Lymph Node Dissection on Oncologic Outcomes in Patients with D'Amico Intermediate and High Risk Prostate Cancer

Treated with Radical Prostatectomy: A Multi-Institutional Study. J Urol 2020;203(2):338-343

17. Uren RF, Howman-Giles R, Thompson JF. Patterns of lymphatic drainage from the skin in patients with melanoma. J Nucl Med 2003;44(4):570-82
18. Földi M, Földi E. Földi's Textbook of Lymphology. Elsevier: 2012.
19. Meershoek P, KleinJan GH, van Oosterom MN, et al. Multispectral-Fluorescence Imaging as a Tool to Separate Healthy from Disease-Related Lymphatic Anatomy During Robot-Assisted Laparoscopy. J Nucl Med 2018;59(11):1757-1760
20. Meershoek P, KleinJan GH, van Willigen DM, et al. Multi-wavelength fluorescence imaging with a da Vinci Firefly-a technical look behind the scenes. J Robot Surg 2021;15(5):751- 760,
21. Berrens AC, Buckle T, van Oosterom MN, et al. Multispectral Fluorescence Imaging as a Tool to Distinguish Pelvic Lymphatic Drainage Patterns During Robot-assisted Lymph Node Dissection in Prostate Cancer. Ann Surg Oncol 2024
22. Unno N, Inuzuka K, Suzuki M, et al. Preliminary experience with a novel fluorescence lymphography using indocyanine green in patients with secondary lymphedema. J Vasc Surg 2007;45(5):1016-21
23. Meijer D, van Leeuwen PJ, Eppinga WSC, et al. Development and Internal Validation of a Novel Nomogram Predicting the Outcome of Salvage Radiation Therapy for Biochemical Recurrence after Radical Prostatectomy in Patients without Metastases on Restaging Prostate-specific Membrane Antigen Positron Emission Tomography/Computed Tomography. Eur Urol Open Sci 2024;61(37-43)
24. SmPC ICG Verdye.
25. Clavien PA, Barkun J, de Oliveira ML, et al. The Clavien-Dindo classification of surgical complications: five-year experience. Ann Surg 2009;250(2):187-96
26. Jeschke S, Lusuardi L, Myatt A, et al. Visualisation of the lymph node pathway in real time by laparoscopic radioisotope- and fluorescence-guided sentinel lymph node dissection in prostate cancer staging. Urology 2012;80(5):1080-6

Supplementary 1. Injection site indocyanine green after injection and OR + 1

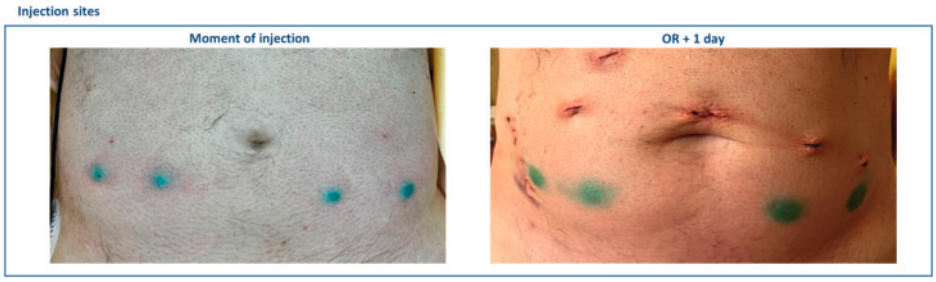

Berrens AC, Tessa Buckle T, van Oosterom MN, Slof LJ, Melsert BM, Nieuwenhuijzen JA, Wit EMK, van Leeuwen PJ, van der Poel HG, van Leeuwen FWB

BJU International, 2025 Sep;136(3):515-522

Chapter 8

Renal Clearance of Fluorescent Agents Can Compromise Image-guided Surgery Along the Urinary Tract

Abstract

Objectives. To study the effect of renally cleared fluorescent agents on image-guided surgery along the urinary tract by using the renally cleared, non-tumour-specific, fluorescent dye fluorescein.

Subjects and methods. Sixteen patients who underwent robot-assisted radical prostatectomy (RARP) with lymph node dissection received an intradermal injection of fluorescein. The slow-release of the fluorescein from the skin into the lymph- and bloodstream were used as a pharmacokinetic model for slow release from receptor-targeted agents. The presence of fluorescein in the urine and the surgical dissection planes around the prostate (representative of cancer margins) during RARP were evaluated. Suction, gauze and irrigation were used to try and reduce fluorescent background signals according to standard operating protocol.

Results. Fluorescein was detected in the urine in the bedside catheter bag after a median of 1.3 h after agent administration and in the surgical field after opening the bladder neck as part of RARP (median of 2.4 h after injection). Suction and application of gauze helped to reduce contamination, but suction combined with irrigation with lukewarm NaCl 0.9% was shown to be most effective. Fluorescein accumulation was seen in the tissue surrounding the bladder neck in 80% of patients.

Conclusions. Renally excreted fluorescent agents risk contamination of the surgical field and possible dissection margins along the urinary tract, a feature that, without proper counter measures, could compromise the accuracy of intra-operative imaging by creating false-positive findings. A clear example of this was the observed bladder neck staining with fluorescein.

Introduction

The use of intra-operative molecular imaging represents asignificant evolution in surgical procedures. Various fluorescent agents are used for the identification/visualisation of different anatomical or molecular features in different indications. For example, i.v. applied agents can be used forangiography (indocyanine green (ICG) or fluorescein), visualisation of bile efflux, and disturbances therein (ICG, mebrofenin and visualisation of ureters (fluorescein) [1–3]. Prostate-specific membrane antigen (PSMA) targeting has proven to be a popular receptor-targeted approach in primary and salvage prostate cancer surgery [4]. Imaging labels (chelates and/or fluorescent dyes) used to functionalise targeting vectors such as PSMA can substantially impact the pharmacokinetic clearance profile [5]. After the body is perfused with a bolus of agent-containing blood through i.v. injection (Figure 1), tumour tissue and tumour-specific receptors can be targeted [6]. During this same first-pass perfusion, some of the agent accumulates in healthy background tissue. This effect is dependent on serum binding [7] and dosing [8 9]. The initial targeting phase is then followed by slow release of non-receptor-bound agent residing in background tissues [10]. This clearance of background tissue may take place over a prolonged period, in some cases requiring a time interval of 17 days between agent injection and surgery [11].

Renal excretion is perhaps the most important and common route of excretion for imaging agents, such as ^{68}Ga-PSMA-11, ^{99m}Tc-PSMA I&S [4], ^{111}In-PSMA I&T [12], IS-002 [8], OTL78 [9], and IR800-IAB2M [11]. A drawback of the use of agents cleared by the kidneys is that contaminated urine can stain the surgical field [13]. When the signal is assumed to be related to the cancerous tissue, non-tumour-specific uptake is likely to compromise surgical margins assessment along the urinary tract and promote over treatment. Indeed, various studies have shown that the use of ^{68}Ga-PSMA-11, ^{99m}Tc-PSMA I&S, IS-002, OTL78, and IR800-IAB2M during PSMA-targeted prostate cancer surgery poses a risk of false-positive results due to contaminated urine [8 9 11 14 15]. These same studies indicate that this effect becomes more prominent with higher dosing. Importantly, therapeutic dosing (mg/kg) tends to promote contamination when compared to the micro dosing commonly used for radio agents (< 100µg/patient) [8 9 11 14].

Given the rising interest in PSMA-targeted prostate cancer surgery it is imperative to increase our general understanding of the potential false-positive effects caused by urine contaminations [4]. To gain insight into the effect of the presence of imaging agent in urine during surgery, we used intradermal injections of the fluorescent dye fluorescein to mimic and visualise the clearance of non-bound PSMA- agent (Figure 1) [10 16 17].

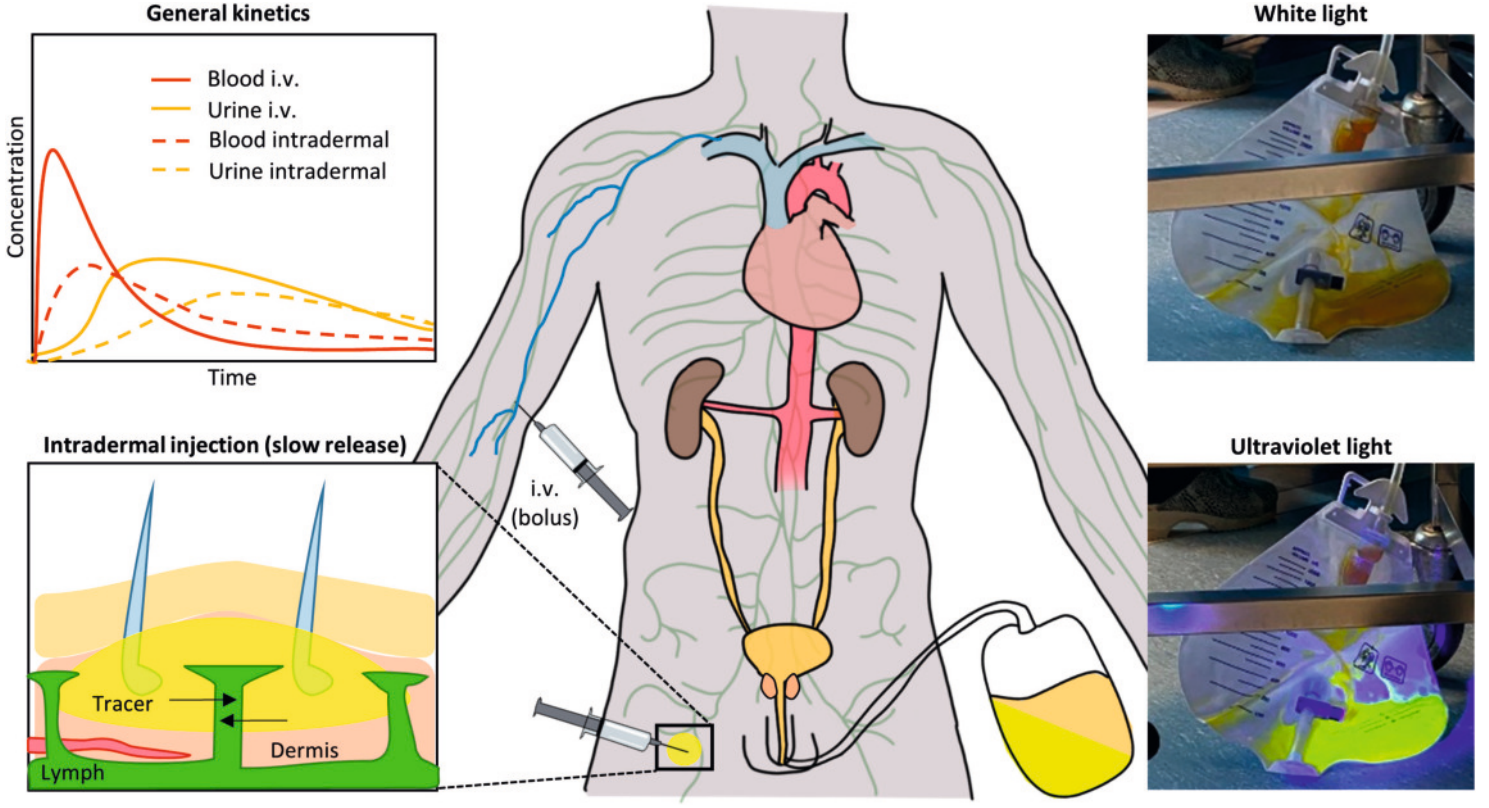

Figure 1. General pharmacokinetics based on ADME Encyclopedia and Buckle et al. [10 12]. Intravenous injection facilitates immediate presence of agent in the bloodstream (early peak). Intradermal injection creates a more stationary agent deposition at the site of injection, followed by slow release from the tissue. As a cause the latter can be used to mimic receptor-targeted agents like PSMA targeted agents that remain available for targeting over a prolonged period of time. As fluorescein is renally cleared it could be seen in the urine in the bedside catheter bag using ultraviolet flashlight.

Methods

A total of 16 patients (Table 1) were included as part of a single-arm, single-centre, prospective, feasibility study (NCT05120973) [19]. This study was approved by the local ethics committee and all patients provided written informed consent. Patients underwent a robot-assisted radical prostatectomy (RARP) with extended pelvic lymph node dissection (ePLND) and sentinel node procedure between March 2022 and August 2023.

Table 1. Patient demographics

Parameter	(n=16)
Median age at surgery, yr (IQR)	66.5 (61.0-69.0)
Median initial prostate-specific antigen, ng/ml (IQR)	15.3 (7.8-21.9)
Clinical T stage, n (%)	
T1	3 (19)
T2	11 (69)
T2b	1 (6)
T3a	1 (6)
Radiological T stage, n (%)	
T2	5 (31)
T2b	1 (6)
T3a	7 (44)
T3b	3 (19)
Radiological N stage PSMA PET/CT, n (%)	
N0	15 (94)
N1	1 (6)
Biopsies ISUP, n (%)	
2	4 (25)
3	7 (44)
4	1 (6)
5	4 (25)
Median risk of LNI according to Briganti 2012, % (IQR) [20]	18.9 (12.5-33.7)
Median time injection fluorescein to first intraoperative imaging, h (IQR)	2.4 (2.0-2.6)
Median time injection fluorescein to urine visible in bedside catheter bag, h (IQR)	1.3 (1.2-1.7)
Pathological T stage	
T2, n (%)	5 (31)
T2c, n (%)	6 (38)
T3a, n (%)	1 (6)
T3b, n (%)	4 (25)
Pathological N stage	
N0, n (%)	10 (62)
N1, n (%)	6 (38)
Pathological ISUP	
2	5 (31)
3	9 (56)
4	1 (6)
5	1 (6)
Surgical margin status	
R0, n (%)	11 (69)
R1, n (%)	5 (31)

h = hours, ISUP = International Society of Urological Pathology, IQR = Interquartile range, LNI = lymph node involvement, n= number, yr = years

Fluorescein administration

Fluorescein (80mg (~1mg/kg); 4ml 2%) was injected unilaterally into the dermis in two deposits of 2ml each. The injection was performed in the operating room, directly after general anaesthesia. The injection was unilaterally placed, either at the medial and lateral side of the upper leg (n=8) or at the left or right lower quadrant of the abdominal wall (n=8). As part of a separate objective of the prospective study protocol, intraprostatic ^{99m}Tc-ICG-nanocolloid was administered [19]. Because of the hepatobiliary clearance pattern of ICG it was not included in this assessment of contamination of urine.

Fluorescein Mechanism of Action and Pharmacokinetics

Fluorescein is excited by blue light (kmax ex = 488 nm) and emits light that appears yellowish-green (kmax em = 515 nm) [20]. Fluorescein can enter the bloodstream either after a systemic bolus injection (routine angiographic use) or following slow release from tissue deposits over time. The latter deposits can either be the result of non-specific accumulations in the interstitial space (0.5 L/kg) that follow bolus injection or can be the direct result of intradermal fluorescein deposition, as was the case in this prospective study protocol. Following intradermal injection of fluorescein, it took approximately 10 min to visualise the (micro-)lymphatics of the skin [20 21]. Fluorescein undergoes rapid metabolism to fluorescein monoglucuronide (80% within 1 h and almost all within 4–5 h [20]) and is mainly eliminated via renal excretion. Glomerular filtration provides a key pathway for excretion of the 10%–20% of fluorescein or fluorescein monoglucoronide that is not bound to plasma proteins. The remaining 80%–90% protein- bound fraction is expected to be cleared via tubular excretion. The plasma elimination half-lives of fluorescein are 23.5 min for 'free' fluorescein and 264 min for fluorescein glucuronide. Because the fluorescein analogues present themselves in ionised form, they are not reabsorbed by the kidneys and are detectable in the urine for 24–36 h post dose; 90% of elimination occurs within 48 h [20]. Notably, the plasma elimination and renal clearance rates are dependent on the molecular structure and will be different for every molecule.

Intraoperative imaging

After placing the patient in the Trendelenburg position and docking of the da Vinci Xi Surgical System (Intuitive Surgical Inc, Sunnyvale, CA, USA), the surgeon commenced the extended pelvic lymph node dissection, followed by RARP. At three timepoints during RARP, the presence of fluorescein within the surgical field was assessed *in vivo*: (i) immediately before opening the bladder neck; (ii) after opening the bladder neck; and (iii) after removal of the prostate. Because the integrated Firefly endoscope of the da Vinci Xi (white-light illumination peak (blue) ~460 nm, fluorescence excitation ~800 nm) cannot differentiate between fluorescein and ICG [22], the photodynamic diagnostic settings of a 1 HUB HD + D- light C light source (Karl Storz, Tuttlingen, Germany) were used to specifically identify fluorescein [23]. In case of contamination with blood or urine, the surgical field was cleared using gauze, suction or irrigation with lukewarm saline (NaCl 0.9%; solubility fluorescein 500 mg/mL) according to standard operating protocol. The

presence of fluorescein in the catheter bag was imaged with a normal (white-light) camera following dye excitation with a standard consumer ultra-violet flashlight (Conrad Electronic Benelux B.V., Oldenzaal, the Netherlands). The presence of fluorescence was objectively determined as positive or negative without quantification of the signal.

Statistical analysis

Descriptive statistics are presented as frequencies with percentages or medians and interquartile range (IQR) calculated using IBM SPSS version 29.

Results

Fluorescein could clearly be observed in the urine of the bedside catheter bag after a median (IQR) of 1.31 h (1.17–1.72) (Figure 1, Table 1). In two patients, fluorescein was still observable using an ultra-violet flashlight in the bedside urine catheter bag 20 h post-surgery.

Imaging of contamination within the prostatic bed

After opening of the bladder neck, fluorescein could be identified in urine that leaked into the abdominal cavity (Figure 2E). Although the catheter showed some autofluorescence when imaged with the fluorescence camera, the bright signal observed seemed to be related to residual urine at the catheter tip (Figure 2H). In six patients, fluorescein was visible using the white-light settings of the Firefly Xi camera. The substantial violet/blue component of the Firefly light source excites fluorescein [22] (Figure 2E,I). During surgery, fluorescein uptake was clearly observed within the bladder neck tissue in 13/16 patients (Figure 2G,H). The fluorescent signal in the urine was blocked by the muscular bladder wall until the incision was made. In contrast to this study, in previous studies (which used a 6.25 times higher dose), fluorescein could be observed within the ureters without opening the urinary tract [24].

Following the removal of the prostate, the presence of fluorescein could clearly be observed in the prostatic bed in all patients (Figure 2E). After imaging to show the full extent of the contamination of the surgical field, suction and gauze were used to help to clear the surgical field (Figure 3). Irrigation of the surgical field with the suction irrigator (if necessary, more than once and, on average, twice) proved most successful for removal of the fluorescein). Despite the high solubility of fluorescein in NaCl 0.9% (up to ~500 mg/mL) [20], it was impossible to wash away all signal (Figure 3C), with a small fraction remaining at the bladder neck (Figure 3D). When the bladder was open, new flushes of fluorescein-containing urine continuously contaminated the view, thus allowing tissue to again absorb the fluorescein. Contamination stopped when the anastomosis was complete (median operating duration 244 min (IQR 222–256.5)).

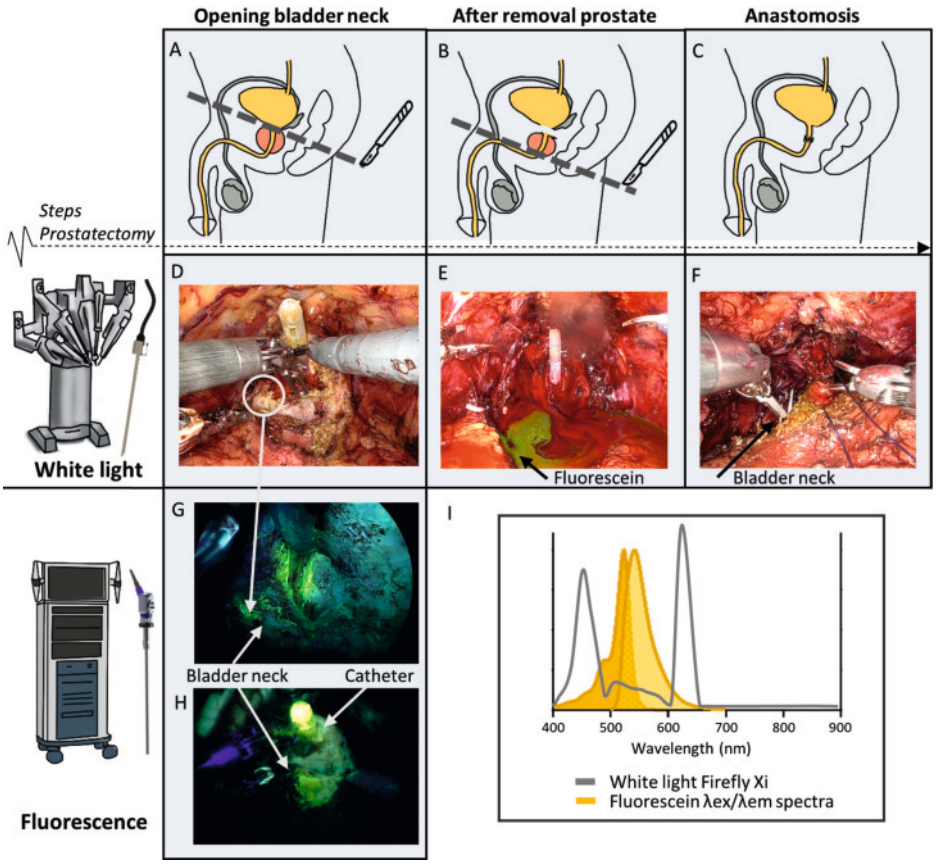

Figure 2. Identification of agent (fluorescein) contamination within the surgical field. (A) Schematic lateral view of the male pelvis demonstrating the moment of opening the bladder at the bladder neck during robot-assisted radical prostatectomy. (B) Schematic lateral view of the male pelvis demonstrating the moment of dissecting prostate from the distal urethra. (C) Schematic lateral view of the male pelvis demonstrating the anatomy after anastomosis. (D) Xi Firefly white-light imaging of the surgical field after opening the bladder. (E) Xi Firefly white-light image of the prostatic bed after removal of the prostate. (F) Xi Firefly white-light imaging of fluorescein visible (yellow) in the bladder neck during anastomosis. (G) Fluorescence imaging using a Karl Storz fluorescence endoscope of the surgical field after opening the bladder. (H) Fluorescence imaging using a Karl Storz fluorescence endoscope of the surgical field after opening the bladder showing the catheter tip illuminating. (I) The excitation and emission spectra of fluorescein and the white-light properties of the Xi Firefly system (based on Meershoek et al. [22]).

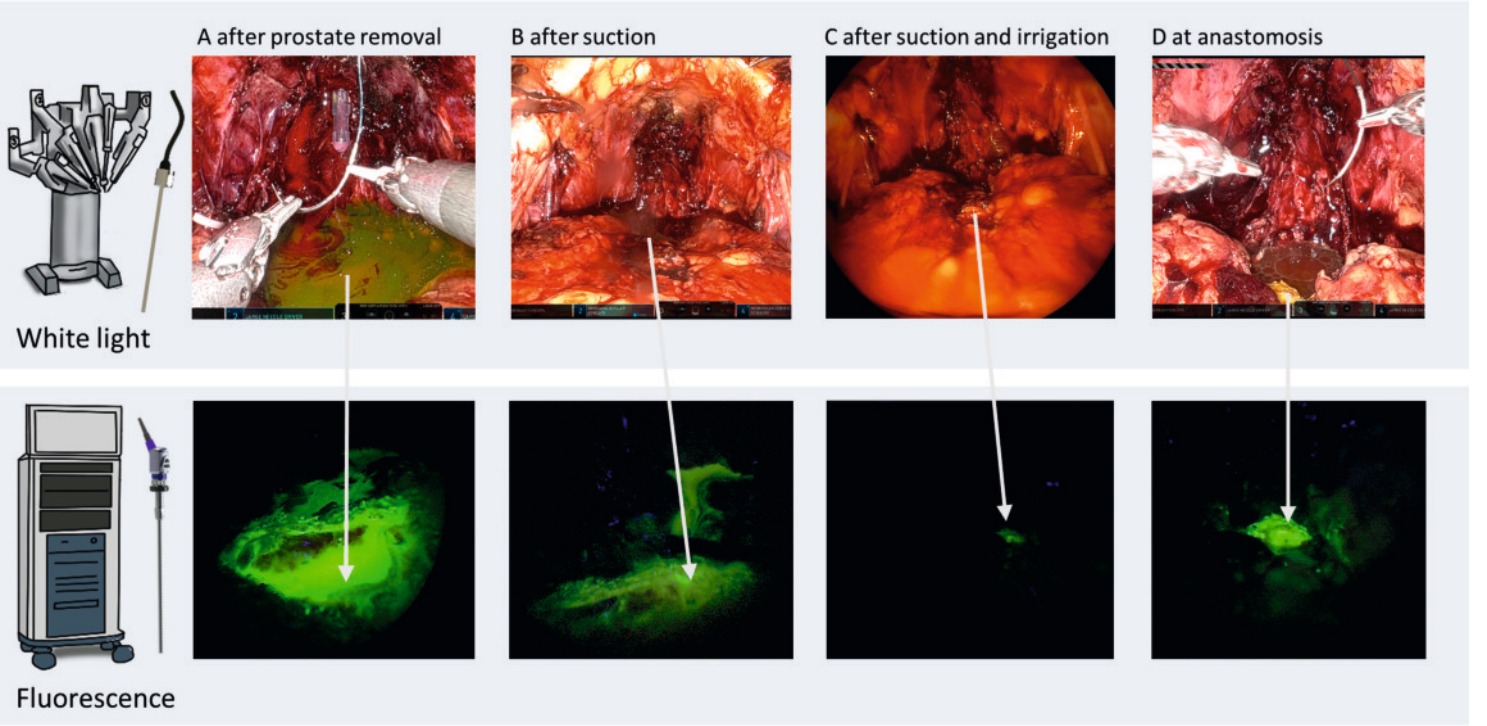

Figure 3. Agent contamination within the surgical field. The agent (fluorescein) contamination is depicted in white light from the Firefly Xi Camera system (top images) and Karl Storz fluorescence endoscope (bottom images). (A) Directly after removal of the prostate without cleaning the surgical field, in white light. (B) After only suction of the visible contamination. (C) After single irrigation with NaCl 0.9% and suction only fluorescein that has been absorbed by the bladder neck remains visible. (D) The bladder neck with the absorbed fluorescein remains visible using white light and fluorescence imaging also at anastomosis.

Discussion

By exploiting the slow-release kinetics of intradermally injected fluorescein it has become possible to study how a renally cleared fluorescent agent can contaminate the surgical field during RARP in a clinical setting. The same may be true for other fluorescent agents known to be cleared via urine, namely, methylene blue, IRDye 800CW and ZW8001 [25]. Monitoring of urine contamination provides insights that are relevant for indications where receptor-targeted fluorescence imaging is actively being exploited to identify tumour within the urinary tract, for example, extracapsular spread and radical margin resections during RARP [26]. This strategy is only reliable when the observed staining directly relates to the PSMA expression in tumour cells. As fluorescein is not known to bind to tumour receptors, such as PSMA, and was seen throughout the surgical field, our evaluation underscores that caution is required when renally cleared dyes are used to identify margins during fluorescence-guided RARP. The same caution should apply when receptor-targeted agents are developed for other cancers of the urinary tract, such as bladder cancer, upper urinary tract cancer, and perhaps even invasive vulva cancer or penile cancer. The fluorescent staining observed within the bladder neck tissue suggests some diffusion into the bladder wall. This may be explained by the fact that exposure of urine containing (lipophilic) organic molecules promotes dye accumulation within and subsequent staining of the top cell layers of the bladder neck resection area. A well-known example of this is mitomycin, an agent used to treat bladder carcinoma among other cancers [27]. In fluorescence-guided surgery, the uptake of agent into the tissue can pose risks; when a surgeon assumes a fluorescent signal is related to the cancerous tissue, non-tumour-specific uptake is likely to promote overtreatment. Strikingly, the non-tumour-specific accumulation of fluorescein in the bladder neck was consistent with a previous study, in which the non-tumourspecific uptake of the renally cleared OTL78 was also observed in the bladder neck [9]. Nguyen et al. [8] also noted non-tumour- specific bladder neck uptake, however, in their study they also confirmed tumour presence in a fluorescent bladder neck with a suspicious thickened appearance under white-light imaging. Studies on Cerenkov luminescence imaging indicate that cauterisation can also influence results, potentially contributing to false positives in the well-vascularised bladder neck [15]. This effect may occur either because tissue damage from cauterisation allows the agent to penetrate more deeply into the tissue or as a result of chemiluminescence [15 28].

Fluorescein contamination was partially eradicated using gauze or suction, but irrigation of the prostatic bed had the best effect. Given the prolonged and continuous release of contaminated urine, 48 h in the case of fluorescein, meticulous cleaning of the surgical cavity is required every time a surgeon intends to use fluorescence to identify the tumour extent. Our study findings suggest that the risk of contamination continues despite using a combination of irrigation and suction, and that the signal intensity merely decreases. Regardless of the surgical approach used, the dissection plane always involves the bladder/urethra, meaning the risk of tissue contamination cannot be avoided,

although, clearly, contamination of the bladder neck will not be apparent during bladder neck-sparing procedures.

Extending the time between agent administration and surgery beyond the renal excretion window will prevent the presence of contaminated urine during surgery. Various time intervals have been reported in clinical studies describing the use of PSMA-targeted agents for primary cancer identification; for example, an interval of 17 h for ^{99m}Tc-PSMA I&S S [14], 24 h for ^{111}In-PSMA I&T [12], OTL78 [9] and IS-002 [8], and 72 h for IR800-IAB2M [11]. That said, the biological half-life ($t_{1/2}$ biol), a feature unique to every molecular design, is a time frame within which urine containing imaging agent has not been reported for any of the PSMA agents. Another key parameter to take into consideration with regard to the biological half-life is that the absolute amount of detectable agent in the urine is highly dependent on the injected dose. When micro-dosing of ^{99m}Tc-PSMA I&S and ^{111}In-PSMA I&T is used (<100 µg/patient), the absolute signal will rapidly drop below detectable levels. The therapeutic dosing used with OTL78 (30 µg /kg [9]), IS-002 (25 µg/kg [8]) and IR800-IAB2M (50 µg/kg [11]) means that substantially more time is needed to allow the signals to drop below detectable levels, a feature that has already motivated the use of dose-reduction studies for these agents to diminish background signals [8 9 11]. Dose reduction, however, may in some cases also impair the identification of the targeted tissue [8].

A conceptual limitation of this study is that we were trying to understand and mitigate the risks of using renally cleared agents to identify lesions within the urinary tract, instead of focusing on designing hepatically cleared agents that would circumvent such issues [5]. This is especially notable given that the value of hepatic clearance of PSMA agents has already been demonstrated; ^{18}F-PSMA-1007 is said to increase the diagnostic confidence offered by PET/CT when interpreting lesions adjacent to the urinary tract, for example, local recurrence [29 30]. This shift from renal to hepatic clearance has also been proposed for intra-operative PSMA-targeted agents [31], a molecular design that appears to warrant further exploration. Limitations of this study include that 80 mg (1.14 mg/kg) intradermal injections of fluorescein, a dye with a relative short biological half-life ($t_{1/2}$ biol = 23.5 min after i.v. injection), can only provide an indication of what urine contamination with receptor-targeted agents may entail. This approach may lead to over- or underestimation of the fluorescent urine content resulting from i.v. administrated doses (see doses of known agents above) at the time of surgery. As fluorescein is relatively inert and easy to rinse away with water, the irrigation results may not imply the success of this approach with other agents. Conversely, tissue attenuation may limit the identification of fluorescein at 1 mm below the tissue surface, while agents functionalised with other dyes may be detected in tissue up to 1 cm deep, thus yielding potentially stronger non-tumourspecific signals [32]. It is unclear how local exposure of the bladder neck to imaging agent-containing urine can lead to absorbance of fluorescein. Furthermore, in this relatively small patient cohort, interpatient variability

in metabolism and renal clearance rates of fluorescein may have influenced the average time between injection and the visibility of fluorescein within the surgical field. As we used fluorescein merely as a model system of urinary clearance, we recommend that future studies on PSMA agents investigate the urinary clearance and contamination in more detail.

In conclusion, by monitoring fluorescein content within urine during RARP, this study showed that renally cleared agents contaminate the surgical field as soon as the bladder neck is opened up until the anastomosis is complete. This yielded non-tumour-specific uptake in the bladder neck; it should therefore it should be kept in mind that renally cleared agents could compromise the accuracy of intra-operative imaging during RARP. Although irrigation and suction helped to substantially reduce the fluorescein contamination, other cleaning methods may be required for other fluorescent agents.

In summary, renally cleared agents may interfere with fluorescence-guided tumour margin assessment in the urinary tract.

References

1. Cassinotti E, Boni L, Baldari L. Application of indocyanine green (ICG)-guided surgery in clinical practice: lesson to learn from other organs-an overview on clinical applications and future perspectives. Updates Surg 2023;75(2):357-65.
2. Baddam DO, Ragi SD, Tsang SH, Ngo WK. Ophthalmic Fluorescein Angiography. Methods Mol Biol 2023;2560:153-60.
3. Delbos L, Gareau-Labelle AK, Langlais EL, et al. Sodium Fluorescein for Ureteral Jet Detection: A Prospective Observational Study. JSLS 2018;22(3).
4. Berrens AC, Knipper S, Marra G, et al. State-of-the- art in Prostate Specific Membrane Antigen (PSMA)-targeted surgery– a systematic review Eur urol Open Science 2023;54:43-55.
5. Hensbergen AW, van Willigen DM, van Beurden F, et al. Image-Guided Surgery: Are We Getting the Most Out of Small-Molecule Prostate- Specific-Membrane-Antigen-Targeted Tracers? Bioconjug Chem 2020;31(2):375- 95.
6. Smith NJ, Green MA, Bahler CD, et al. Comparison of Tracer Kinetic Models for 68Ga-PSMA-11 PET in Intermediate Risk Primary Prostate Cancer Patients. Res Sq 2023.
7. Bunschoten A, Van Den Berg NS, Valdés Olmos RA, Blokland JAK, Van Leeuwen FWB. *Tracers Applied in Radioguided Surgery*. New York: Springer 2016.
8. Nguyen HG, van den Berg NS, Antaris AL, et al. First- in-human Evaluation of a Prostate-specific Membrane Antigen-targeted Near-infrared Fluorescent Small Molecule for Fluorescence-based Identification of Prostate Cancer in Patients with High-risk Prostate Cancer Undergoing Robotic- assisted Prostatectomy. Eur Urol Oncol 2024;7(1):63-72.
9. Stibbe JA, de Barros HA, Linders DGJ, et al. First-in- patient study of OTL78 for intraoperative fluorescence imaging of prostate-specific membrane antigen-positive prostate cancer: a single-arm, phase 2a, feasibility trial. Lancet Oncol 2023;24(5):457-67.
10. Talevi A ed. Intradermal route. In The ADME Encyclopedia: A Comprehensive Guide on Biopharmacy and Pharmacokinetics. Cham: Springer International Publishing, 2022: 566:
11. Hamdy FC, Lamb AD, Tullis IDC, et al. First-in-man study of the PSMA Minibody IR800-IAB2M for molecularly targeted intraoperative fluorescence guidance during radical prostatectomy. Eur J Nucl Med Mol Imaging 2024.
12. Schilham MGM, Somford DM, Kusters-Vandevelde HVN, et al. Prostate-Specific Membrane Antigen-Targeted Radioguided Pelvic Lymph Node Dissection in Newly Diagnosed Prostate Cancer Patients with a Suspicion of Locoregional Lymph Node Metastases: The DETECT Trial. J Nucl Med 2024;65(3):423-29.
13. van Leeuwen FWB, van der Poel HG. Surgical Guidance in Prostate Cancer: "From Molecule to Man" Translations. Clin Cancer Res 2016;22(6):1304-6.
14. Gondoputro W, Scheltema MJ, Blazevski A, et al. Robot-Assisted Prostate-Specific Membrane Antigen-Radioguided Surgery in Primary Diagnosed Prostate Cancer. J Nucl Med 2022;63(11):1659-64.
15. olde Heuvel J, de Wit-van der Veen BJ, van der Poel HG, et al. Cerenkov Luminescence Imaging in Prostate Cancer: Not the Only Light That Shines. J Nucl Med 2022;63(1):29- 35.
16. Pettis RJ, Ginsberg B, Hirsch L, et al. Intradermal microneedle delivery of insulin lispro achieves faster insulin absorption and insulin action than subcutaneous injection. Diabetes Technol Ther 2011;13(4):435-42.
17. Schwager S, Detmar M. Inflammation and Lymphatic Function. Front Immunol 2019;10:308.
18. Berrens AC, Buckle T, van Oosterom MN, et al. Multispectral Fluorescence Imaging as a Tool to Distinguish Pelvic Lymphatic Drainage Patterns During Robot-assisted

Lymph Node Dissection in Prostate Cancer. Ann Surg Oncol 2024.

19. Briganti A, Larcher A, Abdollah F, et al. Updated nomogram predicting lymph node invasion in patients with prostate cancer undergoing extended pelvic lymph node dissection: the essential importance of percentage of positive cores. Eur Urol 2012;61(3):480-7.
20. Safety Data Sheet for Fluorescein sodium 5/11.
21. O'Goshi K, Serup J. Safety of sodium fluorescein for *in vivo* study of skin. Skin Res Technol 2006;12(3):155-61.
22. Meershoek P, KleinJan GH, van Willigen DM, et al. Multi-wavelength fluorescence imaging with a da Vinci Firefly-a technical look behind the scenes. J Robot Surg 2021;15(5):751-60.
23. van den Berg NS, Buckle T, KleinJan GH, van der Poel HG, van Leeuwen FWB. Multispectral Fluorescence Imaging During Robot-assisted Laparoscopic Sentinel Node Biopsy: A First Step Towards a Fluorescence-based Anatomic Roadmap. Eur Urol 2017;72(1):110-17.
24. Meershoek P, KleinJan GH, van Oosterom MN, et al. Multispectral-Fluorescence Imaging as a Tool to Separate Healthy from Disease- Related Lymphatic Anatomy During Robot- Assisted Laparoscopy. J Nucl Med 2018;59(11):1757-60.
25. Faber RA, Verbeek FPR, de Valk KS, Burggraaf J, Vahrmeijer AL, Mieog JSD. A systematic review of clinically available and experimental dyes for intraoperative near- infrared fluorescence imaging of the ureters during laparoscopic surgery.
26. Berrens AC, Scheltema M, Maurer T, et al. Delphi consensus project on prostate-specific membrane antigen (PSMA)-targeted surgery-outcomes from an international multidisciplinary panel. Eur J Nucl Med Mol Imaging 2023.
27. Aeikens B, Niermann R, Schindler E. Investigation about the penetration depth in the normal bladder wall and tumor by local instillation of mitomycin into the urinary bladder. Urol Int 1982;37(6):389-93.
28. Spinelli AE, Durando G, Boschi F. Weak light emission of soft tissues induced by heating. J Biomed Opt 2018;23(4):1-5.
29. Dietlein F, Kobe C, Hohberg M, et al. Intraindividual Comparison of (18) F-PSMA- 1007 with Renally Excreted PSMA Ligands for PSMA PET Imaging in Patients with Relapsed Prostate Cancer. J Nucl Med 2020;61(5):729- 34.
30. Knipper S, Ascalone L, Ziegler B, et al. Salvage Surgery in Patients with Local Recurrence After Radical Prostatectomy. Eur Urol 2021;79(4):537-44.
31. Hensbergen AW, Buckle T, van Willigen DM, et al. Hybrid Tracers Based on Cyanine Backbones Targeting Prostate-Specific Membrane Antigen: Tuning Pharmacokinetic Properties and Exploring Dye-Protein Interaction. J Nucl Med 2020;61(2):234-41.
32. van Willigen DM, van den Berg NS, Buckle T, et al. Multispectral fluorescence guided surgery; a feasibility study in a phantom using a clinical- grade laparoscopic camera system. Am J Nucl Med Mol Imaging 2017;7(3):138-47.

Azargoshasb S, Berrens AC, Slof LJ, Sinaasappel M, van Leeuwen PJ, van der Poel HG, van Oosterom MN, van Leeuwen FWB

Eur Urol. 2024 May;85(5):503-505

Chapter 9

Robot-Assisted Single Photon Emission Computed Tomography: Integrating Nuclear Medicine in Robotic Urologic Surgery

Being at the forefront of surgical innovation, urology actively embraces new technologies, reshaping both surgical procedures (e.g. robotics) and decision-making (e.g. image-guided surgery). The convergence of these advancements in, e.g. robot-assisted prostatectomy, offers new opportunities to impact patient care. In this respect, popular image-guidance techniques during robotic surgery are: integrated fluorescence imaging [1], augmenting the surgeon's view with superficial (≤5 mm deep) target delineation, and tethered gamma radio-guidance [2], facilitating in-depth intraoperative detection of targets preoperatively defined with SPECT/CT or PET/CT patient scans [2]. While the preoperative tomographic imaging approaches of SPECT/CT and PET/CT set the clinical standard for tumor-targeted image-guided surgery [3], unfortunately, registration discordances between pre- and intra-operative settings caused by tissue deformations, limit their value during surgical procedures itself. Therefore, intraoperative tomographic nuclear imaging could fill this void.

As such, we propose a "freehand" intra-abdominal imaging concept, called robot-assisted SPECT. Using a surgical robotic platform equipped with a tracked drop-in gamma probe (Figure 1A), we perform gantry- free imaging to augment the surgical view with tomographic information [4]. This imaging information complements existing radio-/fluorescence-guided modalities. To evaluate this novel concept, we first studied it during the still-experimental sentinel node (SN) procedure in prostate cancer, which is an approach with relatively high nodal signal intensities that has been instrumental in validating novel guidance-technologies in the past (e.g., hybrid tracers, fluorescence endoscopes, the drop-in probe).

Between March and June 2023, five high-risk primary diagnosed prostate cancer patients (median Briganti score of 24 (IQR 18.4-30.5); 2012 nomogram), were included. All patients had clinical tumor stage of cT1c or cT2, without signs of metastases on preoperative PSMA PET/CT (Table 1). Patients underwent a da Vinci robot-assisted radio-guided SN procedure, preceding radiotherapy, without any additional lymph node dissections (local trial nr: IRBd22-231). Using a 1-day protocol, indocyanine green (ICG)-^{99m}Tc-nanoscan (227.21 MBq (IQR 210.01-228.00); GE Healthcare, Netherlands), was administered intraprostatically (4 deposits) approximately 5 hours before surgery. Preoperatively, SNs were identified via lymphoscintigraphy and SPECT/CT, providing a surgical 'roadmap' for the procedure. During surgery, SNs were identified using Firefly fluorescence imaging (Intuitive Inc., USA; integrated in the robotic system) and drop-in gamma tracing (Crystal Photonics GmbH, Germany; manipulated with the ProGrasp robotic instrument) [2]. The drop-in probe readout (counts/second) was displayed in the surgical console using the TilePro function.

To facilitate marker-based tracking, three notches in the housing of the CE-marked, shock resistant and sterilizable drop-in gamma probe were functionalized using sterile PEEK-ring markers (Figure 1A). To segment the drop-in probe from the endoscopic video,

custom vision-based tracking-algorithms (C++; OpenCV) were used, allowing digitization of the probe's traveled path. Custom tomographic reconstruction-algorithms (MATLAB, MathWorks, USA) helped to relate the probe readout to its corresponding geographic location and orientation, facilitating the creation of a freehand SPECT-scan (see QR video link in figure 1C). To model the probe detection during this process, a solid angle model was used, which determines the part of the source-radiation that should reach the detector in an ideal case based on geometric attenuation [5].

The probe with integrated markers could be used in the intraperitoneal cavity without any problems. SNs were successfully identified in all five patients, with no reported adverse reactions. SPECT/CT, fluorescence imaging, drop-in radio-guidance and the innovative robot-assisted SPECT concept, were used to define the origin of the ICG-^{99m}Tc-nanoscan accumulation (Figure 1B). In total, 13 SNs were mapped on preoperative SPECT/CT (median three SNs per patient, IQR: 2-3). All were successfully pursued and identified using the drop-in probe; with a median count rate of 240 counts/second (IQR: 135-653). For superficial lesions a topological concordance between drop-in radio-guidance and fluorescence- guidance was achieved. However, for deeper lesions, only radio-guidance facilitated target localization. This reduced the overall fluorescence identification rate to 77% (10 of 13 SNs; *ex vivo* examination yielded a 100% confirmation rate, (Table 1)). In 2 patients, pathology found nodal metastases.

Incorporating (freehand) robot-assisted SPECT into the robotic platform complements popular fluorescence- and radio-guided surgery strategies, introducing intraabdominal robotic nuclear imaging and improving the alignment between nuclear medicine and surgery. The concept represents a digital surgery approach, wherein the robot console functions as a 'control tower' for acquiring, multiplexing, and displaying complementary imaging data streams. While initial patient numbers are limited, ongoing data collection aims to evaluate the impact of this novel imaging technology on both clinical outcome and surgical decision-making. Enhancing robotic platform sensing capabilities helps broaden the adoption of intraoperative molecular imaging. A key step herein is extending the robot-assisted SPECT concept to PSMA-targeted radioguided surgeries, where dealing with challenging signal-to-background ratios [2] could address an unmet clinical need.

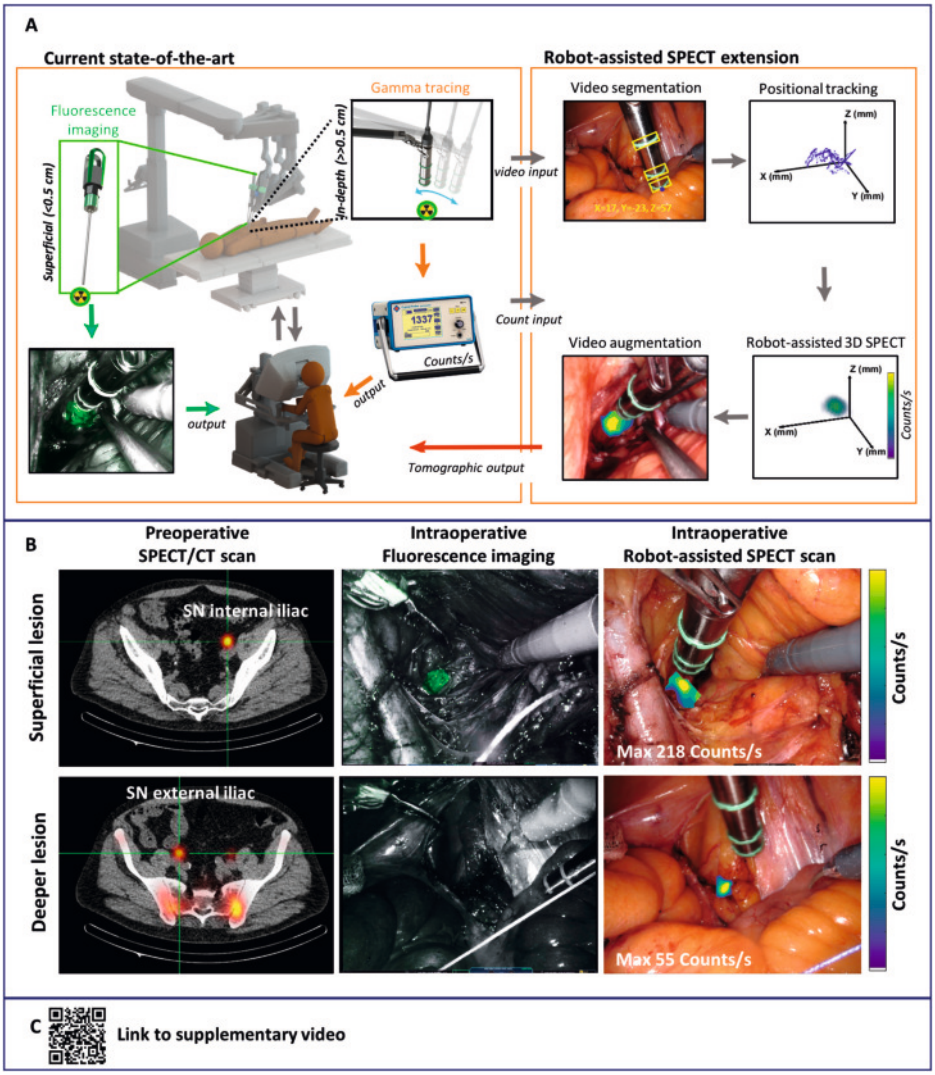

Figure 1. A) System components and illustration robot-assisted SPECT concept in relation to the state-of-the-art in fluorescence imaging and gamma tracing; B) Image guidance data for superficial and deep lesions. SN locations defined on preoperative SPECT/CT (left), fluorescence findings in green (middle), and augmentation of the video-feed with the robot-assisted SPECT scan in blue-yellow heatmap (right); C) A QR code with a link to a Supplementary video explaining the full process to develop a robot- assisted SPECT-CT.

Table 1. Patient characteristics

Patients (n=5)	
Preoperative data	
Age, median (IQR)	63 (60-68.5)
iPSA, median (IQR)	14.0 (9.7-29)
% Risk of LNI according to Briganti nomogram 2012, median (IQR)	24 (18.0-43.3)
Clinical T stage, n (%)	
cT1c	3 (60)
cT2	2 (40)
Radiological T stage, n (%)	
mT2	3 (60)
mT2b	1 (20)
mT3b	1 (20)
Radiological N stage according to PSMA PET/CT, n (%)	
miN0	5 (100)
ISUP grade group, n (%)	
2	1 (20)
3	2 (40)
5	2 (40)
Injected dose (MBq), median (IQR)	227.2 (202.3-230.2)
Time between injection and incision (min), median (IQR)	6.8 (5.9-7.1)
SNs identified at preoperative SPECT/CT, n	13
SNs at preoperative SPECT/CT according to anatomical location, n (%)	
Obturator loge L	3 (23%)
External iliac L	3 (23%)
Internal iliac L	1 (8%)
Common iliac L	-
Obturator loge R	2 (15%)
External iliac R	2 (15%)
Internal iliac R	-
Common iliac R	2 (15%)
Intraoperative data	
SNs pursued during surgery, n	13
Drop-in intraoperative readout (counts/s), median (IQR)	240 (135-653)
Surgical duration (min), median (IQR)	79 (65.5-99.5)
Pathological data	
Pathological N stage, n (%)	
pN0	3 (60)
pN1	2 (40)
Total number of tracer containing SNs removed, n (median)	15 (3)
Total number of additional “suspicious” LNs removed, n	2
Tumor positive SNs, n	2

IQR = interquartile range; iPSA = initial prostate-specific antigen; ISUP = International Society of Urological Pathology; LN= lymph node; LNI = lymph node involvement; PET = positron emission tomography; PSMA = prostate-specific membrane antigen; SN = sentinel lymph node, SPECT = single-photon emission computed tomography.

References

1. Tobis S, Knopf JK, Silvers C, Messing E, Yao J, Rashid H, et al. Robot-assisted and laparoscopic partial nephrectomy with near infrared fluorescence imaging. Journal of endourology. 2012;26(7):797-802.
2. Azargoshasb S, de Barros HA, Rietbergen DD, Dell'Oglio P, van Leeuwen PJ, Wagner C, et al. Artificial Intelligence-Supported Video Analysis as a Means to Assess the Impact of DROP-IN Image Guidance on Robotic Surgeons: Radioguided Sentinel Lymph Node versus PSMA-Targeted Prostate Cancer Surgery. Advanced Intelligent Systems. 2023:2300192.
3. Berrens A-C, Knipper S, Marra G, van Leeuwen PJ, van der Mierden S, Donswijk ML, et al. State of the Art in Prostate-specific Membrane Antigen–targeted Surgery—A Systematic Review. European Urology Open Science. 2023;54:43-55.
4. Fuerst B, Sprung J, Pinto F, Frisch B, Wendler T, Simon H, et al. First robotic SPECT for minimally invasive sentinel lymph node mapping. IEEE transactions on medical imaging. 2015;35(3):830-8.
5. Hartl A, Shakir DI, Lasser T, Ziegler SI, Navab N. Detection models for freehand SPECT reconstruction. Physics in Medicine & Biology. 2015;60(3):1031.

Berrens AC*, Pirkovets K*, Azargoshasb S, Slof L, Cakal B, van Leeuwen PJ, Wit EMK, Sinaasappel M, Wendler T, van der Poel HG, van Oosterom MN, van Leeuwen FWB

Submitted 2025

*These authors contributed equally

Chapter 10

Redefining Robotic Image-guidance — Tomographic Visualization of Lesions During Prostate Cancer Surgery via Gantry-free Robotic SPECT

Abstract

Robotic prostate cancer management is predominately executed based on the surgeon's laparoscopic perception of the intraabdominal tissue surface and available preoperative imaging, even though the localization of subsurface lesions impacts profoundly the surgical approach and precision. Molecular- instrument-sensing of radioactive signals using 'tactile' gamma sensors provides in-depth readouts (zero- dimension). Yet, it remains challenging for surgeons to relate these readouts with the anatomical location of the target. By employing laparoscopic vision to spatially monitor the sensor interaction with the patient, a maximum likelihood expectation maximization algorithm supported conversion of the gamma sensor readout (counts/s) and its pose (3D position and 3D orientation) into tomographic robotic-SPECT (RoboSPECT) scans. These could subsequently be augmented onto the endoscopic vision. Evaluation of this interactive perception concept in 21 patients not only demonstrated safety but also indicated utility in two different radio-guided surgery indications, namely sentinel node- and PSMA-targeted resections.

Introduction

Robot-assisted laparoscopic surgery is the most clinically applied branch of medical robotics. This forward- looking subfield enables minimal-invasive surgery through telerobotic surgeon-patient interactions, thereby relying on a zoomed-in view within the patient using a 3D endoscope and fine tissue manipulation with steerable instruments that improve the surgical dexterity [1 2]. To aid the surgical decision-making process, white-light laparoscopic imaging can be complemented with state-of-the-art sensory enrichments, for example through intraoperative molecular sensors that help to localize structures of interest. Combined, advances in both engineering and molecular imaging enable surgeons to optimally exploit the robot's potential to target and resect e.g. diseased tissue [3 4].

Different urological indications have proven to be key drivers for the adoption of molecular image- guided robotics (m-IGR) over the last decade [5]. They pertain to pelvic lymph node metastases in prostate cancer (PCa): through sentinel lymph node (SN) targeted resections in primary cancer [6], and prostate- specific membrane antigen (PSMA)-targeted lymph node dissection in primary cancer and recurrent cancer [7 8]. The latter procedure has been complemented by the PSMA-targeted resection of local recurrences. In all these procedures, patients are selected based on locoregional disease spread, or lack thereof, seen on PSMA-positron emission computed tomography/computed tomography (PET/CT). Before the operation, patients receive a ^{99m}Tc-labeled radiopharmaceutical, the performance of which is evaluated using non-invasive nuclear imaging in the form of single photon emission computed tomography (SPECT)/CT. Following which both images can be used to create a three-dimensional (3D) 'surgical roadmap' [9]. During surgery the same tracer-avid tissues seen on preoperative imaging can be traced using the miniaturized tethered drop-in gamma sensor technology [10]. This drop-in gamma sensor not only quantitatively identifies the source emissions (in counts/s (cps)); it also leverages the 6 degrees of freedom of the steerable robotic instrument that holds it. In both SN and PSMA-targeted surgeries, the signal intensities found in the preoperative 'roadmaps' have proven to be indicative for surgical detection of set targets [5 11]. Unfortunately, registering static preoperative SPECT/CT images to the deformable soft-tissue environment encountered during the surgical act poses considerable challenges, especially in salvage surgery [12].

Surgeons need to constantly adjust their approach to compensate for the dynamic and often unpredictable scene changes. Real-time perception enhancements (similar to live maps updates using an online navigation system when driving your car due to i.e. road blockages) are needed to support such adjustments [6]. Molecular perception-enhancing strategies in surgery tend to rely on the use of radioactive [13] and/or fluorescence pharmaceuticals [14]. While "superficial" target identification via near-infrared fluorescence laparoscopy is now commonly embedded in modern robotic platforms [4], no such sensory embodiment has been provided for "in depth" radioguided surgery

techniques. With the drop-in gamma probe technology, PCa surgeons are spearheading the expansion of robotic molecular image guidance [3 15]. Hereby lesion localizations is generally achieved via tracing of the radioisotope 99mTc (a γ-emitter with its main peak at 140 keV). Hereby preoperative imaging uses gantry-based scintigraphy and SPECT/CT, while the robotic surgical detection of these signals is made possible by the above-mentioned drop-in gamma sensor technology [16]. However, a recent Delphi consensus on the topic indicates that surgical end-users prefer image-based feedback over the numerical sensor readouts [17]. Meaning there is a desire to advance robotic radioguided surgery with intraoperative visualization of the target. A synergy between gamma tracing and fluorescence imaging, facilitated by for example hybrid tracers (such as indocyanine green (ICG)-[^{99m}Tc]Tc-nanocolloid [10]), can partly address this challenge. A downside that remains is that severe tissue attenuation of fluorescence signals still makes in-depth (> 1 cm) target imaging impossible [18].

In open surgery, gantry-free SPECT provides a valuable alternative source of molecular imaging [19 20]. An innovative technique that improves the fidelity between the intraoperative situation and the above-mentioned SPECT/CT 'surgical roadmaps' and a technique that has even been proposed as replacement of preoperative SPECT imaging in its entirety [21]. Unfortunately, the underlying optical- probe-tracking solutions used in open surgery do not transfer to intraabdominally tracking of drop-in sensor [22]. The latter requires endoscopic- video-based tracking techniques.

Following initial preclinical evaluations [23] a front-to-back redesign of all the hard- and software components needed for drop-in tracking solutions that e.g. rely on marker-based video-processing was created [5 24]. Combined, this allowed us to present the first preliminary clinical SN cases of da Vinci robot-assisted SPECT (SN-RoboSPECT) imaging in PCa patients [25]. In this manuscript, we have (1) extended the evaluation of the RoboSPECT technology (Figure 1) to a larger clinical cohort of SN patients and critically expanded its use towards PSMA-receptor-targeted procedures, and (2) implemented technical improvements on the tracking of the gamma probe and the image reconstruction pipeline. In the SN group fluorescence guidance enabled by the use of a hybrid tracer Indocyanine green (ICG)-^{99m}Tc- nanocolloid helps provide an internal reference for the target location. The PSMA-targeted application sees almost an order-of magnitude lower tracer avidities [5] and is devoid of an intraoperative control, thereby testing the utility of RoboSPECT.

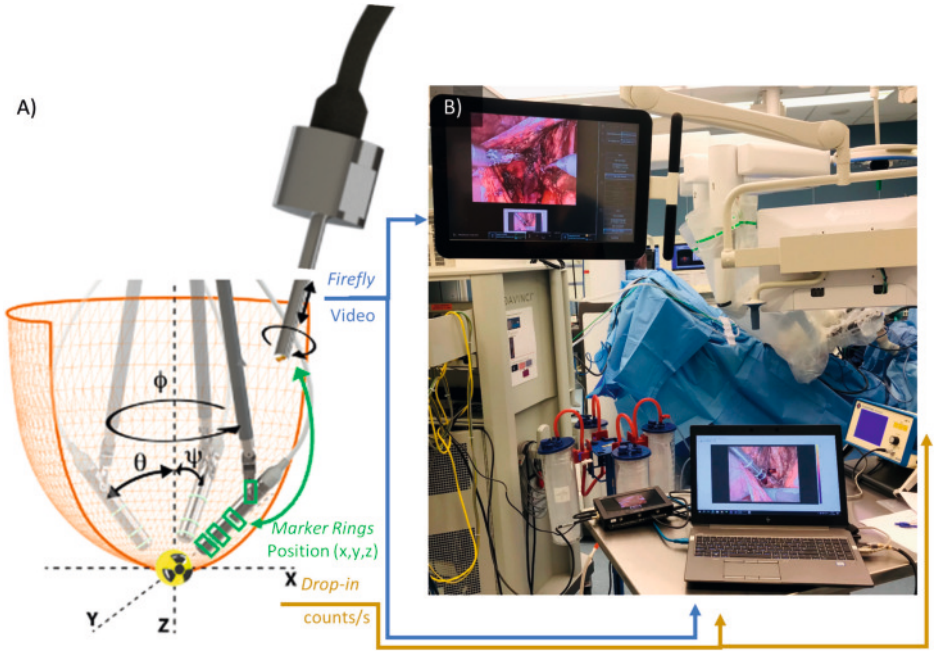

Figure 1. Technical set-up: A) Representation of the drop-in sensor maneuverability in a surgical cavity as monitored using the Firefly Xi endoscope (video tracking is used to segment out the green marker rings and estimate the position and orientation of the sensor tip). B) Visualization of RoboSPECT generation during surgery and augmented reality visualization of the RoboSPECT scan on a laptop and in the assistant display via tilepro (surgeon view is identical to that of the assistant). Drop-in out-/inputs in yellow arrows, Translation ring position to endoscope in green arow, Video out-/inputs in blue arrows.

Results

Probe design and video-tracking

The titanium housing of the medical CE-marked second-generation drop-in sensor (Crystal Photonics GmbH, Berlin, Germany) includes three circular engravings (Figure 2A) that accommodate attachment of three sterilized biocompatible PEEK marker rings (Figure 2B). With the PEEK rings attached the probe remains compatible with a standard 12 mm trocar (Figure 1; final dimension 11.8 mm). In the surgical room, ring attachment was performed by the bedside assistant using a custom press-fitting tool that was designed to support ring attachment in the sterile field (Figure 2C). The oblique ring-design prevents that the functionalized drop-in sensor snags on tissue or the trocar when it is retracted from the patient by the bedside assistant. Use of the ring-functionalized drop-in sensor was safe and did not instigate surgical complications.

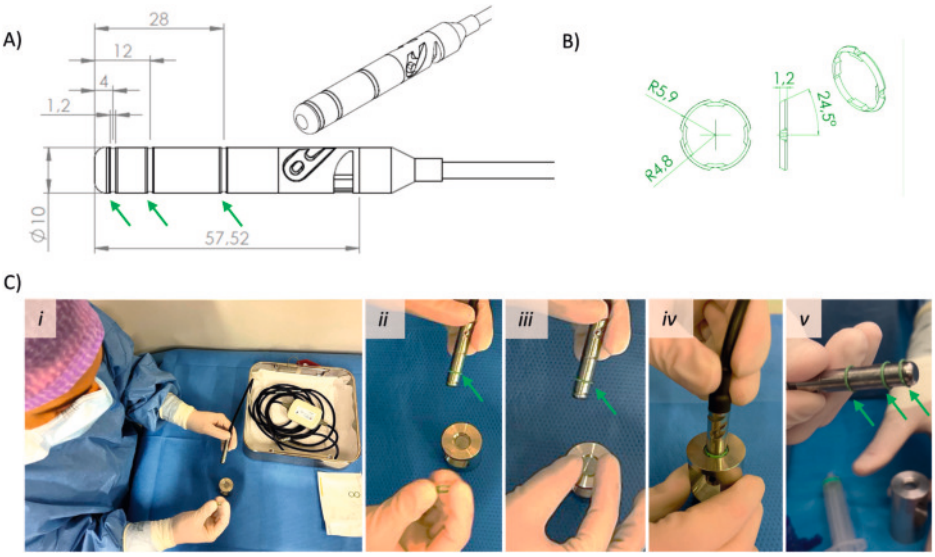

Figure 2. Hardware required for marker-based drop-in sensor tracking: A) Sterilizable and CE-marked drop-in gamma sensor designed with three circular engravings, so-called "notches" in the titanium outer housing. B) PEEK marker rings that are custom made to fit into the "notches" and that have a 24,5° angled facing edge towards the cable end of the probe. An oblique design that prevents the rings from getting snagged on tissue or the trocar opening . C) In a sterile surgical environment, the marker rings can be reproducibly attached by a bedside assistant using a custom- made mounting tool. Green arrows indicate the notches and/or PEEK marker rings located therein.

Custom computer-vision based algorithms that consider both color and geometry of the three PEEK rings supported vision-based tracking of both position and orientation (5 degrees-of-freedom) [24]. To overcome gaps in the tracking due to e.g. 0° angles with respect to the camera, dirty lens, or overlapping tissue, we employed track "stitching" (for lost frames) and track filtering (for tracking outliers). As the tracked sensor position is directly related to the vision at the endoscope tip, operating surgeons were asked to fix the laparoscope position while scanning the target.

3D image reconstruction

The above-mentioned video-tracking allows defining of the probe position (x, y and z) and orientation (yaw and pitch) with respect to the ^{99m}Tc-avid targets (Figure 1). Given the mismatch in data density (i.e., 30 Hz video tracking and 1 Hz gamma sensing), data synchronization and interpolation was required to register the sensor readout to the spatial information (Figure 3). These synchronized readouts were complemented by a drop-in look-up table (LUT; 40x40x59 mm volume: Figure 3) that was generated using GATE Monte Carlo simulations [26] and that considers specific sensor characteristics (collimator detection window radius, length and material, detector shape and material, shielding around detector) [27]. The resulting LUT was validated with the product specifications (forward facing conical detection window of 45°; collimated shielding of

99% at 140 keV; local resolution <1 cm; sensitivity >17000 cps/MBq). Combined the unique data inputs were coupled with an 'on-the-fly' calculation of a system matrix for a subsequent image reconstruction. An iterative maximum likelihood expectation maximization (MLEM) reconstruction was applied in a 100x100x100 mm^3 volume with 2mm isotropic voxels placed in front of the gamma probe at the beginning of the scan. Using an automatic 2D augmented reality projection, the 3D RoboSPECT scans were projected onto the endoscopic white-light view (filtered with a 1.5cm-radius Gaussian filter; Figure 3). Hereby, the distance between the target (i.e., its weighted center of gravity) and the laparoscope's tip could be depicted (Figure 3).

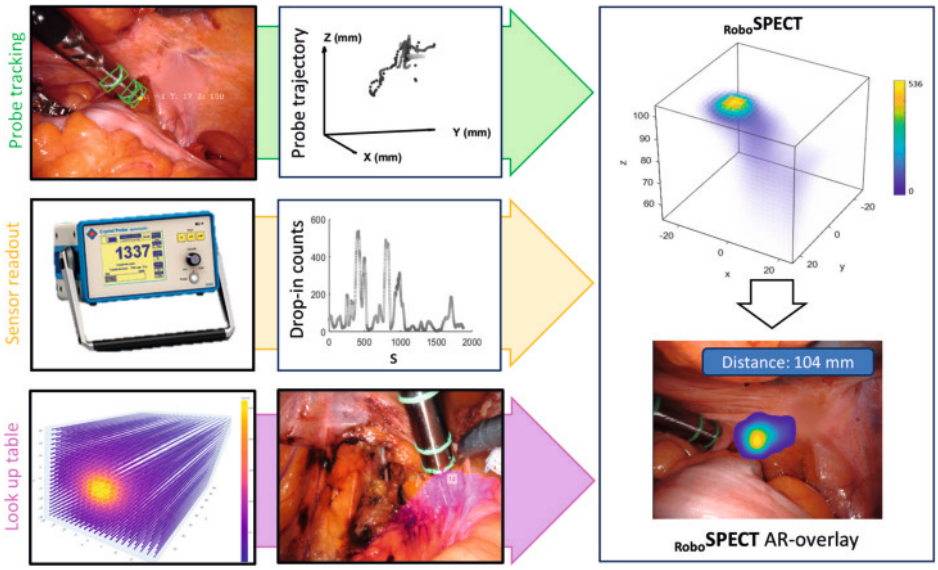

Figure 3. Multiplexing of data streams to enable RoboSPECT generation. Starting with an endoscopic video wherein the 3 green PEEK marker rings help elucidate the scan path (x,y,z position and yaw and pitch angles over time) of the drop-in sensor (workflow in the green arrow). Followed by the recording of the drop-in sensor readout (counts/s) over time (workflow in the yellow arrow). Using a specific lookup table (LUT) the probe view was estimated at different positions (workflow in the pink arrow). When combined with a custom MLEM reconstruction algorithm the synchnoized data inputs could be converted into a tomographic RoboSPECT image (top right image) that can be overlayed on the endoscopic view using augmented reality (AR; botton right image) whereby the distance of the endoscope tip to the target is also presented.

In vivo *target identification of SNs*

Prior to surgery SPECT/CT roadmaps indicated a total of 28 SNs (10 patients; median three SNs per patient, IQR 2–3). These SNs resided in various anatomical locations including, common, external and internal iliac artery, (deep) obturator fossa, presacral and paravesical (Figure 4B).

Of the 28 SNs, five SNs that were seen on SPECT/CT were not removed because they were in surgically difficult to reach anatomical locations prone to surgical complications (mesorectal, perirectal, and presacral). The remaining 23 SNs were identified using the drop-in gamma sensor (median counts: 322, IQR 140-749; median SBR: 7.5, IQR 4.4-14.4) and could be confirmed via *ex vivo* examination (Table 1). An additional three SNs were identified with the drop-in gamma probe and removed that were not seen of SPECT/CT (total 26 SNs), in addition four non-SNs and three non lymphatic tissue lesions were removed. All tumor three positive lesions were SNs (false negatives 0%; diameter 0.8-5 mm). These cases are depicted in Figure 4A. For superficial SNs (19/26 SNs (73%)), topological concordance could be achieved between SN-RoboSPECT and endoscopic fluorescence imaging (see Figure 4A and Table 1). In line with previous work [13], the inability to identify deeper lesions with fluorescence underlines the added value provided by RoboSPECT. Using the latter accurate visualization was provided for 24 SNs, one non lymphatic tissue and one non-SN lesions (sensitivity = 92.3%).

Figure 4A illustrates that the scan path was longest (10^4 mm) for the tumor positive SN that the surgeon could not also detect via fluorescence imaging as it was too deep.

In vivo *target identification of PSMA positive lesions*

Diagnostic PSMA PET/CT indicated 14 lesions in 10 patients, of which only one was false positive compared to pathology. PSMA SPECT/CT was only able to visualize four lesions in three patients (22% true positive lesions). One of the targets identified at PSMA-PET was not pursued with the drop-in probe. A total of 17 ^{99m}Tc-PSMA-avid "hot" lesions (median counts: 19, IQR 12.5-31; median SBR: 2.6, IQR 2.2-2.9) were surgically targeted using the drop-in probe: 14 nodal recurrence (2 cluster nodes) and two local recurrence lesions and one positive resection margin. RoboSPECT imaging identified all 13 PSMA PET-positive lesions as well as the positive margin (Figure 5). These targets were distributed over diverse anatomical locations (i.e., common, external and internal iliac arteries, (deep) obturator fossa, pararectal, paravesical, vas deference, seminal vesical; Figure 4B). At pathology, tumor was identified in 18 lesions: 15 nodal (diameter 2.8-23 mm), two local recurrence lesions (diameter 2-7 mm), and one positive margin (diameter 2mm). 30 lesions that were not considered "hot" were additionally removed as part of the one- sided lymph node dissection (total 47 lesions), and only two (diameter 2.8 and 4 mm) of these contained tumor (Table 1). This means that the drop-in and RoboSPECT sensitivities were 89% and 78%, respectively.

PSMA-RoboSPECT could be repeated during the procedure, allowing scans to be made before and after dissecting different anatomical planes. Doing so helped to illustrate how spatial constraints adapt of the acquisition (volume) and reduces the scanning path. The example in Figure 5A shows a 4-fold reduction in the scanning path length for the same lesion. The example in Figure 5B indicates that the scanning path length may be substantially longer when the scan is made outside of the peritoneum. Interestingly,

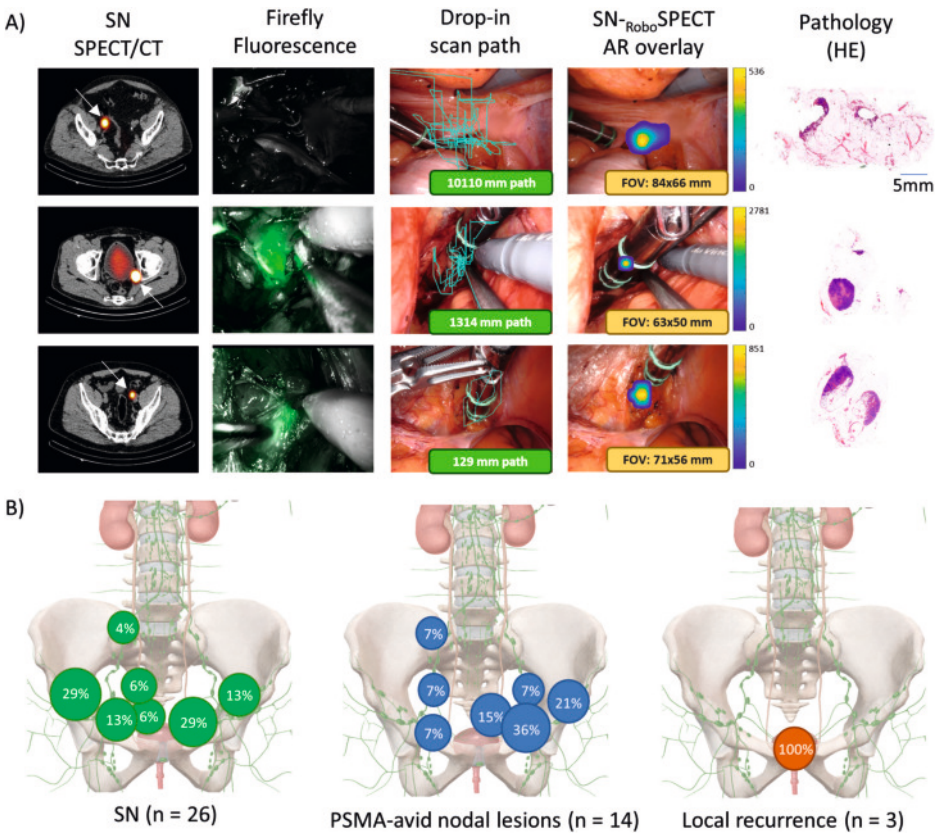

Figure 4. Pre- and intraoperative findings of the 3 tumor positive SNs identified in the study: A) From left to right. First, the anatomical SN location on preoperative SN-SPECT/CT (white arrows). Second, the matching intraoperative Firefly fluorescence images of these SNs with signal in green. Third, the intraoperatively tracked drop-in scanning path (blue line overlayed on the white light endoscopic view) and its length in mm. Fourth, The SN-RoboSPECT images (parula Augmented reality (AR) overlay on the white light endoscopic field of view (FOV)). Fifth, the nodal tumor content as defined at pathology via HE staining and a scale bar for reference. B) Location and relative ditribution of "hot" lesions within the pelvic anatomy for: SN (Common iliac L (4%), paravesical R (6%), presacral R (6%), external iliac L (13%), external iliac R (29%), obturator fossa R (13%), obturator fossa (29%), PSMA-avid nodal lesions (Common iliac L (7%), internal iliac L (7%), internal iliac R (7%), pararectal (15%), external iliac L (21%), obturator fossa R (7%), obturator fossa L (36%), and local recurrence (Vas def L (33%), Vesicle (top) L (33%), surgical margin rectum (33%)).

during the resections of local recurrences, PSMA-RoboSPECT was also able to identify a positive resection margin that occurred following the guided resection of the local recurrence (Figure 5C). Hereby the scanning pathlength required to accurately identify the positive resection margin proved to be 7-fold longer than that of the local recurrence.

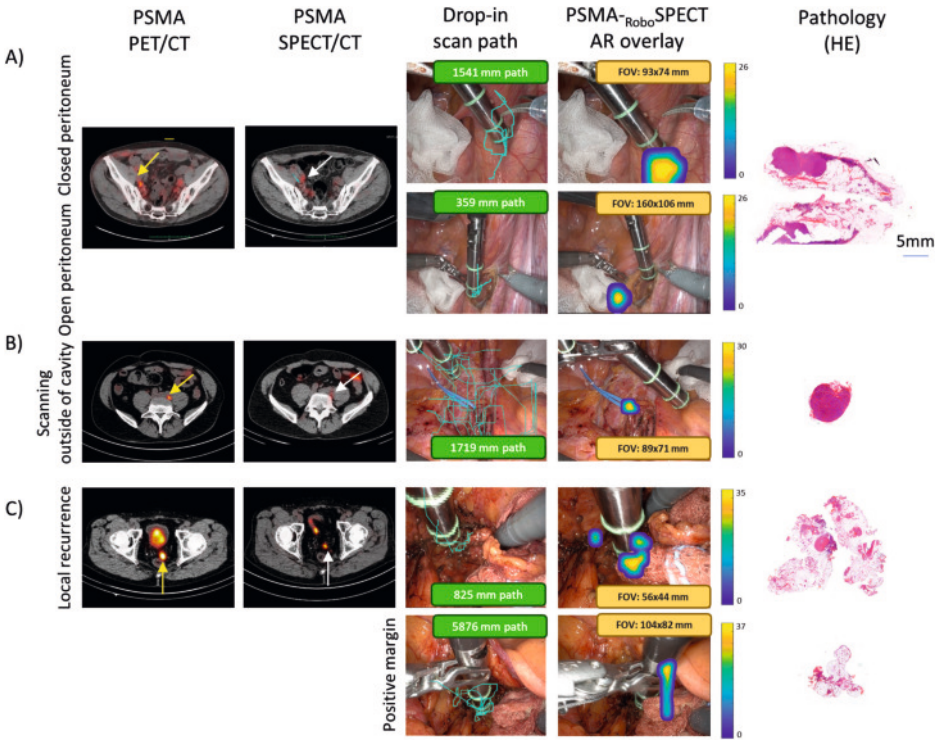

Figure 5. Variations in PSMA-RoboSPECT findings: From left to right. First, PSMA-SPET/CT (yellow arrows indicate lesion locations). Second, PSMA-SPECT/CT (white arrows indicate lesion locations). Third, the intraoperatively tracked drop-in scanning path (blue line overlayed on the white light endoscopic view) and its length in mm. Fourth, The SN-RoboSPECT images (parula Augmented reality (AR) overlay on the white light endoscopic field of view (FOV)). Fifth, the nodal tumor content as defined at pathology via HE staining and a scale bar for reference. A) Differences in scanning and PSMA-RoboSPECT before and after wound opening op the same nodal target. B) Scanning path are bigger when scanning is performed outside of the dedicted wound opening. C) Use of PSMA-RoboSPECT to identify a local recurrence and the positive margins that followed the initial resection.

Discussion

By translating RoboSPECT to the operating room, we have created a unique new gantry-free imaging strategy that supports in-depth molecular target delineation during robotic surgery. RoboSPECT identified ^{99m}Tc- avid targets (SNs, PSMA-avid LNs, local recurrences and a positive margin). In SN procedures it helped identify lesions >1 cm below the tissue surface that could not be detected using fluorescence (see Figure 4A). This means that – when a hybrid tracer is used – RoboSPECT helps to effectively compensate for the shortcomings of fluorescence guided surgery. For PSMA-targeted procedures, RoboSPECT helped identify the lesions with signal- and signal to background intensities that were substantially lower than those identified for the SN application (17-fold and 3-fold, respectively; Figure 5). Intraoperative PSMA-RoboSPECT aligned with diagnostic

PSMA-PET/CT 'roadmaps', thus increasing the target identification accuracy 3-fold when compared to the gantry-based PSMA-SPECT/CT performed prior to surgery. While the drop-in probe, a technology which the involved surgeons were experienced in surgically identified two additional (cluster) lesions, the augmented displays of RoboSPECT images helped advance the target perception. Consequently, it enhanced the precision with which robotic surgeonstarget local disease.

The RoboSPECT imaging technology makes use of interactive perception [28], thereby shifting the image guidance frontier in surgical robotics. This concept, however, is currently reliant on the unique second-generation CE-marked titanium drop-in gamma-sensor housing, a design that enables the functionalization with PEEK marker rings (Figure 2). This uniqueness in drop-in geometry, however, means that the critical 3D tracking solutions that we have employed are currently not transferrable to other tethered sensors e.g. the beta detector by the group of Collamati et al., the gamma detector by LightPoint Medical, or the ultrasound detectors by Hitachi and BK Medical [29]. Doing so would require alternative video-tracking solutions to be employed. In this context, there is literature describing the use of barcode-like stickers as tracking markers in patients [30 31]. Furthermore, proof-of-concept studies indicate that also marker-less artificial intelligence tethered-sensor tracking is clinically feasible [5], yet still with a lower accuracy than the approach of this work. Nevertheless, this could be a strategy that may help to further refine the kinematic tracking-architecture and help make sensor tracking a routine commodity.

Converting the sensors numerical output (cps) into images overlayed on the endoscopic view makes target identification more intuitive and reduces the surgeon's cognitive load. A finding that is in line with the reported value of mobile gamma cameras over gamma probes when applied in open surgery [32]. During the execution of robotic surgical tasks and intraoperative imaging, every motion of the robot is instigated by the surgeons dexterous and decision-making skills [33]. This means that human factors also make the drop-in scan trajectories arbitrary. Nevertheless, the examples shown in Figures 4 and 5 indicate that these trajectories are influenced by the surgeon's confidence of the lesion location (e.g. the role of fluorescence shown in Figure 4A or the identification of a 2mm positive margin in Figure 5C) and spatial constraints (example Figure 5A). This suggests that the level of image guidance provides is reflected in the surgeons' movements (robotic instrument kinematics) as new performance evaluation concept that could in the future also allow for the evaluation of RoboSPECT [5 34].

Looking forward, it is evident that – in analogy to self-driving cars – embedded quantitative and in-depth sensory readouts provide the technological thrust needed to pursue increased autonomy of robotic surgical systems [35]. In turn, computer intelligence can in the future also help improve and standardize RoboSPECT acquisitions, for example by adapting the scan geometry to the source intensity and physical

restrictions encountered at surgery, managing tissue deformations or (unvoluntary) movement of the laparoscope. Before we get to that stage the clinical implementation of RoboSPECT needs to be extended to establish best scanning practices and to define how and to what extend the technology can impact patient outcomes. Such efforts are currently ongoing.

Online methods

Patient population

In total, 21 patients with PCa underwent robot-assisted radioguided surgery procedures using ^{99m}Technetium (Tc) between 2023 and 2024. Ten patients underwent a routine SN procedure in primary PCa and 11 patients with recurrent PCa underwent salvage PSMA-targeted surgery with additional unilateral lymph node dissection as part of clinicaltrials.gov NCT03857113 (institutional review board (IRB) approved study extension IRBd-22-231). In one of the PSMA patients we were not able to properly synchronize the endoscopic and gamma readouts, so that he had to be excluded from further analysis.

Preoperative imaging

In the SN group, patients diagnosed with high-risk primary PCa that were scheduled for EBRT were included. All patients had clinical stage cT1c or cT2 tumor, without signs of metastases on PSMA PET/CT within 90 days before surgery according to local protocol ([^{68}Ga]Ga-PSMA-11, [18F]DCFPyL or [18F]PSMA- JK-7; Table 1). These patients were injected with the radioactive and fluorescent ICG-[^{99m}Tc]Tc-nanocolloid (GE Healthcare, Eindhoven, The Netherlands; ~222MBq; ~6.7h prior to surgery), as described before [5 10]. Early and late lymphoscintigrams (at 15 minutes and 2 hours after injection) were followed by a SPECT and low-dose CT scan. The preoperative SPECT/CT was used to define the general anatomical location of sentinel nodes (SNs).

The patients included in the PSMA-targeted surgery group (salvage setting) were selected based on a maximum of 3 soft-tissue lesions seen on a PSMA PET/CT ([^{68}Ga]Ga-PSMA-11, [18F]DCFPyL or [18F]PSMA-JK-7) within 90 days before salvage surgery according to local protocol. ~20.9 h prior to surgery patients received an intravenous injection of [^{99m}Tc]Tc-PSMA I&S (~566MBq). Preoperative SPECT/CT was performed at the morning of surgery to assist in surgical planning.

Surgical procedures

All procedures were performed using a multiport Da Vinci Xi surgical system (Intuitive Surgical Inc., Sunnyvale, CA, USA). SN procedures benefitted from the system's integrated Firefly fluorescence camera's ability to detect ICG-[^{99m}Tc]Tc-nanocolloid. For all procedures a shock-resistant, sterilizable [10], second-generation drop-in gamma sensor (Crystal Photonics GmbH, Berlin, Germany) was used in combination with 3

Table 1. Patient characteristics (n = 20) and pre-, intra- and post-operative diagnostic *data*

Parameter	Sentinel Node (n=10)	PSMA-Targeted (n=10)
Preoperative data		
Age (yrs), median (IQR)	63.5 (61.3-68.8)	71 (66.3-75.3)
initial prostate-specific antigen (ng/ml), median (IQR)	10.9 (8.3–17.5)	1.2 (0.4-2.0)
LNI risk (%), median (IQR)	18 (13.6–30.4)	n/a
Clinical T stage, n (%)		
cT1c	6 (60)	n/a
cT2	4 (40)	n/a
Radiological T stage, n (%)		
mT2	7 (70)	n/a
mT2b	1 (10)	n/a
mT2c	1 (10)	n/a
mT3b	1 (10)	n/a
Staging according to PSMA PET/CT, n (%)	9 (90)*	10 (100)
Lesions identified at preoperative PET/CT (n)	0	14
Time between PET/CT and surgery (days), median (IQR)	98 (57.0-176.0)	48 (32.8-65.0)
Lesions identified at preoperative SPECT/CT (n)	28 SNs	4 (3 nodal and 1 local recurrence)
Intraoperative data		
Lesions identified using radioguidance, n (%)	26 SNs	17 (14 nodal, 2 local recurrence, 1 positive margin)
Lesions identified using fluorescence, n (%)	19	n/a
Additional lesions removed	7 (4 non-SN, 3 non-lymphatic tissue)	30 (26 nodal, 4 local recurrence)
Pathology data		
Total lesions analyzed, n	33	47
Tumor-positive lesions, n	3 LNs (all of which were “hot”)	18 (16 were “hot”)
Pathological N stage, n (%)		
pN0	7 (70)	0 (0)
pN1	3 (30)	10 (100)

*One patient only received MRI. IQR = interquartile range; LN = lymph node; LNI = Lymph node involvement; MBq = Megabecquerel, PET = positron emission tomography; PSMA = prostate-specific membrane antigen; SN = sentinel lymph node, SPECT = single-photon emission computed tomography

custom PEEK marker rings (Figure 2). The ring-functionalized drop-in gamma sensor was inserted into the abdominal cavity either through or next to a 12-mm trocar within the Alexis portal system (Applied Medical Corp., Rancho Santa Margarita, CA, US). The operating surgeon was able to autonomously grasp and maneuver the drop-in gamma sensor using the ProGrasp Forceps (Figure 1, 4 and 5). Via the Da Vinci TilePro, the input of the sensory readout was directly displayed in the surgeon’s view as counts/s (cps). Signal-to-background ratios (SBRs) were recorded; the maximum probe counts before final resection of the lesion (SN or PSMA-targeted node) were considered the signal value and the average counts on the direct surrounding tissue (<2 cm away from the target) were considered background value. At the end of the procedure, all the tissue was remeasured *ex vivo* using the same drop-in gamma probe. Lesions were classified

as being 'hot' according to surgeon's interpretation during the procedure. The median procedure time was 76 min for SN and 135 min for PSMA.

Complications

Postoperative complications were observed in three PSMA patients (constipation – Clavien-Dindo 1; urinary retention, lymphocele – Clavien-Dindo 2; urinary retention. Transurethral catheter longer *in situ* – Clavien-Dindo 1). There was no relevant blood loss in any of the patients.

Histopathology

SNs were fixed in formalin, cut into 2 mm segments, embedded in paraffin, and stained with hematoxylin and eosin (HE) and the middle slide was additionally stained with a pancytokeratin staining. Non-SNs were cut in 3-mm slices, usually longitudinal to the long axis, and only one HE slide per block was made. During PSMA targeted surgery, all dissected specimens were sent to pathology for histopathological examination. Specimens were formalin-fixed, sliced into 1-2 mm segments, and paraffin-embedded, after which 3 µm thick sections were obtained and stained with HE, and if needed immunohistochemical staining for pancytokeratin AE1/3 (CK AE1/3). Disease positivity was defined as the presence of any PCa deposit in the examined specimens. Pathological assessment was performed by experienced uropathologists.

Probe design and design tracking fiducials

Marker-based tracking was facilitated by using, disposable, clinical-grade green PEEK (Biocompatible PEEK Medical Grade - TECAPEEK MT Green, Ensinger GmbH, Nufringen, Germany). This material is tested according to standard ISO 10993 and can be used with either steam or plasma sterilization. The green color provides a clear contrast with the surrounding tissue and instruments. The rings (Figure 2B) were produced with a 3 axis CNC turning machine with live tooling (DMG CTX 310, DMG MORI AG, Bielefeld, Germany) and were designed in SolidWorks (Dassault Systèmes SolidWorks Corp., Vélizy-Villacoublay, France) to be press-fitted onto the three notches within the housing of gamma sensor (Figure 2C). To allow easy and controlled attachment of the rings while wearing gloves, we fabricated a mounting tool out of sterilizable stainless steel 316 (see Figure 2C; for details on the functionalization unit please see the supporting information section).

Probe tracking software

The output from one "eye" of the Firefly endoscope, recorded with a Blackmagic HyperDeck Studio HD Plus (Blackmagic Design Pty Ltd, South Melbourne, Australia) at a resolution of 1920×1080, was used to capture the surgical procedure in 2D. A custom vision-based tracking algorithm (C++; OpenCV) was employed to segment the marker rings from each individual frame of the endoscopic video, based on their shape and color. Following a checkerboard calibration of the endoscope's intrinsic and extrinsic camera

parameters [22, 36], the known geometric arrangement of the markers (an asymmetric 3-ring pattern [24]) enabled determination of the probe tip's pose in five degrees of freedom (x, y, z position, yaw and pitch angle). The resulting 3D movement trajectory of the probe was digitized using custom algorithms (MATLAB®, the MathWorks, Inc., Natick, MA, United States).

SPECT via Look-up table (LUT)

Our initial work [25] relies on the solid-angle principle for the 3D reconstruction of the radioactivity distribution. Although the solid-angle principle offers reasonable and practical SPECT reconstructions, studies show that employing Monte Carlo based look-up tables provides faster and more accurate system modelling to be used in the MLEM algorithm for SPECT [19 27 37]. A set of previously acquired measurements of a point source is used to model the contribution of each voxel to a measurement. This involved modeling the gamma sensor (based on geometry and materials of collimator, shielding and crystal) in the Monte-Carlo simulation GATE (OpenGATE, 2020) and defining a point source emitting gamma ray with a monochromatic energy of 140.5 keV (the main emission of ^{99m}Tc) [27]). The lookup table covered a range of -20 mm to +20 mm (with a step size of 2 mm) in the probe-right and probe-up directions, and from 8 mm to 67 mm (with a step size of 1 mm) in the probe forward-direction, which yields to a total of 26,460 simulations. For each simulation the stopping criterion was set to 10,000 gamma emissions. With the applied energy window of 140-150 keV, the number of detected counts among the total number of emitted rays leads to the detection probability p(i,j) = P[detected by i | emitted from j].

RoboSPECT reconstruction

Custom tomographic reconstruction algorithms (MATLAB, the MathWorks, Inc., Natick, MA, USA) were used to correlate the probe readout, its respective position and orientation, and the LUT. This resulted in a system matrix consisting of one row per reading and one column per voxel to be reconstructed. The reconstruction process iteratively refined the spatial distribution of radiotracer uptake in the image volume by using the Maximum Likelihood Expectation Maximization (MLEM) algorithm [27 38]. During iterative image refinement, information from multiple angles and positions was incorporated to compensate for attenuation and scatter ultimately yielding high-resolution volumetric reconstructions. An early reconstruction stop was based on a threshold for the solving norm with 100 iterations allowed as maximum. To avoid artifacts at the boundaries of the RoboSPECT scans, readings within a 15 mm vicinity of the boundaries were disregarded during the reconstruction. Minimum scan times were 30 seconds for one target. The reconstruction process took approximately 2.8 min per image.

Statistics

Descriptive statistics are presented as medians and interquartile range (IQR) or as frequencies with percentages. Statistical tests were performed using Python 3.11.12.

References

1. Beasley, R.A., Medical Robots: Current Systems and Research Directions. Journal of Robotics, 2012.
2. Moustris, G.P., et al., Evolution of autonomous and semi-autonomous robotic surgical systems: a review of the literature. Int J Med Robot, 2011. 7(4): p. 375–92.
3. Mazzone, E., et al., Diagnostic Value, Oncological Outcomes And Safety Profile Of Image- Guided Surgery Technologies During Robot-Assisted Lymph Node Dissection with Sentinel Node Biopsy For Prostate Cancer. Journal of Nuclear Medicine, 2021: p. jnumed.120.259788.
4. van Leeuwen, F.W.B., et al., The Rise of Molecular Image–Guided Robotic Surgery. Journal of Nuclear Medicine, 2024. 65(10): p. 1505.
5. Azargoshasb, S., et al., Artificial Intelligence- Supported Video Analysis as a Means to Assess the Impact of DROP-IN Image Guidance on Robotic Surgeons: Radioguided Sentinel Lymph Node versus PSMA-Targeted Prostate Cancer Surgery. Advanced Intelligent Systems, 2023. 5(10): p. 2300192.
6. Groen, H.C., et al., Surgical navigation for targeted retroperitoneal lymph-node removal: a randomised, controlled, phase 3 trial. EClinicalMedicine, 2024. 74: p. 102754.
7. Gandaglia, G., et al., External Validation of Nomograms for the Identification of Pelvic Nodal Dissection Candidates Among Prostate Cancer Patients with Negative Preoperative Prostate-specific Membrane Antigen Positron Emission Tomography. European Urology Oncology, 2025.
8. Maurer, T., et al., PSMA-PET for Lymph Node Detection in Recurrent Prostate Cancer: How do we use the Magic Bullet? Theranostics, 2017. 7(7): p. 2046–2047.
9. Vermeeren, L., et al., Value of SPECT/CT for detection and anatomic localization of sentinel lymph nodes before laparoscopic sentinel node lymphadenectomy in prostate carcinoma. J Nucl Med, 2009. 50(6): p. 865–70.
10. Dell'Oglio, P., et al., A DROP-IN Gamma Probe for Robot-assisted Radioguided Surgery of Lymph Nodes During Radical Prostatectomy. European Urology, 2021. 79(1): p. 124–132.
11. Berrens, A.-C., et al., Strong Correlation Between SUV_{max} on PSMA PET/CT and Numeric Drop-In γ-Probe Signal for Intraoperative Identification of Prostate Cancer Lesions. Journal of Nuclear Medicine, 2024: p. jnumed.123.267075.
12. Brouwer, O.R., et al., Feasibility of intraoperative navigation to the sentinel node in the groin using preoperatively acquired single photon emission computerized tomography data: transferring functional imaging to the operating room. J Urol, 2014. 192(6): p. 1810–6.
13. Meershoek, P., et al., Can Intraoperative Fluorescence Imaging Identify All Lesions While the Road Map Created by Preoperative Nuclear Imaging Is Masked? J Nucl Med, 2020. 61(6): p. 834–841.
14. van der Poel, H.G., et al., Intraoperative laparoscopic fluorescence guidance to the sentinel lymph node in prostate cancer patients: clinical proof of concept of an integrated functional imaging approach using a multimodal tracer. Eur Urol, 2011. 60(4): p. 826–33.
15. Knipper, S., et al., Biochemical Response of <0.1 ng/ml Predicts Therapy-free Survival of Prostate Cancer Patients following Prostate-specific Membrane Antigen-targeted Salvage Surgery. Eur Urol Oncol, 2025. 8(2): p. 270–277.
16. Berrens, A.C., et al., State of the Art in Prostate-specific Membrane Antigen-targeted Surgery-A Systematic Review. Eur Urol Open Sci, 2023. 54: p. 43–55.
17. Berrens, A.-C., et al., Delphi consensus project on prostate-specific membrane antigen (PSMA)–targeted surgery—outcomes from an international

multidisciplinary panel. European Journal of Nuclear Medicine and Molecular Imaging, 2024. 51(10): p. 2893–2902.

18. Oosterom, M.N.v., et al., Extending the Hybrid Surgical Guidance Concept With Freehand Fluorescence Tomography. IEEE Transactions on Medical Imaging, 2020. 39(1): p. 226–235.
19. Wendler, T., et al., Towards intra-operative 3D nuclear imaging: reconstruction of 3D radioactive distributions using tracked gamma probes. Med Image Comput Comput Assist Interv, 2007. 10(Pt 2): p. 909–17.
20. Bluemel, C., et al., 3D scintigraphic imaging and navigation in radioguided surgery: freehand SPECT technology and its clinical applications. Expert Rev Med Devices, 2016. 13(4): p. 339–51.
21. Schilling, C., et al., Intraoperative sentinel node imaging versus SPECT/CT in oral cancer – A blinded comparison. European Journal of Surgical Oncology, 2018. 44(12): p. 1901–1907.
22. Matthias Nathanaël van, O., et al., Navigation of a robot-integrated fluorescence laparoscope in preoperative SPECT/CT and intraoperative freehand SPECT imaging data: a phantom study. Journal of Biomedical Optics, 2016. 21(8): p. 086008.
23. Fuerst, B., et al., First Robotic SPECT for Minimally Invasive Sentinel Lymph Node Mapping. IEEE Trans Med Imaging, 2016. 35(3): p. 830–8.
24. Azargoshasb, S., et al., Optical navigation of a DROP-IN gamma probe as a means to strengthen the connection between robot-assisted and radioguided surgery. Journal of Nuclear Medicine, 2021: p. jnumed.120.259796.
25. Azargoshasb, S., et al., Robot-assisted Single Photon Emission Computed Tomography: Integrating Nuclear Medicine in Robotic Urologic Surgery. Eur Urol, 2024. 85(5): p. 503–505.
26. de Barros, H.A., et al., Robot-assisted Prostate-specific Membrane Antigen-radioguided Salvage Surgery in Recurrent Prostate Cancer Using a DROP-IN Gamma Probe: The First Prospective Feasibility Study. Eur Urol, 2022. 82(1): p. 97–105.
27. Hartl, A., et al., Detection models for freehand SPECT reconstruction. Physics in Medicine & Biology, 2015. 60(3): p. 1031.
28. Bohg, J., et al., Interactive Perception: Leveraging Action in Perception and Perception in Action. IEEE Transactions on Robotics, 2017. 33(6): p. 1273–1291.
29. van Oosterom, M.N., et al., Robotic radioguided surgery: toward full integration of radio- and hybrid-detection modalities. Clinical and Translational Imaging, 2023. 11(6): p. 533–544.
30. Ma, L., et al., Robust and fast laparoscopic vision-based ultrasound probe tracking using a binary dot array marker. Computers in Biology and Medicine, 2022. 145: p. 105406.
31. Hughes-Hallett, A., et al., Intraoperative ultrasound overlay in robot-assisted partial nephrectomy: first clinical experience. Eur Urol, 2014. 65(3): p. 671–2.
32. Heller, S. and P. Zanzonico, Nuclear Probes and Intraoperative Gamma Cameras. Seminars in Nuclear Medicine, 2011. 41(3): p. 166–181.
33. Marinho, M.M., et al. A Unified Framework for the Teleoperation of Surgical Robots in Constrained Workspaces. in 2019 International Conference on Robotics and Automation (ICRA). 2019.
34. Hung, A.J., et al., Surgeon Automated Performance Metrics as Predictors of Early Urinary Continence Recovery After Robotic Radical Prostatectomy—A Prospective Bi-institutional Study. European Urology Open Science, 2021. 27: p. 65–72.
35. Thai, M.T., et al., Advanced Intelligent Systems for Surgical Robotics. Advanced Intelligent Systems, 2020. 2(8): p. 1900138.
36. Azargoshasb, S., et al., The Click-On gamma probe, a second-generation tethered robotic gamma probe that improves dexterity and surgical decision-

making. European Journal of Nuclear Medicine and Molecular Imaging, 2021. 48(13): p. 4142–4151.

37. Alexander, H., et al. Freehand SPECT reconstructions using look up tables. in Proc.SPIE. 2012.
38. Shepp, L.A. and Y. Vardi, Maximum likelihood reconstruction for emission tomography. IEEE Trans Med Imaging, 1982. 1(2): p. 113–22.

Part III

Discussion

Chapter 11

General Discussion and Future Perspectives

As described in this thesis the surgical treatment of prostate cancer is a balanced process. In this chapter, the current surgical approach will be shortly discussed and the author's vision of the future in light of the presented studies will be outlined.

Tailoring prostate cancer surgery

Improvement of surgical care is a multifaceted process, beginning with refined patient selection and extending to comprehensive post-operative care. Enhancement of an (oncological) operation itself comes down to improving (one of) three things: speed, rigor (removal of all cancerous tissue) and "non nocere" (do not harm; remove or sever as little other tissue as possible to avoid complications). During prostatectomy surgeons aim to remove all cancerous tissue whilst very aware of the importance of preserving as much of the surrounding tissue as possible. In contrast, lymph node dissection (LND) prioritizes extensive removal of lymphatic tissue to ensure comprehensive staging without regard of the lymph related complications.

The (extended pelvic) lymph node dissection (ePLND) is therefore an interesting example of an approach that could use improvement and is not without reason a highly debated subject [1-7]. It is still considered the most accurate staging method in primary prostate cancer in spite of its comorbidity and time- consuming nature. In an attempt to refine patient selection for primary extended pelvic lymph node dissection, nomograms are continuously validated [8-10] and new ones developed including outcomes of e.g. prostate-specific membrane antigen (PSMA) PET scan [11].

To improve the "non nocere" part of the surgical approach itself one can remove as little lymph nodes as possible [12-14]. One approach that focuses on only removing the nodes that count is the sentinel node procedure [15-17]. Although a very interesting approach, it has not made the guidelines as standard of care for primary prostate cancer staging. The pattern of the sentinel nodes differs greatly in prostate cancer [18] and is depended on where the tracer is administered within the prostate [19]. In **chapter 6** and **7** of this thesis, we prospectively explored the option of reversing the SN procedure, meaning leaving behind the nodes that the skin drains to and do not contain prostate cancer metastases. We could conclude that it was feasible to visualize the lymphatic patterns of the skin and the prostate simultaneously but it was not a viable solution to spare lymph nodes associated with the skin drainage as they could also contain metastases.

Although proven the best staging method, a question that remains regards the therapeutic value of ePLND. Especially if we have another reliable, less invasive staging method (PSMA PET). Touijer et al. concluded recently from an updated randomized controlled trial that extended LND was protective of metastases but that the biochemical recurrence rate did not differ between extended and limited LND [1]. Furthermore, two recent multi-institutional studies from Japan compared ePLND vs no LND and concluded that there was no significant difference between short-term oncological outcomes [2 5].

The outcomes of a randomized control clinical trial researching the value of ePLND in in cN0 patients in the PSMA PET era (miN0) are still pending (PSMA-select study). In the absence of level 1 evidence, the future perspectives described here build on retrospective data. This perspective includes that for patients with a negative pre- operative PSMA PET/CT, ePLND should not be mandatory, even in high-risk disease. Of course, there will always be the risk of missing metastasis sites, but as current gold standard it has been clinically acceptable for the usual ePLND template to miss up to one third of pelvic metastases [20]. If we stop performing ePLND in the primary setting in miN0 patients, this will reduce operating time, cost and comorbidity. Especially relevant in the patient group that would have had a pN0 outcome. The patients that would have had a pN1 outcome, plus a currently unknown percentage of patients, will eventually develop metastases and become miN1. This gives us the opportunity to perform oligometastatic treatment, including salvage LND or (early) radiotherapy.

Radio- and fluorescence guidance to improve surgical accuracy

Again, it all starts with selecting the right patients based on preoperatively known features like the maximum standard uptake value as discussed in **chapter 4**, but also the number of metastases and PSA values [21]. To perform the best possible (salvage) LND, image-guidance can aid improving all three aforementioned things related to the surgical outcomes (speed, rigor, no harm). It would start with PSMA- targeted tracer administration. A tracer that has both a radio and a fluorescent label as the one described in **chapter 5**. On the day of the surgery, first the surgeon will align the preoperative imaging to the anatomical location of the target using technologies such as ultrasound-guided and electromagnetic tracking navigation [22 23]. As many aspects in the operating room, the navigation can be aided by artificial intelligence (AI) (Figure 1).

When getting closer to the target, thanks to the radiolabel, tools to locate radiotracers like the currently used drop-in gamma probe can be used to guide the surgeon in the direction of the target. This approach can even be facilitated by integrating the drop-in into existing robotic instruments as is shown for the 'click-on' gamma probe [26]. The intraoperative SPECT, as discussed in **chapter 9** and **10** of this thesis, could be used to make a quick scan and overlay the image of the 'hottest' area to guide surgeons towards deeper lying lesions. When near the target, the fluorescent label of the hybrid tracer will prove its worth and can confirm whether the surgeon has reached the cancerous tissue and if all tissue is indeed removed after resection. This way the target is found as fast as possible, and only the target is removed, leaving the non-targeted tissue unharmed. In case of radiological recurrence this approach leaves room for future surgical interventions and radiotherapy before systemic treatment needs to be considered [21]. Important for the quality of life as systemic (hormonal) treatment has considerable impact on a patients' daily life.

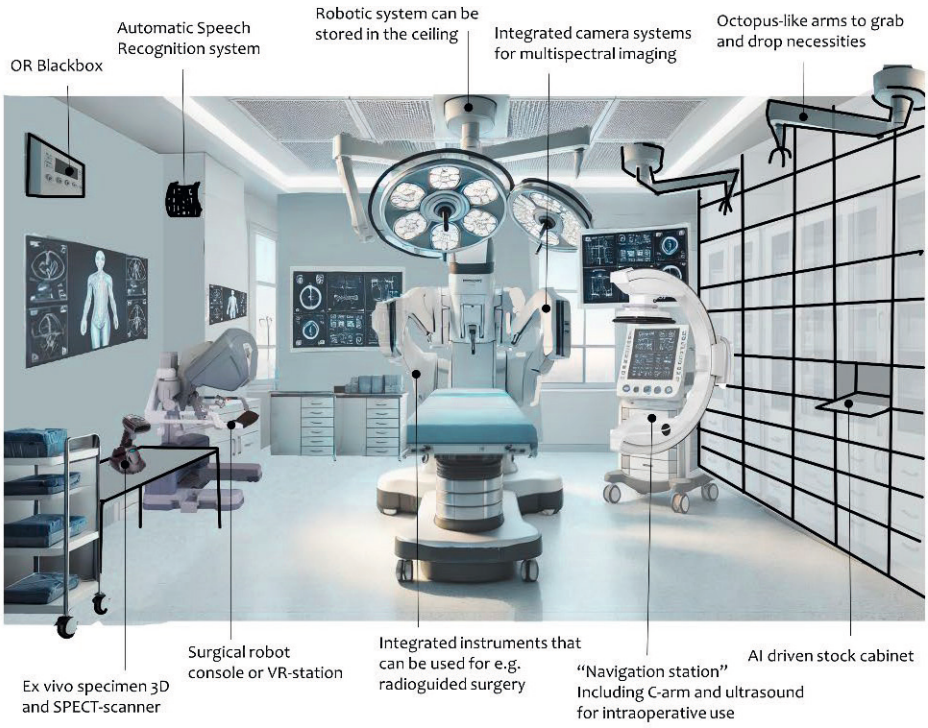

Figure 1. As the author's view on what an operating room may look like in the future this image was made using AI combined with human input. Several features are highlighted. Automatic speech recognition technologies like "Alexa" from Amazon or "Google assistant" are already considered normal in households all over the world. For the OR the technology is currently being developed [24]. A useful application for example would be an AI driven stock cabinet that sends a message to the stockroom when one of the cabinets is empty like is used in many pharmacies. An octopus- like arm can be trained to grab whatever is asked for ("Alexa, vicryl 2-0") and open and drop it in a sterile environment. With the current shortage in OR staff this could save time and man-hours [25]. Similar to a black-box in aviation, an OR black-box can record all data which can be used for training or research. This data could be automatically summarized into an OR-report that only needs to be checked at the end. A feature that is already used by anesthesiologists.

For the robotic system itself, the fluorescence guided approach means the system should have at least the option to excite and filter more types of dyes. Preferably covering all wavelengths to include all upcoming tracers but especially in the far-red spectrum to facilitate incorporation of already commonly used dyes (e.g. Cy5; EMI-137 and the hybrid PSMA tracer presented in this thesis). Lastly, complementary to *in vivo* tracer use, *ex vivo* specimen scanners can aid in direct margin assessment when the *in vivo* observations remain inconclusive [27] (Figure 1).

A few criticial notes: PSMA may have made its way into the daily practice of Urology in the Western World, not all is said yet about this new favorite target. A statement also the experts that responded to our Delphi consensus statements agreed with. There was consensus on PSMA being the best target for prostate cancer we have so far but also on

the statement that other targets need to be continuously explored. One of the things that may play a crucial role in the variety of PSMA-targeting results is the heterogeneity of PSMA intensity as was also demonstrated in **chapter 5** [28-30]. This means PSMA-targeted approach may not be suitable for all patients.

Furthermore, there are more and more robotic systems entering the market with all slightly different instruments and slightly different consoles. Although competition is good for growth, prices and improvements [31], it will make the unanimisation of all added mentioned technologies and features much more complex. Furthermore, to collect all this data first there has to be agreement on what data can be collected, stored and used. Privacy regulations present significant challenges in medical data and will complicate the implementation process. Lastly, training AI models and storing vast amounts of data require energy-intensive data centers, which often rely on fossil fuels. As AI and data-driven technologies grow, their environmental footprint becomes a pressing concern. Fortunately, there is an increasing awareness of the responsibility of hospitals and many initiatives globally that focus on reducing the carbon footprint of hospital care on many different levels [32 33].

To conclude, by improving patient selection and tailoring image-guided prostate cancer surgery we will be able to operate the patients that benefit most in the most effective way, thereby reducing unnecessary (salvage) surgical procedures and delaying costly and impactful treatment.

References

1. Touijer KA, Vertosick EA, Sjoberg DD, et al. Pelvic Lymph Node Dissection in Prostate Cancer: Update from a Randomized Clinical Trial of Limited Versus Extended Dissection. Eur Urol 2024.
2. Sugihara N, Hashine K, Yamashita N, et al. Can Pelvic Lymph Node Dissection in Prostate Cancer Patients with a 5% Briganti Nomogram Cut- off Value Provide an Oncological Benefit? A Large Multi-Institutional Cohort Study in Japan. Acta Med Okayama 2024;78(4):307- 12.
3. Lestingi JFP, Guglielmetti GB, Trinh QD, et al. Extended Versus Limited Pelvic Lymph Node Dissection During Radical Prostatectomy for Intermediate- and High-risk Prostate Cancer: Early Oncological Outcomes from a Randomized Phase 3 Trial. Eur Urol 2021;79(5):595-604.
4. Preisser F, van den Bergh RCN, Gandaglia G, et al. Effect of Extended Pelvic Lymph Node Dissection on Oncologic Outcomes in Patients with D'Amico Intermediate and High Risk Prostate Cancer Treated with Radical Prostatectomy: A Multi-Institutional Study. J Urol 2020;203(2):338-43.
5. Washino S, Kawase M, Shimbo M, et al. Comparison of oncological outcomes between extended and no pelvic lymph node dissection in patients with high- or very high-risk prostate cancer: a multi-institutional study. Prostate International 2024;12(3):160-66.
6. Roberts MJ, Yaxley JW, Stranne J, van Oort IM, Tilki D. Is extended pelvic lymph node dissection REALLY required for staging of prostate cancer in the PSMA-PET era? Prostate Cancer Prostatic Dis 2024.
7. Gandaglia G, Barletta F, Robesti D, et al. Identification of the Optimal Candidates for Nodal Staging with Extended Pelvic Lymph Node Dissection Among Prostate Cancer Patients Who Underwent Preoperative Prostate-specific Membrane Antigen Positron Emission Tomography. External Validation of the Memorial Sloan Kettering Cancer Center and Briganti Nomograms and Development of a Novel Tool. Eur Urol Oncol 2023;6(6):543-52.
8. Fukagawa E, Yamamoto S, Ohde S, et al. External validation of the Briganti 2019 nomogram to identify candidates for extended pelvic lymph node dissection among patients with high-risk clinically localized prostate cancer. Int J Clin Oncol 2021;26(9):1736-44.
9. Gandaglia G, Ploussard G, Valerio M, et al. A Novel Nomogram to Identify Candidates for Extended Pelvic Lymph Node Dissection Among Patients with Clinically Localized Prostate Cancer Diagnosed with Magnetic Resonance Imaging-targeted and Systematic Biopsies. Eur Urol 2019;75(3):506-14.
10. Di Pierro GB, Salciccia S, Frisenda M, et al. Comparison of Four Validated Nomograms (Memorial Sloan Kettering Cancer Center, Briganti 2012, 2017, and 2019) Predicting Lymph Node Invasion in Patients with High- Risk Prostate Cancer Candidates for Radical Prostatectomy and Extended Pelvic Lymph Node Dissection: Clinical Experience and Review of the Literature. Cancers (Basel) 2023;15(6).
11. Vis AN, Meijer D, Roberts MJ, et al. Development and External Validation of a Novel Nomogram to Predict the Probability of Pelvic Lymph-node Metastases in Prostate Cancer Patients Using Magnetic Resonance Imaging and Molecular Imaging with Prostate-specific Membrane Antigen Positron Emission Tomography. Eur Urol Oncol 2023;6(6):553-63.
12. Baas DJH, de Baaij JMS, Sedelaar JPM, et al. Extended pelvic lymph node dissection in robot-assisted radical prostatectomy is an independent risk factor for major complications. J Robot Surg 2024;18(1):140.
13. Briganti A, Chun FK, Salonia A, et al. Complications and other surgical outcomes associated with extended pelvic lymphadenectomy in men with

localized prostate cancer. Eur Urol 2006;50(5):1006-13.

14. Musch M, Klevecka V, Roggenbuck U, Kroepfl D. Complications of pelvic lymphadenectomy in 1,380 patients undergoing radical retropubic prostatectomy between 1993 and 2006. J Urol 2008;179(3):923-8; discussion 28-9.
15. Wit EMK, Acar C, Grivas N, et al. Sentinel Node Procedure in Prostate Cancer: A Systematic Review to Assess Diagnostic Accuracy. Eur Urol 2017;71(4):596-605.
16. KleinJan GH, van Werkhoven E, van den Berg NS, et al. The best of both worlds: a hybrid approach for optimal pre- and intraoperative identification of sentinel lymph nodes. Eur J Nucl Med Mol Imaging 2018;45(11):1915-25.
17. Dell'Oglio P, de Vries HM, Mazzone E, et al. Hybrid Indocyanine Green-(99m)Tc-nanocolloid for Single-photon Emission Computed Tomography and Combined Radio- and Fluorescence-guided Sentinel Node Biopsy in Penile Cancer: Results of 740 Inguinal Basins Assessed at a Single Institution. Eur Urol 2020;78(6):865-72.
18. Droghetti M, Ozman O, Berrens AC, et al. Location- Based Oncological Outcomes of Sentinel Node Dissection in Radical Prostatectomy. J Urol 2024;212(3):409-19.
19. Wit EMK, KleinJan GH, Berrens AC, et al. A hybrid radioactive and fluorescence approach is more than the sum of its parts; outcome of a phase II randomized sentinel node trial in prostate cancer patients. Eur J Nucl Med Mol Imaging 2023;50(9):2861-71.
20. Yaxley JW, Raveenthiran S, Nouhaud FX, et al. Risk of metastatic disease on (68) gallium- prostate-specific membrane antigen positron emission tomography/computed tomography scan for primary staging of 1253 men at the diagnosis of prostate cancer. BJU Int 2019;124(3):401-07.
21. Knipper S, Mehdi Irai M, Simon R, et al. Cohort Study of Oligorecurrent Prostate Cancer Patients: Oncological Outcomes of Patients Treated with Salvage Lymph Node Dissection via Prostate-specific Membrane Antigen- radioguided Surgery. Eur Urol 2023;83(1):62- 69.
22. Pavone M, Seeliger B, Teodorico E, et al. Ultrasound-guided robotic surgical procedures: a systematic review. Surg Endosc 2024;38(5):2359-70.
23. Aguilera Saiz L, Heerink WJ, Groen HC, et al. Feasibility of Image-guided Navigation with Electromagnetic Tracking During Robot- assisted Sentinel Node Biopsy: A Prospective Study. Eur Urol 2025;87(4):482-90.
24. Schulte A, Suarez-Ibarrola R, Wegen D, Pohlmann PF, Petersen E, Miernik A. Automatic speech recognition in the operating room - An essential contemporary tool or a redundant gadget? A survey evaluation among physicians in form of a qualitative study. Ann Med Surg (Lond) 2020;59:81-85.
25. Secondary. https://capaciteitsorgaan.nl/.
26. Azargoshasb S, van Alphen S, Slof LJ, et al. The Click-On gamma probe, a second-generation tethered robotic gamma probe that improves dexterity and surgical decision- making. Eur J Nucl Med Mol Imaging 2021;48(13):4142-51.
27. Pisano G, van Oosterom MN, Berrens AC, et al. Freehand SPECT Combined with 3-Dimensional Light Detection and Ranging as Alternative Means of Specimen Scanning During Prostate Cancer Surgery. J Nucl Med 2024.
28. Heetman JG, Hermsen R, Exterkate L, et al. Immunohistochemical and histopathological validation of (18) F-PSMA-1007 PET/CT for intraprostatic cancerous lesions. Prostate 2023;83(14):1332-41.
29. Vetrone L, Mei R, Bianchi L, et al. Histology and PSMA Expression on Immunohistochemistry in High-Risk Prostate Cancer Patients: Comparison with (68)Ga-PSMA PET/CT Features

in Primary Staging. Cancers (Basel) 2023;15(6).

30. Wang H, Remke M, Horn T, et al. Heterogeneity of prostate-specific membrane antigen (PSMA) and PSMA-ligand uptake detection combining autoradiography and postoperative pathology in primary prostate cancer. EJNMMI Res 2023;13(1):99.
31. Why is competition policy important for consumers? - European Commission (europa.eu). Secondary Why is competition policy important for consumers? - European Commission (europa.eu). https://competition- policy.ec.europa.eu/about/what-competition-policy/why-competition-policy-important-consumers_en.
32. Vu C, Ibarra-Vega A, Yang CD, et al. Interventions to Reduce Surgical Waste Burden: A Systematic Review. Plast Reconstr Surg Glob Open 2024;12(8):e6085.
33. Blok B, Lammers R, Leliveld-Kors A. Ecologisch duurzaam aan de slag in de urologie. Tijdschrift voor Urologie 2025;15:23.

Appendices

Summary
Nederlandse samenvatting
List of publications
List of presentations
PhD portfolio
Dankwoord
Curriculum vitae

Summary

This thesis focuses on gaining more insights in anatomical structures and precise tumor removal during primary and nodal surgery. The two main surgical guidance strategies (fluorescence and radioguidance) are introduced in **chapter 1** and described in more detail throughout this thesis. By means of predominantly prospective studies, conducted in the operating room, new insights to improve precision surgery were sought.

Part I: PSMA-targeted surgery

Throughout the first part of this thesis, emphasis was put on enhancing surgical precision by targeting the prostate-specific membrane antigen (PSMA). **Chapter 2** gives an overview of what tracers and technologies are researched globally. With implementation of new tracers and technologies, the landscape of PSMA-targeted surgery is constantly changing, necessitating ongoing evaluation. A possible challenge that arises with new technologies is that research approaches may differ per institute and great preclinical ideas get lost in the translational process. To address these issues in the early stages of development, a Delphi consensus was conducted as described in **chapter 3**. Here, all current challenges, clinical demands and future perspectives were discussed with an international panel as means to guide future research and clinical implementations. One of the conclusions was that in regard of indication, the strongest consensus was found for the use of PSMA-targeted guidance in nodal surgery outside of the template, independent of primary or salvage setting. The most studied approach in this regard so far was ^{99m}Tc-PSMA-I&S-guided salvage lymph node dissection (**Chapter 2**). Although a promising procedure, the outcomes differed between studies and patients. An approach to reduce these differences is by enhancing patient selection. A clinically relevant approach is studied in **chapter 4**, where we used information from the preoperative PSMA PET scan to identify the patients that may benefit the most of the suggested surgical treatment. We hypothesized that patients that would benefit most are the patients where the targeted tissue can be identified and removed. A higher signal-to-background ratio means that the target is less difficult to distinguish from the surrounding tissues. We demonstrated a strong correlation between the maximum standard uptake value (SUV_{max}) and the intraoperative counts/sec (used to acoustically and optically guide the surgeon in radioguided surgery) and the signal-to-background. Meaning that in patients with a high SUV_{max} the target will stand out more compared to its surroundings.

In order to optimize the potential of PSMA-targeted surgery, a hybrid (meaning a radio and fluorescently labeled) PSMA tracer was developed. In **chapter 5**, 15 human prostates were incubated with the fluorescent batch of this tracer. Our current results showed a comparable accuracy for the hybrid tracer as for preoperative PET imaging in identifying tumor lesions but also revealed challenges that come with *ex vivo*, translational efforts. Nevertheless, our results were promising for the first in-human trial.

Part II– Applications and challenges of image-guided surgery

In the second part of this thesis other approaches to image-guided surgery are discussed focusing on the removal of lymph nodes in prostate cancer surgery. The first two chapters discuss how to avoid important and often overlooked complications of nodal surgery. To explore the option of reversing the sentinel node procedure, meaning leaving behind the nodes that do not contain prostate cancer metastases, the first step was to explore if the lymphatic drainage patterns of the prostate and other organs converge within the pelvic surgical template. To do so it was necessary to identify said drainage patterns intraoperatively. In **chapter 6**, we concluded that it was feasible to identify the drainage patterns from the skin of the abdominal wall and upper leg (the two most common locations for lymphedema) using multispectral fluorescence imaging (tracers: indocyanine green (ICG) and fluorescein). The next step was to find out if those drainage patterns converged. In **chapter 6**, *in vivo*, the lymph vessels were seen closely related but did not clearly follow the same pattern. Fluorescein revealed to be unsuitable for the histopathological analysis. To address the question of convergence, a follow-up study was conducted (**Chapter 7**). Using only ICG that was administered into the dermis of the abdominal wall, we could conclude that lymph nodes related to the abdominal wall could contain prostate cancer metastases. This implies that sparing lymph nodes to avoid complications is not a viable solution to reduce invasiveness of the ePLND.

As mentioned in **part I**, a challenge of image-guided surgery in general is the distinction between the target and the background. Usually expressed as the tumor-to-background or signal-to-background ratio. In our Delphi consensus (**Chapter 3)** no clear consensus was reached on the optimal method to determine this ratio. Both the target vs a rim of surrounding tissue and the target vs a low-intensity tissue section were considered acceptable. Paradoxically, some tracers used in urological procedures are renally cleared. Meaning the tracer leaks into the surgical field when the urinary tract is opened. In **chapter 8,** we visualized how this causes unwanted background staining throughout the procedure that can interfere with the correct interpretation of tracer presence in regard to its surrounding tissue. If that tissue is located in areas that positive surgical margins may be expected, we confirmed it should be taken into consideration that this may result in false positives.

Dependent of tracer clearance pathway, during surgery in the pelvic area background signal from the bladder and the rectum can also interfere with radioguidance. Through the Delphi consensus (**Chapter 3**) it became clear that quantitative and/or visual image-based were the preferred readout type. As described in **chapter 5**, hybrid tracers can facilitate this combination. Although, the challenge remains that fluorescence suffers from tissue attenuation and is of aid only close to the target. We have therefore also explored other ways to improve target identification during radioguided surgery. We researched an innovative way to visualize the 'hottest' regions in both sentinel node procedures and PSMA-targeted procedures (**Chapter 9 and 10**). In order to locate the

gamma probe in regard of its surroundings, first some enhancements were made to track the instruments' movements. Then, by correlating the number of counts/sec (the quantative readout) with the position of the drop-in gamma probe in relation to the anatomy, an intraoperative SPECT could be made. As result, a visual representation (the desired image- based readout) of the 'hottest' region could be projected during surgery, guiding the surgeon towards the target (**Chapter 10**).

Nederlandse Samenvatting

Dit proefschrift focust op het verkrijgen van meer inzicht in anatomische structuren en met precisie verwijderen van kanker tijdens zowel operaties waarbij de primaire tumor wordt verwijderd als bij lymfeklier chirurgie. De twee belangrijkste chirurgische methoden (fluorescentie- en radiogeleid) worden geïntroduceerd in **hoofdstuk 1** en worden in detail uitgewerkt in dit proefschrift. Door middel van voornamelijk prospectieve onderzoeken, uitgevoerd in de operatiekamer, werd gezocht naar nieuwe inzichten om precisiechirurgie te verbeteren.

Deel I: PSMA-gerichte chirurgie

In het eerste deel van dit proefschrift lag de nadruk op het verbeteren van de chirurgische precisie door te richten op het prostaat-specifiek membraan antigeen (PSMA). **Hoofdstuk 2** geeft een overzicht van de huidige tracers en technologieën die wereldwijd onderzocht worden. Met de implementatie van nieuwe tracers en technologieën verandert het landschap van PSMA-gerichte chirurgie voortdurend en is continue evaluatie noodzakelijk. Een mogelijke uitdaging bij nieuwe technologieën is dat onderzoek benaderingen per instituut kunnen verschillen en dat goede preklinische ideeën verloren kunnen gaan in het translationele proces. Om deze kwesties al in een vroeg stadium van ontwikkeling aan te pakken is een Delphi consensus uitgevoerd zoals beschreven in **hoofdstuk 3**. Hiervoor werden alle huidige uitdagingen, klinische behoeften en toekomstperspectieven bediscussieerd door een internationaal panel met het doel toekomstig onderzoek en de klinische implementatie te sturen. Een van de conclusies was dat met betrekking tot de indicatie voor het type begeleiding de sterkste consensus werd gevonden voor het gebruik van PSMA-gerichte tracers om klieren te vinden die buiten het normale template vallen, onafhankelijk van de setting (primair of salvage). De meest onderzochte benadering van PSMA-gerichte chirurgie is ^{99m}Tc-PSMA-I&S-geleide salvage lymfeklier dissectie (**hoofdstuk 2**). Alhoewel dit een veelbelovende procedure is, de uitkomsten verschilden tussen studies en patiënten. Een manier om deze verschillen te verminderen is door de patiënt selectie te verbeteren. Een klinisch relevante benadering dit te verbeteren wordt bestudeerd in **hoofdstuk 4**, waar we informatie van de preoperatieve PSMA PET scan gebruikten om de patiënten te identificeren die het meeste baat zouden hebben bij de voorgestelde chirurgische behandeling. We stelden als hypothese dat patiënten waarbij het tumorweefsel het meest accuraat geïdentificeerd en verwijderd kan worden, het meeste voordeel zouden hebben. Een hoger verschil tussen het signaal en de achtergrond betekent dat het tumorweefsel makkelijker te onderscheiden is van de omliggende weefsels. We toonden een sterke correlatie aan tussen de maximale standaard opname waarde (SUV_{max}; het signaal gemeten van de tumor op de preoperatieve PSMA PET scan) en de intraoperatieve tellingen/seconde (de numerieke waarde die de intensiteit van het signaal weergeeft wat wordt gebruikt om de chirurg akoestisch en optisch te begeleiden bij radiogeleide chirurgie). Dit betekent dat bij patiënten met een hoge SUV_{max} het doelwit meer opvalt in vergelijking met de omgeving. Om het potentieel van PSMA-gerichte

chirurgie te optimaliseren, werd een hybride (d.w.z. zowel radioactief als fluorescent gelabelde) PSMA-tracer ontwikkeld. In **hoofdstuk 5** werden 15 menselijke prostaten geïncubeerd met de fluorescente batch van deze tracer. Onze huidige resultaten toonden een vergelijkbare nauwkeurigheid voor de hybride tracer als voor preoperatieve PET-beeldvorming bij het identificeren van tumorlaesies, maar onthulden ook de uitdagingen die gepaard gaan met *ex vivo*, translationele inspanningen. Desondanks waren onze resultaten veelbelovend voor de eerste studie in mensen.

Deel II – Toepassingen en uitdagingen bij beeldgeleide chirurgie

In het tweede deel van dit proefschrift worden onderdelen van beeldgeleide chirurgie uitgelicht met de focus op het verwijderen van lymfeklieren. De eerste twee hoofdstukken uit dit deel bespreken hoe belangrijke, maar vaak over het hoofd geziene complicaties van lymfeklier chirurgie vermeden kunnen worden. De optie van een omgekeerde schildwachtklierprocedure werd verkend. Dat wil zeggen dat de focus in plaats van op alle klieren verwijderen die mogelijk prostaatkanker bevatten werd verlegd naar de focus op het achterlaten van alle klieren die geen prostaatkankermetastasen bevatten. Om dit uit te voeren was de eerste stap te kijken of de lymfedrainage uit de prostaat kruiste met andere organen binnen het chirurgische template passend bij een lymfeklierdissectie van het kleine bekken. Hiervoor was het nodig deze drainage patronen intra-operatief te kunnen identificeren. In **hoofdstuk 6** konden we concluderen dat het mogelijk was om het drainage patroon van zowel de lymfe vanuit de huid van de onderbuik en het bovenbeen (de twee meest voorkomende locaties van lymfe oedeem) als de prostaat te identificeren door fluorescente tracers met verschillende golflengten (indocyanine groen (ICG) en fluoresceïne) te gebruiken. De volgende stap was om te onderzoeken of deze drainage patronen ook kruisten. In **hoofdstuk 6**, *in vivo*, werden de lymfebanen van de huid en de prostaat nauw verwant gezien maar volgden niet duidelijk exact hetzelfde patroon. Daarbij bleek fluoresceïne ongeschikt voor de nodige histopathologische analyse. Dus om de vraag of de lymfedrainage patronen ook kruisten te beantwoorden werd een vervolgonderzoek uitgevoerd (**hoofdstuk 7**). Door alleen ICG te gebruiken welke in de lederhuid van de buikwand werd toegediend, konden we concluderen dat lymfeklieren gerelateerd aan de buikwand metastasen van prostaatkanker konden bevatten. Dit impliceert dat het sparen van lymfeklieren om geen reële oplossing is om de uitgebreidheid en daarmee het hogere risico op complicaties van de ePLND te verminderen.

Zoals ook vermeld in **deel I**, is een uitdaging van beeldgeleide chirurgie in het algemeen het onderscheid tussen het doelwit (het tumorweefsel) en de achtergrond. Dit wordt meestal uitgedrukt als de tumor-tot- achtergrond of signaal-tot-achtergrond ratio. In onze Delphi-consensus (**hoofdstuk 3**) werd geen duidelijke consensus bereikt over de optimale methode om deze verhouding te bepalen. Zowel het doelwit ten opzichte van omringend weefsel als het doelwit ten opzichte van elk weefsel met lage intensiteit werden als acceptabel beschouwd. Paradoxaal genoeg worden sommige tracers die bij

urologische procedures worden gebruikt, door de nieren geklaard. Dit betekent dat de tracer in het operatieveld lekt wanneer de urinewegen worden geopend. In **hoofdstuk 8** hebben we gevisualiseerd hoe dit ongewenste achtergrondkleuring veroorzaakt tijdens de procedure die de juiste interpretatie van de aanwezigheid van de tracer ten opzichte van het omringende weefsel kan verstoren. Als dat weefsel zich bevindt in gebied waar ook positieve snijranden kunnen voorkomen moet in overweging worden genomen dat dit in vals- positieve uitslagen kan resulteren. Afhankelijk van het type klaring (nier/lever) kan tijdens chirurgie in het bekkengebied ook bij gebruik van radiogeleide tracers het achtergrondsignaal van de blaas en het rectum de interpretatie verstoren.

Door de Delphi-consensus (**hoofdstuk 3**) werd duidelijk dat kwantitatieve en/of visuele terugkoppeling van het signaal de voorkeur had ter begeleiding. Zoals beschreven in **hoofdstuk 5** kunnen hybride tracers zowel het kwantitatieve als het visuele combineren. De uitdaging blijft echter dat het fluorescentie signaal afhankelijk is van de afstand tot aan het doelwit en dus in de praktijk alleen nuttig is wanneer je dicht in de buurt bent. Daarom hebben we ook andere manieren onderzocht om het identificeren van het doelwit tijdens radiogeleide chirurgie ook te kunnen visualiseren zoals je dat bij fluorescentie geleiding kunt. Hiervoor onderzochten we een innovatieve manier om de ‘heetste’ gebieden gebaseerd op de numerieke uitslagen bij radiogeleide chirurgie te visualiseren als een soort hoogtekaart bij landschappen. We hebben dit gedaan bij zowel schildwachtklierprocedures als PSMA-gerichte procedures (**hoofdstuk 9 en 10**). Om de locatie van de gammasonde ten opzichte van zijn omgeving te bepalen, werden eerst enkele verbeteringen aangebracht om de bewegingen van de instrumenten te volgen. Vervolgens kon een intra- operatieve SPECT worden gemaakt door het aantal tellingen/seconde (de kwantitatieve uitlezing) te correleren met de positie van de drop-in gammasonde ten opzichte van de anatomie. Als resultaat hiervan kon tijdens de operatie de gewenste visuele weergave van het ‘heetste’ gebied over de anatomie worden geprojecteerd, waardoor de chirurg naar het doelwit werd geleid (**hoofdstuk 10**).

List of publications

Publications related to this thesis

- **Back table evaluation of a novel 99mTc-hPSMA tracer – proof of concept using excised specimens of primary prostate cancer**
  Berrens AC, Contieri R, Buckle T, Ottens V, Donswijk ML, van Willigen D, da Silva Guimaraes M, van Leeuwen FWB, van der Poel HG. *Submitted 2025*

- **Redefining Robotic Image-Guidance – Tomographic Visualization of Lesions During Prostate Cancer Surgery via Gantry-Free Robotic SPECT**
  Berrens AC†, Pirkovets K†, Azargoshasb S, Slof L, Cakal B, van Leeuwen PJ, Wit EMK, Sinaasappel M, Wendler T, van der Poel HG, van Oosterom MN, van Leeuwen FWB. *Submitted 2025*

- **Back-table specimen scanning using gantry-free hybrid fhSPECT/LiDAR imaging: a feasibility study during PSMA-radioguided surgery**
  Pisano G, van Oosterom MN, Ottens VA, Berrens AC, Slof LJ, Çakal BA, Rietbergen DDD, van der Poel HG, van Leeuwen PJ, van Leeuwen FWB. *Surgical Endoscopy 2025*

- **Anatomical Distribution of Disease in Patients with pN1 Prostate Cancer who have a Biochemical Recurrence: A PSMA-PET/CT-Based Analysis**
  Zuur LG, de Bie KCC, Wever L, Ettema RH, Berrens AC, van Basten JPA, van Melick HHE, Donswijk ML, Oprea-Lager DE, Vogel WE, van der Poel HG, Vis AN, van Leeuwen PJ. *British Journal of Urology International 2025*

- **Lymphatic Drainage Of The Abdominal Wall Within The Extended Nodal Dissection Template During Prostate Cancer Surgery - Mapping Overlapping Patterns**
  Berrens AC, Vis AN, van Leeuwen PJ, Wit EMK, van Leeuwen FWB, van der Poel HG. *Lymphatic Research and Biology 2025*

- **Robot-Assisted PSMA-Radioguided Surgery For Local Recurrence In The Prostatic Bed**
  Falkenbach F, Mazzucato G, Schmalhofer ML, Tian Z, Karakiewicz PI, Graefen M, Budäus L, Mandel P, Leeuwen FWB, van Oosterom MN, Berrens AC, van der Poel HG, Shenas F, Koehler D, Knipper S, Maurer T. *British Journal of Urology International 2025*

- **Renal Clearance of Fluorescent Agents Can Compromise Image-Guided Surgery Along the Urinary Tract**
  Berrens AC, Buckle T, van Oosterom MN, Slof LJ, Melsert BM, Nieuwenhuijzen JA, Wit EMK, van Leeuwen PJ, van der Poel HG, van Leeuwen FWB. *British Journal of Urology International 2025*

- **Freehand SPECT Combined with 3-Dimensional Light Detection and Ranging as Alternative Means of Specimen Scanning During Prostate Cancer Surgery***
  Pisano G, van Oosterom MN, Berrens AC, Slof LJ, Rietbergen DDD, van der Poel HG, van Leeuwen PJ, van Leeuwen FWB. *Journal of Nuclear Medicine 2024*

- **Multispectral Fluorescence Imaging as a Tool to Distinguish Pelvic Lymphatic Drainage Patterns During Lymph Node Dissection in Prostate Cancer** Berrens AC, Buckle T, van Oosterom MN, Slof LJ, van Leeuwen PJ, Wit EMK, Bekers EM, Donswijk ML, van Leeuwen FWB, van der Poel HG. *Annals of Surgical Oncology 2024*

- **Sterke Correlatie Tussen de Intensiteit van Prostaatkanker Recidieven op de PSMA PET/CT-scan en het Intra-Operatieve Gammasonde Signaal**
  Berrens AC, Sorbi MA, Donswijk ML, De Barros HA, Azargoshasb S, van Oosterom MN, Rietbergen DDD, Bekers EM, van der Poel HG, van Leeuwen FWB, van Leeuwen PJ. *Tijdschrift voor Urologie 2024*

- **Location-Based Oncological Outcomes of Sentinel Node Dissection in Radical Prostatectomy**
  Droghetti M, Özman O, Berrens AC, van Vliet R, Schiavina R, Brunocilla E, Bekers EM, Donswijk ML, van Leeuwen FWB, van der Poel HG. *Journal of Urology 2024*

- **Complete Biochemical Response Below 0.1 ng/ml Predicts Long-Term Therapy-Free Survival of Prostate Cancer Patients Following PSMA-Targeted Salvage Lymph Node Dissection, a Retrospective Multicenter Study Including 553 Patients**
  Knipper S, Lischewski F, Koehler D, Eiber M, van Leeuwen FWB, de Barros HA, Berrens AC, van Leeuwen PJ, van der Poel HG, Ambrosini F, Falkenbach F, Budäus L, Steuber T, Graefen M, Tennstedt P, Gschwend JE, Horn T, Heck MM, Maurer T. *European Urology Oncology 2024*

- **Strong Correlation SUV_{max} on PSMA PET/CT and Numerical Drop-In Gamma Probe Signal for Intraoperative Identification of Prostate Cancer Lesions***
  Berrens AC†, Sorbi MA†, Donswijk ML, De Barros HA, Azargoshasb S, van Oosterom MN, Rietbergen DDD, Bekers EM, van der Poel HG, van Leeuwen FWB, van Leeuwen PJ. *Journal of Nuclear Medicine 2024*

- **Robot-assisted Single Photon Emission Computed Tomography: Integrating Nuclear Medicine in Robotic Urologic Surgery**
  Azargoshasb S, Berrens AC, Slof LJ, Sinaasappel M, van Leeuwen PJ, van der Poel HG, van Oosterom MN, van Leeuwen FWB. *European Urology 2024*

- **^{99m}TcPSMA- radioguided Surgery in Oligorecurrent Prostate Cancer: the Randomised TRACE-II Trial**
  Zuur LG, de Barros HA, van Oosterom MN, Berrens AC, Donswijk ML, Hendrikx JJMA, Bekers EM, Vis AN, Wit EM, van Leeuwen FB, van der Poel HG, van Leeuwen PJ. *British Journal of Urology International 2024*

- **Delphi Consensus Project on Prostate-specific Membrane Antigen (PSMA)-Targeted Surgery - Outcomes from an International Multidisciplinary Panel**
  Berrens AC, Scheltema M, Maurer T, Hermann K, Hamdy FC, Knipper S, Dell'Oglio P, Mazzone E, de Barros HA, Sorger JM, van Oosterom MN, Stricker PD, van Leeuwen PJ, Rietbergen DDD, Valdes Olmos RA, Vidal-Sicart S, Carroll PR, Buckle T, van der Poel HG, van Leeuwen FWB. *European Journal of Nuclear Medicine and Molecular Imaging 2023*

- **State of the Art in Prostate-specific Membrane Antigen–targeted Surgery—A Systematic Review**
  Berrens AC, Knipper S, Marra G, van Leeuwen PJ, van der Mierden S, Donswijk ML, Maurer T, van Leeuwen FWB, van der Poel HG. *European Urology Open Science 2023*

- **A Hybrid Radioactive and Fluorescence Approach is More Than the Sum of Its Parts; Outcome of a Phase II Randomized Sentinel Node Trial in Prostate Cancer Patients**
  Wit EMK, KleinJan GH, Berrens AC, van Vliet R, van Leeuwen PJ, Buckle T, Donswijk ML, Bekers EM, van Leeuwen FWB, van der Poel HG. *European Journal of Nuclear Medicine and Molecular Imaging 2023*

- **Prevalence of High-risk Prostate Cancer Metastasis to Cloquet's Ilioinguinal Lymph Node. Letter**
  de Barros HA, Berrens AC, Donswijk ML, Wit EMK, van Leeuwen FWB, van Leeuwen PJ, van der Poel HG. *Journal of Urology 2023*

- **Three-way Multiplexing in Prostate Cancer Patients — Combining a Bimodal Sentinel Node Tracer with Multicolor Fluorescence Imaging. Image of the month**
  Berrens AC, van Oosterom MN, Slof LJ, van Leeuwen FWB, van der Poel HG, Buckle T. *European Journal of Nuclear Medicine and Molecular Imaging 2023*

- **The Effect of Salvage Radiation Therapy on Survival, Functional Outcomes, and Quality of Life in Men with Persistent Prostate-specific Antigen After Robot-Assisted Radical Prostatectomy: Which Patient Benefits More?**
  Özman O, Berrens AC, Pos F, van Leeuwen PJ, van der Poel HG. *Practical Radiation Oncology 2022*

- **Implementation of Radioguided Surgery in Prostate Cancer**
  Berrens AC, van Leeuwen PJ, Maurer T, Hadaschik BA, Krafft U. *Quarterly Journal of Nuclear Medicine and Molecular Imaging 2021*

Bookchapter

- **Robot-assisted Radical Prostatectomy: Advanced Surgical Techniques - Bookchapter on Fluorescence Guided Node Dissection**
  Berrens AC, Özman O, Maurer T, van Leeuwen FWB, van der Poel HG. *Published by Springer 2022*

Publications not related to this thesis

- **Human colon stem cells are the principal epithelial responders to bacterial antigens**
  de Vries MH, Meddens CA, Hijma HJ, Berrens AC, Jansen SA, Kooiman BAP, Snapper S, Clevers H, Mokry M, Kuijk EW, Nieuwenhuis EES. *Frontiers in Immunology 2025*

Group authorship

- **Survival Outcomes of Patients with Muscle-Invasive Bladder Cancer According to Pathological Response at Radical Cystectomy with or without Neo-Adjuvant Chemotherapy: a Case-Control Matching Study**
  van Ginkel N, Hermans TJN, Meijer D, et al. *International Urology and Nephrology 2022*

- **Intermediate-term Survival of Robot-Assisted Versus Open Radical Cystectomy for Muscle-Invasive and High-Risk Non-Muscle Invasive Bladder Cancer in The Netherlands**
  Hinsenveld FJ, Boormans JL, van der Poel HG, et al. *Urologic Oncology 2020*

** Both awarded with the 'Alavi-Mandell Award for young academics' by the Society of Nuclear Medicine and Molecular Imaging 2025*

List of presentations

Presentations at (international) scientific conferences	Location	Year
European Association of Urology (EAU)		
- Oral presentation, AI tracking of gamma probe	Milan	2023
- Oral presentation, multispectral fluorescence imaging	Milan	2023
- Poster presentation, correlation SUV_{max} PSMA PET/CT and gamma probe	Paris	2024
European Association of Nuclear Medicine (EANM)		
- Poster, long-term outcomes of SN prostate	Barcelona	2022
- Invited lecture, Delphi consensus using Surveymonkey	Hamburg	2024
- Oral presentation, robotic SPECT	Hamburg	2024
Nederlandse Vereniging voor Urologie (NVU)		
- Oral presentation, TRACE-study	Nieuwegein	2021
- Oral presentation, follow-up SN prostate	Arnhem	2022
- Oral presentation, unilateral ePLND	Barneveld	2022
- Oral presentation, robotic SPECT	IJmuiden	2024
- Oral presentation, mapping drainage patterns	IJmuiden	2024
European Multidisciplinary Congress Urological Cancers (EMUC)		
- Poster, multispectral fluorescence imaging	Budapest	2022
- Poster, correlation SUV_{max} PSMA PET/CT and gamma probe*	Marseille	2023
- Poster, Delphi consensus PSMA-targeted surgery	Marseille	2022
European Molecular Imaging Meeting (EMIM)		
- Oral presentation, multispectral fluorescence imaging	Salzburg	2023
Amsterdam Research meeting		
- Oral presentation, multispectral fluorescence imaging	Amsterdam	2022
- Oral presentation, Delphi consensus PSMA-targeted surgery	Amsterdam	2023
Regional scientific information evening		
- Oral presentation, multispectral fluorescence imaging	Amsterdam	2023
- Oral presentation, how to use the firefly in daily urological practice	Rotterdam	2025
Lectures & symposia		
Lecture on multispectral imaging in Urology - minor Biomedical Imaging	Online	2022
Lecture on multispectral fluorescence imaging - State of the Art (SOTA); training for urologists and residents	Garderen	2023
Oral presentation at webinar on innovations in prostate cancer surgery	Online	2024
Oral presentation at symposium on lymphatics in prostate cancer surgery	Leiden	2024

**awarded as highly rated abstract*

PhD Portfolio

Courses	**Year**	**ECTS**
Basic Oncology	2021	3.0
Ethics and integrity in science	2021	2.0
Scientific writing	2021	1.5
Good clinical practice	2021	0.3
Basiscursus Regelgeving & Organisatie voor onderzoekers (BROK)	2022	1.5
Excel Basics	2021	0.2
Introduction to R	2021	1.3
Medical Statistics in R	2021	1.5
How to influence yourself positively	2023	0.3
Design your thesis with Indesign	2023	0.1
Medical statistics	2024	1.0
Scientific activities		
Preparing a publication	2021-2025	2.0
Participating in (international) scientific conferences	2021-2024	4.0
Supervision medical masterstudents	2022, 2023	1.0
OOA Retreat 2023	2023	2.0
OOA Retreat 2024	2024	2.0
Meetings	2021-2024	4.0
- Weekly Interventional Molecular Imaging laboratory meeting (LUMC)		
- Twice a week multidisciplinary consultations prostate cancer		
- Fortnightly Amsterdam Urology research meeting		
- Annual supervisory committee meeting		
Other		
Medical Business Project (MBP) (4 months)	2021	5.7
Mentor at 'Giving Back' (1 yr)	2021	0.0
Total ECTS		35.9

Dankwoord

Dit proefschrift had niet tot stand kunnen komen zonder een heleboel bijzondere mensen die ik graag wil bedanken.

Allereerst gaat mijn grootste dank uit aan **alle patiënten** die hebben meegedaan aan de onderzoeken beschreven in dit proefschrift. Op zo'n moment in je leven besluiten dat je wilt bijdragen aan wetenschap omdat dit anderen kan helpen heeft veel indruk op mij gemaakt.

Beste prof. dr. van der Poel, beste **Henk**, bedankt voor de begeleiding als mijn promotor. Ik bewonder hoe jij elke dag zo gemotiveerd bent en blijft om op hoog niveau onderzoek te doen en ook anderen kan blijven enthousiasmeren. Ik ken niemand die tegelijk een SPSS-syntax kan uitleggen, diensttelefoon kan opnemen en daarna een spot-on vraag kan stellen over een onderzoek wat nog ergens op de achtergrond in een teams-meeting werd besproken. Tijdens onze tweewekelijkse meetings was jij altijd op de hoogte van alle studies. Met scherpe vragen wist je mij te motiveren zelf verder te denken en zo te groeien in het onderzoek. Die kennis neem ik de rest van mijn carrière mee. Bedankt voor het vertrouwen deze mooie studies te coördineren, en dat ook dit boekje wel goed kwam, het is gelukt!

Beste prof. dr. van Leeuwen, beste **Fijs**, er was een keer een meeting ergens op een dinsdag ochtend in het lab in het LUMC waar we concludeerden dat ons brein anders werkt, maar we wel hetzelfde doel hadden. Daar hebben we gelukkig om kunnen lachen en sindsdien veel mooie projecten opgezet en afgerond. Ik heb in de afgelopen jaren veel van jou geleerd. Jij hebt mij laten zien hoe je met een groep van hele verschillende achtergronden met veel doorzettingsvermogen tot een gezamenlijk project en indrukwekkende eindresultaten kan komen. Ook weet ik nu hoe je zo efficiënt mogelijk data uit verschillende ideeën kunt halen. Ik bewonder je gedrevenheid en de passie om steeds weer nieuwe dingen te ontdekken en te ontwikkelen. Bedankt voor alle jaren betrokkenheid en begeleiding.

Pim, je bent voor mij en velen een voorbeeld dat het kan om met veel toewijding copromotor, PI, af en toe TV-bekendheid, vader, partner, en ook nog medisch specialist te zijn. Jij wist me gemotiveerd te houden door soms eens een hele andere kijk te suggereren en te leren van de kleine overwinningen een boost te krijgen. Ik waardeer je als copromotor, met heel veel kennis van onderzoek, een sterk relativerend vermogen en hoe je een spiegel kan voorhouden, maar bovenal als persoon. Bedankt voor het altijd meedenken met alles wat er ook buiten onderzoek speelde en de telefoontjes om "even in te checken".

Beste prof. dr. van Moorselaar, beste **Jeroen**, er is geen congres, refereeravond of Amsterdam research meeting geweest waar jij niet als eerste op stond met een vraag om mij scherp te houden. Dank voor de wijze lessen (en gezelligheid), ook tijdens de borrelavonden bij de EAU en EMUC.

Lieve AvL-collega's. **Marja**, **Daniëlle** en **Nadia**. Jullie kamer was de veilige haven van de urologie. Of het nou voor een afspraak, een dropje, levens advies, troostende woorden of om even te ontladen was, ik was altijd welkom. Dank voor alles!! Prostaat VS-ers, **Erik**, **Jolien**, **Jeroen** en **Corinne**, zonder jullie geen urologie afdeling. Bedankt voor het informeren en enthousiasmeren van de patiënten. **Jakko** en **André** bedankt voor jullie geduld, sterke verhalen en aanstekelijke enthousiasme tijdens alle studie-uren op OK. **Esther**, hoe jij je weg hebt gebaand als hele bedreven uroloog (en als enige vrouw) in het PKNW heb ik veel respect voor. Ook jij natuurlijk bedankt voor alle inzet en gezelligheid tijdens al die studie-uren op OK, maar ook voor het delen van het lief en leed van onderzoek doen. **Maarten Donswijk**, heel erg bedankt voor al je hulp met nucleaire vraagstukken en dat ik met altijd voor advies bij je terecht kon. **Elise Bekers** en **Marcos da Silva Guimaraes** voor alle uren die jullie in de pathologie van de prostaten zijn gedoken. **Jeroen Hendrikx** en de hele **afdeling nucleaire geneeskunde** voor de hulp met protocollen en scans nodig voor de onderzoeken. **Jeany** en **Roos**, zonder jullie was geen een studie daadwerkelijk van start gegaan. Veel dank voor alles wat jullie mogelijk hebben gemaakt ondanks alle onmogelijke vragen. Heel veel dank gaat uit naar de collega's van het **opnamebureau**, de **bio-imaging facility** en natuurlijk de **PA-uitsnijkamer.** Bedankt dat ik precies (net na) 18u nog aan mocht komen met studiemateriaal en altijd welkom was om in jullie domein om te komen imagen. Verder weet ik dat het altijd gezegd wordt, maar lieve **OK robot-vakspecialisten** o.a. **Jessica**, **Maaike**, **Daphne**, **Ellen**: dank voor jullie geduld! Zonder jullie was het nooit gelukt alle patiënten succesvol te opereren, alle data te verzamelen én de operatietijd binnen de perken te houden. Uiteraard ook dank voor de betrokkenheid, OOA-commissie: **Lonneke van de Poll** en **Koert Kuhlmann**.

Interventional Molecular Imaging (IMI)-collega's. **Tessa**, de rots waar ik altijd bij terecht kon in het LUMC. Jij had altijd tijd voor een korte meeting tussendoor om meer uitleg te geven of over data te sparren. Bedankt voor het helpen netwerken op congressen, je motivatie en geduld! **Matthias**, **Leon**, **Samaneh**, **Katie** bedankt voor de ontelbare uren op OK waarbij jullie altijd klaar stonden om de studies in goede banen te leiden (inclusief nametingen die tot in de late uurtjes door konden gaan). Jullie specifieke kennis en kunnen is van onschatbare waarde geweest voor dit proefschrift. Ook **Maarten**, **Danny**, **Tom**, **Martin**, **Daphne**, heel erg bedankt voor de samenwerking en de goede banden met het LUMC.

Dear international colleagues. Dear **Sophie Knipper**, **Tobias Maurer**, **Roberto Contieri**, **Mattheo Droghetti** and many more, I am very grateful that you were willing to share your knowledge with me and for all the valuable contributions to this thesis.

Natuurlijk ook heel erg bedankt voor de afgelopen jaren aan fijne samenwerking **AvL Urologen**, **AUMC-onderzoekers** en **EMC-collega's**. Al ben ik er nog maar net begonnen wil ik ook de **Radiotherapie LUMC** bedanken voor het vertrouwen, ik kijk uit naar de komende jaren. Lieve **Ben & Guida, Jos, Mig & Pe**, **schoonfamilie**, **Erasmiaans vrienden** dank voor alle support en altijd geïnteresseerd naar mijn werkverhalen luisteren. **Dhr** en **mevrouw V,** zonder jullie steun en vertrouwen had dit proefschrift niet tot stand kunnen komen. Heel erg bedankt daarvoor.

Lieve paranimfen, lieve **Jetske** en **Lotte**. Als ik naar onze groepsfoto kijk waar drie broekies verkleed als 'pinguïn', 'bierflesje' en 'tiroler dame' op een geneeskunde feest staan had ik nooit durven dromen dat we met z'n drieën een PhD in het AvL zouden gaan doen. Koffie met jullie heeft me vaak op de been gehouden en ik ben heel blij dat ik jullie aan mijn zijde heb op het podium. **Jet**, we hebben soms lachend, soms huilend onze bachelor, coschappen en eerste ANIOS-banen doorstaan. Ik ben oneindig dankbaar dat we alles met elkaar kunnen delen van lief en leed naar domme stickers. Ik ben blij als jij blij bent. **Lot**, jij bent de sterkste persoon die ik ken. Het is niet normaal hoe jij je staande hebt gehouden en nu met een opleidingsplek, een huis en gezin het leven tegemoet lacht. Ik waardeer je altijd scherpe en nuchtere kijk en ben heel dankbaar dat je altijd voor me klaarstaat.

Lieve AvL Uro PhDs. **Marias**, met dezelfde attitude als jij het chille bureau claimde op onze eerste werkdag ben jij door je PhD gevlogen. Ik bewonder je werkethos en jouw brein wat zo systematisch door data vliegt en het dan ook nog goed kan opschrijven. Ik wil je bedanken voor alle keren dat je zei dat het wel goed kwam. Dan wel door een schouderklopje in het O of om 5u s'ochtends met kebab in Marseille. Trots op je, Maar(r)tje. Stokbrood in je gezicht! **Hilda**, in jouw voetsporen probeerde ik te volgen al bleek die lat best hoog te liggen. Ik vind het ongelofelijk hoe jij de afgelopen jaren door hebt geknokt en nu met een PhD, een opleidingsplek en Daniël het leven viert. Ik ben dankbaar dat jij op al mijn vragen een antwoord wist en ik daardoor als onderzoeker kon groeien. Gelukkig zitten we samen in Leiden, ik hoop nog vaak met je bij te kletsen. **Sarah**, dank dat je het allerlangst O3.22 met me wilde delen; van onwetend naar de grootste kenners. Waar de wegen ook naartoe leiden, ik hoop je nog vaak te spreken (voorkeur met een biertje in de hand) en over het leven te filosoferen. (Don) **Manon**, hockey en EAU buddy, maar bovenal zeer gewaardeerde kamergenoot. Bedankt voor alle uren aan gezelligheid, moral support en soms de terechte terugfluitingen als ik weer FOMO had. Heel knap hoe jij ondanks aanvaring met een hockeybal alles zo snel hebt weten af te ronden. Declareren! **Sophia** bedankt voor je nuchterheid, je betrokkenheid bij je collega's en natuurlijk je aanstekelijke lach. Ik hoop dat we nog heel vaak aan Petra van de stem kastjes mogen denken. **Lotte**, jouw enthousiasme, positiviteit en manier van omdenken is niet te evenaren. Al moet niemand jouw serieuze kant onderschatten. Dat maakt je zo'n veelzijdige topper. Verander alsjeblieft nooit. **Inge**, ik bewonder jouw liefde voor de medemens en hoe jij af en toe vlijmscherp uit de hoek kan komen om ons

bij de morele les te houden. P.s. Is dit kokos? **Jo**, ik ken niemand die zo hard werkt als jij en dan ook nog eens zo veel tijd heeft voor anderen. Hopelijk zitten we later samen in zo'n fantastisch opgezet Onco netwerk! **Vera**, met veel vertrouwen droeg ik m'n grootste project aan je over. Dank voor je tomeloze enthousiasme. Het is mooi om te zien hoe je ermee aan de slag bent gegaan en eigen hebt gemaakt. Je mag me altijd bellen. **Hans** en **Hielke-Martijn**, jullie hielpen mij ondanks m'n bureau midden in de kamer met veel liefde op weg het eerste jaar, veel dank daarvoor! En natuurlijk was mijn laatste jaar door jullie nog veel leuker **Renee**, **Rick**, **Sanne** & **Jeroen**.

Dank ook voor jullie bijdrage **Roos** en **Malou**, ik vond het erg leuk jullie als student te begeleiden.

Lieve **Karen**, **Emilie**, **Ruby**, **Lot**, **Myrtle**, **Chantal**, **Stijn, Joos,** en alle andere **parels van O3**. Wat zou het saai zijn geweest zonder al die geweldige, lieve, grappige, hyperintelligente mensen op de gang. Dank voor jullie gezelligheid alle jaren. 12u lunch?

Lieve **Capone**, lieve **borrelaars**, of je elkaar nou elke woensdag (en vrijdag) ziet of ineens met maanden ertussen maakt voor ons niet uit. De pasta pesto en lauwe Bavaria zijn gelukkig ingeruild, maar de vriendschappen zijn blijven bestaan. Ik ben dankbaar dat we onvoorwaardelijk elkaars cheerleaders zijn waarbij het niets uitmaakt wie wat is gaan doen. Lieve **Car** en **Fleur**, dank voor het zijn van geweldige huisgenoten en steunpilaren op de Ceintuurbaan.

Lieve **HTTV**, ik had nooit kunnen dromen dat als je ergens gaat wonen op je 19e je er zoveel mensen ontmoet die onmisbaar blijken te worden in je leven. Iedereen, maar met name alle **11/12/13/14-HTTV-ers** en natuurlijk **Val**: heel erg bedankt voor alle liefde, het luisteren naar al mijn gezwets en vooral de lol. **Janne**/**Pip**, ik wil jou nog in het bijzonder bedanken. Jij staat altijd voor me klaar. Bij elk mooi of verdrietig moment weet ik dat je aan me denkt en er altijd een kaartje van jou in de bus ligt. Op nog heel veel mooie reisjes!

Lieve **Spoof**, toen wij in groep 1 als de langste en de kortste kleuter uit de klas besloten vrienden te worden hadden we nooit kunnen voorspellen dat we dat 25+ jaar later nog zouden zijn. Bedankt dat jij (en natuurlijk je fam) er altijd voor me bent, op nog 100 jaren meer!

Lieve **Oma**, bedankt voor het luisterend oor en alle wijze raad tijdens onze wekelijkse maandag-avond-fietstocht-telefoontjes.

Lieve BSFs, lieve **Marilise** en **Josephine**. Bedankt dat jullie er onvoorwaardelijk voor me zijn, me ophypen als ik twijfel en voor jullie eerlijke en ongezouten mening als ik juist die nodig heb. Ik ben zo trots op jullie! **Lise**, met al je creativiteit (dank voor alle hulp

met photoshop!!), intellect en doorzettingsvermogen weet ik zeker dat je eigenhandig de wereld een beetje beter (en groener) gaat maken. **Fien**, ik ken niemand die zoveel vrienden heeft als jij en dan ook nog even een universitaire master rockt. Elk bedrijf mag in z'n handjes knijpen als jij er komt werken. Op nog een miljoen inside jokes, LYNV!

Lieve **Pap** en **Mam**, waar moet ik beginnen. Jullie hebben altijd zo erg in mij geloofd. Ook als ik het zelf niet kon geloven. Ik ben zo dankbaar voor alles wat jullie mij geleerd hebben. Natuurlijk tijdens alle fijne jaren op de PB in Rotterdam, maar ook juist nu bel ik graag voor advies. Hoe jullie laten zien hoe je er kan zijn voor andere mensen en jullie steentje bijdragen om de wereld een beetje mooier te maken is heel bijzonder. Ik ben heel trots dat ik jullie dochter ben. "Doe je ding, doe je dansje!"

Lieve **Lex**, bedankt voor je onvoorwaardelijke steun en hoe trots je op me bent. Bedankt dat je af en toe vraagt of ik wel door heb dat het best bijzonder is om een PhD te doen. Jij weet hoe je me weer aan het lachen krijgt en motiveert me mijn beste zelf te zijn. Ik hoop dat we nog heel vaak in de keuken mogen dansen. Jij bent thuis.

Curriculum Vitae

Anne Claire Berrens was born on the 12th of July 1993 to her parents Frank and Marianne. She grew up with her two younger sisters Marilise and Josephine in Rotterdam and completed her secondary education at Erasmiaans Gymnasium in 2011. After learning Spanish in Salamanca, Spain, and traveling around South-America, she moved to Groningen to study medicine at the Rijksuniversiteit Groningen. Inspired by her family's love of travel, many trips followed including clinical internships at hospitals in Quito, Ecuador and Kumi, Uganda. After clinical rotations in Isala Hospital, Zwolle, a research internship at the University Medical Centre Utrecht (Hubrecht Institute) followed where she grew and studied organoids of the intestine.

After graduating as a medical doctor in 2019, she spent a COVID-ridden year working at the department of Urology of the Franciscus Gasthuis en Vlietland. She then continued her career by pursuing a PhD at the Netherlands Cancer Institute – Antoni van Leeuwenhoek hospital in Amsterdam under supervision of prof. dr. HG van der Poel and prof. dr. FWB van Leeuwen. During this time, she successfully initiated, conducted and completed two subsequent, prospective, clinical trials (SPLIT-study) while also coordinating the Ferrotran trial locally. The primary focus of her PhD has been on improving intraoperative identification of different tissues during prostate cancer surgery. During her PhD she also drew up the protocol for the next prospective clinical study regarding the mentioned hybrid PSMA tracer in this thesis, which will commence in 2026. Furthermore, she initiated a national database for the unanimous registration of sentinel node surgery, which is now open in three centers.

In addition to her scientific efforts, she broadened her horizons as a part-time consultant for 'medical business project' and as a mentor to a 15-year old through 'Giving Back'. Outside the hospital, you can find her spending time with good friends and good food. Anne Claire has now once again returned to her roots and lives in Rotterdam where she worked as a resident not in training at the Urology department of the Erasmus Medical Centre for one year. As of 2026, she found her place at the Radiotherapy department of the Leiden University Medical Center, where she will be a resident in training to become a medical specialist in this field.